THE UNIVERSITY
of EDINBURGH

Effect of C9orf72 hexanucleotide repeat expansions on human induced pluripotent stem cell derived oligodendrocytes

Elaine M Cleary

Doctor of Philosophy

University of Edinburgh

2017

Table of Contents

List of abbreviations 8
Declaration 11
Acknowledgements 12
Abstract 13
Publications relating to this thesis 16
Chapter 1. General Introduction 17
1.1 MND and FTD 17
1.1.1 Clinical features of ALS 17
1.1.2. Clinical features of FTD 17
1.1.3 Links between ALS and FTD 18
1.1.4 Cellular autonomy versus non-cellular autonomy in neurodegeneration 18
1.2 Genetics of ALS and FTD 19
1.3 C9orf72 HRE 21
1.3.1 Molecular Genetics 21
1.3.2 C9orf72 HRE related phenotypes 22
1.3.3 C9orf72 HRE genotype-phenotype correlations 22
1.3.2 Detection of the C9orf72 HRE 24
1.3.4 Pathogenic mechanisms of the C9orf72 HRE 26
1.3.5 Disease modifiers 34
1.4 Studying ALS 35
1.4.1 Pathology studies and neuroimaging 37
1.4.2 Animal models of disease 37
1.4.3 hiPSC models of disease 39
1.4.3.1 Cellular reprogramming 39
1.4.3.2 Studying ALS using hiPSC based models 40
1.4.3.3 Limitations of disease studies on hiPSC based cells 42
1.4.3.4 Generating isogenic controls using CRISPR/Cas9-mediated gene editing 44
1.5 Oligodendrocytes in ALS and FTD 45
1.5.1 Oligodendrocyte function 45
1.5.2 Oligodendrocytes in ALS/FTD 46
1.5.3 In vivo development of oligodendrocytes 47
1.5.4 Generating hiPSC derived oligodendrocytes 52
1.6 Scope of study 53
Chapter 2. Materials and Methods 55

2.1 Cell culture reagents 55
2.1.1 Media and supplements 55
2.1.2 Cytokines Growth Factors and Inhibitors 57
2.1.3 Other Tissue Culture Reagents 57
2.1.4 Cell lines 58
2.1.5 Plastics 59
2.2 Cell culture 59
2.2.1 Generating and validating iPSC lines 59
Figure 2.1 Characterisation of hiPSC lines 60
2.2.2 Tissue culture routine 61
2.2.3 hiPSC maintenance 61
2.2.3 Neuralisation and patterning 63
2.2.4 Differentiation of oligodendrocytes 64
2.2.6 Magnetic-Activated Cell Sorting (MACS) 66
2.2.7 Fluorescence-Activated Cell Sorting (FACS) 67
2.2.8 Gene editing of hiPSCs 68
2.2.9 Electrophysiology 69
2.3 Immunocytochemistry 70
2.3.1 Solutions and reagents 70
2.3.2 Live immunostaining and fixing 71
2.3.3 Blocking and antibody incubation 71
2.3.4 Imaging of slides 72
2.3.5 Image analysis 72
2.3.6 Sholl analysis 72
2.4 Molecular biology 72
2.4.1 DNA extraction 72
2.4.2 PCR for C9orf72 genotyping 73
2.4.3 Capillary electrophoresis and analysis 77
2.4.4 Sanger sequencing 77
2.4.5 Agarose gel electrophoresis 78
2.4.6 RNA extraction 78
2.4.7 cDNA synthesis 79
2.4.8 qRT-PCR 79
2.4.9 RNA-FISH 80

2.4.10 Western blotting....81
2.4.11 Transfections/HEK cells....84
2.4.12 Statistical analysis....85
2.5 Immunohistochemistry....85
2.5.1 Solutions and reagents....85
2.5.2 Immunohistochemistry protocol....86
2.5.3 Antibodies....87
2.5.4 Imaging of slides....87
Chapter 3. Molecular genetic testing for the C9orf72 hexanucleotide repeat expansion....88
3.1 Introduction....88
3.1.1 PCR based methods....89
3.1.2 Objectives....90
3.2 Results....91
3.2.1 Original flanking PCR....92
3.2.2 Redesigned flanking PCR....96
3.2.3 Original RP-PCR....104
3.2.4 Re-designed RP-PCR....106
3.2.5 Screening for C9orf72 HRE in the Scottish ALS population....113
3.2.6 Clinical diagnostic testing for C9orf72 HRE in the Scottish MND and FTLD population....114
3.3 Discussion....116
3.3.1 PCR assays for detecting C9orf72 expansions....116
3.3.2 C9orf72 repeat expansions in the Scottish ALS population....120
3.3.3 Future directions....120
3.4 Conclusion....121
Chapter 4. Derivation of oligodendrocytes from patient derived induced pluripotent stem cells with C9orf72 hexanucleotide expansions....123
4.1 Introduction....123
4.1.1 Generation of human oligodendrocytes from hiPSCs....123
4.1.2 Signalling for oligodendrocyte conversion....124
4.1.3 Protocol for oligodendrocyte generation....125
4.1.4 Objectives....127
4.2 Results....128
4.2.1 Maintenance of the C9orf72 hexanucleotide expansion in vitro....128
4.2.3 Creation of an isogenic control line....129

4.2.4 Derivation of OPCs and oligodendrocytes from neural precursor cells.....130
4.2.5 Presence of other cell types.....134
4.2.6 Maturation of C9orf72 HRE oligodendrocytes from hiPSCs.....135
4.3 Discussion.....136
4.3.1 Validation of hiPSC lines.....136
4.3.2 Presence of the C9orf72 HRE.....137
4.3.3 Creation of isogenic control.....137
4.3.4 Differentiation of hiPSC to oligodendrocytes.....138
4.3.5 Maturation of C9orf72 HRE oligodendrocytes from hiPSCs.....139
4.4 Conclusion.....140
Chapter 5. Investigating pathological features of oligodendrocytes from patient derived induced pluripotent stem cells with C9orf72 hexanucleotide expansions.....141
5.1 Introduction.....141
5.1.1 Pathological features of C9orf72 HRE.....141
5.1.2 Oligodendrocyte pathology in ALS.....142
5.1.3 Objectives.....142
5.2 Results.....142
5.2.1 C9orf72 mRNA expression levels in O4+ cells.....142
5.2.2 Presence of RNA foci.....144
5.2.3 Presence of DPR.....151
5.2.4 TDP-43 and p62 pathology.....157
5.2.5 MBP and MCT1 mRNA expression levels.....159
5.2.6 Baseline cell death and susceptibility to tunicamycin.....160
5.3 Discussion.....161
5.3.1 Loss of function of C9orf72.....161
5.3.2 RNA foci detected in OPCs and oligodendrocytes.....162
5.3.3 RAN translation.....164
5.3.4 TDP-43 mislocalisation and p62 accumulation.....165
5.3.5 MBP and MCT1 mRNA expression levels.....166
5.3.6 Cell death and susceptibility to ER stress.....166
5.4 Conclusions.....167
Chapter 6: General Discussion.....168
6.1 Genetic testing for C9orf72.....169
6.2 Disease modelling in ALS with hiPSC derived cells.....173

6.2.1 Reprogramming methods....173
6.2.2 Gender of cell line donors....174
6.2.3 Isogenic controls....174
6.2.4 Genomic stability of hiPSCs....175
6.2.5 Verification of pluripotency of cell lines....176
6.3 Derivation of hiPSC derived oligodendrocytes....176
6.4 Pathology of C9orf72 HRE hiPSC derived oligodendrocytes....179
6.4.1 Loss of function....179
6.4.2 Gain of function (RNA)....180
6.4.3 Gain of function (protein)....182
6.4.4 TDP-43 and p62 accumulation....183
6.4.5 Cell death and ER stress susceptibility....183
6.4.6 Other potential pathogenic mechanisms in oligodendrocytes....184
6.5 Further research....185
References....186

Tables

Table 2.1 Cell line details....60
Table 2.2 Details of different plate formats....65
Table 2.3 Highly homologous sequences to gRNAs and primers for Sanger sequencing....69
Table 2.4 Primary antibodies used, with dilutions used and details of origin....70
Table 2.5. Secondary antibodies used, with dilutions used and details of origin....71
Table 2.6 C9orf72 genotyping primer sequences....73
Table 2.7 qRT-PCR primer details....77
Table 2.8 Western blotting antibodies....79
Table 3.1 Variability detected at 3' end of the repeat expansion in *C9orf72* positive ALS patients....112

Figures

Figure 1.1 Proportion of familial and sporadic ALS cases attributed to mutations in different genes....20
Figure 1.2 Summary of the main methods currently used in molecular genetic testing for *C9orf72* expansion repeats....26
Figure 1.3 Schematic of main proposed pathological mechanisms for *C9orf72* HRE....27

Figure 1.4 Potential dipeptide repeat proteins arising from RAN translation…… 32
Figure 1.5 Caudalization of the neural tube by retinoic acid…….. 48
Figure 1.6 Signaling regulation of OPC specification and development…… 49
Figure 1.7 Oligodendrocyte differentiation and maturation: markers and morphology……. 51
Figure 2.1 Characterisation of hiPSC lines…….. 61
Figure 3.1 Size ranges and detection methods for C9orf72 $(G_4C_2)_n$ repeats……. 88
Figure 3.2 Primer locations for *C9orf72* PCR …… 91
Figure 3.3 Flanking PCR optimisation of polymerase mix and gradient PCR to determine annealing temperature …… 93
Figure 3.4 Assessment of co-solvents in flanking PCR……... 94
Figure 3.5 Calibration of original flanking assay…… 95
Figure 3.6 Original flanking PCR examples…… 96
Figure 3.7 Gradient PCR for HPE flanking PCR…… 97
Figure 3.8 Example of Sanger sequencing of HPE flanking PCR products to calibrate fragment size to number of repeats……..…… 98
Figure 3.9 Optimisation of cycling conditions for flanking PCR……...… 100
Figure 3.10 Optimised flanking PCR results……. 102
Figure 3.11 Flanking PCR for cell line DNA……. 103
Figure 3.12 Optimisation of original 5’ RP-PCR assay……. 105
Figure 3.13 Original 3’ RP-PCR examples……..…. 106
Figure 3.14 5’RP-PCR assay with heat pulse extension compared to constant temperature extension……... 107
Figure 3.15 Improved PCR amplification of expanded alleles using the re-designed 5’ RP-PCR assay compared to the original assay…… 108
Figure 3.16 Comparison of 3’RP-PCR with varying ramp rate and denaturation temperature……....109
Figure 3.17 Optimisation of the re-designed 3’ RP-PCR assay……. 110
Figure 3.18 3’RP-PCR artefact which is only present in the presence of normal alleles greater than 15 repeats, which is not observed for 5’RP-PCR. ……. 111
Figure 3.19 Sensitivity of RP-PCR for mosaicism…… 112
Figure 3.20 Distribution of repeat lengths of the *C9orf72* $(GGGGCC)_n$ tract in Scottish ALS patients…….……. 113
Figure 4.1. Schematic of protocol used to generate oligodendrocytes from hiPSCs…… 126
Figure 4.2 Genotyping results from hiPSC lines…….. 128
Figure 4.3 Genotyping results for creation of isogenic line……. 130

Figure 4.4 Immunocytochemical staining and quantification of oligodendrocyte lineage markers……..…….... 131
Figure 4.5 Quantification of O4 positive cells at week 3 by FACS…….. 133
Figure 4.6 Overlap of O4 marker with PDGFRa and MBP…… 134
Figure 4.7 Immunocytochemical staining of GFAP and β-III tubulin positive cells and quantification……..……135
Figure 5.1 Transcript levels of *C9orf72* in oligodendrocytes……... 144
Figure 5.2 RNA-FISH validation with controls and carriers…… 145
Figure 5.3 hiPSC derived PDGFR-α positive oligodendrocyte precursor cells with *C9orf72* HRE exhibit nuclear GGGGCCexp RNA foci while controls do not……147
Figure 5.4 hiPSC derived O4-positive oligodendrocytes with *C9orf72* HRE exhibit nuclear GGGGCCexp RNA foci……149
Figure 5.5 hiPSC derived GFAP-positive astrocytes and MBP-positive oligodendrocytes with *C9orf72* HRE exhibit nuclear GGGGCCexp RNA foci…….150
Figure 5.6 Sholl analysis on O4 positive cells with and without RNA foci……..… 151
Figure 5.7 Novus C9RAN antibody testing on transfected HEK cells……..… 152
Figure 5.8 Millipore C9RAN antibody testing on transfected HEK cells……..… 153
Figure 5.9 Biogen C9RAN antibody testing on transfected HEK cells……..….. 155
Figure 5.10 Immunohistochemistry using Biogen anti-PA antibody…….…156
Figure 5.11 Western blots with anti-GA, anti-GP and anti-PA antibodies……... 157
Figure 5.12 TDP-43 mRNA expression levels, TDP-43 and p62 immunocytochemistry and Western blots……..……158
Figure 5.13 mRNA expression levels of MBP and MCT1……... 160
Figure 5.14 GGGGCCexp carrying oligodendrocytes show no baseline survival phenotype (population) by FACS and response to ER stress…… 161

List of abbreviations

AD	Alzheimer's disease
ADARB2	adenosine deaminase, RNA specific B2
ALS	Amyotrophic lateral sclerosis
ALYREF	Aly/REF export factor
AMPA	α-amino-3-hydroxy-5-methyl-4-isoxazolepropionic acid
AP	alanine-proline
ATXN2	ataxin-2
bp	base pairs
BMP	Bone morphogenic protein
C9orf72	Chromosome 9 open reading frame 72
CDM	Chemically defined medium
CEPH	Centre for the Study of Human Polymorphisms
CNS	central nervous system
CNTF	ciliary neurotrophic factor
CpG	Cytosine-phosphate-guanine
CRISPR	clustered regularly interspaced short palindromic repeat
DENN	differentially expression in normal and neoplasia
DNA	deoxyribonucleic acid
DMSO	Dimethyl sulphoxide
DPBS	Dulbecco's phosphate buffered saline
DPR	dipeptide repeat protein
EDTA	Ethylenediaminetetraacetic acid
EGF	epidermal growth factor
ER	endoplasmic reticulum
ES	embryonic stem cell
FACS	Fluorescent activated cell sorting
FGF2	Fibroblast growth factor 2
FTD	Frontotemporal dementia
FTLD	frontotemporal lobar degeneration
FUS	Fused in sarcoma/Translocated in sarcoma
GA	glycine-alanine

GFAP	glial fibrillary acidic protein
GFP	green fluorescent protein
GP	glycine-proline
GR	glycine-arginine
gRNA	guide RNA
hnRNP	heterogeneous ribonucleoprotein particle
HRE	hexanucleotide repeat expansion
hiPSC	Human induced pluripotent stem cell
IGF-1	Insulin-like growth factor 2
ITS	Insulin-transferrin-sodium selenite
KLF4	Kruppel-like factor 4
LIF	Leukaemia inhibitory factor
MACS	Magnetic activated cell sorting
MAPT	Microtubule associated protein tau
MBP	Myelin baseic protein
MCT1	Monocarboxylate transporter 1
MND	motor neuron disease
MRI	magnetic resonance imaging
mRNA	messenger ribonucleic acid
MS	Multiple Sclerosis
NT-3	Neurotrophin-3
OCT4	octamer-binding transcription factor 4
OPC	oligodendrocyte precursor cell
OPTN	optineurin
PBS	Phosphate-buffered saline
PCR	polymerase chain reaction
PDGF	Platelet derived growth factor
PDGFR-α	Platelet derived growth factor receptor α
PGRN	progranulin
PLP1	Proteolipid protein 1
PMD	Pelizaeus-Merzbacher Disease
PPA	Primary progressive aphasia

PR	proline-arginine
qRT-PCR	quantitative reverse transcriptase PCR
RA	Retinoic acid
RAN	repeat-associated non-ATG
RNA-FISH	RNA fluorescent *in situ* hybridisation
RP-PCR	Repeat-primed PCR
SAG	Smoothened agonist
SNP	single nucleotide polymorphism
SSC	Saline sodium citrate
Shh	Sonic hedgehog
SOD1	superoxide dismutase 1
SOX2	sex-determining region-Y-box-2
SQSTM1	sequestosome 1
SRSF2	serine and arginine rich splicing factor 2
pTDP-43	phosphorylated 43kDa transactive response -DNA binding protein
T3	Triiodo-L-Thyronine
TALENs	transcription activator-like effector nucleases
TARDBP	transactive response-DNA binding protein
TBK1	TANK-binding kinase 1
TMEM106B	transmembrane protein 106B
UBQLN2	ubiquilin-2
UPR	Unfolded protein response
UTR	untranslated region
VCP	valosin containing protein
VWMD	Vanishing White Matter Disease
ZFN	zinc finger nuclease

Declaration

I declare that the thesis presented herein has been composed by me and this is my own work, unless otherwise stated. Where others have contributed to elements of this work, this is clearly stated in the text. I also declare that no element of this work has been submitted for any other degree or professional qualification.

Elaine Cleary

Acknowledgements

Firstly, I would like to thank my supervisors, Prof Siddharthan Chandran, Prof Mary Porteous and Dr Jon Warner, for their guidance and support throughout this project. Their varied scientific and clinical backgrounds have helped immensely towards broadening my way of thinking.

I would also like to thank Dr Dario Magnani for his help in supervising my day-to-day bench work and for reading my thesis at the end. I extend my thanks to all members of the Chandran lab and South East Scotland Genetics Service for all their help and support. From the Chandran lab, I must thank the technical staff: David Story, Dr Karen Burr, Nicola Miller, Karen Gladstone and Rinku Rajan, for all their help looking after the cells, without whom, this project would not have been feasible. They were also incredibly supportive and kept me going with many laughs along the way. For their help in teaching me new techniques, I thank Dr Bhuvaneish Selvaraj, Dr Navneet Vasistha, and Dr Chen Zhao. I would also like to acknowledge Dr Mandy Johnstone and Dr Shyamanga Borroah for their encouragement and chats that made out of hours working much more bearable! Megan Torvell, Dr Nina Rzechorzek and Dr Samantha Barton have been great friends and also kept me going through this process.

Within the South East Scotland Genetics Service, I would like to thank my office mates for keeping a smile on my face whilst writing up: Jenna Jenkinson, Michelle Sinclair and Tara Azam, who also helped hugely in the running of the *C9orf72* genetic testing service while I was away tending to cells!

All of my friends have been tremendously supportive over the past few years, but I'd like to mention Laura Wales, Dave Wales, Adam Jackson, Louise Keay and Sarah Nicol for being so understanding and encouraging along the way. And for helping keep some sort of balance in my life throughout my PhD, I must thank Lisa, Allan, Colin, Gillian and Karolina for their help.

And last, but in no way least, I must thank my family for their unrelenting support – my husband, Gavin Cleary for never letting me give up, my parents Fiona and David Evans and my sister Yvonne for always being there when I needed them.

Abstract

A hexanucleotide repeat expansion in the *C9orf72* gene is the most common cause of familial amyotrophic lateral sclerosis and frontotemporal dementia. Genetic testing for this pathogenic mutation is challenging due to its GC rich, repetitive nature. I developed PCR based assays to detect the presence of the pathogenic variant, which were used in screening an archival cohort of Scottish ALS patients, and have also been implemented within a diagnostic setting. These PCR assays allow amplification of larger repeat expansions than have previously been reported, and can determine whether a C9orf72 expansion of greater than 100 repeats is present or not. It is not well understood how the repeat expansion leads to disease, but several potential mechanisms have been hypothesised, including reduced expression, RNA toxicity and protein toxicity via dipeptide repeat proteins produced through repeat associated non-AUG translation. Motor neurons are an understandably well studied target in amyotrophic lateral sclerosis, however the role of glia, particularly oligodendrocytes, in the pathogenesis of the disease has recently been highlighted from studies on rodent models and post mortem tissue. To investigate the effect of the *C9orf72* repeat expansion on oligodendrocytes, we have applied a differentiation protocol to hiPSCs with the expansion and controls, including an isogenic control which has been generated in the lab. There was no difference in the production of neuronal and glial cell types between these cell lines. I went on to look for evidence of the main proposed pathological mechanisms of C9orf72 repeat expansions: loss of function or gain of function through either RNA or protein toxicity. hiPSC derived oligodendrocytes from both carrier and control showed low expression of C9orf72 mRNA, and there was no difference due to the presence of a repeat expansion. Carrier hiPSC derived oligodendrocytes displayed sense RNA foci, which did not appear to have an effect on cellular morphology. The detection of dipeptide repeat proteins proved challenging, and the results were inconclusive as to their presence in hiPSC derived oligodendrocytes. I went on to show there was no evidence of mislocalisation of TDP-43 in C9orf72 carrier oligodendrocytes. Finally, the study showed similar levels of cell death in basal conditions in carrier and control cells, and no clear difference in the response to endoplasmic reticulum stress. Further research will be required to elucidate the role of oligodendrocytes in C9orf72 related amyotrophic lateral sclerosis.

Lay summary

Motor neuron disease (MND) is a devastating disease where motor nerves in the brain and spinal cord stop working and eventually die. This means that messages from the brain can no longer reach the muscles, leading to weakness and wasting. The most common form of MND is called amyotrophic lateral sclerosis (ALS). In some cases of the disease, it is passed on through families. The most common reason for this is that there is a fault in a gene called C9orf72. This faulty gene has extra material in it, and this can be quite difficult to detect. I have developed genetic tests for detecting this gene fault that are quicker and more reliable than were available before.

The genetic tests which I have developed allow us to work out whether or not ALS is likely to be caused by a fault in the C9orf72 gene, which is important to help patient's families know if they might also be at risk of the disease. In the Scottish patients which were tested, about 1 in 10 cases of ALS which has been recorded in the last 20 years have been found to have this gene change.

Lots of research into the disease has focussed on the motor nerves, however recently it has become clear that some of the cells which support the nerves may not be working properly either. These cells, which are called oligodendrocytes, usually insulate the nerves. They also help to transfer energy to nerves. In people with motor neuron disease, these cells may not be as good at supporting the nerves as they should be.

It is difficult to investigate oligodendrocytes in patients as they are inaccessible. To get around this problem, we can take skin cells from a patient who has a genetic fault in C9orf72, and then generate stem cells. Stem cells are cells which are able to form any type of cell in the body. I took these stem cells, which still have the same genetic fault, and by feeding them specific chemicals over several months, encouraged them to form oligodendrocytes. By comparing these oligodendrocytes to ones which were made in the same way from healthy people, I tried to find any differences that might be due to the genetic fault. I found that both groups of cells formed oligodendrocytes in the same way.

There are a few ways that the C9orf72 gene fault could cause MND. It might be that there is less of the gene product made, or it might be that the product that is made is different from the normal product in a way that is detrimental to the cells. I wanted to see if any of these could be affecting oligodendrocytes. I found that there was the same amount of the gene product in oligodendrocytes even when the gene fault was there. The extra DNA present in the C9orf72

gene fault leads to ‘RNA foci’ being made, which might stick to important proteins in the cell and stop them working. The oligodendrocytes that were made from patients with the gene fault had this sticky RNA. Finally, the gene fault might cause abnormal proteins to build up in the cells. I looked at a number of different proteins which can lead to disease in this way, but they were either not seen in the oligodendrocytes or proved too difficult to detect. Finally, I looked to see if the levels of cell death were higher in the oligodendrocytes with the gene fault and found that they were similar to those without it. Further research is needed to see if oligodendrocytes are involved in motor nerve death in ALS.

Publications relating to this thesis

Devlin AC, Burr K, Borooah S, Foster JD, **Cleary EM**, Geti I, Vallier L, Shaw CE, Chandran S, Miles GB. Human iPSC-derived motoneurons harbouring TARDBP or C9ORF72 ALS mutations are dysfunctional despite maintaining viability. Nature Communications (2015) 6:5999. doi 10.1038/ncomms6999

Livesey MR, Magnani D, **Cleary EM**, Vasistha NA, James OT, Selvaraj BT, Burr K, Story D, Shaw CE, Kind PC, Hardingham GE, Wyllie DJ, Chandran S. Maturation and electrophysiological properties of human pluripotent stem cell-derived oligodendrocytes. Stem Cells (2016) 34(4):1040-53. doi: 10.1002/stem.2273

Cleary EM, Pal S, Azam T, Moore DJ, Swingler R, Gorrie G, Stephenson L, Colville S, Chandran S, Porteous M, Warner JP. Improved PCR based methods for detecting C9orf72 hexanucleotide repeat expansions. Molecular and Cellular Probes (2016) 30(4):218-24. doi:10.1016/j.mcp.2016.06.001

Black, HA, Leighton DJ, **Cleary EM**, Rose E, Stephenson L, Colville S, Ross D, Warner J, Porteous M, Gorrie GH, Swingler R, Goldstein D, Harms MB, Connick P, Pal S, Aitman TJ, Chandran S. Genetic epidemiology of motor neuron disease-associated variants in the Scottish population. Neurobiology of Aging (accepted December 2016). doi: 10.1016/j.neurobiolaging.2016.12.013.

Future publications (submitted)

Selvaraj BT, Livesey MR, Zhao C, James OT, **Cleary EM**, Perkins EM, Dando O, Lillico SG, Lee YB, Nishimura AL, Poreci U, Thankamony S, Pray M, Vasistha NA, Magnani D, Booroah S, Burr K, Story D, McCampbell A, Shaw CE, Kind PC, Whitelaw BA, Wilmut I, Hardingham GE, Wyllie DJA, Chandran S. C9ORF72 repeat-expansion causes vulnerability of motor neurons to Ca^{2+}-permeable AMPA receptor-mediated excitotoxicity. Under review in Nature Communications.

Henstridge CM, Sideris DI, Carroll E, Rotaris S, MacKenzie C, Smith C, von Armin CAF, Ludolph AC, Lulé D, Porteous M, Warner J, **Cleary EM**, Newton J, Colville S, Stephenson L, Swingler R, Chandran S, Leighton D, Gillingwater TH, Abrahams S, Spires-Jones TL. Synapse loss in the prefrontal cortex underlies cognitive decline in amyotrophic lateral sclerosis. Submitted to Nature Medicine (May 2017).

Chapter 1. General Introduction

1.1 MND and FTD

The first description of disorders with motor symptoms resembling motor neuron disease (MND) and with cognitive and behavioural symptoms resembling frontotemporal dementia (FTD) were noted in the late 19th century (Ferrari et al., 2011). In the 150 years since they were first reported, there has been increasing evidence that there is a clinical overlap between these two devastating neurodegenerative disorders, for which there is currently no effective treatment (Ferrari et al., 2011).

1.1.1 Clinical features of ALS

Amyotrophic lateral sclerosis (ALS) is the most common form of MND. It is an adult-onset neurodegenerative condition which affects the upper and lower motor neurons. In the majority of cases, it is a rapidly progressive disease which causes muscle weakness, then paralysis, and within three to five years, death through respiratory failure (Zoccolella et al., 2008). However, the phenotype is variable and a fifth of patients survive for longer than 5 years (McDermott and Shaw, 2008). The incidence of ALS is gender and age related, and affects 2.6 per 100 000 females and 3.9 per 100 000 males per year in the UK, with a peak incidence between 75-79 years (Alonso et al., 2009). The lifetime prevalence is around 1 in 350 for males and 1 in 472 for females in the UK (Alonso et al., 2009; Johnston et al., 2006). The underlying pathological mechanisms have been proposed to include neuroinflammation, glial activation, neuronal trafficking deficits, excitotoxicity, mitochondrial dysfunction and oxidative stress (Pasinelli and Brown, 2006). An alteration in protein homeostasis is also thought to play a role in pathogenesis, and in this respect targeting endoplasmic reticulum (ER) stress has emerged as a potential therapeutic target in ALS (Matus et al., 2013). There are currently no effective drug treatments available for ALS, aside from the glutamate release inhibitor Riluzole, which only has a slight impact on survival (Miller et al., 2012). The disease tends to begin in one area and then spreads through the motor system (Ravits, 2014).

Within the Scottish population, there are approximately 160 patients diagnosed with ALS each year, and at any one time, there are approximately 400 people living with the condition (Pal, personal communication).

1.1.2. Clinical features of FTD

FTD covers a heterogeneous range of neurodegenerative disorders which cause cognitive and behavioural impairments, as a result of frontotemporal lobar degeneration (FTLD) (Neary et al., 1998). FTD is one of the commonest causes of early onset dementia, affecting 3.5 per 100

000 people aged 45-64, per year, in a detailed study in Cambridgeshire (Mercy et al., 2008). The majority of FTD cases have onset in the fifth or sixth decade of life, and present with characteristic progressive behavioural changes, executive dysfunction and language difficulties, without major memory deficits (Perry and Miller, 2013). The disorder is broadly classified into the clinical variants of behavioural variant FTD and primary progressive aphasia (PPA). Early symptoms of behavioural variant FTD are changes in personality, disinhibition and apathy which can result in tactless and socially inappropriate behaviour and impulsiveness. There may also be loss of interest in people and activities, as well as a loss of empathy and responsiveness to the needs of others. Stereotyped behaviours, such as repetitive movements and compulsive ritualistic behaviours may also manifest. Patients tend to be unaware of their own condition and it is usually reported by a family member of caregiver. Patients with PPA show a progressive loss of language skills, which is shown by deficits in object naming, syntax, or understanding of words. Word-finding difficulties characterise semantic-variant PPA while non-fluent variant PPA leads to agrammatism and speech apraxia (Bang et al., 2015).

1.1.3 Links between ALS and FTD

Both genetic and neuropathological findings suggest that ALS and FTD are conditions which are at opposite ends of a disease spectrum, and many patients are found to suffer combined symptoms (Morris et al., 2012). Approximately 15% of ALS patients have concurrent FTD (Elamin et al., 2011; Lomen-Hoerth et al., 2002), and up to 50% have some evidence of cognitive or behavioural defects (Lomen-Hoerth et al., 2003). Conversely, up to 40% of patients with FTD have motor impairments, with approximately 12.5% developing motor neuron disease (Burrell et al., 2011; Lomen-Hoerth et al., 2002). Distinct populations of neurons are susceptible in ALS and FTD, and these clinical phenotypes correlate with the pattern of neuronal loss. Upper and lower motor neurons are affected in ALS while frontal and anterior or medial temporal neurons are lost in FTD (Neumann et al., 2006). Neuropathologically, ALS and FTD are classified based on the major protein aggregates which are detected. In ~60% of FTD and ~90% of ALS cases, phosphorylated 43kDa transactive response (TAR)-DNA binding protein (pTDP-43) inclusions are found in neurons and glia of the areas with most severe neurodegeneration (Mackenzie et al., 2007; Neumann et al., 2006).

1.1.4 Cellular autonomy versus non-cellular autonomy in neurodegeneration

Historically, research on neurodegenerative conditions such as ALS and FTD has focused on the principal cells, neurons, whose loss results in disease. The prevailing view was of cell

autonomous effects, where the neurons themselves were defective (Lobsiger and Cleveland, 2007). However, with increased understanding of the function of non-neuronal neighbouring cells, glial, it is becoming apparent that there is damage to multiple cell types, which converges to result in neuronal loss and a clinical phenotype. The main glial cell types in the central nervous system are astrocytes, microglia, and oligodendrocytes, and these cells are now thought to be implicated in the development and progression of ALS (Boillée et al., 2006; Di Giorgio et al., 2007; Philips et al., 2013). These interactions between different cell types are known as non-cell autonomous effects, and include cross-talk between neurons and glia, and between different types of glial cells (Meyer and Kaspar, 2016). It is therefore of interest to study various cell types in the context of ALS, both to investigate any cell autonomous effects, and then ultimately to elucidate how the cells interact to result in disease.

1.2 Genetics of ALS and FTD

It is estimated that around 5% of ALS patients have an affected first degree relative, which suggests that there is a genetic component to the disease risk (Byrne et al., 2011b). The discovery of pathogenic variants in superoxide dismutase 1 (SOD1) (Rosen et al., 1993), TARDBP (Kabashi et al., 2008; Sreedharan et al., 2008) and the noncoding (G_4C_2)n hexanucleotide repeat expansion (HRE) in chromosome 9 open reading frame 72 (*C9orf72*) (DeJesus-Hernandez et al., 2011; Renton et al., 2011), have been major advances towards understanding pathogenic mechanisms in ALS.

There are now over 25 genes that have been implicated in the disease, which is usually inherited in a dominant manner. However, the identification of pathogenic variants in sporadic cases of ALS has blurred the distinction between familial and sporadic disease (Boylan, 2015; Renton et al., 2014). Cases are generally classified as familial when there is a first-degree relative with ALS. They are 'probably' familial if a second degree relative has ALS, and possibly also if a first or second degree relative has been diagnosed with FTD (Byrne et al., 2011a). Cases with an underlying genetic cause could be classified erroneously as sporadic due to reduced penetrance, small family size, inaccurate diagnoses in family members, incomplete family history or death from other causes, prior to disease onset in genetically at risk family members (Byrne et al., 2011a). Currently, a genetic cause can be identified in 60-70% of familial ALS cases and ~10% of apparently sporadic cases as shown in Figure 1 (Renton et al., 2014).

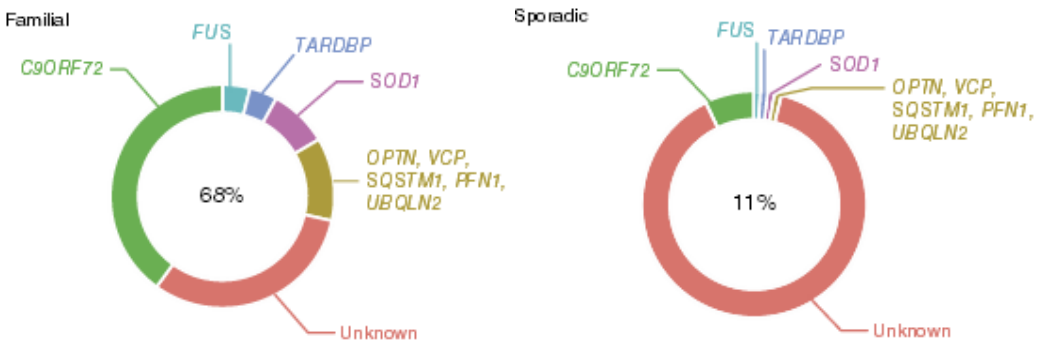

Figure 1.1 Proportion of familial and sporadic ALS cases attributed to mutations in different genes

68% of familial ALS cases of European ancestry, and 11% of sporadic cases, have pathogenic variants in one of the known genes listed above. Reproduced with permission (Renton et al., 2014).

Developments in high-throughput DNA sequencing of patients with ALS has increased the number of genes known to be associated with ALS, and although most of these genes are rare causes of the disease, investigating the functional characteristics of these and more common ALS genes, has elucidated some of the molecular pathways involved in ALS pathogenesis (Boylan, 2015). Pathogenic variants in the functionally related RNA-binding proteins encoded by *TARDBP* and Fused in sarcoma/Translocated in sarcoma (*FUS)* genes, have suggested that RNA-processing defects are implicated in ALS pathogenesis (Kwiatkowski et al., 2009; Vance et al., 2009).

Around 40% of patients who are diagnosed with FTD have a family history of dementia (Rosso et al., 2003), with 10% of cases showing a clear autosomal dominant inheritance pattern (Rohrer et al., 2009). Pathogenic variants in microtubule associated protein tau (*MAPT*) (Hutton et al., 1998) and progranulin (*PGRN*) have been identified in FTD patients (Baker et al., 2006), and together with *C9orf72* expansions, account for 60% of inherited cases (Le Ber, 2013). Most of the other genes which are implicated in FTD overlap with those that are associated with ALS, including *C9orf72* HRE, *TARDBP*, and valosin containing protein (*VCP*). This observation that genetic variants in the same genes can cause either ALS or FTD is further evidence that these disorders are part of a disease continuum (Ling et al., 2013). Cases of combined ALS-FTD are familial in ~30% of cases (Goldman et al., 2005). The *C9orf72* HRE is the commonest genetic cause of combined ALS-FTD, with rare cases also being caused by pathogenic variants in VCP, sequestosome-1 (*SQSTM1*), optineurin (*OPTN*) and ubiquilin-2 (*UBQLN2*) (Al-Chalabi and Hardiman, 2013; Hardy and Rogaeva, 2014). Furthermore, loss of function mutations in TANK-binding kinase 1 (*TBK1*) have also been

implicated in ALS and FTD, reinforcing a link between autophagy and ALS pathology (Freischmidt et al., 2015; Pottier et al., 2015).

It is clear that ALS and FTLD are genetically heterogeneous, and it may be the case that pathogenic variants in different genes cause the disease via diverse mechanisms (Valori et al., 2014). There have also been reports of oligogenic inheritance in ALS and FTD but the consequences of this to the clinical phenotype are not known (Lashley et al., 2014; van Blitterswijk et al., 2012).

The identification of pTDP-43 inclusions in affected neurons of ALS (Neumann et al., 2006) and the later identification of pathogenic variants in TDP-43, revealed a link between the genetics and pathology of the condition (Kabashi et al., 2008; Sreedharan et al., 2008). Other proteins also found to contain pathogenic mutations in ALS have since been identified in cellular inclusions, including SOD1, FUS and UBQLN2 (Deng et al., 2011; Deng et al., 2010; Shibata et al., 1996) reinforcing this link. It is important to note that these aggregates, particularly pTDP-43, are common to both familial and sporadic cases, which also have similar clinical features (Al-Chalabi et al., 2012). In FTD cases, there are often similar intracellular protein accumulations associated with the disorder and these can be categorized into molecular subtypes (Mackenzie et al., 2009). The most common neuronal inclusions in FTD cases are formed of ubiquitin, which is associated with pTDP-43 (Mackenzie et al., 2006; Neumann et al., 2006). In other cases, there are accumulations of hyperphosphorylated tau protein in neurons and glia, or FUS (Mackenzie et al., 2009; Munoz et al., 2009; Neumann et al., 2009).

1.3 C9orf72 HRE

A hexanucleotide $(G_4C_2)_n$ repeat expansion in a non-coding region of *C9orf72* has been identified as a significant cause of FTD, ALS and ALS-FTD (DeJesus-Hernandez et al., 2011; Renton et al., 2011).

1.3.1 Molecular Genetics

The *C9orf72* HRE was identified by studies of the risk locus at 9p21.2, which had previously been identified through both linkage studies in affected families and genome wide association studies for ALS and FTD (Laaksovirta et al., 2010; Luty et al., 2008; Morita et al., 2006; Shatunov et al., 2010; Valdmanis et al., 2007; Van Deerlin et al., 2010; van Es et al., 2009; Vance et al., 2006).

The *C9orf72* gene has 11 exons, with two alternatively spliced non-coding exons 1a and 1b. There are three major mRNA transcripts that encode two protein isoforms of 481 and 222 amino acids. The repeat expansion is in the upstream regulatory region in variant 1

(NM_018325.4) and in intron 1 of transcript variants 2 and 3 (NM_145005.6 and NM_001256054.2).

The G_4C_2 repeat number is normally between 2 and 25 in controls (median of 2 repeats) but is frequently expanded to greater than 1000 in disease cases (DeJesus-Hernandez et al., 2011; Renton et al., 2011).

The C9orf72 protein is found in both the nucleus and cytoplasm, and is thought to be similar in structure to the differentially expressed in normal and neoplasia (DENN) proteins, which have a guanine (GDP and GTP) nucleotide exchange factor (GEF) domain, and are thought to play a role in membrane trafficking and autophagy (Farg et al., 2014; Levine et al., 2013; Tang, 2016). There is evidence from both immunoprecipitation experiments and *in vitro* binding assays that C9orf72 binds with Rab1a, and the data suggests that C9orf72 acts as a Rab1a effector, and plays a role in the initiation of autophagy (Webster et al., 2016). It is also thought to play a role in promoting the clearance of protein aggregates via p62 (Ciura et al., 2016; Sellier et al., 2016) Autophagy is a cellular process whereby cytosolic components are transported to the lysosome for degradation. This process is critical in neurodegenerative diseases which are associated with diminished clearance of toxic protein or RNA inclusions (Jain and Ganesh, 2016).

1.3.2 *C9orf72* HRE related phenotypes

The HRE in the *C9orf72* gene is the commonest genetic variant found in Caucasian ALS cases. It accounts for ~6% of sporadic ALS and FTD cases, and 40% and 25% of familial ALS and FTD cases, respectively (Majounie et al., 2012). In addition, the HRE in *C9orf72* is associated with a clinically varied presentation and prognosis (Devenney et al., 2015). As well as ALS and FTD, there are a variety of clinical syndromes which have been associated with the HRE, including Huntington-like disease, Alzheimer's disease (AD) (Beck et al., 2013), ataxia (Lindquist et al., 2013) and some psychiatric diseases (Bieniek et al., 2014). It is unclear whether the expansion directly causes this wide spectrum of disease, or whether it indirectly affects susceptibility to neurodegeneration (Burrell et al., 2016).

1.3.3 *C9orf72* HRE genotype-phenotype correlations

The pathogenic size range of the expansion has not been well defined, and was originally hypothesised to be around 30 repeats (Renton et al., 2011), which is based partly on the size detected in controls, and partly on limitations in polymerase chain reaction (PCR) based detection, as the GC-rich nature and size of the repeat hampers PCR (Dobson-Stone et al., 2013). The largest UK study to date using Southern blotting showed that the 68 *C9orf72*

expansions detected in their extensive series (2974 cases with FTLD, ALS, AD, sporadic Creutzfeldt-Jakob disease, Huntington Disease-like syndrome) were approximately 800-4400 repeats in length (Beck et al., 2013). Further large scale studies will be needed to further delineate the pathogenic size range. There is one report in the literature of a patient who developed FTLD in his late fifties, who had ~65 repeats, but no family studies were carried out so it is not possible to conclusively say that the expansion was the cause of the disease in this case (Dobson-Stone et al., 2013). Short (45-78 repeats) expansions were detected in 5.6% of 72 *C9orf72* HRE positive index cases in another study, with co-segregation with disease observed in two families (Gijselinck et al., 2016). Conversely, there is also one report of a stable 70 repeat allele in an unaffected 89-year-old individual expanding in four of his offspring, but further studies are required to determine whether anticipation is commonly associated with this repeat expansion (Xi et al., 2015a). Analysis of families from the CEPH cohort suggests an overall intergenerational change rate of 0.29%, with all detected changes occurring in normal alleles which were greater than 10 repeats (Beck et al., 2013). There have been reports in three families of a decrease in age of onset between parents and offspring of between 16-25 years, suggesting that anticipation may be occurring, although the underlying molecular genetic basis of this is still unclear (Gijselinck et al., 2016).

The detection of *C9orf72* expansions in 11/7579 (0.15%) of 54-year old healthy controls, suggests that the mutation has incomplete penetrance since this frequency is higher than would be expected given the prevalence of ALS/FTD (Beck et al., 2013). Other studies have suggested that penetrance appears to be age-related, with approximately 50% penetrance at the age of 58 years and almost full penetrance by 80 years (Majounie et al., 2012). In an extensive UK study, large expansions were detected at a frequency of 1 in 600 in the control population tested (cohort of unaffected 54 year olds) (Beck et al., 2013). Recent evidence suggests that the average age of onset for ALS and FTD in *C9orf72* cases is 57.9 and 63.6 years. As this is higher than the age of the control population used in the study by Beck et al., it seems likely that the frequency of unaffected mutation carriers has been overestimated as they may go on to develop either ALS or FTD.

It is currently unclear whether there is a correlation between repeat length and age of onset, disease severity or speed of progression, because relatively few cases have been tested using Southern blotting, and the studies which have been done have given conflicting results (Fong et al., 2012). The Xpansize-72 study found no correlation between repeat length and age at onset or sample collection, except for FTD where there was an inverse correlation between age of onset and repeat length in frontal cortex (van Blitterswijk et al., 2013b). The largest

study in the United Kingdom to date has suggested there was no correlation between repeat size and clinical presentation, disease course or severity, but repeat size does correlate inversely with age of onset (Beck et al., 2013). This study has not shed light on the potential role of intermediate alleles (30-800 repeats) as none were detected (Beck et al., 2013). This was in contrast to another more recent study where 5.6% of *C9orf72* HRE index cases were found to have short (45-78 repeats) expansions (Gijselinck et al., 2016). Currently therefore, using Southern blotting in a diagnostic setting to generate information on repeat size does not provide any extra clinically useful information for patients.

DNA hypermethylation is a proposed disease modulator in *C9orf72* HRE carriers. Hypermethylation of nearby cytosine-phosphate-guanine (CpG) islands and the *C9orf72* repeat expansion itself have been observed (Xi et al., 2014; Xi et al., 2015b; Xi et al., 2013), and repressive histone trimethylation has also been noted in the region, and has been found to be associated with shorter disease duration in ALS (Belzil et al., 2013). However, in contrast, a study on *C9orf72* lymphoblasts and brain tissue suggested that hypermethylation was protective, as it resulted in reduced vulnerability to oxidative and autophagic stress (Liu et al., 2014). Hypermethylation resulted in reduced RNA foci and dipeptide repeat protein (DPR) production, as well as the expected reduction in expression levels (Liu et al., 2014). Methylation levels are reportedly similar in ALS and FTD, however *C9orf72* hypermethylation was associated with shorter repeat sizes, increased age at death and longer disease duration for FTD (Russ et al., 2015). More large scale studies are required to ascertain whether there are any correlations between age of onset and methylation with repeat size (Gijselinck et al., 2016).

1.3.2 Detection of the *C9orf72* HRE

Genetic testing in ALS and FTLD is important in contributing to a definitive diagnosis, can avoid prolonged and unnecessary investigations from being carried out and can allow a more accurate risk to the wider family to be determined. Pre-symptomatic patients with known ALS genetic variants may offer insight into early disease processes if appropriate research studies are performed, as has been demonstrated for Huntington's Disease (Tabrizi et al., 2009). Genetic test results will likely be increasingly used to stratify patients in clinical trials, particularly for gene-targeted therapy (Boylan, 2015). Such trials have already been carried out, albeit on a small scale, for therapies targeting SOD1 mediated disease (Miller et al., 2013b).

Molecular genetic testing for the G_4C_2 repeat expansion is challenging due to its highly GC rich, repetitive nature and frequent large size. A summary of the main techniques that are

currently used is shown in Figure 1.2. It is challenging to amplify large expansions by conventional flanking PCR assay, and for this reason, repeat primed (RP-) PCR is commonly used, as for other repeat expansion disorders (Warner et al., 1996). This technique allows detection of the presence or absence of a repeat expansion, but does not allow sizing of the expansion. The 30 repeat cut-off is frequently used in the literature to denote the pathogenic size range for *C9orf72* expansions, however this is likely to have arisen as a result of the limitations of RP-PCR in determining the expansion size. Southern blotting is often quoted as being the 'gold standard' method (Akimoto et al., 2014), however this is not without drawbacks. Aside from being a time-consuming and cumbersome technique, which requires a large amount of high quality DNA (minimum 1-3µg), interpretation of results can be complicated as the signal from heterogeneous sized repeat expansions are difficult to differentiate from background probe hybridisation (Buchman et al., 2013). This is particularly true when assessing expansions in DNA derived from whole blood samples, which show a smear rather than distinct bands (Hubers et al., 2014). Difficulties in assessing the exact size of the repeat lengths have been reported by others and this is thought to be due to extensive somatic heterogeneity (Beck et al., 2013; Nordin et al., 2015). It is also possible that due to the repetitive nature of the DNA fragments, that they adopt unusual structures which can result in abnormal migration during agarose gel electrophoresis, making inference of size and repeat number inaccurate (Mirkin, 2007). There are a number of Southern blotting protocols that have been developed, and each has differing advantages and disadvantages. One method is to enhance the signal by using a probe containing the $(G_4C_2)_n$ repeat rather than flanking sequence, however this may interfere with the detection of normal alleles (Beck et al., 2013; Hubers et al., 2014). It is desirable to ensure the size range of detection allows normal alleles to be visualised in addition to expansions, but this is difficult to achieve without loss of resolution in the sizing of large expansions (Hubers et al., 2014).

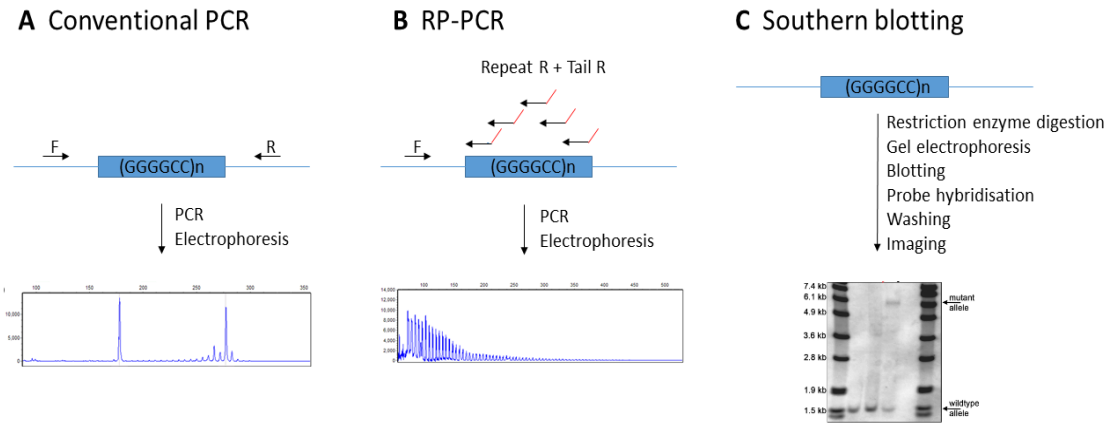

Figure 1.2 Summary of the main methods currently used in molecular genetic testing for *C9orf72* expansion repeats.

(a) Conventional PCR, where primers flanking the repeat are used to generate products which can then be accurately sized following capillary or agarose gel electrophoresis. (b) RP-PCR, where one flanking primer is used, alongside a primer specific for the repeat with a tail which has no homology to the human genome, and a primer for the tail. This produces products corresponding to each repeat unit, which can be detected following capillary electrophoresis, giving a ladder of fragments with a saw-tooth pattern. (c) Southern blotting, where DNA is digested with specific restriction enzymes which result in different sized fragments depending on the number of repeats present. These are separated by agarose gel electrophoresis before the products are transferred to a filter (blotting) and a probe to detect the expansion containing fragment is hybridised. After washing, the blot can be imaged or developed depending on whether chemiluminescent or radioactive techniques are used.

1.3.4 Pathogenic mechanisms of the *C9orf72* HRE

The pathology of *C9orf72* HRE cases shows pTDP-43 positive inclusions in anterior horn neurons, dentate gyrus and sometimes neocortex, but the more unusual feature is the presence of p62 positive, pTDP-43 negative inclusions in the pyramidal cells of the hippocampus and cerebellum (Al-Chalabi et al., 2012; Therrien et al., 2013). There are three proposed, non-mutually exclusive hypotheses surrounding the potential pathogenic mechanisms of the *C9orf72* hexanucleotide expansion (Figure 1.3):

A. Loss of function (haploinsufficiency)

B. Gain of function via RNA foci

C. Gain of function via C9RAN peptides (Ling et al., 2013).

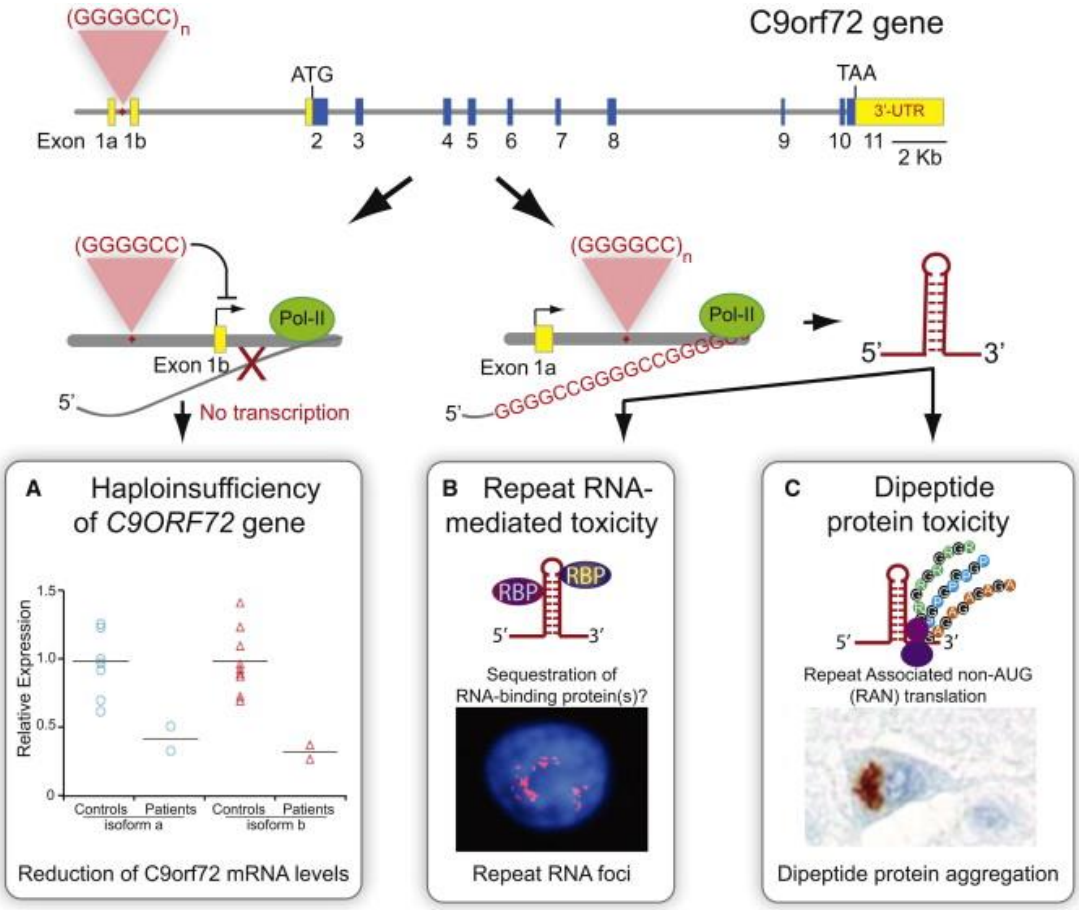

Figure 1.3 Schematic of main proposed pathological mechanisms for *C9orf72* HRE (Ling et al., 2013)

A schematic of the *C9orf72* gene, showing the intronic location of the (GGGGCC)n repeat expansion (yellow = UTRs; blue = exons). There are at least three non-mutually exclusive mechanisms by which a C9orf72 repeat expansion could mediate pathogenesis: (A) It could prevent or reduce transcription of the gene resulting in reduced expression of the protein (haploinsufficiency) (Gijselinck et al., 2012); (B) RNA foci containing repeat RNA could mediate toxicity via sequestration of RNA-binding proteins (DeJesus-Hernandez et al., 2011); (C) Dipeptide repeat proteins, generated via Repeat associated non-AUG (RAN) translation, may exert a toxic effect (Mori et al., 2013c). Image reproduced with permission.

There is a great deal of interest in determining whether one of these proposed pathogenic mechanisms is predominantly responsible for the resulting disease. It is hoped that understanding the disease mechanism may lead to targeted therapies from being developed (Gitler and Tsuiji, 2016). It may be that there is a complex interplay between each mechanism, and they are actually all responsible to some extent, for example RNA toxicity could make cells more susceptible to loss of C9orf72 (Sivadasan et al., 2016). How these proposed *C9orf72* HRE specific mechanisms lead to the resulting TDP-43 mislocalisation and p62

inclusion formation, is still an area of investigation, with defective nucleocytoplasmic transport being a prime candidate (Boeynaems et al., 2016; Freibaum et al., 2015; Jovicic et al., 2015).

1.3.4.1 Loss of function

When the *C9orf72* hexanucleotide repeat was first described, it was noted that the mutation affected *C9orf72* expression in a transcript specific manner by quantitative reverse transcriptase (qRT)-PCR (DeJesus-Hernandez et al., 2011). The transcripts vary in that the repeat expansion is found either in the promoter (NM_018325.4) or in the first intron (NM_145005.6 and NM_001256054.2) which may explain this transcript specific expression pattern (van Blitterswijk et al., 2015). These findings have been replicated in numerous studies of post-mortem tissue (Fratta et al., 2013; Gijselinck et al., 2012) and hiPSC derived neuronal cells from patients (Almeida et al., 2013; Donnelly et al., 2013), although this finding has not been consistent (Sareen et al., 2013). Determining the effect of the *C9orf72* expansion on protein expression levels initially proved challenging due to a lack of reliable commercial antibodies, and difficulties distinguishing the two protein isoforms, however studies have now shown that there is a reduction in protein levels of the longer C9orf72 isoform in expansion carriers (DeJesus-Hernandez et al., 2011; Waite et al., 2014; Xiao et al., 2015).

The development of specific antibodies to the two different C9orf72 protein isoforms has shown reduced levels of the long isoform in frontal and temporal cortex, and a redistribution of the short isoform from the nuclear membrane to the plasma membrane in motor neurons of *C9orf72* expansion cases (Xiao et al., 2015). This has also contributed to our understanding of the normal function of C9orf72 protein, which has been found to interact with Importin β1 and Ran-GTPase which form part of the nuclear pore complex, suggesting that C9orf72 is involved in nucleocytoplasmic transport (Xiao et al., 2015). Given that TDP-43 requires nuclear trafficking, it is possible that this provides a mechanistic link between C9orf72 loss of function and TDP-43 mislocalisation, which was found to correlate with loss of the short isoform of C9orf72, Importin β1 and Ran-GTPase from the nuclear membrane. Support for the role of loss of function in disease, comes from the observation that *C9orf72* HREs have been found to impede nucleocytoplasmic transport (Freibaum et al., 2015; Zhang et al., 2015).

There are several hypotheses which could explain how the HRE in *C9orf72* could influence expression levels, including that the complex secondary structures (G-quadruplexes and R-loops) which are formed by the repeat (Fratta et al., 2012; Reddy et al., 2013) result in abortive transcription (Haeusler et al., 2014). Hypermethylation of nearby CpG islands and the *C9orf72* repeat expansion itself is another proposed mechanism resulting in reduced expression in

expansion carriers (Xi et al., 2014; Xi et al., 2015b; Xi et al., 2013), and histone trimethylation, a repressive chromatin mark, has also been noted in the region (Belzil et al., 2013). One study showed that C9orf72 hypermethylation resulted in a faster disease progression, suggesting that hypermethylation was deleterious (Xi et al., 2013), however this has not been replicated and others have found that it may actually be a protective factor (Liu et al., 2014; Russ et al., 2015). A recent study found a correlation between methylation status and expansion length, with lower methylation levels being found in short expansion carriers (Gijselinck et al., 2016).

Evidence from human genetics suggests that *C9orf72* loss of expression is not likely to be the primary mechanism of pathogenesis, as a study on 389 ALS patients failed to detect any coding mutations in *C9orf72* (Harms et al., 2013). A further study on 276 Chinese patients with ALS revealed one patient with a novel splice site variant, (c.601-2A>G) which was associated with reduced mRNA levels, but there was no segregation studies performed (Liu et al., 2016). In addition, a patient who was found to be homozygous for *C9orf72* HRE, did not display a clinical phenotype outwith the normal range, which would not be expected if the disease was only mediated via loss of function (Fratta et al., 2013).

Animal models have been generated to try and elucidate the impact of *C9orf72* loss of function. In zebrafish, knockdown of the *C9orf72* orthologue led to motor neuron axonopathy and motor deficits, and the phenotype was reversed by introducing human *C9orf72* (Ciura et al., 2013). Similarly, homozyogous loss of the *C9orf72* orthologue in *C. elegans* results in motility defects and stress susceptibility (Therrien et al., 2013). These models suggest that haploinsufficiency may contribute to *C9orf72* pathogenesis, however in contrast these findings have not been consistent in mouse models (Koppers et al., 2015; Lagier-Tourenne et al., 2013). Reducing C9orf72 levels in mouse brain and spinal cord by injecting antisense oligonucleotides by stereotactic intracerebroventricular injection, did not result in behavioural or motor phenotypes, nor did it result in TDP-43 cytoplasmic mislocalisation (Lagier-Tourenne et al., 2013). Similarly, the generation of a conditional *C9orf72* knockout mouse using the Cre/loxP system, which inactivated *C9orf72* in neurons and glia from E10.5, did not result in motor neuron loss, reduced motor function or TDP-43 accumulation (Koppers et al., 2015). Interestingly, more recent studies which have generated homozygous mutant mice which constitutively lack C9orf72, have shown that this leads to splenomegaly, myeloid cell expansion, immune response deficits and impaired microglial function (Atanasio et al., 2016; O'Rourke et al., 2016). Thus, loss of function of C9orf72 in non-neuronal tissues could still influence the development of disease.

1.3.4.2 Gain of function via RNA foci

The nuclear and/or cytoplasmic accumulation of repeat expansion containing RNA has been reported in several conditions caused by noncoding repeat expansions such as type 1 myotonic dystrophy and fragile X tremor and ataxia syndrome (Todd and Paulson, 2010). The presence of $(G_4C_2)_n$ sense RNA foci in the cells of patients with G_4C_2 repeat expansions in *C9orf72* was reported when details of the mutation emerged (DeJesus-Hernandez et al., 2011). As seen in other noncoding repeat expansions (Todd and Paulson, 2010), (C_4G_2)n antisense RNA foci were also detected in neuronal and glial cells from post-mortem tissue of *C9orf72* HRE carriers (Mizielinska et al., 2013). Antisense foci were present in fewer cells than sense foci, but the average number of foci per cell was higher (Mizielinska et al., 2013). Either sense or antisense foci alone, or both types, have been detected in individual cells (Mizielinska et al., 2013). Having a higher percentage of neurons containing foci in frontal cortex has been correlated to a lower age of disease onset, suggesting that RNA foci are implicated in disease pathology (Mizielinska et al., 2013).

RNA foci have been reported in a wide variety of cell types including fibroblasts, hiPSCs, immortalized lymphoblasts, astrocytes and microglia from *C9orf72* expansion patients (Almeida et al., 2013; Donnelly et al., 2013; Lagier-Tourenne et al., 2013). The presence of sense RNA foci has been quantified in post-mortem tissue, which suggested that a higher proportion of neuronal cells contained foci (21-37%, depending on brain region) than astrocytes (~5%), oligodendrocytes (~10%) or microglia (~13%) (Mizielinska et al., 2013). This observation is consistent with higher C9orf72 expression levels in neurons than glia in mice (Suzuki et al., 2013). Most RNA foci are observed in the nucleus, although they are also detected in the cytoplasm, consistent with an intermediary role in DPR production (Mizielinska et al., 2013).

The mechanism by which RNA foci are proposed to cause disease relates mainly to the sequestration of essential RNA binding proteins (O'Rourke and Swanson, 2009), which could potentially affect the expression and downstream processing of hundreds of genes in a cell type dependent manner (Yokoyama et al., 2014). The identification of proteins which bind to *C9orf72* RNA foci is important in determining their contribution to pathogenesis (Mizielinska et al., 2013). Initial studies investigating the binding partners of sense and antisense RNA foci did not reach consensus on the most important binding partners. Using an RNA pulldown assay based on sense RNA foci on whole cell lysates from human neuronal cell lines and cerebellum tissue, followed by mass spectrometry, 103 proteins which bound to $(G_4C_2)_5$ were identified (Cooper-Knock et al., 2014). Several well-characterised targets were investigated

further to determine if there was co-localization in cerebellar granule neurons or motor neurons, which showed that there was some degree of overlap (19-30%) between sense RNA foci and heterogeneous ribonucleoprotein particle (hnRNP) A1, hnRNP H1/F, Aly/REF export factor (ALYREF) and serine and arginine rich splicing factor 2 (SRSF2) (Cooper-Knock et al., 2014). Several of the targets had been identified previously in association with sense RNA foci including hnRNP A1 (Sareen et al., 2013), hnRNP H1/F and SRSF2 (Lee et al., 2013). Further studies suggested that antisense RNA shared similar binding partners (Cooper-Knock et al., 2015; Haeusler et al., 2014). The multitude of proteins identified, and the low percentage of RNA foci displaying co-localization, suggests that a dynamic sequestration of multiple targets may be occurring, rather than an irreversible binding to a single factor (Cooper-Knock et al., 2014). Other proposed binding partners include RNA specific B2 adenosine deaminase (ADARB2) (Donnelly et al., 2013), nucleolin (Haeusler et al., 2014) and Pur-alpha (Xu et al., 2013).

Support for a role of RNA foci has come from studies which have used antisense oligonucleotides to reduce the abundance of sense RNA foci and reverse the toxicity in patient fibroblasts and hiPSC derived neurons (Donnelly et al., 2013; Lagier-Tourenne et al., 2013; Sareen et al., 2013). However, the link between RNA foci and DPRs is still poorly understood so it can be challenging to tease apart these two entities. The RNA pulldown described previously suggested that several mRNA export adaptors were associated with sense RNA foci, which could potentially be involved in the export of expanded *C9orf72* mRNA into the cytoplasm where they could be translated (Cooper-Knock et al., 2014). RNA foci have also been observed in the cytoplasm in fibroblasts from *C9orf72* HRE carriers (Donnelly et al., 2013; Lagier-Tourenne et al., 2013; Sareen et al., 2013). Studies using hiPSC derived neurons carrying *C9orf72* HREs, primary rodent neurons and *Drosophila* have shown that sense repeat RNA localizes in neurites where it associates with ribonucleoprotein transport granules and interferes with local translation, which is associated with neuritic branching defects (Schweizer Burguete et al., 2015).

Conversely, several studies using transgenic *Drosophila* which express *C9orf72* G_4C_2 repeat expansions have provided some evidence against RNA toxicity. Such flies show evidence of RNA foci and DPRs (Freibaum et al., 2015; Mizielinska et al., 2014; Tran et al., 2015). To then try and determine the contributions of RNA and DPRs, two fly lines were engineered with G_4C_2 repeats, one of which contained regular stop codons within it, which prevented the formation of DPRs (Mizielinska et al., 2014). Both fly lines expressed RNA foci, but only the pure repeat (without stop codons) led to toxicity and early death, suggesting that DPRs are

responsible for this effect (Mizielinska et al., 2014). Another group have generated an intronic G_4C_2 repeat containing *Drosophila* line, which does not display neurodegeneration (Tran et al., 2015). It is likely that this difference in phenotypes is due to the relative expression levels of the G_4C_2 repeats in each model, as the Mizielinska et al. flies express this as an mRNA with a 3'UTR, allowing export to the cytoplasm and efficient production of DPRs, which lead to neurodegeneration. Because the Tran et al. flies express the G_4C_2 repeat in the context of an intron, they show high levels of RNA foci in the nucleus, but low DPR levels, suggesting that the sense RNA in the nucleus is insufficient to lead to neuronal loss. Neither of these models investigate the contribution of antisense RNA, which should be investigated before RNA toxicity is excluded as a pathogenic mechanism in the fly model (Gitler and Tsuiji, 2016).

1.3.4.3 Gain of function via C9RAN peptides

The occurrence of repeat-associated non-ATG (RAN) translation (Zu et al., 2011) in *C9orf72* expansion cases results in the production of DPRs from both sense and antisense strands, in each possible reading frame (Ash et al., 2013; Gendron et al., 2013; Mori et al., 2013c; Zu et al., 2013). The DPR which are formed from the sense strand are polymers of glycine-alanine (GA), glycine-proline (GP) and glycine-arginine (GR), while glycine-proline (GP), alanine-proline (AP) and proline-arginine (PR) are translated from the antisense strand, as shown in Fig 1.4 (Gendron et al., 2013). Although poly-GP is produced from both sense and antisense strands, the carboxyl terminal tails will differ (Zu et al., 2013).

Figure 1.4 Potential dipeptide repeat proteins arising from RAN translation (Gendron et al., 2013).

Schematic showing the potential DPRs which could arise from RAN translation of expanded G_4C_2 (sense) and C_4G_2 (antisense) repeats in *C9orf72*. Note that poly-GP dipeptides can be formed in both directions.

All DPR proteins have been found in neuronal cytoplasmic inclusions in post-mortem *C9orf72* expansion cases (Ash et al., 2013; Gendron et al., 2013; Mori et al., 2013c; Zu et al., 2013),

where they appear to co-localise with p62, but not pTDP-43 inclusions (Mackenzie et al., 2013; Mori et al., 2013a; Mori et al., 2013c). A small number of patients with a *C9orf72* HRE, who died prematurely of causes unrelated to their presenting FTD, showed high levels of DPR in some pyramidal cells and interneurons in the cerebral cortex and hippocampus, but very little evidence of TDP-43 pathology which may suggest that DPR accumulation precedes TDP-43 mislocalisation (Baborie et al., 2015; Proudfoot et al., 2014). In a sample of 10 ALS cases, there was little evidence of DPR accumulation in the spinal cord or co-localisation with TDP-43, and DPR were rare in motor neurons (Gomez-Deza et al., 2015). Given that TDP-43 inclusions are present in *C9orf72*-related ALS cases, it is difficult to establish where DPR accumulation fits into the neurodegenerative process (Gomez-Deza et al., 2015). The most recent studies have used an extensive array of antibodies against each of the DPR species, and investigated their presence in a variety of different brain regions, including frontal lobes and spinal cord which are most prone to neurodegeneration, and other regions which are of less clinical relevance to ALS and FTD (Mackenzie, 2016). These have confirmed the previous suggestions that there is a lack of correlation between the presence of DPR and neurodegeneration or clinical features (Davidson et al., 2016; Mackenzie et al., 2015).

Much of the evidence suggesting that DPR are toxic have come from studies where DPRs have been expressed in cell lines or model organisms, therefore caution should be exercised when interpreting these results as the expression levels may differ significantly from those seen in patients with *C9orf72* repeat expansions. The expression of poly-GA, poly-GP and poly-GR, independent of $(G_4C_2)_n$ RNA in cultured cells, resulted in toxicity in cultured neuronal cells and in cortical neurons *in vivo* (Yamakawa et al., 2015). Numerous studies have found that the most abundant DPR inclusion protein in patients is poly-GA (Mackenzie et al., 2015; Mori et al., 2013c; Zhang et al., 2014b). Poly-GA expression in primary neurons led to impaired proteasome activity, endoplasmic reticulum stress and neurotoxicity, all in the absence of RNA foci (Zhang et al., 2014b). Poly-GA has also been found to sequester Unc119, which is thought to play a role in neurodegeneration (May et al., 2014). Poly-GA appears to form an amyloid like structure, and has properties which suggest that cell-to-cell transmission may be possible (Chang et al., 2016). A mouse model which produces poly-GA in the CNS shows neurodegeneration and behavioural problems which are similar to those seen in ALS and FTD (Zhang et al., 2016). In this study, poly-GA was found to form aggregates which can sequester HR23 and nuclear pore proteins, providing a link between poly-GA accumulation and deficiencies in the ubiquitin proteasome system (Yamakawa et al., 2015; Zhang et al., 2016).

Other studies have focussed on the arginine-rich DPRs poly-GR and poly-PR. Expression of these in *Drosophila* cause neurodegeneration, independent of RNA toxicity (Mizielinska et al., 2014). The arginine-rich DPRs were also found to bind nucleoli in cultured cells, impairing mRNA splicing and production of ribosomal RNA, leading to cell death (Kwon et al., 2014).

1.3.4.4 TDP-43 and p62 pathology

Loss of nuclear TDP-43 and cytoplasmic mislocalisation is characteristic of most types of ALS, including *C9orf72* expansion cases (Neumann et al., 2006). Although the neuropathology of *C9orf72* ALS cases are similar to non-*C9orf72* cases in terms of loss of anterior horn and cranial nerve nuclei motor neurons, and microglial activation, there are also some differences. ALS associated with *C9orf72* HREs also have large inclusions, with RNA foci and DPRs, which also contain ubiquitin and p62, rather than TDP-43 (Mackenzie et al., 2014). These are particularly found in extra-motor regions including the hippocampus and cerebellum (Cooper-Knock et al., 2012).

The link between *C9orf72* specific pathologies and TDP-43 mislocalisation is intriguing. Post-mortem studies have suggested that there is no difference in the proportion of sense RNA foci containing motor neurons with and without nuclear TDP-43 (Cooper-Knock et al., 2014). However, the occurrence of antisense RNA foci has been shown to be significantly associated with TDP-43 mislocalisation in motor neurons, as shown by co-labelling experiments (Cooper-Knock et al., 2015).

Recently, there has been an intense interest around deficiencies in nucleocytoplasmic transport related to *C9orf72* HREs (Boeynaems et al., 2016; Freibaum et al., 2015; Jovicic et al., 2015; Zhang et al., 2015). The trafficking of RNA and protein between the nucleus and cytoplasm is a highly regulated process (Burns and Wente, 2012). Disruption of normal nucleocytoplasmic transport could lead to the characteristic cytoplasmic accumulation of TDP-43 observed in ALS and FTD cases attributed to *C9orf72* HREs (Gitler and Tsuiji, 2016). Although several studies have now implicated nucleocytoplasmic transport impairment in pathology, using a range of different methods and model systems, there is no consensus on whether the root cause of this defect is related to toxic RNA or DPRs (Gitler and Tsuiji, 2016).

1.3.5 Disease modifiers

As the majority of ALS cases (95%) are not familial in nature, it seems clear that there are significant environmental factors which influence the disease (Al-Chalabi and Hardiman, 2013). Twin studies have been used to estimate the heritability of ALS and suggest that approximately 60% of the risk of ALS is genetic and the remaining 40% is due to

environmental influences (Al-Chalabi et al., 2010). Another study investigating concordance between parents and offspring has suggested a lower genetic risk of around 40% (Wingo et al., 2011).

The environmental influences are largely unknown for ALS, partly due to the infinite nature of possible influences and the difficulty in extracting meaningful information of exposures from patients over their lifetimes (Al-Chalabi and Hardiman, 2013; Burrell et al., 2016). Many environmental factors have been suggested to be linked with ALS, including smoking, physical exercise, and exposure to metals or pesticides (Al-Chalabi and Hardiman, 2013).

It may be the case that there are different environmental factors influencing disease in specific genetic backgrounds, and therefore studies should stratify for known genetic factors to enable detection of such interactions (Al-Chalabi and Hardiman, 2013).

For *C9orf72*, there are no specific environmental influences that have thus far been reported to influence disease presentation or progression. There have been several studies which have investigated the influence of other genetic factors on disease such as variants in transmembrane protein 106B (TMEM106B), intermediate repeats in ataxin-2 (ATXN2) and the presence of mutations in other known ALS-associated genes (Gallagher et al., 2014; van Blitterswijk et al., 2013a; van Blitterswijk et al., 2014a; van Blitterswijk et al., 2014b). The TMEM106B genotype does not appear to influence ALS, with risk alleles only affecting FTD presentation (van Blitterswijk et al., 2014b). There is some evidence that intermediate repeats (>23 repeats) in ATXN2 influence the propensity to develop ALS as compared to FTD in *C9orf72* HRE carriers (van Blitterswijk et al., 2014a), however this finding was not replicated in a larger study (Chiò et al., 2016). The influence of genomic instability around the HRE is another interesting area, with a 10 base pair deletion adjacent to the 3' end of the repeat being associated with a lower prevalence of psychosis (Snowden et al., 2016). It is not clear whether this is a direct effect or due to *cis*-acting factors that are linked to this specific variant, and further studies are required to confirm this finding in other populations (Snowden et al., 2016).

1.4 Studying ALS

The progressive loss of motor neurons is a defining feature of ALS. Animal and cellular models have been used to study the roles of ALS related genes and pathogenic mutations; however there is still limited knowledge of the specific molecular mechanisms leading to neurodegeneration (Qiang et al., 2013). There has been a shift in the focus of research on intrinsic motor neuron defects, to non-cell-autonomous effects, as it has become clear that ALS is a disease of the motor system rather than just motor neurons (Taylor et al., 2016; Valori

et al., 2014). Studies in mice where mutant SOD1 is expressed exclusively in motor neurons have given support to this concept, as early onset of disease does not occur (Yamanaka et al., 2008a). The reduction of mutant SOD1 in motor neurons, even before symptom onset, does not slow disease progression indicating non-cell-autonomous effects are at play (Boillée et al., 2006).

The main glial cells types in the CNS: astrocytes (Lobsiger and Cleveland, 2007), microglia (Boillée and Cleveland, 2008) and more recently oligodendrocytes (Kang et al., 2013; Lee et al., 2012; Philips et al., 2013; Rohan et al., 2014) have been investigated in the context of ALS. This has mainly been done both through post-mortem studies and *SOD1* mutant rodent studies where cell-type specific expression allowed the contribution of mutant glial cells to disease to be assessed (Lobsiger and Cleveland, 2007).

Astrocytes are an abundant cell type in the CNS, and play a significant role in homeostasis. They are involved in the ion buffering, neurotransmitter recycling and metabolic support to neurons (Sofroniew and Vinters, 2010). In the context of ALS the most intensely studied glial influence has been mutant *SOD1* astrocytes, which are thought to be toxic to motor neurons and drive disease progression (Ferraiuolo et al., 2011). The targeted reduction of mutant SOD1 expression in astrocytes in mouse models either delayed disease onset or slowed disease progression (Wang et al., 2011; Yamanaka et al., 2008b). Astrocytes generated directly from fibroblasts with a *C9orf72* HRE were found to be toxic to motor neurons in co-culture experiments (Meyer et al., 2014).

Microglia are macrophages which reside in the CNS, acting as immune defenders and destroying any cellular debris (Kreutzberg, 1996). They secrete cytokines and upon activation following an injury or pathological insult to neuronal tissue, will rapidly transform from their resting ramified state to a migratory ameboid morphology. Once activated, microglia tend to be anti-inflammatory and provide neuroprotection in the early stages of ALS, but later a self-propagating cycle of neuronal injury occurs as microglia release reactive oxygen species and pro-inflammatory cytokines in response to neurotoxic signals released from motor neurons (Appel et al., 2011). In a mouse model lacking murine C9orf72, abnormal microglia were observed, along with age-related neurodegeneration thus providing further evidence that microglial mediated inflammation plays a role in ALS (O'Rourke et al., 2016).

The role of oligodendrocytes in ALS, the subject of this thesis, will be discussed in detail in section 1.5.

1.4.1 Pathology studies and neuroimaging

Histopathological studies on post-mortem material analyse disease down to the cellular level, investigating single neurons and synapses in the areas sampled (Turner and Verstraete, 2015). In the majority of cases, analysis focuses on the end-stage of disease, and due to the nature of the sampling, the process of death may confound results (Turner and Verstraete, 2015). One pathology study included three *C9orf72* HRE carriers who died prematurely of non-FTD related disease, allowing some insight into earlier disease processes (Baborie et al., 2015). Histopathological studies allow investigations of cell loss (type, layer, quantification), the presence of specific protein inclusions and molecular characterization (Turner and Verstraete, 2015).

Neuroimaging, on the other hand, allows *in vivo* analysis on a whole-brain scale to be carried out, and typically reflects findings that have been revealed through post-mortem studies, whilst also allowing longitudinal studies in both pre-symptomatic and symptomatic individuals and analysis of network properties and efficiency (Turner and Verstraete, 2015). Clinically, magnetic resonance imaging (MRI) is mainly used to exclude the presence of structural changes which could account for symptoms (Filippi et al., 2010). MRI is increasingly being used in biomarker discovery, for example corticospinal tract hyperintensity has been identified as a feature in ALS patients (Goodin et al., 1988). Future studies aim to find new biomarkers which may be useful in monitoring patients during clinical trials (Grolez et al., 2016). Detailed imaging of living brains of *C9orf72* HRE carriers, particularly if DPR could be detected, could help establish the links between DPRs and pathology, since the model systems and post-mortem results appear disconnected (Gitler and Tsuiji, 2016). Such technology has allowed amyloid fibrils to be imaged *in vivo* using specific binding compounds and positron emission tomography, in Alzheimer disease (Mitsis et al., 2014).

1.4.2 Animal models of disease

There are several animal models for ALS and FTD, and the majority of studies have focused on rodent models of these diseases. As the first genetic cause of ALS identified, mutant SOD1 based models which recapitulate several aspects of the disease, have been extensively studied to aid understanding of the underlying pathogenesis (McGoldrick et al., 2013). It has proved more challenging to develop rodent models for TDP-43 based disease, as they do not result in an ALS-like phenotype and results are highly variable depending on transgene expression levels (McGoldrick et al., 2013).

The various models which have been generated to investigate the effects of loss of C9orf72 function have been discussed in section 1.3.4.1. These studies have shown that different results

are obtained when investigating different animal models, making it hard to draw conclusions regarding the contribution of C9orf72 haploinsufficiency to the disease phenotype.

For C9orf72, a murine model which expresses the 66 GGGGCC repeats throughout the central nervous system has been developed by adeno-associated virus mediated transgenesis, and shown to replicate both neuropathological and clinical aspects of human *C9orf72* mediated ALS/FTD (Chew et al., 2015). Other strains of transgenic mouse which have been generated from a bacterial artificial chromosome which contains part of the human *C9orf72* gene with an HRE of approximately 500 repeats, has shown the production of RNA foci and DPRs, but did not induce neurodegeneration (Peters et al., 2015). Similarly, another bacterial artificial chromosome (BAC) induced model with 100-1000 repeats had similar findings, while also reporting evidence of nucleolar stress (O'Rourke et al., 2016). The differences between these models are likely to be due to the expression levels of the repeat expansion, as the adeno-associated virus model expresses this under the control of the chicken β-actin promoter, and is thus produced at a higher level than in the BAC models, which are more physiologically relevant to the human disease (O'Rourke et al., 2016).

A major issue with transgenic animal models relates to the expression levels of the proposed pathological entities (McGoldrick et al., 2013). For example, poly-GR may well be toxic to cells if expressed at a high level, but unless it is actually expressed at a similar level in human cells, then this offers limited insight into the *in vivo* human pathogenic processes. A clear example where this has been demonstrated is in the poly-GA transgenic mouse model, which was found to have double the poly-GA levels found in a mouse model which expressed the $(G_4C_2)_{66}$ repeat (Zhang et al., 2016). Another important factor is that mouse models are inbred, which may affect the phenotype related to a pathogenic genetic variant compared to the more heterogeneous genetic backgrounds of humans (Saha and Jaenisch, 2009).

Although much can be learnt from animal models, it is clear from other diseases that findings do not always translate between species (Benatar, 2007). An example of a drug which failed to translate between a murine model of ALS and human clinical trials was creatine, which extended survival and conserved motor neuron function in mice but had no apparent benefit to ALS patients (Shefner et al., 2004). Partly, the lack of translation may be due to the majority of studies being carried out on SOD1 disease models which may not reflect the underlying pathology of the majority of ALS cases, or because drugs have been tested presymptomatically on rodents but are then administered to patients in the late stages of disease (McGoldrick et al., 2013) The toxicity profiles of drugs also differ between animals, meaning that drug screens

on animal models may not always reveal results which are appropriate to humans (Singh and Gupta, 1985).

1.4.3 hiPSC models of disease

Studying neurodegenerative disease is challenging, as access to living tissue is impractical, and post-mortem tissue is unlikely to represent early disease processes. Animal models of neurodegenerative disease provide insight, but have limitations in recapitulating human disease, and findings may not translate to human systems (Bradl and Lassmann, 2009). The advent of technology to reprogram somatic cells to generate human induced pluripotent stem cell (hiPSC) lines using ectopic expression of transcription factors octamer-binding transcription factor 4 (OCT4), sex-determining region-Y-box-2 (SOX2), Kruppel-like factor 4 (KLF4) and C-MYC (Takahashi et al., 2007), and the ability to direct their differentiation to specific cells of interest using morphogenic signals has offered a novel means to generate central nervous system cell types. hiPSC lines can be maintained and expanded in culture for many passages while retaining a capacity to generate all three embryonic germ layers like embryonic stem (ES) cells (Takahashi et al., 2007; Thomson et al., 1998).

hiPSC technology is particularly exciting in the context of neurodegenerative diseases, as patient derived cells with pathogenic genetic variants can be studied. Early studies using hiPSC technology have provided a 'proof of principle' by recreating phenotypes that have previously been noted in animal models, or human pathology studies (Sandoe and Eggan, 2013). The generation of enriched populations of particular cell types allow for cell autonomous effects to be studied, and reductionist model co-culture systems can allow assessment of non-cell autonomous effects between specific cell types (Qiang *et al.*, 2013). Such cells can also be used as a platform for drug screening where clear phenotypes are observed or may be used in cell-replacement therapies in the future (reviewed in Cundiff and Anderson, 2011).

1.4.3.1 Cellular reprogramming

There are a number of transcription factors, including OCT4, Nanog and Sox2, which are vital in ES cell maintenance, and give these cells their characteristic pluripotency and self-renewal properties. Expression of these transcription factors suppresses the expression of differentiation genes and promotes pluripotency gene expression (Loh et al., 2006). This led to speculation that forced expression of such genes in somatic cells could revert them to a pluripotent state, which was shown to be the case in mice by Takahashi and Yamanaka in 2006 (Takahashi and Yamanaka, 2006).

There are various methods which can be used to reprogram somatic cells by inducing the expression of defined sets of transcription factors within the cells, and these include transgene-based and transgene-free methods. Transgene-based methods involve the integration of genes encoding these transcription factors into the host genome, utilizing retroviral or lentiviral vectors (Brock et al., 2012). These methods are widely used but suffer from the risk of insertional mutagenesis, as the integration site is random and could inactivate a vital gene or otherwise disturb normal gene expression (Brock et al., 2012). Because of the limitations associated with a viral-mediated reprogramming methods, several other methods which are integration free, have now been developed. Non-integrating Sendai viruses and adenoviral vectors have been used to reprogram human somatic cells to hiPSCs (Fusaki et al., 2009; Zhou and Freed, 2009), whilst episomal approaches are becoming increasingly popular as they are cost-effective, transgene-free and viral-free (Yu et al., 2009). In the mouse, small molecules have been used in place of exogenous transcription factors (Hou et al., 2013), however this approach has not yet proved successful for generating hiPSCs.

Reprogramming is an inefficient process, and stochastic events during clonal selection can influence the transcriptional and epigenetic states of the cells (Lund et al., 2012b). Because many cell types can be formed during the reprogramming process, including transformed cells or intermediates (Chan et al., 2009; Mikkelsen et al., 2008), it is important that newly generated cell lines are checked for pluripotency, through both showing the expression of transcription factors such as Nanog and OCT4 and the ability to generate all three germ layers (Ellis et al., 2009). It is also important to check that resulting hiPSCs are free from chromosomal abnormalities, and as cells in culture for extended time periods may acquire abnormal karyotypes, this should be done regularly during their maintenance (Taapken et al., 2011).

1.4.3.2 Studying ALS using hiPSC based models

Using hiPSC derived cells is an attractive *in vitro* method to study cellular mechanisms underlying ALS as it allows human cells to be studies which are either from sporadic cases or familial cases which contain physiologically relevant expression of a mutated gene (Richard and Maragakis, 2015). Most of the early studies using this technique have focused on investigating motor neurons in culture, while later work has now extended to non-neuronal cells and the impact that these may be having on disease pathogenesis (Richard and Maragakis, 2015).

Human iPSC-derived neurons have been generated from patients with *C9orf72* HREs by several groups, who have shown that they display RNA foci, which is one of the key

pathological features associated with the repeat expansion (Almeida et al., 2013; Devlin et al., 2015; Donnelly et al., 2013; Sareen et al., 2013). Further characterisation of these hiPSC-derived neurons has suggested that (GGGGCC)n RNA foci could be sequestering several RNA binding proteins (such as ADARB2, hnRNPA1, hnRNPA1B2, Pur-α, FUS and TDP-43), and thus potentially disrupting their normal function (Donnelly et al., 2013; Sareen et al., 2013). These studies have been largely inconclusive, however, and the role of RNA foci in pathogenesis remains unclear. The presence of DPRs, particularly poly(GP), have been shown in hiPSC-derived neurons (Almeida et al., 2013; Donnelly et al., 2013).

RNA-sequencing of hiPSC derived neurons has suggested that *C9orf72* HREs are associated with misregulation of genes involved in cell adhesion, synaptic transmission and neural differentiation (Donnelly et al., 2013; Sareen et al., 2013). *C9orf72* HRE hiPSC-derived neurons show enhanced vulnerability to glutamate-mediated cytotoxicity (Donnelly et al., 2013) and the autophagy inhibitor chloroquine (Almeida et al., 2013).

C9orf72 HRE hiPSC-derived neurons also offer a means of screening potential therapeutics. Studies have shown that antisense oligonucleotides that specifically target the GGGGCC containing transcripts can reduce RNA foci and revert transcriptional changes and vulnerability to glutamate toxicity (Donnelly et al., 2013; Sareen et al., 2013). The use of hiPSCs in drug screening should offer more physiologically relevant results, in terms of both drug efficacy and toxicity, from drug screening compared to using animal models (Rubin, 2008).

Reprogramming skin fibroblasts from patients with a heterozygous SOD1 A4V variant to produce hiPSCs, and converting these to motor neurons revealed that these cells were more prone to apoptosis, had a smaller soma, and a reduced number of neuronal processes, which were also shorter, when compared to an isogenic control line in which the A4V variant had been corrected using zinc finger nuclease (ZFN)-mediated gene targeting (Kiskinis et al., 2014). Similar studies have been performed on hiPSC-derived neurons with pathogenic variants in TARDBP, which indicated that these cells showed an increase in TDP-43 protein in the insoluble fractions (Bilican et al., 2012; Egawa et al., 2012).

Most studies of ALS using hiPSC derived cellular models have focused on generating neuronal cells to investigate the influence of genetic variants on specific clinically relevant neuronal subtypes, however more recent studies have been carried out to investigate glial influences in neurodegenerative disease using this type of approach. Such cells can be used to investigate the roles of cell autonomous and non-cell autonomous factors for these variants in motor neuron dysfunction. Particular interest has been shown to the role of astrocytes in ALS derived

from hiPSCs carrying the pathogenic M337V variant have been co-cultured with control motor neurons and shown not to have a non-cell autonomous cytotoxic effect on these cells (Serio et al., 2013). This contrasts with studies using co-cultures with post-mortem derived astrocytes from sporadic cases and *SOD1* mutation carriers, which led to 45-70% reduced survival in motor neurons compared to controls (Haidet-Phillips et al., 2011).

1.4.3.3 Limitations of disease studies on hiPSC based cells

Like ES cell lines, which have been found to have variable differentiation efficiencies (Osafune et al., 2008), there have been similar concerns of differences between hiPSC lines (Hu et al., 2010). Not only are there differences in the differentiation capabilities of cell lines, but it is becoming increasingly clear that there are phenotypic differences between cell lines even with the same pathogenic mutation. For example there are differences reported in the electrophysiological properties of hiPSC-derived neurons with *C9orf72* HREs (Devlin et al., 2015; Sareen et al., 2013). Also, despite the same antibodies being used for detecting DPRs, these have not been consistently detected in all studies (Sareen et al., 2013).

One way in which the variability between hiPSC lines can be accounted for is to use large cohorts of both patient and control lines, such as was carried out by the Huntington's Disease hiPSC consortium who assessed 14 hiPSC lines (Consortium, 2012). This is a highly rigorous approach, particularly where there are multiple research groups who are performing phenotypic assessments, although it is still unclear how many lines may need to be studied to elucidate subtle phenotypes (Sandoe and Eggan, 2013), which may be even more difficult to detect when studying a genetic variant, such as the *C9orf72* HRE, which is so clinically variable. Clearly, although this approach is scientifically a sound approach, there are significant practical and cost implications which may limit the number of cell lines which can be assessed (Sandoe and Eggan, 2013).

It is thought that one of the major causes of variation between different hiPSC lines is the genetic background of the donor, which was shown in a study of the transcriptional profiles of 25 hiPSC lines which were derived from three donors and aimed to determine the relative variation caused by tissue source versus donor genetic background to the transcriptional profiles of the derived hiPSCs (Rouhani et al., 2014). One approach which has been used to limit this effect is to use family members of affected individuals as a source of control cell lines (Ebert et al., 2009), however such a strategy must take into account the genetic status of the individual and the likelihood of them being pre-symptomatic carriers, and is less appropriate for studies of sporadic disease (Sandoe and Eggan, 2013). More recently, the problems with genetic background have been overcome through the ability to generate

isogenic control lines where pathogenic variants are corrected using gene targeting technology such as ZFN, transcription activator-like effector nucleases (TALENs) or clustered regularly interspaced short palindromic repeat (CRISPR)/Cas9-mediated gene editing (Soldner et al., 2011).

A potential limitation of studies on hiPSC-derived neurons is that they represent cells which are at an earlier developmental stage compared to those that manifest disease *in vivo (Lee and* Huang, 2015*)*. The dynamics of pathogenesis are likely to be hugely different between a patient and *in vitro* cells differentiated from hiPSCs, particularly for neurodegenerative diseases which are associated with aging (Saha and Jaenisch, 2009). Various strategies have been utilised to artificially 'age' hiPSC derived cells, including the application of oxidative stress (Nguyen et al., 2011), expression of progerin (Miller et al., 2013a) and excessive glutamate induced stimulation (Koch et al., 2011). Recently, one study which looked at the gene expression profiles of a variety of cell types including hiPSCs, hiPSC-derived neurons and post-mortem tissues has suggested that hiPSC-derived neurons lose their aging signatures, which is in contrast with neurons generated via direct reprogramming from fibroblasts (iNeurons), which retain them (Mertens et al., 2015).

Some other limitations of hiPSC models are that the cells undergo significant epigenetic changes during reprogramming, and the prolonged culture times and cell selection *in vitro* might introduce variation within the system (Lee and Huang, 2015). During reprogramming, there is a reduction in cytosine methylation throughout the genome (Leitch et al., 2013). It is thought that there is some degree of epigenetic memory whereby the DNA methylation patterns in hiPSCs are related to those seen in their cell type of origin, which may affect their differentiation capacity (Kim et al., 2010). Also, abnormalities in X-chromosome inactivation may occur and could have an impact on cellular phenotypes (Mekhoubad et al., 2012). This makes it challenging to study diseases with significant epigenetic components using hiPSCs (Saha and Jaenisch, 2009). Given the observation that *C9orf72* HREs are associated with repressive epigenetic marks (Belzil et al., 2013), which could contribute to haploinsufficiency by reducing mRNA expression levels (Gendron et al., 2014), it is important to consider the effect of reprogramming on this locus. Recently, a study has shown that following reprogramming there was a reduction in DNA methylation at the *C9orf72* promoter of hiPSCs compared to the hypermethylated state detected in an immortalized lymphocyte cell line from which they were derived (Esanov et al., 2016). A time-course study then revealed that as hiPSCs were differentiated to neural precursor cells, the levels of cytosine methylation at the *C9orf72* promoter increased with differentiation which suggests that methylation patterns are

established during early neurodevelopment (Esanov et al., 2016). This study was limited to one patient, and another small study has revealed that two hiPSC lines with *C9orf72* HREs were hypermethylated compared to fibroblasts and ES cells (Cohen-Hadad et al., 2016). Thus further studies are required to determine what influences *C9orf72* methylation status during reprogramming and differentiation of hiPSCs.

Long term cell culture of pluripotent stem cells can lead to the accumulation of karyotypic abnormalities, particularly those which confer a growth advantage (Baker et al., 2007; Cowan et al., 2004; Draper et al., 2004), and the reprogramming process to generate hiPSCs is also associated with copy number variation (Hussein et al., 2011). There are a number of common abnormalities which have been found in large scale studies of hESCs and hiPSCs which involve partial or whole gains of chromosomes 12, 17, 20 or X (Baker et al., 2007; Spits et al., 2008; Taapken et al., 2011). It is therefore important that hiPSCs are checked for the presence of karyotypic abnormalities regularly, as these could alter the developmental properties and malignant potential of the cells (Lund et al., 2012a).

A final challenge in using hiPSC derived cells for disease modelling is that human diseases rarely affect a single cell type, and are usually mediated via complex interactions between different cell types which are difficult to recreate *in vitro*. Nevertheless, studies on ALS have shown that hiPSC derived cells can be used to help elucidate glial influences on neurons, for example, by setting up co-culture systems (Almad et al., 2016; Ferraiuolo et al., 2016; Serio et al., 2013). Furthermore, recent developments in three-dimensional culture systems, particularly in creating cerebral organoids from hiPSCs hold potential in creating enhanced three-dimensional model systems in which to study neurodegenerative disease, as has been shown for Alzheimer's Disease (Zhang et al., 2014a). For such late-onset diseases, *in vivo* approaches whereby chimeras are created from the grafting or transplantation of hiPSC derived cells into suitable model organisms, may be an informative approach for investigating disease processes (Saha and Jaenisch, 2009).

1.4.3.4 Generating isogenic controls using CRISPR/Cas9-mediated gene editing

The ability to generate isogenic cell lines is a significant breakthrough which overcomes the problems of background genetic variation between cell lines (Jaworska et al., 2016). Gene correction can be carried out using site-specific nucleases such as ZFNs, TALENs or CRISPR/Cas9 systems to generate double strand breaks in specific genomic locations, which are then repaired using non-homologous end joining, or homologous recombination where a repair template is included (Jaworska et al., 2016). This technology can be used to remove

disease associated repeat expansions from cells: for example, the CRISPR/Cas9 system has been used to remove the $(CGG)_n$ repeats from Fragile X syndrome hiPSCs as well as $(CAG)_n$ repeat expansions in Huntington Disease models (An et al., 2014; Park et al., 2015). CRISPR/Cas9 nucleases are generally preferred for use in hiPSCs compared to ZFNs and TALENs as they are easier to design and relatively low cost (Singh et al., 2015). CRISPR regions are transcribed to form pre-CRISR RNA (pre-crRNA) which are then processed to generate a target-specific crRNA. The locus also gives rise to trans-activating crRNA which aids in the processing of the pre-crRNA (Deltcheva et al., 2011). These RNA species form a complex with CRISPR-associated protein 9 (Cas9), and together they act as a DNA endonuclease (Gasiunas et al., 2012). This can cleave a 23 bp target DNA sequence which includes a 20 bp guide RNA within the crRNA, which can be modified to target regions of interest (Hsu et al., 2013; Jiang et al., 2013). Because the targeting relies on guide RNA in the CRISPR/Cas9 system, protein engineering is not required, and the specificity can be determined simply by cloning the appropriate DNA sequence into a vector which encodes crRNA (Kim and Kim, 2014).

1.5 Oligodendrocytes in ALS and FTD

1.5.1 Oligodendrocyte function

Oligodendrocytes are a type of glial cell which were first known for their role in generating myelin sheaths on CNS axons, which increase electrical resistance and decrease capacitance allowing fast action potential conduction (Simons and Nave, 2016). Oligodendrocytes extend many processes, which contacts and wraps around neuronal axons, and subsequently condense to form myelin (Bunge et al., 1962; Bunge, 1968). Myelin is required for establishing nodes of Ranvier, which allow fast saltatory conduction through neurons of small diameter (Bunge, 1968). More recently it has become clear that oligodendrocytes also have a key role in providing trophic support to neurons (Nave, 2010), mainly through the transfer of lactate via monocarboxylate transporter 1 (MCT1) (Funfschilling et al., 2012; Lee et al., 2012).

Disorders of myelin include multiple sclerosis (MS), Pelizaeus-Merzbacher disease (PMD) and Vanishing White Matter Disease (VWMD). All of these are devastating neurological conditions which highlight the importance of myelin (Clayton and Popko, 2016). In all of these disorders of CNS myelination, ER stress is thought to play a role, highlighting the susceptibility of oligodendrocytes to this type of stress (Clayton and Popko, 2016). This is presumably because myelin is rich in lipids and contain large amounts of proteins, the production of which places a strain on the cellular secretory systems (D'Antonio et al., 2009; Lin and Popko, 2009).

1.5.2 Oligodendrocytes in ALS/FTD

Recent studies have suggested that oligodendrocyte pathology may contribute to disease in ALS. In ALS, the presence of p62 and pTDP-43 intracytoplasmic inclusions has been detected in the oligodendrocytes of patients (Mackenzie et al., 2011; Neumann et al., 2006; Seilhean et al., 2009). As well as the presence of these inclusions, myelin abnormalities, demyelination and oligodendrocyte degeneration have all been observed in ventral spinal cord gray matter of ALS patients (Kang et al., 2013). The presence of pTDP-43 inclusions in oligodendrocytes has been confirmed by double-labelling immunofluorescence with antibodies for TDP-43 and the oligodendrocyte marker anti-tubulin polymerisation promoting protein (p25α) (Brettschneider et al., 2014; Fatima et al., 2015; Song et al., 2007). Neuroimaging on a small number of ALS cases suggested that there is no significant difference in the overall cerebral myelin content compared to controls, but revealed reduced myelin in the frontal lobes which correlated with reduced cognitive scores in these patients with ALS (Kolind et al., 2013). Another study comparing histology and post-mortem MRI has tried to elucidate the MRI metrics which correlate to myelin content and the myelin sheath deterioration which is seen in end-stage disease, and this could allow investigations into earlier myelin changes in future MRI studies on patients (Meadowcroft et al., 2015).

Alterations in myelin composition in a rat $SOD1^{G93A}$ ALS model have been reported, even in pre-symptomatic stages of the disease, although whether it was a secondary effect to axonal dysfunction was not established (Niebroj-Dobosz et al., 2007). Post-mortem spinal cord and motor cortex samples from ALS patients also showed reduced myelin, indicated by luxol blue staining, compared to unaffected controls (Kang et al., 2013). In the $SOD1^{G93A}$ mouse ALS model, morphological changes are seen in oligodendrocytes before symptom onset and increase with disease course, before the cells die (Philips et al., 2013). The overall number of oligodendrocytes appears constant despite their increased death, so there appears to be compensatory increases in oligodendrocyte precursor cell proliferation and differentiation (Kang et al., 2013; Philips et al., 2013). However, the resulting cells are dysfunctional in terms of myelination and trophic support which is displayed by reduced myelin basic protein (MBP) and monocarboxylate transporter (MCT1) expression respectively (Kang et al., 2013; Philips et al., 2013). The loss of MCT1 from oligodendrocytes has been found to contribute to neurodegeneration (Lee et al., 2012). Ablation of motor neurons by ricin injection was not sufficient to cause the oligodendrocyte changes observed in the $SOD1^{G93A}$ mouse, and selectively removing mutant SOD1 expression in oligodendrocytes delayed disease onset suggesting that oligodendrocytes may play a role early in disease (Kang et al., 2013).

A recent study using ribosome tagging in SOD1 ^{G37R} and SOD1 ^{G85R} mutant mice to selectively analyse gene expression in motor neurons, astrocytes and oligodendrocytes has suggested that at disease onset, there are fewer genes which are dysregulated in oligodendrocytes than motor neurons, and that the changes are of lower magnitude (Sun et al., 2015). This study did not detect a decrease in MCT1 mRNA at either disease onset or early symptomatic stages of the disease, but did find a decrease in production of the main myelin proteins including MBP (Sun et al., 2015). This argued against early changes in oligodendrocytes being drivers of disease development, instead suggesting that changes were secondary to alterations in motor neurons and the surrounding environment, although this study did not investigate mRNA expression in oligodendrocyte precursor cells (Sun et al., 2015).

Most studies on oligodendrocytes in ALS to date have focused on *SOD1* models of the disease, as well as post-mortem tissue from sporadic patients. Mechanisms of cell autonomous and cell non-autonomous effects may differ in sporadic disease, and disease associated with pathogenic variants in other genes. This has been highlighted in a recent publication which compares hiPSC derived oligodendrocytes from both sporadic ALS patients and those with pathogenic mutations in a variety of ALS-associated genes (Ferraiuolo et al., 2016). There has not been extensive investigation of oligodendrocyte dysfunction in FTD, with one small study suggesting that p62 inclusions were present in oligodendrocytes in an ALS/FTD patient but not in five FTD patients tested (Arai et al., 2003).

The involvement of ER stress in ALS pathogenesis has been shown in post-mortem studies, animal models and *in vitro* cellular studies (Matus et al., 2013). ER stress activates the unfolded protein response (UPR) which is a signal transduction pathway which enhances the protein folding capacity and quality controls within the ER to regain homeostasis (Walter and Ron, 2011). ER stress may be the result of the accumulation of misfolded or unfolded proteins, problems with lipid synthesis or a reduction in calcium stores (Walter and Ron, 2011). Given the previously mentioned susceptibility of oligodendrocytes to ER stress in myelination disorders (section 1.5.1), this is an area which is worthy of investigation in oligodendrocytes with ALS related mutations.

1.5.3 *In vivo* development of oligodendrocytes

Oligodendrocyte development *in vivo* has been well characterised in animal models, particularly rodents, and is clearly defined by morphological features and expression of specific markers over time (Pfeiffer et al., 1993). The brain and spinal cord are thought to contain different subclasses of early OPCs, which arise from different origins and are characterized by the expression of different transcription factors and cell-specific markers. In

human fetal forebrain, distinct OPCs form from the ganglionic eminence and the cortical subventricular zone (Jakovcevski and Zecevic, 2005a; Rakic and Zecevic, 2003). It is unclear whether the resulting oligodendrocytes from these different sources have variation in their roles, myelination capacity or function within the context of disease. In mice, oligodendrocytes from the spinal cord have been found to form longer myelin sheaths than those derived from the cortex, independent of neuronal influences (Bechler et al., 2015). As well as any intrinsic differences between oligodendrocytes from different regions, there are also differences in the cellular microenvironments that these cells find themselves in which may influence their myelination and remyelination capacities and predisposition to demyelination (Ornelas et al., 2016).

Spinal cord derived oligodendrocytes, which are of interest in ALS, develop from the ventral ventricular zone of the neural tube (Kang et al., 2013). Their early specification is closely related to the transcriptional control of rostral-caudal and dorsal-ventral patterning of the neural tube by the morphogenic gradients of Sonic Hedgehog (Shh) and bone morphogenic protein (BMP) (Emery and Lu, 2015; Richardson et al., 2000). The developing neural tube is patterned along the rostral-caudal axis, primarily mediated by a gradient of retinoic acid (RA) (Figure 1.5). High levels of RA are produced by the caudal paraxial mesoderm and form a boundary between spinal cord and hindbrain. After spinal cord formation, RA is released from the somites, refining positioning along the rostral-caudal axis (Davis-Dusenbery et al., 2014).

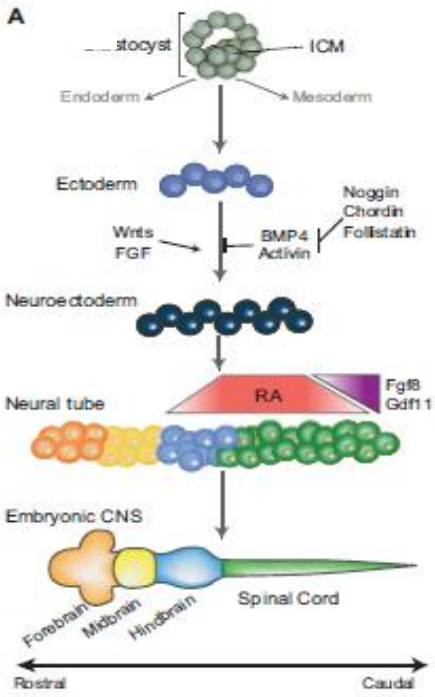

Figure 1.5 Caudalization of the neural tube by retinoic acid

Figure 1.5 Caudalization of the neural tube by retinoic acid

The inner cell mass (ICM) forms the three germ layers (ectoderm, mesoderm and endoderm) during gastrulation. The dorsal portion of ectoderm is specified to neuroectoderm early in development, by inhibition of active and BMP signalling and activation of Wnt and FGF signalling. The neural tube is then formed, and patterned along the rostral-caudal axis (anterior-posterior) by a RA gradient. The initial boundary between spinal cord and hindbrain versus forebrain and hindbrain is set by high RA levels. Upon spinal cord formation, the release of RA from somites refined the position along the rostral-caudal axis. The opposing factors, Fgf8 and DGF11 specify more caudal cell types. The spinal cord is also then patterned along the dorsal-ventral axis. Reproduced with permission. (Davis-Dusenbery et al., 2014).

Following caudalization, the anterior-posterior patterning is then determined by a gradient of Shh. Shh is secreted from the notochord and floor plate where a higher concentration leads to ventral patterning of the neural tube (Figure 1.6), while BMP and Wnt signalling from the roof plate lead to dorsal neural tube formation, and inhibit generation of the oligodendrocyte lineage (He and Lu, 2013). These morphogens result in the formation of 6 distinct progenitor domains along the dorsal-ventral axis: floor plate, p3, pMN, p2, p1 and p0. These domains all form specific cell types that express different homeodomain and basic helix-loop-helix transcription factors, which then act as downstream activators of Shh, and interact to generate the boundary between adjacent domains (Briscoe et al., 2000). OPCs mainly arise from the ventral pMN domain, following the production of motor neurons from a pool of precursors which are characterised by expression of Oligodendrocyte lineage transcription factor 2 (Olig2), as shown in Figure 1.6 (Jacob and Briscoe, 2003; Richardson et al., 2000). Using a mouse model with an Shh-green fluorescent protein (GFP) fusion, it has been shown that the Shh expression exponentially decays along the dorsal-ventral axis, with maximal expression at p3, dropping at pMN, and is undetectable at p2 (Chamberlain et al., 2008), thus ventral cells are exposed to higher Shh concentration and for a longer time period than dorsal cells.

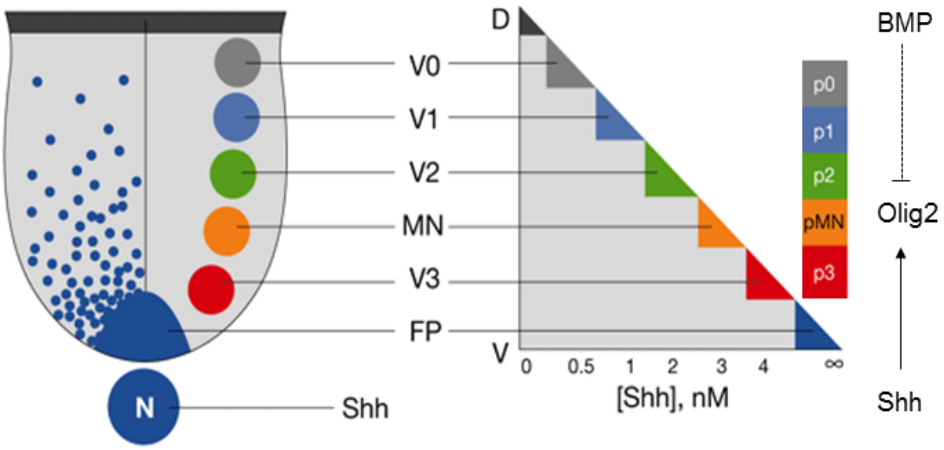

Figure 1.6 Signaling regulation of OPC specification and development

Figure 1.6 Signaling regulation of OPC specification and development

Ventral Shh from the notochord promotes OPC production in the pMN domain of the developing neural tube by promoting Olig2 expression, and competes against dorsal BMP signalling. Adapted, (Jacob and Briscoe, 2003). Reproduced with permission, copyright of Cold Spring Harbor Laboratory Press (Emery and Lu, 2015).

Olig2 is a transcription factor which promotes motor neuron fate initially through binding to neurogenin-1 and neurogenin-2 (Zhou et al., 2001), and then after undergoing dephosphorylation at Ser147, switches to promote oligodendrocyte fate via preferential binding to different partner transcription factors (Li et al., 2011). OPCs arise from cells which co-express Olig2 and Nkx2.2, and the latter is thought to inhibit expression of neurogenins, providing for the neurogenic-gliogenic switch which is required for OPC production (Li et al., 2011; Ribes and Briscoe, 2009). Olig2 is thought to be essential for early ventral OPC generation which produces 85-90% of the final oligodendrocyte population and is a consistent marker for the oligodendrocyte lineage, (Bradl and Lassmann, 2010; Emery and Lu, 2015; Fogarty et al., 2005; Vallstedt et al., 2005). The remaining 10% of OPCs arise more dorsally, later in rodent development, and these do not initially express Olig2 (Cai et al., 2005; Vallstedt et al., 2005), suggesting that there is compensation by other factors such as Olig1, and that Olig2 is not essential for specifying the oligodendrocyte lineage (Zhou and Anderson, 2002). Mice which are homozygously deleted for Olig2 fail to develop motor neurons or oligodendrocytes within their spinal cords, and die at birth (Takebayashi et al., 2002).

Various transcription factors are expressed in OPCs as they migrate from where they are generated to throughout the central nervous system. Olig2 expression continues, and appears to promote expression of Sox10 and Nkx2.2 (Liu et al., 2007; Zhou et al., 2001). Sox9 and Sox10 promote the expression of PDGFR-α (Finzsch et al., 2008), which promotes survival and proliferation of OPCs via the binding of its ligand platelet-derived growth factor (PDGF) (Barres et al., 1993; Calver et al., 1998).

For differentiation of oligodendrocytes to occur, OPCs must exit the cell cycle and this process must be highly regulated to control the timing of myelination and to ensure there is a pool of OPCs remaining (Emery and Lu, 2015). The Notch, BMP and Wnt signalling pathways inhibit OPC production and differentiation during development, and there are prodifferentiation factors which act to antagonize these inhibitory effects allowing differentiation to occur (Emery and Lu, 2015). These include Olig2 in combination with Brg1 (Yu et al., 2013), and the downstream target zinc finger homeobox transcription factor Zfhx1b which antagonizes

signals via BMP, Notch and Wnt signalling pathways allowing differentiation to occur (Weng et al., 2012).

OPCs can be characterised by the expression of platelet-derived growth factor receptor α (PDGFR-α) (Pringle et al., 1992) and have either bipolar morphology, or a few short branches (Jakovcevski and Zecevic, 2005b) as shown in Figure 1.7. In humans, OPCs are first detected at 10 gestational weeks (gw) (Jakovcevski et al., 2009). These cells then continue proliferating from 10-15 gw, before migrating dorsally from the cortical ventricular zone and subventricular zone (Jakovcevski et al., 2009). Development progresses from late OPCs to immature oligodendrocytes, characterised by expression of the O4 sulfatide (Jakovcevski and Zecevic, 2005b; Schachner et al., 1981) to pre-myelinating oligodendrocytes, with mature myelin basic protein (MBP) expressing, highly branched cells first appearing at 18gw and then increasing in number with time (Jakovcevski et al., 2009), as shown in Figure 1.7. Postnatally, oligodendrocytes are found throughout the central nervous system, and are most abundant in white matter tracts (Rowitch, 2004). Following terminal differentiation, postmitotic oligodendrocytes undergo morphology changes, extending elaborate processes which then contact axons. Subsequently, most of these processes are withdrawn and the axons are ensheathed and nodes of Ranvier form (Emery and Lu, 2015). Myelination begins in the final trimester and continues over several decades (Back et al., 2001; Jakovcevski et al., 2007).

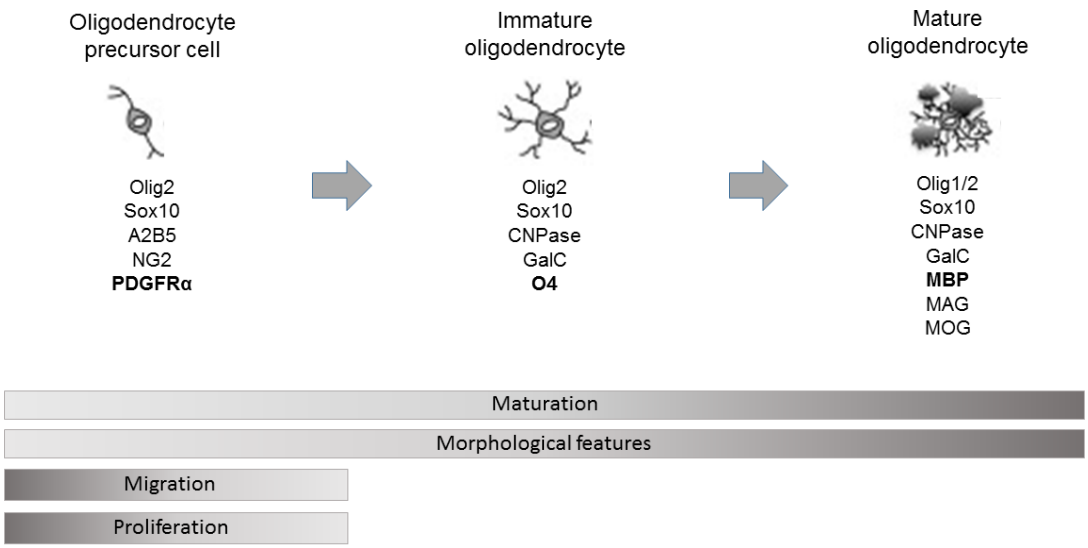

Figure 1.7 Oligodendrocyte differentiation and maturation: markers and morphology

At least three stages of oligodendrocyte maturation can be defined: oligodendrocyte progenitor cells, immature oligodendrocytes and mature oligodendrocytes. Stages are

identifiable by increasingly complex morphology with time, and the expression pattern of different transcription factors and cell surface markers. Oligodendrocyte precursor cells can also be defined by their ability to proliferate and migrate. CNPase, 2′,3′-cyclic nucleotide 3′-phosphodiesterase; GalC, galactocerebroside C; MAG, myelin associated glycoprotein; MOG, myelin oligodendrocyte glycoprotein. Markers in bold are used in this study. Adapted (Barateiro and Fernandes, 2014).

1.5.4 Generating hiPSC derived oligodendrocytes

The ability to generate differentiated cells from patient derived hiPSCs allows the study of cell autonomous factors in disease. For neurodegenerative diseases such as amyotrophic lateral sclerosis, hiPSC technology is particularly useful as brain and neuronal tissue from patients are inaccessible during early and intermediate stages of disease. To generate oligodendrocytes from hiPSCs, knowledge of their *in vivo* development can be used to attempt to recapitulate this *in vitro*.

Protocols to derive OPCs and oligodendrocytes were first developed for murine systems, and these have been used to guide development of human based protocols, taking into account key differences in the signalling pathways involved in NPC patterning between mouse and human (Li et al., 2009). There are several published protocols for deriving OPCs and oligodendrocytes from human ES cells, all of which are time-consuming and take months rather than weeks as is the case in mouse (Hu et al., 2009a; Izrael et al., 2007; Kang et al., 2007; Nistor et al., 2005; Stacpoole et al., 2013). Initial attempts to apply protocols optimised on ES cells to hiPSCs were very low yielding with less than 0.01% of cells being O4 positive (Ogawa et al., 2011), and few cells displaying MBP (Pouya et al., 2011). Most early studies focused on generating OPCs from hiPSCs for transplantation studies (Wang et al., 2013), whereas for studying disease phenotypes, the study of more differentiated cells would also be desirable. The majority of oligodendrocyte protocols published prior to the beginning of this study had only been optimised on hESC lines, and their applicability to hiPSCs was controversial (Alsanie et al., 2013).

To show that hESC and hiPSC derived oligodendrocytes are functional, an assessment of their myelination capacity is required. Other groups have shown that transplantation of hiPSC derived OPCs can myelinate and rescue early lethality in the congenitally hypomethylated shiverer mouse model (Douvaras et al., 2014; Wang et al., 2013). Other less costly and time consuming methods to assess myelination have been developed in the form of *in vitro* myelinating co-culture systems, including dissociated CNS cultures and *ex vivo* slice cultures (Jarjour et al., 2012). Although mouse ESC derived oligodendrocytes have been shown to myelinate using such techniques, such techniques have not yet been widely applied to human

iPSC derived oligodendrocytes (Kerman et al., 2015). There has been a report of hiPSC derived oligodendrocytes myelinating rat dorsal root ganglion neurons in an *in vitro* system (Thiruvalluvan et al., 2016). Recently, an *in vitro* human co-culture system between wild type Hb9-GFP+ motor neurons and hiPSC derived oligodendrocytes has been described (Ferraiuolo et al., 2016), and although this system did not permit myelination, this represents a step towards the goal of generating human systems to understand human disease.

Finally, although studying hiPSC oligodendrocytes *in vitro* may allow us to identify cell autonomous effects within these cells, ultimately to understand how oligodendrocytes contribute to pathogenesis in diseases such as ALS requires investigation of their effect on neurons. Transplantation studies of hiPSC derived oligodendrocytes *in vivo* could allow their effects to be assessed at a cellular and organism level (Douvaras et al., 2014). Other approaches to understand oligodendrocyte-neuron interactions are *in vitro* techniques: the application of oligodendrocyte conditioned media to motor neurons to assess the effect of any soluble factors released from oligodendrocytes, or setting up co-culture experiments with neurons to assess cell contact mediated effects. Such experiments have recently been carried out for a hiPSC derived oligodendrocytes with a variety of ALS causing mutations, and have shown that they contribute to motor neuron death *in vitro* via both soluble factors, and cell-contact mediated effects (Ferraiuolo et al., 2016).

1.6 Scope of study

A major aim of this study was to investigate the effect of the *C9orf72* HRE on oligodendrocytes, as it is currently unknown to what extent oligodendrocytes contribute to disease in cases of ALS caused by mutations in *C9orf72*. In order to investigate this, I have applied a differentiation protocol to generate oligodendrocytes from hiPSCs derived from controls and patients with *C9orf72* HREs. To reduce genetic variability between the lines, we generated an isogenic control by taking one hiPSC line which carried a *C9orf72* HRE and specifically deleting the repeat expansion using CRISPR/Cas9- mediated gene editing.

To investigate the influence of *C9orf72* HRE on hiPSC derived oligodendrocytes, the differentiation potential of the cell lines was first compared to investigate whether the mutation led to differences in the generation of oligodendrocytes and other cell types.

I then went on to assess whether there was evidence for any of the main proposed pathological mechanisms involved in *C9orf72* expansion cases, by measuring C9orf72 mRNA expression, RNA foci formation and investigating whether DPR were present. I also examined whether there was any TDP-43 mislocalisation or p62 inclusions. I also investigated whether there were

any differences in oligodendrocyte cell morphology in the presence of *C9orf72* HRE, including whether RNA foci influenced this. Finally, I investigated whether there was an increased vulnerability to ER stress in *C9orf72* HRE containing hiPSC derived oligodendrocytes.

As part of this thesis, I developed PCR based strategies for detection of the *C9orf72* HRE, which proved challenging and became a substantial undertaking. I used these assays not only for validating the presence of the expansion in the cell lines and in screening for HRE corrected isogenic cell lines, but also to screen a historical cohort of 450 Scottish ALS patients. I have also introduced this test into the National Health Service diagnostic service, where it is directly used for diagnostic and predictive testing for patients.

Chapter 2. Materials and Methods

2.1 Cell culture reagents

2.1.1 Media and supplements

Essential 8™ Complete: Essential 8™ Basal Medium (Life Technologies, A1516901)

Essential 8™ Supplement (Life Technologies, A1517101) 1:50

Chemically Defined Medium (CDM): 1:1 Iscove's Modified Dulbecco's Medium (Life Technologies, 21980-32): F-12 (Life Technologies, 31765-027)

Bovine Serum Albumin (Europa Bioproducts, EQBAC62) 5%

Chemically Defined Lipid (Life Technologies, 11905-031) 1:100

Monothioglycerol (Sigma, M6145) 1:25

Insulin (Roche 1376497) 7mg/ml

Transferrin (Roche 652202) 15mg/ml

Penicillin-Streptomycin (Life Technologies, 15070-63)

Phase I: CDM

N-acetyl cysteine (Sigma, A8199) 1mM

SB431542 (R&D Systems, 1614/1) 10µM

LDN193189 (Stratech, S2618) 100nM

Phase II: CDM

N-acetyl cysteine (Sigma, A8199) 1mM

Fibroblast growth factor 2 (FGF2) (Peprotech, 450-33) 5ng/ml

Heparin (Sigma, H3149) 5 ng/ml

	RA (Sigma, R2625) 0.1 µM
Phase III:	Adv DMEM/F12 (Life Technologies, 12634-010)
	Antibiotic-antimycotic (Gibco, 15240-062) 1:100
	B-27® (Life Technologies, 17504-044) 1:100
	N-2 (Life Technologies, 17502-048) 1:200
	Glutamax™ (Life Technologies, 35050-038) 1:200
	FGF2 (Peprotech, 450-33) 5ng/ml
	Heparin (Sigma, H3149) 5ng/ml
	Purmorphamine (Merck Millipore, 540220) 1µM
	RA (Sigma, R2625) 1µM
Phase III-FGF	As Phase III minus FGF2 and heparin
Oligo Base:	Adv DMEM/F12 (Life Technologies, 12634-010)
	Antibiotic-antimycotic (Gibco, 15240-062) 1:100
	B-27® (Life Technologies, 17504-044) 1:100
	N2 (Life Technologies, 17502-048) 1:100
	Glutamax™ (Life Technologies, 35050-038) 1:100
	Heparin (Sigma, H3149) 5µg/ml
Oligo Pro:	Oligo base
	Insulin-like growth factor (IGF-1) (Peprotech, 100-11) 10ng/ml
	FGF2 (Peprotech, 450-33) 20ng/ml
	Purmorphamine (Merck Millipore, 540220) 1µM

PDGF-AA (Peprotech, 100-13A) 20ng/ml

Smoothened agonist (SAG) (Merck Millipore, 566660) 1µM

Triiodo-L-Thryonine (T3) (Sigma, T6397) 60ng/ml

Oligo Diff: Oligo base

Insulin-transferrin-sodium selenite (ITS) (Life Technologies, 41400-045) 1:100

T3 (Sigma, T6397) 60ng/ml

IGF-1 (Peprotech, 100-11) 10ng/ml

2.1.2 Cytokines Growth Factors and Inhibitors

N-acetyl cysteine (Sigma, A8199), 500mM in DPBS

SB431542 (R&D Systems, 1614/1) 10mM in DMSO

LDN193189 (Sigma, S2618) 100µM in DMSO

FGF2 (Peprotech, 450-33) 20µg/ml in 0.1% BSA in DPBS

RA (Sigma, R2625) 1mM in ethanol

Purmorphamine (Merck Millipore, 540220) 1mM in DMSO

Heparin (Sigma, H3149) 5mg/ml in Advanced DMEMF12

IGF-1 (Peprotech, 100-11) 20µg/ml in 0.1% BSA in DPBS

PDGF-AA (Peprotech, 100-13A) 20µg/ml in 0.1% BSA in DPBS

SAG (Merck Millipore, 566660) 1mM in H_2O for embryo transfer

T3 (Sigma, T6397) 20µg/ml in Advanced DMEM/F12

2.1.3 Other Tissue Culture Reagents

GFR BD Matrigel™ basement membrane matrix (SLS, 354230) 1:2

Matrigel™ was thawed at 4°C for 1-2 hours and diluted in cold Advanced DMEM/F12 using chilled stripettes and tips. Stored at -20°C.

Laminin (Sigma, L2020-1MG) 1:100

Laminin (1mg/ml) was thawed at 4°C briefly before resuspending 1:100 in cold Advanced DMEM/F12. Stored at -20°C.

Fibronectin (Sigma, F2006-2MG)

1mg/ml in PBS pH 7.4

hiPSC freezing mix: Complete Essential 8™ Media + DMSO (1:10)

Poly-L-ornithine (Sigma, P3655) 100µg/ml in H_2O

Trypsin (Life Technologies, 25200-056)

Dispase (Life Technologies, 17105-041)

Collagenase Type IV (Life Technologies, 17104-014)

Accutase (Sigma, A6964)

Papain Dissociation System (Worthington Biochemical Corporation, LK003150)

DNase (Worthington Biochemical Corporation, LS002060)

Tryptan blue (Sigma, T8154)

Water for embryo transfer (Sigma, A8199)

Phosphate buffered saline (PBS) pH 7.4 (Ca-, Mg-) (Life Technologies, 10010-015)

Dulbecco's phosphate buffered saline (DPBS) (Ca-, Mg-) (Life Technologies, 14190-094)

2.1.4 Cell lines

Written informed consent was obtained from each of the participants who donated fibroblasts for this study.

Control 1 = 33D9 – derived from a healthy 56 year old male. Reprogrammed by retrovirus.

Control 2 = 34D6 – derived from a healthy 40 year old female. Reprogrammed by retrovirus.

The derivation, characterisation and validation of these control cell lines has previously been described (Bilican et al., 2012; Devlin et al., 2015).

Carrier 1 = DN19V4 – derived from a 58 year old male ALS patient with a *C9orf72* HRE. Reprogrammed by retrovirus.

Carrier 2 = Becker S6 – derived from a 39 year old female ALS patient with a *C9orf72* HRE. Reprogrammed by Sendai virus. The derivation, characterisation and validation of this cell line has previously been described (Devlin *et al*, 2015).

Cell lines were already established when this project commenced. Thanks to Dr. Shyamanga Booroah, who reprogrammed Carrier 2, under the supervision of Dr. Ludovic Vallier at the Wellcome Trust-Medical Research Council Stem Cell Institute, Anne McLaren Laboratory for Regenerative Medicine, Department of Surgery, University of Cambridge, UK. The other cell lines were obtained from Prof. Chris Shaw at Kings College London.

2.1.5 Plastics

2ml aspirator pipettes (Fisher, 10332282)

6 well Nunc plates (Fisher, TKT-190-110E)

12 well Nunc plates (Fisher, 10098870)

24 well Nunc plates (Fisher, TKT-190-010Y)

4 well plates (Fisher, TKT-190-130V)

FACS tubes (Falcon, 4009013)

10µl filter tips (Thermo-scientific, AXC-4135)

200µl filter tips (Thermo-scientific, AXC-4138)

1000µl filter tips (Thermo-scientific, AXC-4140)

500ml filter units (Fisher, 10229090)

150ml receiver bottle (Scientific Laboratory Supplies, FIL8020)

50ml steriflip (Millipore, SCGP00525)

2.2 Cell culture

2.2.1 Generating and validating iPSC lines

hiPSCs were generated from fibroblasts of patients with ALS and healthy controls. Single clones from two ALS patients with *C9orf72* HREs and two healthy controls without *C9orf72* HREs were used in this study. Reprogramming was performed by either retrovirus or Sendai virus. A summary of the cell lines used, including their patient of origin and reprogramming method, is shown in Table 2.1. Many thanks to Chris Shaw's laboratory (King's College, London) for reprogramming the cell lines and sharing them, and to Dr. Shyamanga Booroah

for reprogramming Carrier 2, under the supervision of Prof. Ludovic Vallier at the University of Cambridge.

Cell line	Age and sex	Reprogramming method
Control 1	56 years, male	Retrovirus
Control 2	40 years, female	Retrovirus
Carrier 1	58 years, male	Retrovirus
Carrier 2	39 years, female	Sendai virus

Table 2.1 Cell line details

The pluripotency of the hiPSC lines was confirmed by the expression of pluripotency markers NANOG, SOX2, TRA-1-60 and OCT3/4. The ability to form all three germ layers was also confirmed by immunocytochemistry, as shown in Figure 2.1a. The potential to develop neuroectoderm was demonstrated by expression of Nestin and Sex-determining region Y-box 1 (SOX1); mesoderm by expression of Brachyury and Eomes; and endoderm by expression of forkhead box protein A2 (FoxA2) and GATA-4 as shown in Figure 2.1b. Thanks to Karen Burr for performing this work, which has already been published for Controls 1 and 2, and Carrier 2 (Devlin et al., 2015).

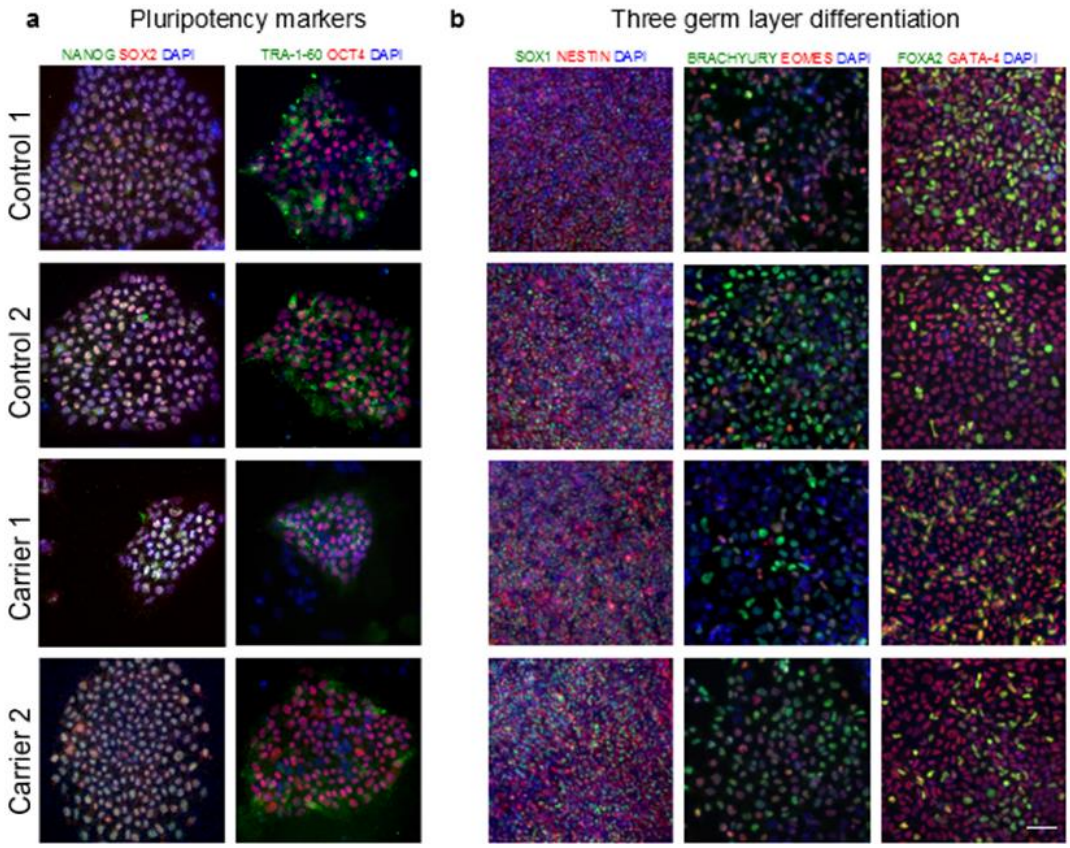

Figure 2.1 Characterisation of hiPSC lines

Figure 2.1 Characterisation of hiPSC lines

(a) Immunocytochemical staining of pluripotency markers NANOG, SOX2, OCT4 and TRA-1-60 in hiPSCs from controls 33D9 and 34D6 and C9orf72 hexanucleotide expansion patients. (b) Immunocytochemical staining showing the three germ layers differentiated from each of the control and patient-derived hiPSCs: SOX1 and NESTIN indicate neuroectoderm; BRACHYURY and EOMES indicate mesoderm; FOXA2 and GATA-4 indicate endoderm. Scale bar = 50μm.

2.2.2 Tissue culture routine

Aseptic technique was used throughout. All cells were incubated at 37°C, with 5% CO2 and normoxia.

Mycoplasma testing was performed monthly. MycoRAZOR™ (Cambio, M040-100) was used to treat any infected hiPSC cultures.

Karyotyping of hiPSC was performed regularly by G-banding, through TDL Genetics.

Control 1 - abnormal at P49 (47, XYY)

Control 2 - normal at P51

Carrier 1 - normal at P21

Carrier 2 - normal at P42, later become abnormal (Trisomy 12)

2.2.3 hiPSC maintenance

Matrigel™ dissolved in Advanced DMEM/F12 1:60 was used to coat all plates for hiPSCs.

hiPSCs were stored in liquid nitrogen. Once cultures got beyond passage 60, they were replaced with stocks of earlier passage.

Thawing hiPSCs: hiPSCs were removed from liquid nitrogen or -80°C freezer and quickly thawed in the water bath at 37°C. Cell were washed in 9ml E8 media and centrifuged at 2500 rpm for 2.5 min. The supernatant was removed and the hiPSCs resuspended in 0.5-1ml E8 medium, before being transferred to a fresh well with coating removed and containing 2ml E8 medium. The plate was placed in the incubator and shaken gently to spread the colonies on the dish and then left overnight before being handled.

hiPSC cultures were cleaned up using three different methods: pruning, haircut or selective passaging. Pruning was used to remove colonies which are not hiPSCs or which look

unhealthy. Haircutting was used if the colonies look good but are surrounded by single cells. Selective passaging is picking out good colonies from the culture and transferring them to a new plate.

Pruning: Colonies to be removed were marked with the objective marker on the microscope, and then a 2ml tip was used to aspirate off the marked colonies quickly using the vacuum. Cells were then fed or passaged.

Haircuts: Media was removed from the well requiring haircut, and 0.5 ml collagenase (2mg/ml) was added to the well and left for 2-5 min until single cells began to lift and come away from the edge of the colonies. The collagenase was then removed and 1ml DPBS added, which was then gently pipetted around the well to remove the single cells. Cells were then passaged.

Selective passage: Coating was removed from a fresh 6-well plate, and 2ml of Complete E8 medium added to each well. Healthy colonies were marked with the objective marker on the microscope, and then a 1ml pipette was used to remove the marked colonies which were then moved to the freshly prepared plate. The plate was shaken gently to spread the colonies on the dish and then left overnight before being handled.

Passaging hiPSCs: hiPSCs were passaged when they reached around 90% confluence, or when the majority of the colonies were large. Coating was removed from a fresh 6-well plate, and 2ml of Complete E8 medium added to each well. The media from the wells being passaged was removed and 0.75-1ml Dispase/Collagenase (1:1) mix was added to each well. The plates were placed into the 37°C incubator for 20-45 min. Once the colonies had lifted, 1ml DPBS was added to each well and used to flush the colonies from the well and transfer to a 15ml falcon tube. The colonies were then pipetted up and down to mechanically dissociate the cells. They were left to settle for 1-2 min before the supernatant was removed. The cells were washed in 2ml DPBS and then resuspended in E8 media (0.5ml per well), and distributed into a fresh plate. The plate was shaken gently to spread the colonies on the dish and then left overnight before being handled.

hiPSCs were fed daily and passaged approximately once a week.

Freezing hiPSCs: Protocol as per passaging, except that instead of resuspending the pellet in E8 media, hiPSC freezing mix was used. The cell suspension was then transferred to a cryovial before being transferred to the -80°C freezer, before being transferred to liquid nitrogen.

Pelleting hiPSCs: Protocol as per passaging, except that once the pellet has been washed in DPBS, the cell suspension was transferred to a 1.5ml tube and centrifuged at 3000 rpm for 3-5min. The DPBS was then removed, before spinning again and removing any residual DPBS. The tubes were then placed in dry ice to snap freeze, before being stored in the freezer.

hiPSC maintenance was carried out by Dr. Karen Burr, Nicola Miller, with assistance from Dr. Dario Magnani, Dr. Navneet Vasistha and Dr. Bhuvaneish Thangaraj Selvaraj, with all lab members contributing to weekend feeding. Verification of pluripotency of the lines was carried out by Dr. Karen Burr as described in earlier publications using these cell lines (Bilican et al., 2012; Devlin et al., 2015).

2.2.3 Neuralisation and patterning

2.2.3.1 Lifting hiPSCs to Phase I (Day 0)

1ml of Dispase/Collagenase (1:1) was added to hiPSCs being passaged and cells were incubated for 20-45 min until cells had lifted. 1ml of DPBS (Life Technologies, 14190-094) was used to flush colonies from the well and transfer them to a 15ml falcon, where the cells were left to settle for 1-2min. The supernatant was removed and cells washed in DPBS for 1-2 min. The supernatant was then removed and replaced with 10ml Phase I medium before being transferred to a 90mm dish and placed in the incubator on an orbital shaker.

2.2.3.2 Phase I (Day 1-7)

The first media change after the hiPSCs have been lifted was carried out either the same day if the media had turned cloudy, or the following day, and was always performed after allowing cells to settle in a 15ml falcon tube. Cell were then fed every 2-3 days, by replacing the media in the 90mm dish directly.

2.2.3.3 Phase II (Day 7-14)

After 7 days in Phase I medium, the spheres are transferred to a fresh 90mm dish containing 10ml of Phase II medium. They are again placed on an orbital shaker in the incubator and have a full media change every 2-3 days.

2.2.3.4 Plating down Phase II neurospheres (Day 14)

6 well plates can be coated with Laminin (10µg/ml) and either left in the fridge (4°C) overnight or in the incubator (37°C) for four hours before use. Neurospheres and media are transferred from their 90mm dish to a 15ml falcon tube. After the spheres have settled for 1 min, the medium was aspirated off and resuspended in Phase II medium. After laminin has been removed from the fresh 6 well plates, the neurospheres are distributed evenly between the wells. The spheres were left to settle overnight and then after 2-3 days, once neural cells could

be identified, spheres were picked. Sometimes, spheres were kept plated down for up to 7 days in which case, they had a full media change every 2-3 days.

2.2.3.5 Phase III (Day 16-23)

Neural precursor cells were selected from the plated down Phase II spheres. In cases where the cultures were purely neuronal, Phase II media was removed along with any floating dead spheres and then replaced with 10ml Phase III media. A cell scraper was then used to detach the spheres from the well. The free floating spheres were then transferred to a fresh 90mm dish, and then placed on an orbital shaker in the incubator.

In cases where the cultures were mixed (not purely neuronal), the neural rosettes were marked using an objective marker, and then a 200µl pipette was used to transfer them to a fresh 90mm plate prepared with 10ml Phase III medium. They were then placed on an orbital shaker in the incubator.

After either selection method, the spheres were then given a full media change with 10ml Phase III media every 2-3 days.

2.2.3.6 Phase III-FGF (Day 23-37)

After 7 days of Phase III media, the medium is changed to Phase III-FGF. Cells had a full media change every 2-3 days for two weeks.

These steps were performed by technical staff in the laboratory, including Dr. Karen Burr, Nicola Miller, and Rinku Rajan. A schematic showing the main stages is shown in Chapter 4.

2.2.4 Differentiation of oligodendrocytes

Oligoprogenitors and oligodendrocytes were generated from spinal conversion neurospheres. When the neurospheres had been fed Phase IIII – FGF for two weeks, the medium was switched to Oligo Pro. After a minimum of two weeks, with a full media change every 2-3 days, these spheres can be dissociated and plated down for conversion to oligodendrocytes. Oligodendrocyte progenitor spheres can be maintained for up to two months, with chopping required when the spheres reach 5-10mm.

2.2.4.1 Dissociation and plating down

Oligooprogenitor spheres were dissociated using Papain dissociation system. The dissociation solutions were reconstituted according to the manufacturer's instructions. Oligoprogenitor spheres (~0.5 ml) were transferred to a 15ml falcon tube and washed with 10ml DPBS. Once the spheres had settled at the bottom after 1-2 min, the supernatant was removed. 1ml Papain/DNase mix was added and the cells incubated at 37°C for 20-30min, with pipette

mixing of the media half every ten minutes. Once the spheres started to dissociate, they can be vigorously pipetted up and down until they are fully broken down. The cells were then centrifuged at 2.5rpm for 3.5 min, before the supernatant was removed. The pellet was then resuspended in 600µl of Inhibitor/DNase. A discontinuous density gradient was prepared by adding 1ml of reconstituted albumin-ovomucoid inhibitor solution to a fresh 15 ml tube. The cell suspension was then carefully layered on top and left for 1 min while any remaining spheres and debris settle at the bottom. A clear interface between the layers of the gradient was clearly visible, and the upper layer and the supernatant of the lower layer were slowly collected and transferred to a fresh 15 ml tube. Any spheres and debris should be left behind and discarded. The cell suspension was centrifuged at 2.5rpm for 2.5min and the supernatant was then discarded. The cell pellet is then resuspended in Oligo Pro medium. Cells were counted using Tryptan blue and a haemocytometer, before plating.

Depending on the experimental needs, different formats of plates were used. All plates were first coated with poly-ornithine, which was then washed off three times with Water for Embryo transfer, and then coated with a mixture of Laminin/Matrigel™/Fibronectin (L/M/F) in Advanced DMEM/F12.

For dry coating: Laminin 10µg/ml
Matrigel™ 1:20
Fibronectin 20µg/ml

For wet coating: Laminin 10µg/ml
Matrigel™ 1:20
Fibronectin 10µg/ml

Plate format	Volume of poly-ornithine	Coating type	Volume of L/M/F	Number of cells plated per well	Volume of media for plating
24 well + glass coverslip	500µl	Dry	40µl	40 000	40µl
12 well	1ml	Wet	600µl	500 000	1ml
6 well	1ml	Wet	1ml	1 500 000	2ml

Table 2.2 Details of different plate formats

This table shows the volume of poly-ornithine coating used, whether dry or wet coating was required, and the volume of L/M/F mixture. The final cell number and media required for plating down is also shown.

For plating, in all cases, the L/M/F coating was first removed before an appropriate volume of cells were added to each well. For 24 well plates, cells were diluted in Oligo Pro media such

that there were 40 000 cells per 40µl. These plates were then carefully placed in the incubator for 2-3 hours before wells were flooded with 0.5ml Oligo Diff. For the other plate types, the cells were added to the plates and the Oligo Pro media subsequently adjusted to the volume shown in Table 2.2. The plates were rocked from side to side to spread the cells evenly across the plate surface before being placed in the incubator. After plate down, cells had a half-media change every 2-3 days with Oligo Diff.

2.2.5.2 Chopping spheres

Spheres were chopped when they reached between 5-10mm. DNase (25mg) was dissolved in 5ml of Advanced DMEM/F12. The spheres requiring chopping were moved to the centre of the dish and the majority of media removed. Using a sterile blade, the spheres were chopped until there were no large lumps and all pieces were around the same size. 5ml Advanced DMEM/F12 was used to wash the chopped spheres and they were then transferred to a fresh 15ml tube and pipetted up and down several times. The spheres were centrifuged at 400 rcf for 1 min before the supernatant was removed. 500µl of DNase was added and the spheres were incubated at 37°C with occasional shaking, for 10 min. 10ml Advanced DMEM/F12 was then added to the spheres to wash them. After allowing the spheres to settle for a few minutes, the supernatant was removed and replaced with 12ml Oligo Pro medium. The spheres and media were then transferred to a fresh 90mm plate and put back on an orbital shaker in the incubator.

2.2.6 Magnetic-Activated Cell Sorting (MACS)

For qRT-PCR and Western blotting, week-3 cell cultures were dissociated with Accutase, and separation of O4+ oligodendrocytes was achieved by MACS.

2.2.6.1 MACS solutions and reagents

MACS buffer: Made up in PBS pH 7.4 (Ca-, Mg-) (Life Technologies)

B-27® (Life Technologies, 17504-044) 1:50

N-2 (Life Technologies, 17502-048) 1:100

EDTA (Life Technologies, 15575-038) 0.8mM

$MgCl_2$ (Sigma, M1028) 2mM

D+-Glucose solution (Sigma, G8769) 4.5%

MACS® FcR blocking reagent, human (MACS, 130-059-901)

anti-O4 MicroBeads (MACS, 130-096-670)

MACS® LS columns (MACS, 130-042-401)

MACS® Smart Strainer 100µm (MACS, 130-098-463)

2.2.6.2 MACS protocol

Throughout the protocol, MACS buffer was kept on ice. Cells were lifted by replacing media with 1ml Accutase per well of a 6-well plate, and incubating at 37°C for ~5min until cells lift off. 1ml of Oligo Diff media was then added, and cells were collected into a 15ml falcon tube before being centrifuged at 2.5 rpm for 2.5 min. The supernatant was removed from the cell pellet, which was then resuspended in 12ml cold MACS buffer. The cell suspension was then passed through a 100µm MACS® Smart Strainer into a fresh 15ml falcon tube. The cells were centrifuged for 2.5 min at 2.5 rpm. The supernatant was then removed and the cell pellet resuspended in 70µl MACS buffer and 20µl MACS® FcR blocking reagent, before being incubated at 4°C for 10 min. 10µl of Anti-O4 microbeads were then added, and further incubated at 4°C for 15 min. An LS column was prepared within a magnetic stand, with a 15ml falcon tube for collection. The column was prepared by rinsing through 3ml MACS buffer. Once the cells had incubated with Anti-O4 Microbeads, 3ml MACS buffer was added and the cells centrifuged for 2.5 min at 2.5 rpm. The supernatant was removed and the cells resuspended in 500µl of MACS buffer before being applied to the MACS® LS column. The column was then washed 3 times with 3ml MACS buffer to remove the negative cell fraction. The column was then removed from the magnet, and a plunger used to elute the positive (O4) cell fraction into a fresh 15ml tube. 3ml MACS buffer was then added and the cells centrifuged for 2.5 min at 2.5 rpm. The supernatant was then removed and the cells resuspended in Oligo Diff media. Cells were counted using Tryptan blue, and were then either plated down (as described in Section 2.2.4) or pelleted for biochemical or molecular studies (as described for iPSCs in Section 2.2.2).

2.2.7 Fluorescence-Activated Cell Sorting (FACS)

2.2.7.1 FACS solutions and reagents

Accutase (Sigma, A6964)

FACS buffer: Made up in DPBS (Ca-, Mg-) (Life Technologies)

Bovine Serum Albumin (Europa Bioproducts, EQBAC62) 0.2%

O4 antibody (R&D Systems, MAB1326)

Alexa Fluor 647 Anti-mouse IgM (Life Technologies, A21238)

CellEvent™ Caspase-3/7 Green Flow Cytometry Assay kit (Life Technologies, C10427)

2.2.7.2 FACS protocol

Throughout the protocol, FACS buffer was kept on ice. Cells were lifted by replacing media with 1ml Accutase per well of a 6-well plate, and incubating at 37°C for ~5min until cells lift off. 1ml of Oligo Diff media was then added, and cells were collected into a 15ml falcon tube before being centrifuged at 2.5 rpm for 2.5 min. The supernatant was removed and the cell pellet resuspended in 100µl of FACS buffer. 1µl of O4 primary antibody (diluted 1:5 in FACS buffer) was added and incubated on ice for 30 min. 3ml FACS buffer was then added to wash the cells, followed by centrifugation at 1.5 rpm for 5 min. The pellet was then resuspended in 200µl of Alexa Fluor 647 Anti-mouse IgM (diluted 1:2000 in FACS buffer) before incubating on ice, in the dark, for 30 min. 3ml FACS buffer was then added to wash the cells, followed by centrifugation at 1.5 rpm for 5 min. The pellet was then resuspended in 300µl CellEvent™ Caspase-3/7 (diluted 1:1000 in FACS buffer), and incubated at 37°C for 30 min. Secondary only and unstained controls were performed with each sample set.

Flow cytometry was then performed on a FACSCalibur (Becton Dickinson, San Jose, CA). Cells were analysed by forward and side scatter for Alexa Fluor 488 fluorescence through a 530 ± 30 nm band-pass and for Alex Fluor 647 through a 695 ± 40 nm band-pass. Unstained cells were used to set the background fluorescence; a false positive rate of 0.5% was accepted.

Thanks to Dr. Karen Burr and Dr. Navneet Vasistha for optimising the FACS protocol and helping with running the samples on the FACSCalibur.

2.2.7.3 Tunicamycin stress

Tunicamycin (Sigma T7765) was dissolved in DMSO to a concentration of 1.2mM. This was then added to oligodendrocyte cultures in media to produce a final concentration of 0.5µM. Cells were subjected to tunicamycin stress for 48 hours prior to FACS analysis being performed.

2.2.8 Gene editing of hiPSCs

Cas9 and guide (g)RNA were cloned into an expression plasmid pSpCas9(BB)-2A-GFP (Px458) as described in a published protocol (Ran et al., 2013). CRISPR gRNA sequences were designed using the web tool http://crispr.mit.edu. The sequences of the gRNA's were as follows: gRNA-1 AACTCAGGAGTCGCGCGCTAGGG and gRNA-2 GGCCCGCCCCGACCACGCCCGG.

Using Accutase, hiPSC were dissociated to produce a single cell suspension. Using the Amaxa 4D nucleofector system (program CA137), $8x10^5$ cells were then nucleofected with 2 µg of each Cas9-gRNA-1 and Cas9-gRNA-2 plasmids following the manufacturer's instructions.

The transfected cells were then plated onto Matrigel coated plates and fed with Essential 8 medium plus ROCK inhibitor (10 µM). Once cells were confluent, they were once again dissociated to single cells and re-plated at low density (2000 cells/ 10 cm dish) to permit clonal analysis. Individual colonies were picked and screened by PCR based methods for deletion of the expanded *C9orf72* allele (Selvaraj, submitted).

Assessment of off-target effects was carried out by Sanger sequencing of highly homologous regions of the genome.

Location and sequence of highly homologous target	Primer sequences (5'-3')
Chr2:-231921408 AGGTCAGGAGTCCCGCGCAA	F: CTCAGTCAGTCGCCTCCTC R: AGCCCCAATTCCTAAGCAT
Chr7:-151551819 ATCATCAGGAGGCCCGCCCTA	F: CTGGAGTATGGAGCCCTCAG R: GAGGATAGGGCTGTGTGACA
Chr3:46924939 TGGCCGCCCCGCCCACGCCCGG	F: GTGTGGCTGCAAAGTTGAGA R: TGTGCATGTGTGTGTGTGTGAG
Chr3:+98241587 CGCCCAGCCCGACCACGCCCGG	F: CCTTCATCCTGGTGCTCTCA R: GTGCTGTGGTCTGAGCTAGA
Chr22:-37731099 GCCCCGCTCCGCCCACGCCCGG	F: TAGCTCAGAGGGTTAGGGC R: AATCAAAACAGGGGCGGTTC

Table 2.3 Highly homologous sequences to gRNA targets and primers for Sanger sequencing (red sequence highlights difference in sequence between target and gRNA).

The creation of the isogenic control was carried out by Dr. Bhuvaneish Thangaraj Selvaraj in combination with Bruce Whitelaw and Simon Lillico at the Roslin Institute (University of Edinburgh). PCR based screening methods were optimised based on the methods developed by myself and I also contributed by carrying out fluorescent capillary electrophoresis and analysing traces to select clones of interest.

2.2.9 Electrophysiology

Electrophysiology recordings were undertaken by Dr Matt Livesey and Dr Owain James. Whole-cell patch clamping was used to record macroscopic currents, which were typically low-pass filtered online at 2kHz, digitized to 10 kHz and recorded to computer using WinEDR V2 7.6 Electrophysiology Data Recorder. Rectification indices were calculated as described (Livesey et al., 2016).

2.3 Immunocytochemistry

2.3.1 Solutions and reagents

4% Paraformamyde (Sigma, 158127) in PBS

Triton™ (Sigma X-100)

Goat serum (DAKO, X0907)

Hoescht (Invitrogen, H3569) 1:1500

4-,6-diamidino-2-phenylindole (DAPI) (Sigma, D9542) 1:5000

FluorSave™ (Calbiochem, 345789)

PBS pH 7.4 (Ca-, Mg-) (Life Technologies, 10010-015)

Primary antibodies:

Antibody	**Type**	**Company**	**Catalogue number**	**Dilution**
SOX1	Goat polyclonal	R&D Systems	AF3369	1:100
Nestin	Mouse monoclonal	Millipore	MAB5326	1:100
Brachyury	Goat polyclonal	R&D Systems	AF2085	1:100
Eomes	Rabbit polyclonal	Abcam	Ab23345	1:600
FOXA2	Goat polyclonal	R&D Systems	AF2400	1:100
GATA-4	Goat polyclonal	Santa Cruz	SC25310	1:100
Olig2	Rabbit polyclonal	Millipore	2519344	1:300
PDGFRα	Rabbit monoclonal	Cell Signaling	52415	1:200
O4	Mouse IgM	R&D Systems	MAB1326	1:600
MBP	Rat	Abcam	Ab7349	1:50
GFAP	Rabbit polyclonal	DAKO	20334	1:500
β-III tubulin	Mouse IgG2b	Sigma	T8660	1:1000
TDP-43	Mouse IgG1	Abnova	H00023435	1:200
p62	Mouse IgG1	BD Biosciences	610832	1:200

Table 2.4 Primary antibodies used, with dilutions used and details of origin.

Secondary antibodies:

Antibody	**Type**	**Company**	**Catalogue number**	**Dilution**
Alexa Fluor 647	Goat anti-mouse IgM	Life Technologies	A21238	1:1000

Alexa Fluor 488 (green)	Goat anti-rat IgG	Life Technologies	A11006	1:1000
Alexa Fluor 488 (green)	Goat anti-rabbit IgG (H+L)	Life Technologies	A11008	1:1000
Alexa Fluor 647 (far red)	Goat anti-Mouse IgG2b	Life Technologies	A21242	1:1000
Alexa Fluor 555 (red)	Goat anti-rabbit IgG1	Life Technologies	A21428	1:1000
Alexa Fluor 488 (green)	Goat anti-mouse IgG1	Life Technologies	A21121	1:1000

Table 2.5 Secondary antibodies used, with dilutions used and details of origin.

2.3.2 Live immunostaining and fixing

Live immunostaining was performed with O4 antibody. O4 antibody was diluted 1:300 in Oligo Diff media. The media from the well was then removed, leaving behind ~150µl of media to prevent the cells drying out. 150µl of the diluted antibody was then added. The cells were then incubated at 37°C for 1 hour to allow antibody binding, before fixing.

Fixing was performed by aspirating off media, and then adding ~0.5ml 4% PFA and incubating at room temperature for 10 min. Cells were then washed with PBS three times. Fixed cells were used immediately for RNA-FISH or kept for up to 7 days at 4°C prior to immunocytochemistry.

2.3.3 Blocking and antibody incubation

For all antibodies except for PDGFR-α, cells were permeabilised prior to blocking and antibody incubation. In the case of PDGFR-α, permeabilisation was not performed until after this primary antibody had been added, therefore for co-staining with other antibodies an extra primary antibody incubation was required. All steps were performed at room temperature.

Cell membranes were permeabilised by applying 0.2% Triton X to the cells for 10 min. This was then removed and replaced by 3% goat serum as a blocking agent, for 1 hour. Primary antibodies, diluted in 3% goat serum were then applied and incubated for 1 hour. Cells were then washed three times, for 5 min each, with PBS. Secondary antibody, diluted in 3% goat serum, were then added to cells for 30 min. Cells were then washed three times, for 5 min each, with PBS. Hoescht or DAPI was then added for 5 min before washing three more times, for 5 min each, with PBS. Where coverslips were used, a drop of Fluorsave was placed on a microscope slide before mounting. Slides were left to dry overnight before being stored at 4°C.

2.3.4 Imaging of slides

Imaging was performed using a Carl Zeiss Axio Observer microscope (Zeiss, Oberkochen, Germany), either x20 or x63 magnifications, and analyzed using Axiovision v4.8.1 (Zeiss) software. Fields were selected based upon uniform DAPI staining and imaged in three/four fluorescent channels as required.

2.3.5 Image analysis

For quantitative immunocytochemistry, Image J64 (v1.47) was used to convert images to grayscale and the DAPI channel was used to create regions of interest. Cell quantification was perfomed manually with Image J64 (v1.47) software for an area of 162.4 μ^2. Positive staining was indicated by signal which was clearly stronger than any background fluorescence in cell free areas. For all cell counting, at least three independent images per coverslip were taken, and a minimum of three independent cultures from three independent conversions were assessed.

2.3.6 Sholl analysis

Sholl analysis was performed using a plugin in ImageJ (Ferreira et al., 2014). Images were converted to 8-bit, and a threshold applied to remove background. A line was selected from the centre of the soma to the furthest point. The starting radius was set at 10µm as this was estimated to be the average cell body size after measuring a representative sample. The step size was set at 2.5µm. The software calculated the number of intersections the cell made at each radius around the cell body and this value was recorded in Microsoft Excel.

2.4 Molecular biology

2.4.1 DNA extraction

2.4.1.1 Isolation of DNA from cultured cells

Approximately 1 million cells were harvested using trypsin (for iPSCs) or Accutase (for oligodendrocytes). DNA was extracted using the Wizard SV Genomic DNA Purification System (Promega), according to the manufacturer's instructions for cell culture DNA.

2.4.1.2 Isolation of DNA from patient leukocytes

Historic DNA samples relating to the Scottish Regenerative Neurology Tissue Bank were extracted from whole blood samples by phenol-chloroform or manual salting out. Recent samples were extracted by the Nucleon BACC3 genomic DNA kit (Tepnel Life Sciences). Samples for diagnostic testing were extracted from whole blood or saliva using the Chemagic DNA blood kit (Perkin Elmer), according to the manufacturer's instructions.

2.4.2 PCR for C9orf72 genotyping

2.4.2.1 C9orf72 genotyping reagents and solutions

Multiplex PCR kit (Qiagen Ltd, 206143)

DyNAzyme EXT DNA Polymerase (ThermoFisher Scientific, F505-L), 1U/µl

DMSO (Sigma, D8418)

Betaine (Sigma, B0300), 5M

7-deaza-2'-dGTP (Roche, 10988537001), 10mM

dNTPs (Scientific Lab Supplies, 28406551), 100mM each A,C,G,T

HPE dNTP mix: 35µM dCTP and dGTP, 10 µM dATP and dTTP

Primers stocks at 100µM (IDT):

Primer	Sequence (5'-3')
F1	TAA CCA GAA GAA AAC AAG GAG GGA
F2	FAM-CTG TAG CAA GCT CTG GAA CTC AGG AGT CG
F3	FAM-AGC AAG CTC TGG AAC TCA GGA GTC G
R1	GCC CCC GGG CCC GCC CCG ACC AC
R2	FAM-GCA GGC ACC GCA ACC GCA GC
R3	CCG CCT CCT CAC TCA CCC ACT
R4	ATG CCG CCT CCT CAC TCA CCC ACT
R6	CCT CAC TCA CCC ACT CGC CAC
R8	CGG GCG CAG GCA CCG CAA CC
Repeat R	TAC GCA TCC CAG TTT GAG ACG CCC CGG CCC CGG CCC CGG CCC C
Repeat F	TAC GCA TCC CAG TTT GAG ACG GGG GCC GGG GCC GGG GCC GGG G
Repeat F3	TAC GCA TCC CAG TTT GAG ACG GGC CGG GGC CGG GGC CGG
Tail R	TAC GCA TCC CAG TTT GAG ACG

Table 2.6 C9orf72 genotyping primer sequences

All primers were SNP checked. In chapter 3 there is a schematic which shows where these primers bind against the reference sequence.

2.4.2.2 Original flanking PCR assay

PCR mix:	x1 (µl)
Qiagen Multiplex Mastermix	12.5
DMSO	1.75
Betaine, 5M	3

F2 primer (FAM) + R1 primer, 5µM	5
H_2O	0.75
DNA, 20ng/µl	2
	25

Cycling was performed using a GeneAmp® 9700 (Life Technologies) using the following conditions:

94°C – 15 minutes

94°C – 1 minute
68°C – 1 minute
72°C – 1 minute
} 35 cycles

72°C – 10 minutes

2.4.2.3 Nested RP-PCR

The original flanking PCR (section 2.4.2.2) was performed, followed by product clean up with Agencourt Ampure XP (Beckman Coulter, A63881) and then nested PCR as follows:

3' RP PCR mix	x1 (µl)
Qiagen Multiplex Mastermix	10
Q solution	4
F2 primer (FAM), 5µM	1.5
Repeat R primer, 5µM	0.75
Tail R, 5µM	1.5
H_2O	1.5
PCR product (1:500)	1
	20

Cycling was performed using a GeneAmp® 9700 (Life Technologies) using the following conditions:

95°C – 15 minutes

95°C – 1 minute
*71°C – 1 minute
72°C – 1 minute
} 30 cycles

72°C – 10 minutes

*A 5 point gradient PCR (65-74°C was performed) but data were presented from optimal Ta=71°C.

2.4.2.4 Original RP-PCR assays

3' RP PCR mix	x1 (µl)	5' RP PCR mix	x1 (µl)
Qiagen Multiplex Mastermix	12.5	Qiagen Multiplex Mastermix	12.5
Betaine, 5M	3	Betaine, 5M	3
DMSO	1.75	DMSO	1.75
7-deaza-2'-dGTP	0.2	7-deaza-2'-dGTP	0.2
R2 primer (FAM), 5µM	1.9	F2 primer (FAM), 5µM	1.9
Repeat F primer, 5µM	0.9	Repeat R primer, 5µM	0.9
Tail R, 5µM	2.9	Tail R	2.9
H_2O	0.85	H_2O	0.85
DNA,~200ng/µl	1	DNA (~200ng/µl)	1
	25		25

Cycling was performed using a GeneAmp® 9700 (Life Technologies) using the following conditions:

95°C – 15 minutes

95°C – 1 minute
71°C – 1 minute
72°C – 2 minutes
} 10 cycles

95°C – 1 minute
60°C – 1 minute
72°C – 2 minutes
} 25 cycles

72°C – 10 minutes

2.4.2.5 HPE flanking PCR assay

	x1 (µl)
Optimized DyNAzyme EXT buffer, 10x	1.6
Betaine, 5M	7.2
HPE dNTP mix	0.3
F3 primer (FAM)+ R6 primer, 5µM	5
DyNAzyme EXT DNA Polymerase, 1U/µl	2.4
H_2O	2.5
DNA, 20ng/µl	1
	20

Cycling was performed using a Veriti® thermal cycler (Life Technologies) using the following conditions:

94°C – 7 minutes

95°C – 45 seconds

98°C – 10 seconds

61°C – 30 seconds

78°C – 5 seconds*

78°C – 2 seconds (x7)

86°C – 2 seconds (x7)

78°C – 2 seconds (x7)

90°C – 2 seconds (x7)

78°C – 10 minutes

(35 cycles)

*slow ramp (12% = 0.6°C/second)

2.4.2.6 HPE RP-PCR assays

3' RP	x1 (µl)	5' RP	x1 (µl)
Optimized DyNAzyme EXT buffer, 10x	1.6	Optimized DyNAzyme EXT buffer, 10x	1.6
Betaine, 5M	7.2	Betaine, 5M	7.2
HPE dNTP mix	0.3	HPE dNTP mix	0.3
R8 primer (FAM), 5µM	2	F2 primer (FAM), 5µM	2
Repeat F3 primer, 5µM	1	Repeat R primer, 5µM	1
Tail R, 5µM	3	Tail R	3
DyNAzyme EXT DNA Polymerase, 1U/µl	2.4	DyNAzyme EXT DNA Polymerase, 1U/µl	2.4
H_2O	1.5	H_2O	1.5
DNA, ~200ng/ µl	1	DNA, ~200ng/ µl	1
	20		20

Cycling conditions were as described for the HPE flanking assay (section 2.4.2.4).

2.4.3 Capillary electrophoresis and analysis

All RP-PCR products were ran neat whereas flanking PCR products were diluted 1:100 before loading. 2µl of sample was added to 9.5µl Hi-Di (Life Technologies, 4311320) and 0.5µl Genescan™ LIZ600 size standard (Life Technologies, 4366589) and denatured for 3 min at 95°C prior to capillary electrophoresis using an ABI 3130xL Genetic Analyzer (Life Technologies). POP-7 polymer (Life Technologies, 4335615) was used, with a 50cm capillary array was used (Life Technologies, 4315930).

For long injection protocol, the GeneScan™ LIZ1200 size standard (Life Technologies, 4379950 was used.

Data was analysed using GeneMarker® software v2.4.0 (Soft Genetics).

2.4.4 Sanger sequencing

2.4.4.1 Sanger sequencing reagents and solutions

Agencourt Ampure XP (Beckman Coulter, A63881)

BigDye® Terminator v3.1 Cycle Sequencing kit (Life Technologies, 4337455)

BigDye® Terminator v1.1 and v3.1 Sequencing buffer (Life Technologies, 4336699) 5x

Cleanseq® (Beckman Coulter, A29154)

2.4.4.2 Sanger sequencing protocol

For Sanger sequencing of the flanking PCR products, PCR was performed as described and then sequencing was carried out using R2 primer. For sequencing of the C9orf72 3' region, repeat-primed PCR was performed as described above for HPE PCR 3'RP, with primer R6 used in place of R8. In both cases, PCR products were purified using Agencourt Ampure XP, as per the manufacturer's instructions, using a Biomek® NX robot (Beckman Coulter). Sequencing was then performed using BigDye® Terminator v3.1 (Life Technologies). Reactions were set up as shown below:

	x1 (µl)
BigDye v3.1	0.5
BigDye Sequencing buffer, 5x	1.75
R2 or R6 Primer, 3.2µM	1
H_2O	4.75
Purified PCR product	2
	10

Cycling were performed using a GeneAmp® 9700 thermal cycler (Life Technologies) using the following conditions:

96°C – 75 seconds

94°C – 15 seconds
55°C – 10 seconds
62°C – 4 minutes
} 30 cycles

CleanSeQ was used, according to the manufacturer's instructions to clean-up sequencing products prior to running on an ABI 3130xL Genetic Analyzer (Life Technologies).

Sequencing was analysed using Mutation Surveyor v4.0.8 (Soft Genetics) or Sequence Scanner v1.0 (Applied Biosystems).

2.4.5 Agarose gel electrophoresis

BlueJuice™ loading buffer (ThermoFisher Scientific, 10816-015), 10x

Tris-Borate EDTA (TBE) (Sigma, T3913), 0.5x

UltraPure ™ Agarose (ThermoFisher Scientific, 16500-500)

GelRed (Cambridge Biosciences, BT41003), 10 000x

100bp DNA ladder (Promega, G2101)

1kb DNA extension ladder (Invitrogen, 10511012)

Gels were prepared by melting agarose at the desired concentration (0.8-2%) in 0.5x TBE buffer using a microwave. Once the agarose had cooled, GelRed was added and the gel poured in a casting tray. Electrophoresis was preformed in BioRAD tanks at 100V in 0.5x TBE buffer. PCR products were visualised by UV transillumination and photographed using an AlphaDigiDoc system. When loading, samples were mixed with BlueJuice™ loading dye, and appropriate DNA ladders were run alongside the samples.

2.4.6 RNA extraction

Following MACS sorting, approximately 1 million cells were pelleted and either snap frozen in dry ice and stored at -80°C, or taken directly for RNA extraction. RNA was isolated with the RNeasy kit (Qiagen, 74104) following the manufacturer's instructions, with homogenization performed by pipette mixing. RNA was eluted in 32µl RNase-free water. Genomic DNA was removed by treatment with Turbo DNA-free™ (Ambion, AM1907),

according to the manufacturer's instructions. RNA concentration was estimated using spectrophotometry (NanoDrop 1000).

2.4.7 cDNA synthesis

cDNA was synthesized by using 1µg of total RNA with the DyNAmo cDNA Synthesis Kit (Life Technologies. F470-L), using random hexamers in a 20µl reaction. The manufacturer's protocol was used. Briefly, 2µl of random hexamer primers were added to 1µg RNA (in a total volume of 7µl), with 10µl RT Buffer and 2µl RT enzyme (M-MuLV RNase H^+ reverse transcriptase). These were placed in a thermal cycler to allow primer extension (25°C for 10 min), cDNA synthesis (37°C for 30 min), followed by reaction termination (85°C for 5 min). A 'minus RT' control was included, where the RT enzyme was replaced with RNase-free water.

2.4.8 qRT-PCR

Real-time qPCR reactions were set up in triplicates with the DyNAmo ColorFlash SYBR Green qPCR Kit (ThermoFisher Scientific, F-416L) according to the manufacturer's instructions. Primers were used at 200nM, and reactions run on an iCycler System (Bio-Rad). All results were normalized to β-actin and GAPDH using the delta delta Ct method, and were from 3 technical replicates of 5 independent biological samples. Primer sequences, annealing temperatures and reaction efficiencies are provided Table 2.6. Primers were designed using NCBI (website) with the exception of isoform specific C9orf72 primers (Fratta et al., 2013).

Gene	Primers (5'-3')	Ta (°C)	Efficiency (%)	r^2
MBP	F: TGTACAAGGACTCACACCACC	60	109.5	0.997
	R: ACGGGGTTTTCATCTTGGGT			
MCT1	F: GACCTTGTTGGACCCCAGAG	60	107.0	0.996
	R: AGCCGACCTAAAAGTGGTGG			
C9orf72 V1	F: TCATCTATGAAATCACACAGTGTTC	60	98.9	0.966
	R: GGTATCTGCTTCATCCAGCTT			
C9orf72 V2	F: GCGGTGGCGAGTGGATAT	60	96.0	0.982
	R: TGGGCAAAGAGTCGACATCA			
C9orf72 V3	F: GAGCAGGTGTGGGTTTAGGAGA	60	103.9	0.922
	R: TGGGCAAAGAGTCGACATCA			
B-actin	F: GTTACAGGAAGTCCCTTGCCATCC	60	97.8	0.992
	R: CACCTCCCCTGTGTGGACTTGGG			
GAPDH	F: GAGTCCACTGGCGTCTTCAC	60	98.3	0.987
	R: ATGACGAACATGGGGGCAT			

TDP-43	F: CGGCCTAGCGGGAAAAGTAAAAGA	65	94.4	0.915
	R: AGCACCGTCCCATCGTCTT			

Table 2.7 qRT-PCR primer details

All PCR products were shown to be specific by a single band of the expected size after agarose gel electrophoresis and through post-PCR melt-curve analysis on the iCycler System (Bio-Rad).

2.4.9 RNA-FISH

For experiments where RNA-fluorescence *in situ* hybridisation (RNA-FISH) was combined with immunocytochemistry for the O4 marker, O4 live staining was performed prior to fixation as described in section 2.3.2.

2.4.9.1 RNA-FISH solutions and reagents

All solutions and reagents must be RNase free.

16% paraformaldehyde (Agar Scientific, AGR1026) 1:4 in PBS pH7.4 (Ca-, Mg-)

Pre-hybridisation solution: Made up in Water for embryo transfer (Sigma, A8199)

Formamide (Sigma F9037) 1:2

20x Saline sodium citrate (SSC) (Sigma, S8015) 1:10

Hybridisation solution: Made up in Water for embryo transfer (Sigma, A8199)

Formamide (Sigma F9037) 1:2

20x SSC (Sigma, S8015) 1:10

50% dextran sulphate (Millipore, S4030) 1:10

10mg/ml Yeast tRNA (Invitrogen, 15401-029) 1:10

10mg/ml salmon sperm DNA (Invitrogen, 15632-011) 1:10

Alexa 546-conjugated $(GGCCCC)_4$ oligonucleotide probe (IDT, custom made) 100ng/µl

Alexa 546-conjugated $(CAGG)_6$ oligonucleotide probe (IDT, custom made) 100ng/µl

RNase A (Sigma R4642)

2.4.9.2 RNA-FISH protocol

Cells cultured on glass coverslips were fixed in sterile 4% paraformaldehyde for 15 min, before being washed 3 times with PBS. Membranes were permeabilized using 70% ethanol for 10

min (note this step was omitted if PDGFRα staining was performed). Cells were then incubated in pre-hybridisation solution for 10 min. During this time, the probe was denatured by heating to 95°C for 5 min and then snap freezing on ice. The probe was then diluted in hybridisation solution to a final concentration of 0.16ng/µl. The diluted probe was then added to the coverslips which were incubated in a humid chamber at 45°C for 2 hours. The coverslips were then washed in pre-hybridisation solution twice, for 30 min at 45°C, followed by a final 30 min wash in 2x SSC at room temperature. If immunostaining was performed in addition, the protocol described in section 2.3 followed from the blocking stage. If immunostaining was not required, Hoescht or DAPI was then added for 5 min before washing three more times, for 5 min each, with PBS. A drop of Fluorsave was placed on a microscope slide before mounting the coverslip. Slides were left to dry overnight before being stored at 4°C.

For the RNase A experiments, after fixation, cells were incubated with 100 µg/ml RNase A (Sigma) for 1 h at 37°C.

2.4.10 Western blotting

2.4.10.1 Western Blotting solutions and reagents

RIPA buffer: Made up in Water for embryo transfer (Sigma, A8199)

Tris-hydrochloric acid pH 7.4 (Fisher, BP152-500) 50mM

Sodium chloride (Fisher S/3160160) 150mM

Triton X-100 (Sigma, T9284) 1%

Sodium deoxycholate (Sigma, D6750) 0.5%

Sodium dodecyl sulfate (Sigma, L3771) 0.1%

EDTA (Life Technologies, 15575-038) 2mM

Urea buffer: Urea (Sigma, U4883) 9M

Sodium dodecyl sulfate (Sigma, L3771) 1%

Tris (Fisher, BP152-500) 25mM

EDTA (Life Technologies, 15575-038) 1mM

PI: Complete Mini Protease Inhibitor tablets (Roche, 04 693 124 001)

PhosSTOP: Phosphatase Inhibitor Cocktail tablets (Roche, 04 906 837 001)

Pierce BCA Protein Assay kit (Thermo Scientific, 23227)

NuPAGE® Sample Reducing Agent (Life Technologies, NP0009)

NuPAGE® LDS Sample buffer (Life Technologies, NP0007)

4-20% Precise Protein gel (Thermo Scientific, 25224)

SDS PAGE running buffer, BupH™ Tris-HEPES (Thermo Scientific, 28398)

Protein ladder: Precision Plus Protein™ All Blue Standards (Bio-RAD, 161-0373)

10x SDS PAGE Transfer buffer: Made up in deionised water

Tris (Fisher, BP152-500)

Glycine (Sigma, G8898)

1x SDS PAGE Transfer solution: Made up in deionised water

10x SDS PAGE Transfer buffer (1:10)

Methanol (1:5)

Odyssey® blocking buffer (LiCor, 927-40100)

PBS-T: 0.1% Triton X-100 in PBS

Coomassie blue stain (Thermo Scientific, 20278)

Coomassie blue destaining solution: Acetic Acid (SLS, CHE1014) 7.5%

Methanol (Sigma, 322415) 5%

2.4.10.2 Protein preparation

Frozen cell pellets (MACS sorted O4+) were lysed on ice in 100µl RIPA buffer, which was supplemented with fresh protease inhibitors (PI, 1:25; PhosSTOP, 1:10). The lysate was homogenised by pipetting regularly during a 30 min incubation on ice. Cell lysates were then centrifuged at 13 000 rpm for 30 min at 4°C. The cleared lysate (soluble fraction) was transferred to a fresh tube.

The cell pellet was washed with 200µl RIPA buffer to minimise carry-over of the soluble fraction and then centrifuged at 13 000 rpm for 15 min before the lysate was discarded. The pellet was then resuspended in 50µl urea buffer (which was supplemented with fresh protease inhibitors (PI, 1:25; PhosSTOP, 1:10) and incubated on ice for 10 min. Lysates were then sonicated at 40 000Hz for two pulses of 10 s, followed by 1 min. The lysates were then left at room temperature for 20 min before being centrifuged at 13 000 rpm for 30 min at 4°C. The

supernatant (detergent insoluble fraction) was transferred to a fresh tube. The protein concentration of the soluble fraction was determined using the Pierce BCA Protein Assay kit, following the manufacturer's protocol.

2.4.10.3 SDS-PAGE

4-20% Precise Protein gels were used. The comb was removed, and the gel rinsed in deionised water before being placed in the tank, where the wells were flooded with SDS PAGE running buffer. For the soluble fraction, 20µl volume was loaded, including 10 µg of sample, NuPAGE® Sample Reducing Agent (1:4), and NuPAGE® LDS Sample buffer (1:10). For the insoluble fraction, 5µl of sample and NuPAGE® Sample Reducing Agent (1:4), and NuPAGE® LDS Sample buffer (1:10) was loaded. All samples were heated to 95°C before loading. Protein ladder was added to one well. Gels were run at 110V for 70 min.

2.4.10.4 Transfer

The membrane was activated by soaking in 100% methanol for a minimum of 30s. The gel was removed from its casing, washed in deionised water before being rinsed with 1x SDS PAGE transfer solution. The transfer assembly was set up in a BioRAD electrophoresis tank with the membrane between two foam sponges and a wet sheet of filter paper on either side. The transfer was carried out at 30V for 1 hour.

2.4.10.5 Blocking, antibody incubation and washing

The membrane was placed protein side up in a LiCor staining box and incubated for 1 hour in Odyssey® blocking buffer at room temperature on a shaker. Primary antibodies were diluted in Odyssey® blocking buffer and incubated overnight at 4°C. The membrane was then washed 3 times for 10 min each, in PBS-T. Secondary antibody, diluted in Odyssey® blocking buffer, was then added and incubated for 1 hour at room temperature. The membrane was then washed 3 times for 10 min each, in PBS-T before being transferred to PBS before being imaged.

If further probing was required, this process was repeated.

Antibody	Type	Company	Catalogue number	Dilution
TARDBP primary	Rabbit	ProteinTech	10782-2-AP	1:2000
P62 primary	Mouse IgG1	BD Biosciences	610832	1:1000
GAPDH primary	Mouse IgG1	Calbiochem	CB1001	1:15000
Secondary (800)	Mouse IgG1	Li-Cor	925-32210	1:15000
Secondary (680)	Rabbit	Li-Cor	925-68071	1:15000

Table 2.8 Western blotting antibodies

2.4.10.6 Imaging of membrane

Imaging of the membrane was performed using an Odyssey Fc imager (Li- CO R Biosciences, UK).

2.4.10.7 Coomassie staining

After the gel had run, it was removed from its casing and rinsed in deionised water. It was placed protein side up and covered with Coomassie blue stain and left overnight on a shaker at room temperature. Destaining was performed using Coomassie blue destaining solution, with two 30 min washes followed by a final 1 hour wash.

2.4.11 Transfections/HEK cells

2.4.11.1 Reagents and solutions

Opti-MEM® I Reduced Serum Medium (Life Technologies, 31985062)

Lipofectamine® 2000 (Life Technologies, 11668019)

Plasmids for expression of DPR were obtained from Biogen Idec.

2.4.11.2 Transfection protocol

Human Embryonic Kidney (HEK) 293 cells were plated down in a 24 well plate, with 100 000 cells per well. The following day, when 70-90% confluent, the cells were transfected with plasmids. Lipofectamine® 2000 was gently mixed, diluted at 20µl/ml in Opti-MEM medium, and incubated for 5 min at room temperature. Meanwhile, plasmids (0.5µg for each DPR + 0.5µg GFP per well) were diluted in Opti-MEM medium. The Lipofectamine solution was then added to the diluted plasmid in a 1:1 ratio, gently mixed and incubated at room temperature for 20 min. 100µl of this complex was then added to each well containing cells and medium. Cells were incubated at 37°C in a CO_2 incubator overnight, prior to checking for transgene expression and subsequence immunocytochemistry.

2.4.12 Statistical analysis

All experiments were carried out on a minimum of three independent cultures. Within each experiment, three or more technical repeats were analysed. All data represented is from one hiPSC clone per individual with *C9orf72* associated ALS.

All quantitative immunocytochemistry was performed blind. All data is presented with error bars which represent the standard error of the mean (SEM). Comparisons between control and carrier lines was based on their individual data points. All data points were tested for normality using Anderson-Darling test, using Minitab17. Since most data was not normally distributed, non-parametric tests were used the Mann-Whitney test was mainly used. Statistical tests were run in GraphPad Prism5. P values <0.05 were considered statistically significant.

2.5 Immunohistochemistry

2.5.1 Solutions and reagents

Xylene (VWR Chemicals, 28975.325)

Ethanol (VWR Chemicals, 20821.330)

10mM citric acid, pH 6: Made up in distilled water

Citric acid (Fisher Scientific, C/6160/53)

pH to 6.0 with Sodium hydroxide

3% hydrogen peroxide: Made up in distilled water

Hydrogen peroxide (Sigma, 349887)

Blocking solution: Made up in PBS

Horse serum (Vector laboratories, S-2000), 3%

Triton-X100, 0.2%

PAP pen (Vector laboratories, H-4000)

Vectastain® Universal Elite ABC kit (Vector Laboratories, PK-7200), containing:

Normal Horse Serum

Biotinylated, Universal (Anti-Mouse IgG/Rabbit IgG) Antibody

Reagent A (Avidin DH)

Reagent B (Biotinylated Horseradish Peroxidase H)

TNS: Made up in distilled water

Trizma® base (Sigma, T6066), 6g per litre

pH to 7.4 with Nitric Acid (Fisher Scientific, N/2300/PB17)

DAB Peroxidase Substrate kit (Vector Laboratories, SK-4100), made up in TNS:

Buffer stock solution (1:50)

DAB stock solution (1:25)

Hydrogen Peroxide solution (1:50)

Nickel solution (1:50)

Haematoxylin (Thermo Scientific, LAMB/170-D)

Lithium carbonate (Sigma, L4283), saturated solution

DpX mountant (Sigma, 44581)

2.5.2 Immunohistochemistry protocol

Paraffin sections (cut to 4μm) which were previously prepared in Colin Smith's laboratory, were dewaxed in xylene and taken down to water through graded alcohols, by immersing in the following solutions for the times stated:

- Xylene – 3 min
- Xylene – 3 min
- 100% Ethanol – 3 min
- 95% Ethanol – 3 min
- 70% Ethanol – 3 min
- Water – 3 min

Antigen retrieval was then performed by placing the slides in 10mM citric acid, pH 6 and heating in a pressure cooker to 125°C for 30 seconds. The slides were then washed in PBS twice for two minutes each time, before being incubated in 3% hydrogen peroxide. The slides were then washed in PBS, before being marked with a PAP pen.

Blocking solution was then added to the slides, and incubated at room temperature for 1 hour in a humidified chamber. The primary antibody was prepared in 1% horse serum in 0.2% Triton-PBS. Excess blocking solution was removed and replaced with primary antibody solution, and incubated overnight at room temperature.

The slides were washed 3 times, for 10 min each in PBS. Secondary antibody (Biotinylated, universal; from Vectashield kit, diluted 1:200 in 1% horse serum in PBS) was then added and incubated for 2 hours. The slides were then washed 3 times, for 10 min each in PBS. Meanwhile, a mixture of Reagent A (1:200) and B (1:200) was prepared in PBS and left for 20 minutes, before being applied to the slides for 1 hour.

The slides were washed 3 times, for 10 min each in PBS, followed by two 10 min washes in TNS. DAB solution was freshly prepared and applied to the slides for approximately 3 min (test slide checked under microscope to determine optimal time, and all slides treated in this way). The slides were then washed in TNS for 10 min, before being transferred to distilled water. Counterstaining was performed by immersing slides in haemotoxylin for 1 min, followed by dipping in saturated lithium carbonate solution. The slides were then dehydrated into xylene by passing through the following solutions, for the stated times:

- 70% ethanol – 30 seconds
- 95% ethanol – 1 min
- 100% ethanol – 2.5 min
- Xylene – at least 1 min

The slides were then fixed in DpX mountant.

2.5.3 Antibodies

The DPR antibodies were produced by Biogen Idec., and raised in rabbit.

2.5.4 Imaging of slides

Immunoreactivity was assessed at 20x objective, representative images were taken using a Zeiss Axiovision microscope with Axiovision 4.8 software via a digital camera.

Chapter 3. Molecular genetic testing for the *C9orf72* hexanucleotide repeat expansion

3.1 Introduction

Genetic testing for the *C9orf72* HRE can help to define a diagnosis, and allows the risk to other family members to be assessed. Detection of the *C9orf72* HRE is challenging because of its large size and GC rich, repetitive nature. The main techniques that are currently used were described in Figure 1.2. The amplification of large expansions (>1000 repeats) is generally unfeasible using a conventional flanking PCR, and therefore other techniques including RP-PCR and Southern blotting are required for the detection of these (Warner et al., 1996). A summary of our current understanding of the repeat size ranges, and capacity to detect them is shown in Figure 3.1.

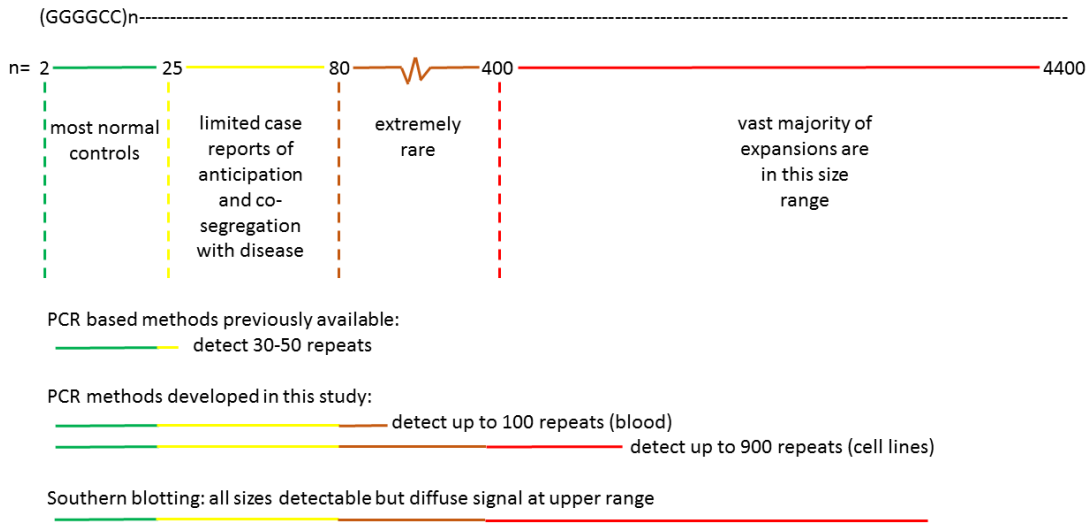

Figure 3.1 Size ranges and detection methods for C9orf72 $(G_4C_2)_n$ repeats

The coloured line indicates the range of possible $(G_4C_2)_n$ repeat sizes, where n= number of repeat units, and the colour shows the estimated likelihood of causing disease (green being least likely to red most likely). The majority of normal controls tested have less than 25 repeats. Short expansions (25 to 80 repeats) have been reported to segregate with disease in several families, whilst other in other cases have suggested anticipation can occur (Gijselinck et al., 2016; Xi et al., 2015a). There is then a jump in reported expansion sizes, with cases typically having between 400 and 4400 repeats (Beck et al., 2013). Current PCR methods allow identification of normal alleles and RP-PCR can detected whether an expansion is 30-50 repeats. The RP-PCR method described here can indicate that an expansion is at least 100 repeats and the flanking assay can detect up to 900 repeats in cell lines. Southern blotting can cover the entire range, but gives a weak signal at the larger size range.

A further challenge, which applies both to flanking PCR and Southern blotting, is the somatic heterogeneity which is seen in *C9orf72* HREs, particularly from blood samples presumably as they become increasingly unstable (Hubers et al., 2014). This results in a diffuse signal, which can be difficult to differentiate from background noise, and also makes assessment of the size of the expansion extremely challenging (Buchman et al., 2013).

3.1.1 PCR based methods

Within both research and diagnostic settings, it is desirable to have high-throughput, rapid PCR based tests which are highly accurate and use small quantities of input DNA (20-100ng). PCR is a widely used technique, and with optimisation can be used to amplify most DNA templates. However, the amplification of GC-rich and long repetitive sequences remains challenging. DNA with $(GGGGCC)_n$ expansions can form stable secondary structures such as G-quadruplexes (Haeusler et al., 2014; Sket et al., 2015), which are thought to prevent DNA polymerase from extending the template during PCR. In terms of genetic testing for the presence of the *C9orf72* HRE, a conventional flanking PCR can be used to accurately define the size of most normal alleles (up to around 30 repeats). RP-PCR can be used to determine whether there is an expansion present or not, although cannot reliably provide information on the size of large expansions. The difficulties surrounding PCR amplification of the *C9orf72* HRE have been highlighted by a blinded international study which showed a wide variability in results obtained by different research laboratories using PCR methods (Akimoto et al., 2014). Furthermore, the presence of variable deletions and insertions at the 3' end of the repeat expansion (van der Zee et al., 2013), can affect the reliability of PCR assays targeting this region (Rollinson et al., 2015). Broadly, there have been two approaches to overcoming this problem, firstly reagent development and secondly optimization of cycling conditions (Orpana et al., 2012).

The addition of co-solvents is a common approach to improve PCR amplification, particularly for GC-rich sequences. These co-solvents include DMSO (Seto et al., 1995; Sun et al., 1993), betaine and glycerol (Henke et al., 1997). These are thought to work by disrupting base pairing, reducing secondary structure formation and reducing the melting temperature of the DNA (McDowell et al., 1998). Similarly the inclusion of modified nucleotides such as 7-deaza-2'-deoxyguanosine triphosphate (7-deaza dGTP) can also enhance amplification (Dierick et al., 1993; McConlogue et al., 1988). Combinations of these reagents often work best (Musso et al., 2006), and it can be hard to predict which will work for a given template. This must be determined empirically, and care must be taken as DMSO, for example, can inhibit DNA polymerase in high concentrations (Landre et al., 1995). Developments in DNA polymerase

blends have also improved amplification of long, GC-rich templates (Hećimović et al., 1997; Mukai and Nakagawa, 1996).

Alterations in conventional PCR cycling methods have also been applied to difficult templates. Examples of these include 'Two-step hot PCR' (Schuchard et al., 1993), 'Slowdown PCR' (Frey et al., 2008) and 'Hotstart and Touchdown PCR' (D'Aquila et al., 1991; Don et al., 1991). Another method which has emerged is 'Heat Pulse Extension (HPE) PCR' which has been applied to long-range PCR for Fragile X syndrome and Myotonic Dystrophy Type I, both of which are caused by large GC-rich triplet repeat expansions (Orpana et al., 2013; Orpana et al., 2012). In this technique, multiple short heat pulses are introduced to the extension stage of the PCR cycle, which are thought to destabilize any secondary structures which would otherwise cause the Taq polymerase to stall, improving PCR amplification efficiency (Orpana et al., 2012). The two reported applications of this technique have used a conventional style 'flanking PCR' to detect amplicons which are up to a maximum of 5 kb in size (Orpana et al., 2013). The larger *C9orf72* expansions detected by Southern blot may not be amenable to PCR amplification, but I was interested to determine if HPE PCR could increase the current upper limit of detection by PCR. Also, since RP-PCR can be used to detect even the largest expansions, I wanted to determine whether the HPE PCR conditions would be successful for this type of assay.

3.1.2 Objectives

This chapter describes the original design and optimisation of PCR assays for the *C9orf72* HRE, which were then redesigned after the discovery of genomic instability in the 3' region of the repeat. The aim of this work was to improve the detection range of PCR based methods for the *C9orf72* HRE, as at the beginning of the study the published methods were limited to detection of alleles up to around 30 repeats by either flanking or RP-PCR, and Southern blotting was required to determine if there were greater than this number of repeats (DeJesus-Hernandez et al., 2011; Renton et al., 2011). Expanding the detection range of short expansions by PCR is an important step towards helping to define the lower pathogenic size range of *C9orf72* HRE. Having reliable PCR based assays to detect the presence of a *C9orf72* HRE was vital to the quality control of the later cell culture based work described in chapters 4 and 5 of this thesis, as well as the generation of an isogenic control line.

The PCR assays described were used to determine the prevalence of the *C9orf72* HRE in over 500 Scottish MND patients who had donated a DNA sample to the Scottish MND Register between 1989-2015. In addition, the methods were applied in a clinical diagnostic setting for

ALS and FTD patients within the South East Scotland Regional Genetics Service, with over 160 patients being tested between January 2013-November 2016.

3.2 Results

I designed a number of primers flanking the *C9orf72* HRE using a combination of Primer 3 (NCBI) and manual design. The primers were checked using OLIGO primer analysis software (Molecular Biology Insights, Inc, USA) to check for the predicted formation of secondary structures such as hairpins, dimers and self-complementation. The sequences and positions of these primers are detailed in Figure 3.2.

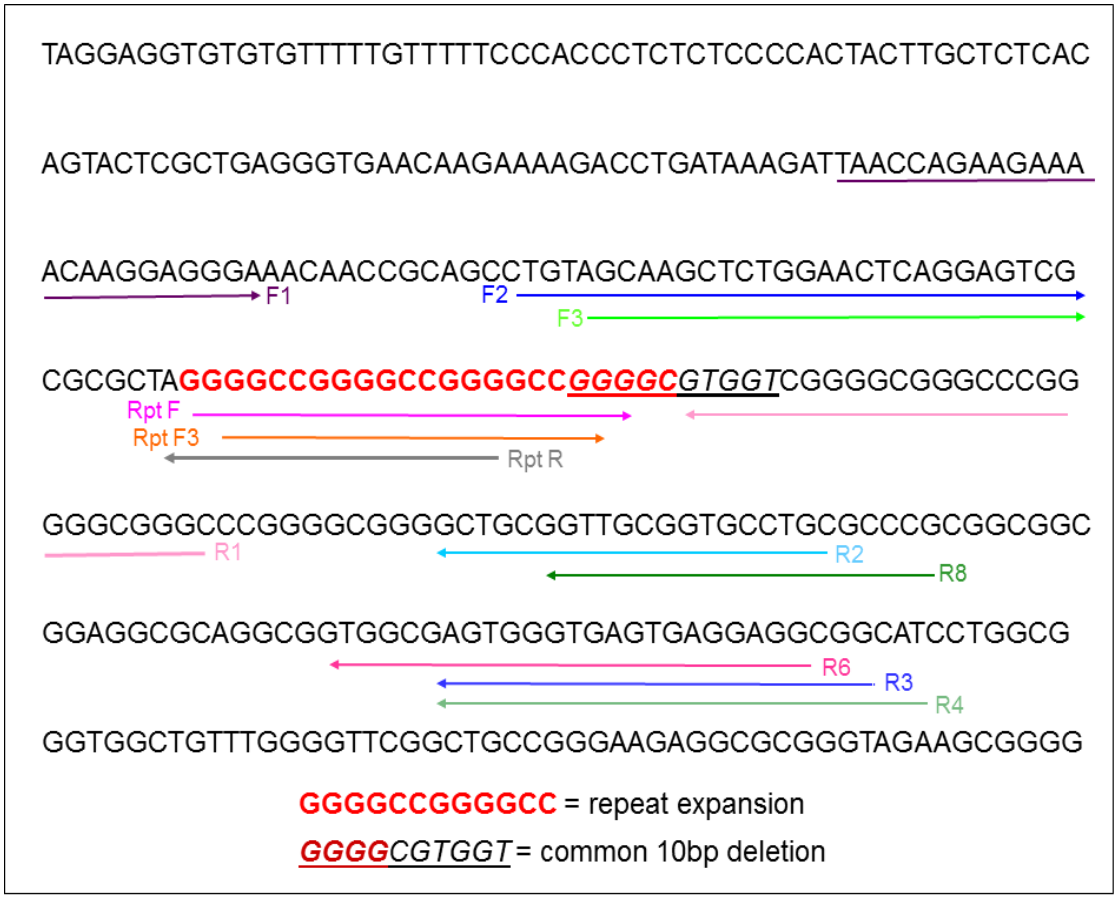

Figure 3.2 Primer locations for *C9orf72* PCR

Sequence flanking the *C9orf72* hexanucleotide repeat expansion (highlighted in red) with the location of the common 10 bp deletion which can hamper PCR (underlined). From GRCh37.p9 primary assembly, chr9: 27574028-27574389. F = forward, R = reverse and Rpt = Repeat. The main primers which have been used are shown and a complete list of sequences are detailed in Chapter 2 (Table 2.6).

3.2.1 Original flanking PCR

To design the optimal flanking PCR, I selected primers as close to the repeat expansion site as possible, to enable the best possible resolution and theoretical upper size limit of detection by capillary electrophoresis. Initially, I used primers F1+R2 and F3+R3 as these were well matched combinations in terms of their melting temperatures. I first attempted PCR with the conditions used in one of the first published RP-PCR assays (Renton et al., 2011), using the Roche Fast Start High Fidelity PCR system (Roche, 04 738 284 001). Despite numerous attempts, which included making alterations to magnesium concentration, running annealing temperature gradients and introducing a hot start to help denature the template, there was either no amplification, or a predominance of non-specific products of varying size when separated by agarose gel electrophoresis (example shown in Figure 3.3a). However, amplification was more successful for both primer sets using Qiagen Multiplex Mastermix and Q solution (Figure 3.3a), with the manufacturer's recommended cycling conditions (annealing temperature (T_a) = 60°C, 35 cycles) including a 15-minute initial denaturation step to activate the Hot Start Taq polymerase. Although primers F1+R2 showed some presumed non-specific products of approximately 600bp in size, the smaller size of the specific fragment (70 bp) was more desirable than that obtained with primers F3+R3 (150 bp). To try and improve the specificity of the reaction, I ran a gradient PCR for annealing temperatures of 60-70°C on three samples. The resulting gel shows that increasing the annealing temperature decreases the non-specific band intensity, and that an annealing temperature of 68°C permits a single band to be obtained for each sample (Figure 3.3b).

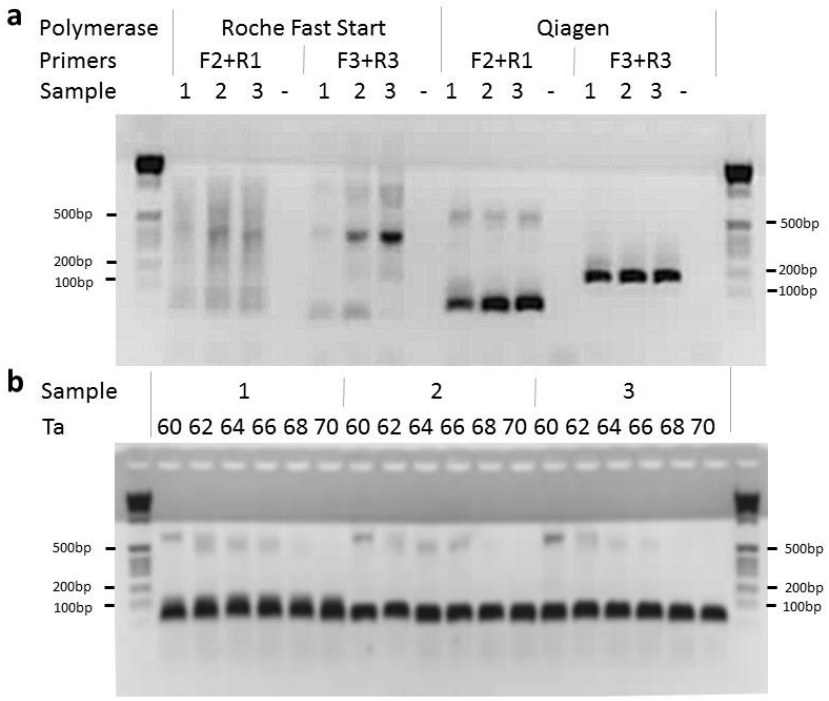

Figure 3.3 Flanking PCR optimisation of polymerase mix and gradient PCR to determine annealing temperature

(a) Products from flanking PCR of three normal control samples (1-3), and a zero (-) using either Roche Fast Start polymerase or Qiagen multiplex mastermix, and primer sets F2+R1 or F3+R3. (b) Gradient PCR for three samples using Qiagen multiplex mastermix and primers F2+R1, to assess the specificity of the reaction. The upper non-specific band is seen to gradually decrease in intensity as annealing temperature increases, and is not present at 68°C. Size in base pairs (bp).

When running a number of normal controls using these conditions, I identified several samples which were apparently heterozygous for repeat sizes, and in these cases it was apparent that there was severe preferential amplification of the smaller alleles (Figure 3.4a). To try and overcome this, I carried out further optimisation by comparing Q solution to what had been determined as the optimal co-solvents for the RP-PCR (7% DMSO and 0.6M Betaine). This showed that the presence of DMSO and betaine promoted improved amplification of the larger alleles, as reflected by their approximately 4-5 fold increased fluorescence compared to Q solution (Figure 3.4b).

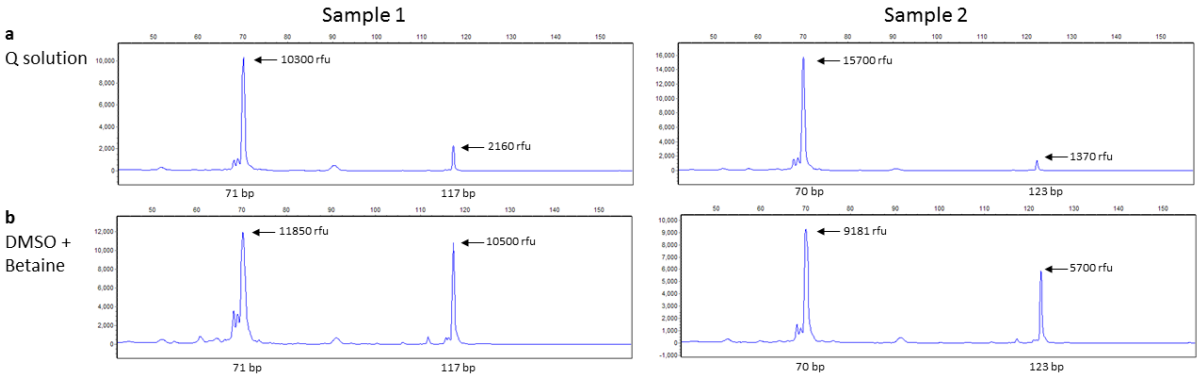

Figure 3.4 Assessment of co-solvents in flanking PCR

(a) Capillary electrophoresis trace following PCR amplification of two DNA samples with heterozygous normal repeat sizes, with Qiagen Muliplex Mastermix and Q solution. (b) Capillary electrophoresis trace following PCR amplification of the same two DNA samples with heterozygous normal repeat sizes, with Qiagen Multiplex Mastermix and 7% DMSO and 0.6M betaine. All fragment analysis traces are from GeneMarker (Soft Genetics) and x axis corresponds to size (bp) and y axis to relative fluorescent units.

To calibrate the flanking PCR sizes to repeat number, it would have been desirable to sequence the products from homozygous samples. However, the fragment of 70 bp which was commonest, was too short for Sanger sequencing, Therefore, I performed PCR on four samples which gave this fragment size on the flanking PCR (F2+R1), using primers F1+R4, and sequenced the products, which revealed they contained two GGGGCC repeats (Figure 3.5a). To check the specificity of the flanking primers F1+R2, I carried out a nested RP-PCR, using primers for the repeat sequence (F2+Repeat R+Tail R), on PCR products which were apparently heterozygous for normal repeat sizes. This revealed a saw-tooth pattern with peaks approximately every 6 bp, which suggested that the flanking PCR was specific to the *C9orf72* expansion (Figure 3.5b-c). This also provided another method by which to check the sizes against the number of repeats as the repeat containing primer had 3 repeats, and therefore the first peak (75 bp) of the saw-tooth pattern corresponds to 3 repeats and the others can be counted from this (Figure 3.5c). Therefore, for sample 1, the 70 and 117 bp peaks in the flanking PCR correspond with 2 and 10 repeats respectively, and for sample 2, the 100 and 117 bp peaks in flanking PCR correspond with 7 and 10 repeats respectively.

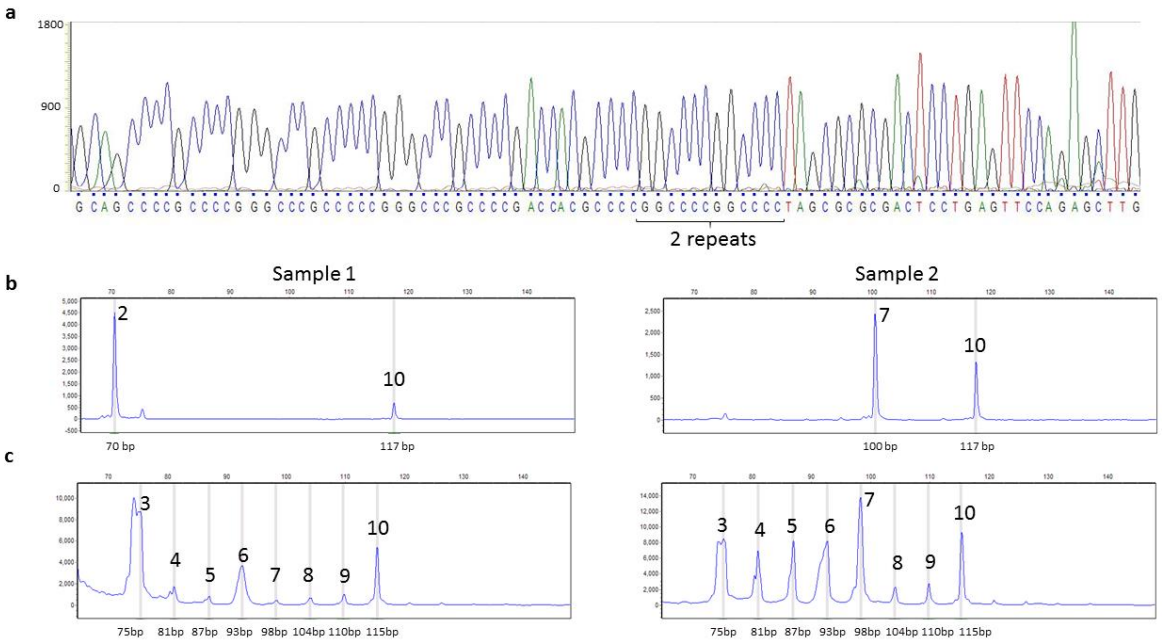

Figure 3.5 Calibration of original flanking assay

(a) Sequencing result from a flanking PCR product, from a sample which gives a homozygous 70 bp allele, showing the presence of two GGGGCC repeats (in reverse strand). Unidirectional sequencing only was performed. Sequencing trace was obtained from Sequence Scanner (Applied Biosystems). Y axis represents relative fluorescent units (rfu) (b) Flanking PCR products from two heterozygous normal samples after Ampure clean-up to remove primers, and prior to nested RP-PCR. (c) Products from samples in b, after nested RP-PCR. Repeat sizes are noted above the peaks, and corresponding size in base pairs (bp) is noted below the peak. All fragment analysis traces are from GeneMarker (Soft Genetics) and x axis corresponds to size (bp) and y axis to rfu.

A range of control DNA samples were tested using these conditions, and revealed expected patterns with the majority having an allele at approximately 70 bp, and some having an additional larger allele. This assay was used in diagnostic testing for 92 samples from 2013-2015. The upper size limit of the assay was determined to be approximately 26 repeats and was not expected to amplify alleles that were greater than around 30 repeats. Some example traces with a range of normal alleles are shown in Figure 3.6, and it can be seen from these that preferential amplification of the smaller allele becomes an increasing problem when there is a second allele with greater than 20 repeats present.

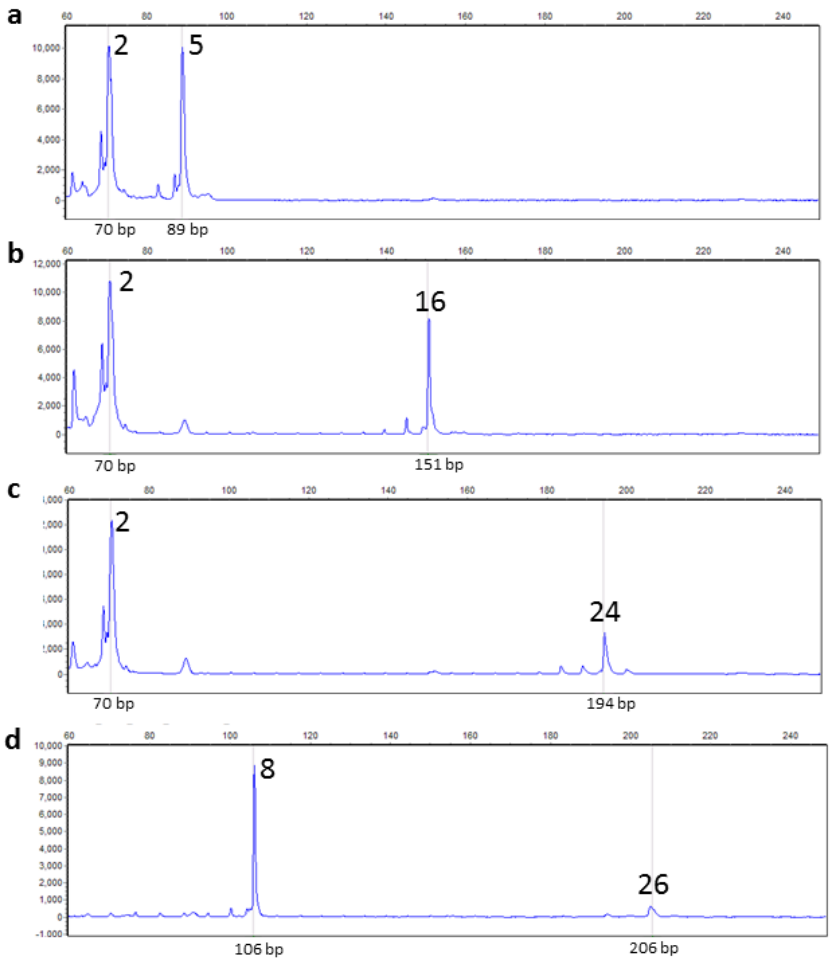

Figure 3.6 Original flanking PCR examples

Capillary electrophoresis traces from flanking PCR products of heterozygous normal samples with (a) 2 and 5 repeats, (b) 2 and 16 repeats, (c) 2 and 24 repeats and (d) 8 and 26 repeats. These show the preferential amplification of larger alleles which becomes more pronounced when there is an allele greater than ~20 repeats. All fragment analysis traces are from GeneMarker (Soft Genetics) and x axis corresponds to size (bp) and y axis to relative fluorescent units.

3.2.2 Redesigned flanking PCR

Following the observation of common deletions and insertions at the 3' end of the HRE (Rollinson et al., 2015; van der Zee et al., 2013), and which were under the site of one of the flanking PCR primers (R1), I decided to re-design these primers. At the same time, I decided to try altering the PCR mixture and cycling conditions based on an assay that had been developed for another GC-rich PCR template which used heat-pulse extension PCR (Orpana et al., 2012). Although this method reportedly relies heavily on unusual cycling conditions, the polymerase mix that is used, DyNAzyme EXT Taq (ThermoScientific), is suited to

difficult templates and long range PCR. The aim was to investigate whether these changes to PCR conditions could increase the size range which could be detected above 30 repeats.

I applied these conditions for several primer sets (F2+R2, F2+R3, F2+R4), and also ran annealing temperature gradients for these, however there was either no amplification or non-specific products were generated (data not shown). Because some of these primers were mis-matched for their melting temperature and the fragments were shorter than recommended for HPE PCR, I designed new reverse primers and found that a combination of F3+R6 gave the expected allele sizes for a number of samples which were of known repeat size from previous testing. It became clear after running several samples that these reaction conditions were allowing amplification of larger alleles than the original PCR assay, and that preferential amplification was reduced.

Having identified a cell line DNA sample which appeared to have an allele which was 576 bp (estimated 88 repeats), I ran an annealing temperature gradient using this sample (Figure 3.7). The highest level of fluorescence for the larger repeat allele (1350 rfu) was obtained at 58°C, with this product becoming gradually less abundant as the annealing temperature increased, until at 64°C and above there is very little or no amplification of even the 2 repeat allele.

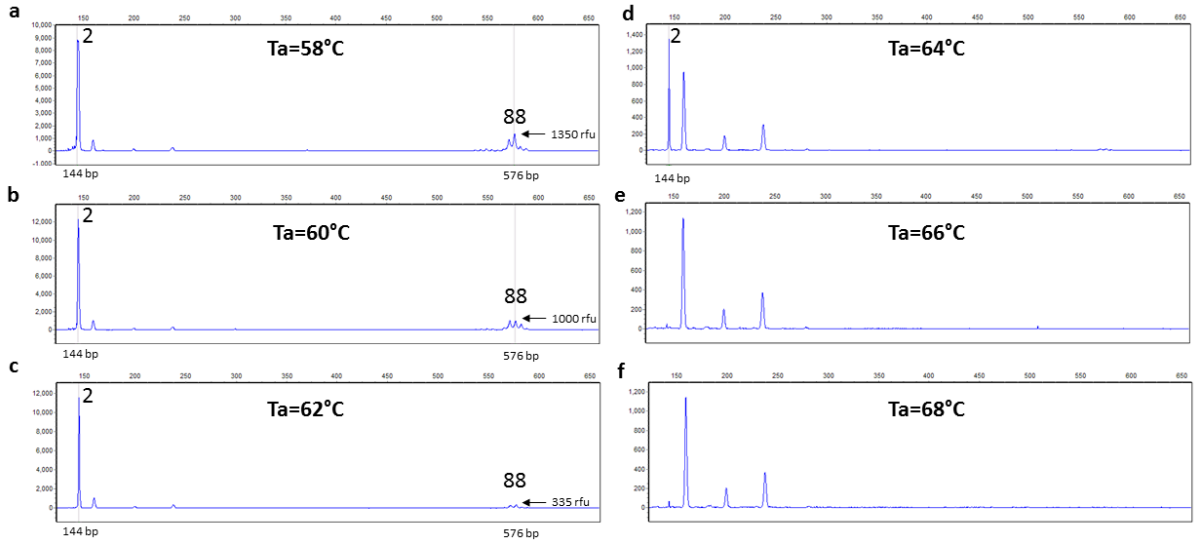

Figure 3.7 Gradient PCR for HPE flanking PCR

Capillary electrophoresis traces from flanking PCR products showing an annealing temperature gradient for primers F3+R6 on a cell line DNA sample with 2 and 88 (GGGGCC) repeats. (a) 58°C shows the highest yield of 88 repeat containing material (b) 60°C (c) 62°C and (d) 64°C only permits weak amplification of the 2 repeat allele (e) 66°C and (f) 68°C does not allow amplification. All fragment analysis traces are from GeneMarker (Soft Genetics) and x axis corresponds to size (bp) and y axis to relative fluorescent units.

As the products were slightly larger for this PCR than the original one, Sanger sequencing was directly performed to check that the specificity of the product and to calibrate the fragment sizes to repeat numbers (example in Figure 3.8). A range of flanking PCR product sizes were sequenced (up to 20 repeats). I also ran 41 samples which had been genotyped using the original assay and confirmed that these gave concordant sizing results.

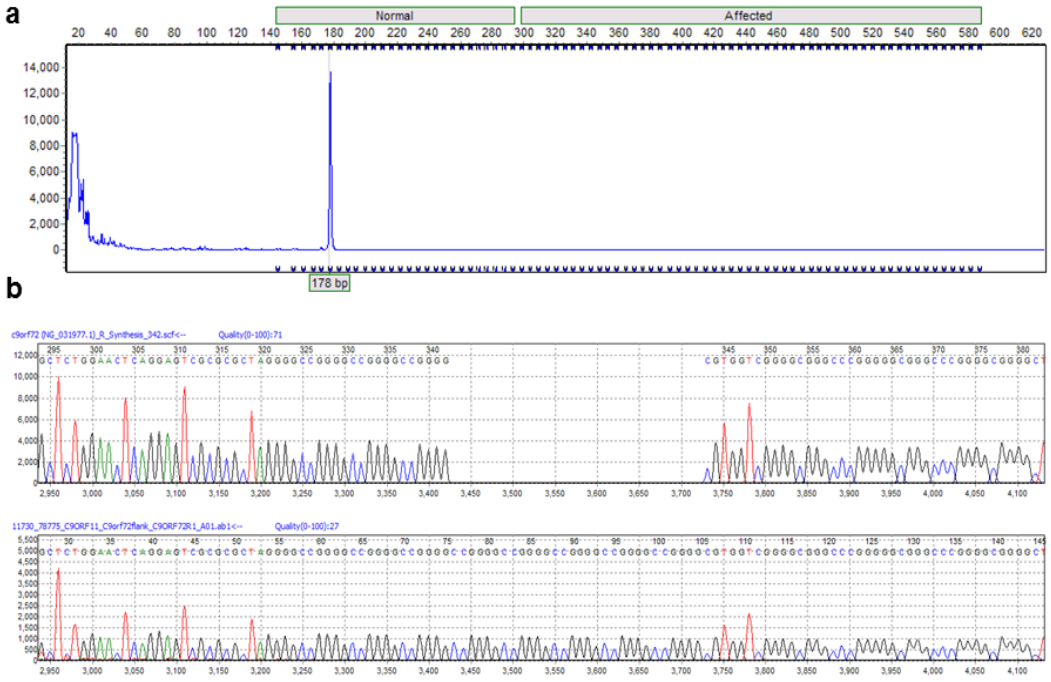

Figure 3.8 Example of Sanger sequencing of HPE flanking PCR products to calibrate fragment size to number of repeats

(a) Capillary electrophoresis trace of flanking PCR products from a patient who is homozygous, with one allele at 178 bp. Fragment analysis traces are from GeneMarker (Soft Genetics) and x axis corresponds to size (bp) and y axis to relative fluorescent units. (b) Sanger sequencing of the product reveals that it contains 8 GGGGCC repeats. Traces are from Mutation Surveyor (Soft Genetics) (upper panel is reference sequence (NG_031997.1)) and lower is the sample that gave a 178 bp band on the flanking PCR.

Because of the somewhat unconventional cycling conditions, I decided to test which aspects of this were necessary for amplification by comparing this for samples with the large normal alleles. Heat pulse extension was compared to constant temperature extension, and then the the two-step denaturation and the slow ramping were subsequently removed. A schematic of the cycling conditions which were compared is shown in Figure 3.9a. The first feature that I tested was whether the heat pulses to 86°C or 90°C during the extension phase altered the intensity of the products. The results of this comparison, as exemplified by the results for a sample with 8 and 26 repeats, showed that replacing the heat pulses with constant temperature extension at 78°C for 6 minutes made little difference to the amplification of larger allele (both show >9000 rfu) (Figure 3.9b,c). Considering the potential detrimental effects of pulsing on the PCR machine, and the observation that a constant temperature extension improved the RP-PCR assays, I decided to use constant temperature extension for further optimisation. I then investigated whether the slow ramp (12% or 0.6°C/s) from annealing to extension temperature or two-step denaturation (94°C for 45s, then 98°C for 10 s) improved amplification. Replacing the two-step denaturation step with a single denaturation step (94°C for 55 s) resulted in a marginally reduced yield of the larger product (8800 rfu vs 9200 rfu) (Figure 3.9d), as did increasing the ramp rate to 100% (9100 rfu vs 9200 rfu) (Figure 3.9e). Finally, I compared the results of constant extension for 3 min versus 6 min (Figure 3.9f). For alleles up to 90 repeats in size, this appeared to make little difference, but there was a smear apparent in two positive cell line DNA samples that was more apparent with the longer extension time. Along with the results obtained for RP-PCR, the cycling conditions which were determined as optimal include constant temperature 6 min extension, two-step denaturation and slow ramping.

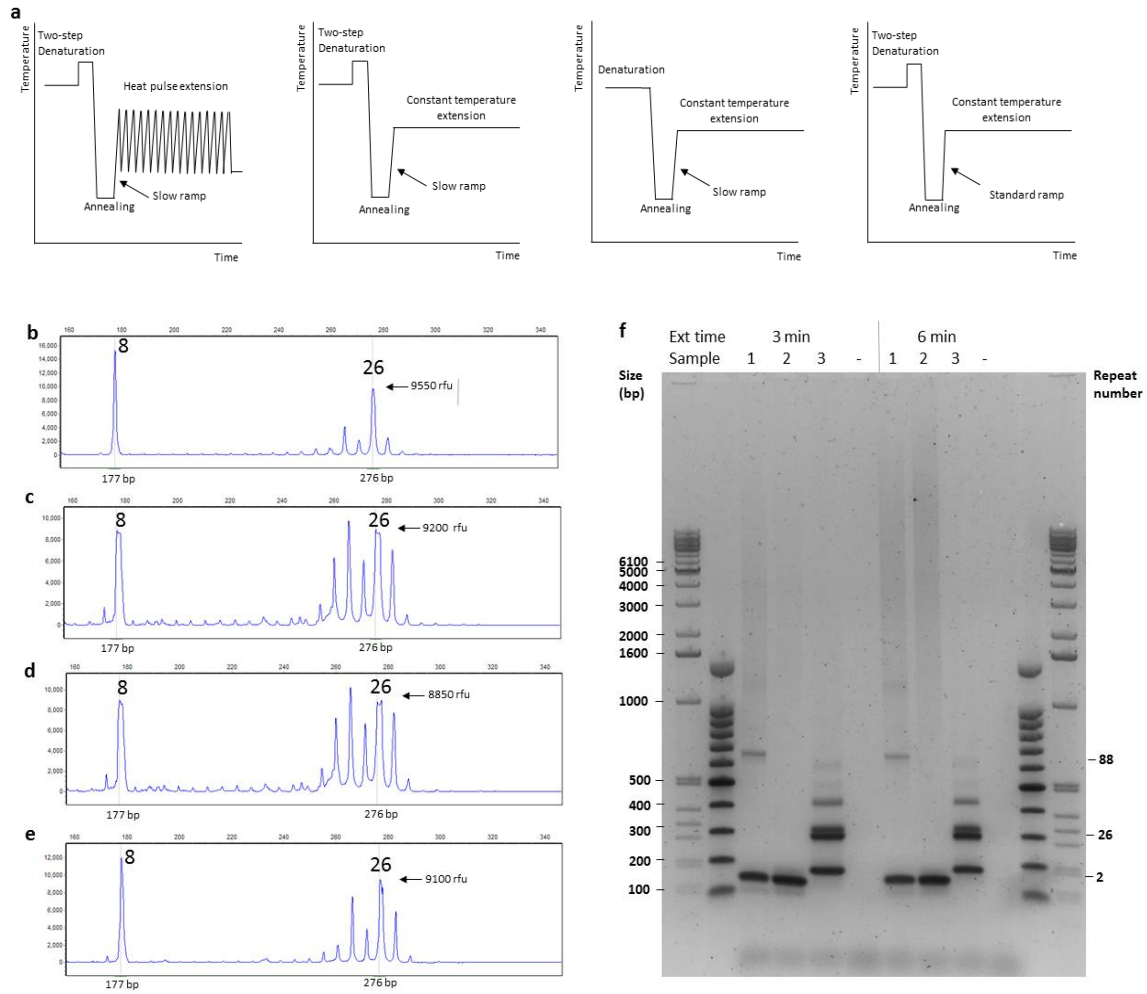

Figure 3.9 Optimisation of cycling conditions for flanking PCR

(a) Schematic of PCR cycling conditions which were compared. (b-e) Capillary electrophoresis traces showing an 8 and 26 repeat carrier with flanking PCR performed with (b) heat pulse extension, two-step denaturation and slow ramping, (c) constant temperature extension, two-step denaturation and slow ramping, (d) constant temperature extension, single-step denaturation and slow ramping and (e) constant temperature extension, high denaturation and normal ramping. (f) Agarose gel electrophoresis images showing PCR products after 3 or 6 minute constant temperature extension, two-step denaturation and slow ramping for (1) a cell line from an expansion carrier with 88 repeats present (2) a cell line from an expansion carrier with unknown repeat number (3) an 8 and 26 repeat carrier (-) negative PCR control. All fragment analysis traces are from GeneMarker (Soft Genetics) and x axis corresponds to size (bp) and y axis to relative fluorescent units.

These conditions allowed balanced amplification of normal alleles between 2 and 26 repeats in length (Figure 3.10a-c). Particularly because of the large smears of greater than 1000 bp that I had observed for several expanded samples after agarose gel electrophoresis, I wanted to determine what the upper range of the PCR assay was. I obtained two samples, from whole

blood with short expansions detected by Southern blot which were kindly sent by James Polke (Institute of Neurology, UCL, Queen Square, London). One of these samples had approximately 60 repeats, and was mosaic for a longer expansion (James Polke, personal communication), while the second sample had somatic mosaicism for 70-120 repeats estimated by Southern blotting (Fratta et al., 2015). Both of these samples had amplification of short expansions which were detectable following PCR with this assay, and these revealed a high level of mosaicism (Figure 3.10d-f). The highest peaks in the '60' repeat sample corresponded with 71 repeats by the PCR method, while the '70-120' repeat samples peaked at approximately 82 repeats. I observed that several patient samples which were positive for *C9orf72* expansions on RP-PCR, revealed a large diffuse smear from 1 - >10 kb when the flanking PCR products were separated by agarose gel electrophoresis (Figure 3.10f).

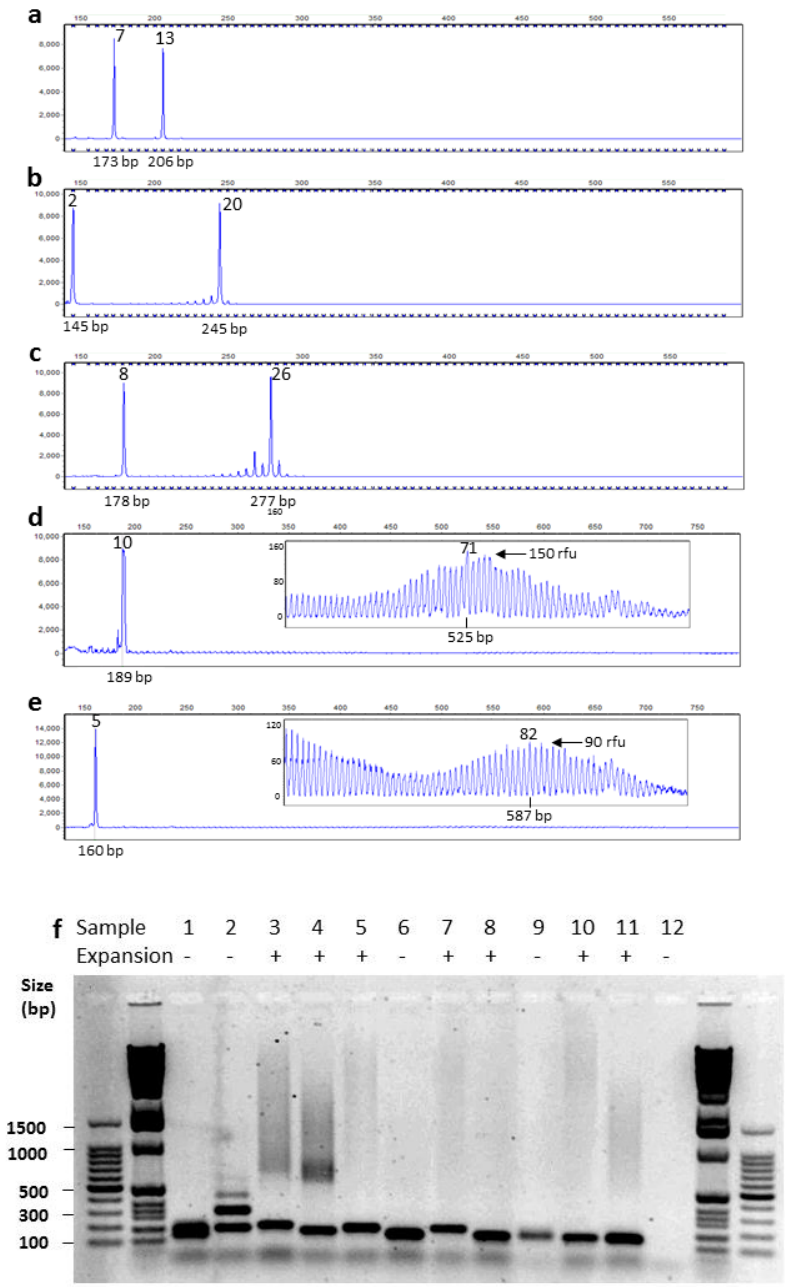

Figure 3.10 Optimised flanking PCR results

Flanking PCR products separated by capillary electrophoresis (a-e) from blood derived DNA with (a) 7 repeat and 13 repeat alleles (b) 2 and 20 repeat alleles (c) 8 repeat and 26 repeat alleles (d) a sample estimated to have 5; 60 repeats, with somatic mosaicism for a large expansion by Southern blot and (e) a sample estimated to have 5; 70-120 repeats by Southern blot (Fratta et al., 2015). All traces are from GeneMarker (Soft Genetics) and x axis corresponds to size in base pairs (bp) and y axis to relative fluorescent units. The inner box shows the zoomed in trace where the x axis is consistent with that of the overall trace. (f) Agarose gel electrophoresis of flanking PCR products from blood DNA with 100 bp and 1 kb extension DNA ladders. Lane: 1. Normal control (2;5 repeats). 2. Normal control (8;26 repeats). 3. Expansion

carrier (10;60 mosaic repeats). 4. Expansion carrier; (5;70-120 repeats). 5. Expansion carrier (8 repeats; expansion). 6. Normal control (2; 2 repeats). 7. Expansion carrier (8 repeats; expansion). 8. Expansion carrier (2 repeats; expansion). 9. Normal control (2; 5 repeats). 10. Expansion carrier (2 repeats; expansion). 11. Expansion carrier (2 repeats; expansion). 12. No DNA control.

The smears that I had observed on agarose gel electrophoresis following flanking PCR of expanded carriers were intriguing and I was interested in determining what the upper detection limit of the PCR was. As it had been observed that cell line DNA gave sharper bands and lower size than peripheral blood DNA using Southern blotting (Beck et al., 2013; van Blitterswijk et al., 2013b), I decided to test such samples by PCR. I obtained lymphoblast cell line (LCL) derived DNA from Coriell Cell Repositories, and tested these to try and establish the upper size range of amplification by PCR. After agarose gel electrophoresis, it was observed that several of the cell lines showed bands up to a size of 5.7kb, corresponding with approximately 900 repeats (Figure 3.11). Expanded material was detected in 4 out of 7 lines tested, which is presumably because the other lines contained expansions which were beyond the size limit of detection by this method, which is supported by previously published Southern blotting results for ND10966, ND11836 and ND14442 (Liu et al., 2014). Comparison of our PCR results with these suggest that the very largest expansions are not amplified.

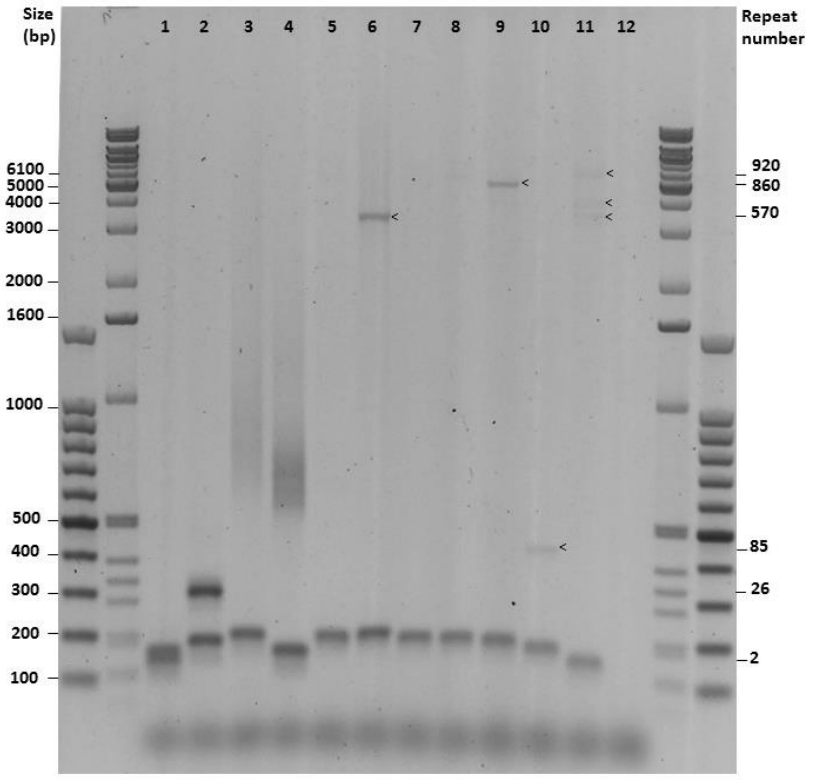

Figure 3.11 Flanking PCR for cell line DNA

Figure 3.11. Flanking PCR for cell line DNA

Agarose gel electrophoresis of flanking PCR products with 100 bp and 1 kb extension DNA ladders. Lane 1-4 Blood derived DNA: 1. Normal control (2;5 repeats). 2. Normal control (8;26 repeats). 3. Expansion carrier (10;60 mosaic repeats). 4. Expansion carrier; (5;70-120 repeats). 5-11 Coriell Cell Repositories *C9orf72* HRE positive LCL DNA: 5. ND09373 (10; Undetected expansion). 6. ND09438 (11; 570 repeats). 7. ND10966 (9; Undetected expansion). 8. ND10973 (9; Undetected expansion). 9. ND11836 (8; 860 repeats). 10. ND12199 (6; 85 repeats). 11. ND14442 (2; 600,700,920 repeats). 12. No DNA control.

3.2.3 Original RP-PCR

Because the largest expansions cannot be detected by flanking PCR, another method such as RP-PCR is required to determine if there is an expanded allele preent. I initially tried using the Roche FastStart polymerase and conditions as described in one of the first described assays (Renton et al., 2011), but had no success. However, as with the original flanking PCR, using the Qiagen Multiplex Mastermix with standard cycling conditions (primer F2+Repeat R, T_a=71°C) was more successful. This generated a product, which was predominantly 75 bp, with some evidence of a saw tooth pattern, as would be expected from a sample with heterozygous repeat sizes (Figure 3.12a). To try and overcome the apparent preferential amplification and encourage a more prominent saw-tooth pattern, I then tested seven control samples with a range of co-solvents (7% DMSO, 0.6M betaine and a mixture of both) and compared the results (representative images, Figure 3.12b-d), which demonstrate a higher yield of product for the DMSO and betaine mixture. A positive control sample was kindly sent by James Polke (Institute of Neurology, UCL, Queen Square, London) and this was used to further optimise this assay (Figure 3.12e). I first established the optimal primer concentrations of flanking, repeat and Tail R (Figure 3.12f). I then altered the cycling conditions to promote the binding of the repeat primer by using a high anneal (T_a=71°C) for the first ten cycles, and then reducing to T_a=60°C for a further 25 cycles to allow Tail R to bind which increased the product yield further, and led to longer fragments being produced (Figure 3.12g). Finally, I added 7-deaza-dGTP to the PCR mix, to try and further disrupt secondary structure formation, which led to a further increase in the product yield (Figure 3.12h).

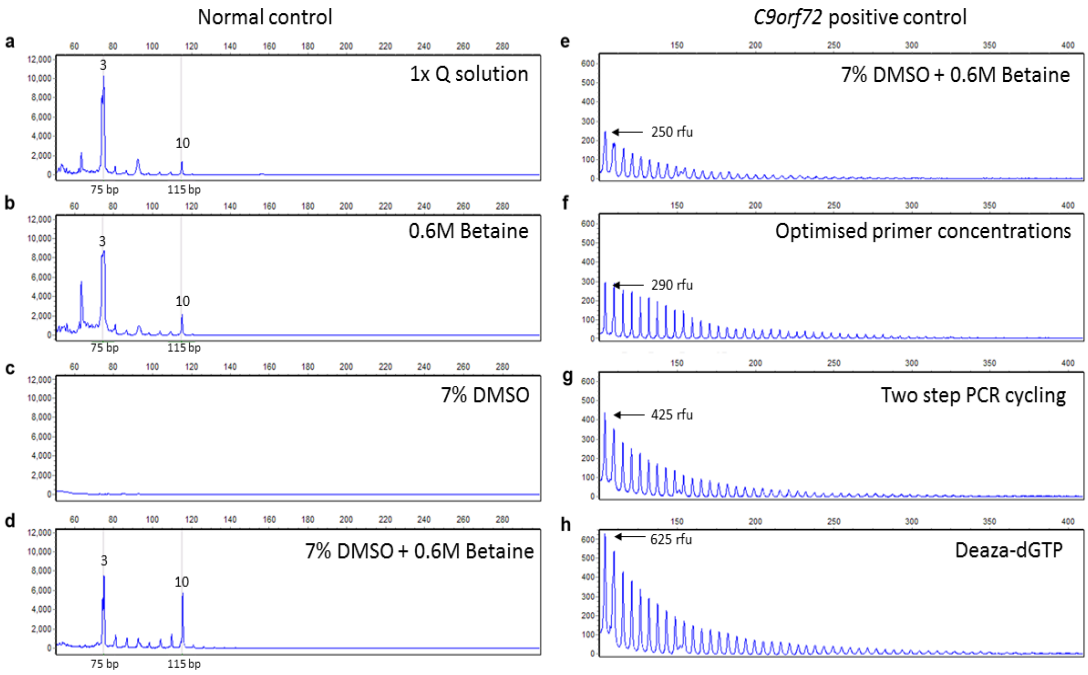

Figure 3.12 Optimisation of original 5' RP-PCR assay

Capillary electrophoresis traces of 5'RP-PCR products from normal controls (a-d) and *C9orf72* hexanucleotide expansion carriers (e-h) during optimisation of 5'RP-PCR. Using standard cycling conditions, T_a=71°C, different co-solvents were used to determine the optimal PCR mix for a sample with 2 and 10 repeats (a) 1x Q solution (b) 0.6M Betaine (c) 7% DMSO and (d) 7% DMSO plus 0.6M betaine. (e) This combination of DMSO and betaine allowed detection of the expanded repeat allele (zoomed in traces shown). (f) The PCR amplification was gradually improved by optimising primer concentrations and ratios between flanking primer, repeat primer and Tail R. (g) A two-step PCR protocol which involved lowering T_a to 60°C for the final 25 cycles to encourage priming by Tail R. (h) The addition of 7-deaza dGTP increased the signal strength and maximum product sizes obtained. All traces are from GeneMarker (Soft Genetics) and x axis corresponds to size (bp) and y axis to relative fluorescent units.

In line with recommendations for other repeat expansion disorders, I also developed an RP-PCR assay for the 3' end of the repeat. The optimised conditions for the 5' RP-PCR assay were then applied to PCR with primer R2, which appeared to have a similar amplification pattern, but tested whether there was a repeat from the 3' direction (Figure 3.13). The maximum size of fragments produced by the RP-PCR assays was around 350 bp, which corresponded to around 50 repeats. Thus, this assay could allow detection of an allele with an expansion of 30 repeats or more, which was the range suggested by the original paper to be pathogenic (Renton et al., 2011).

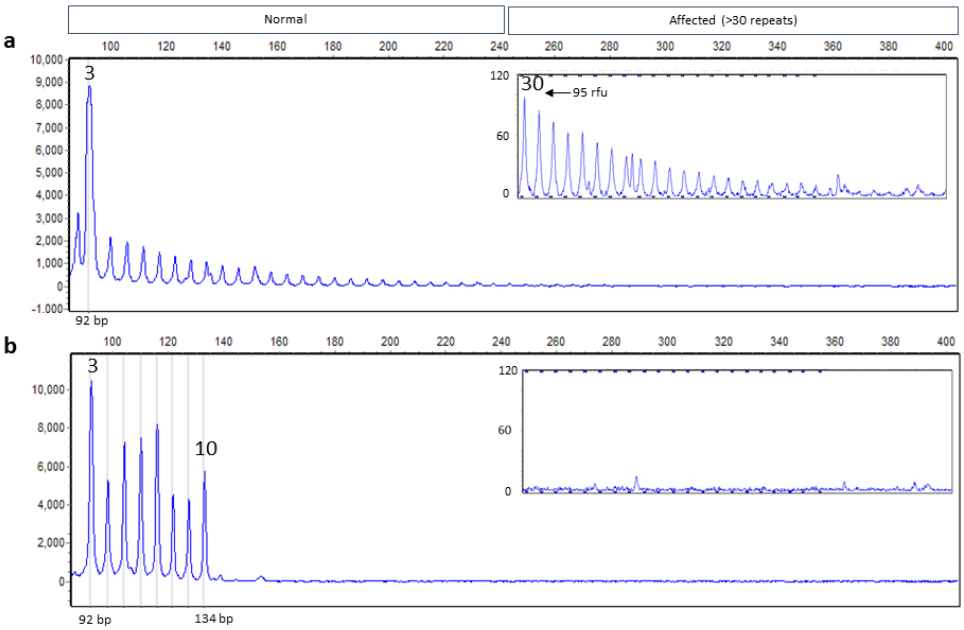

Figure 3.13 Original 3' RP-PCR examples

Capillary electrophoresis traces of 3'RP-PCR products from (a) a *C9orf72* HRE carrier (b) a normal heterozygous control with a maximum of 10 repeats. Repeats are counted from the first peak, which corresponds with the number of repeats in the primer (3). All traces are from GeneMarker (Soft Genetics) and x axis corresponds to size (bp) and y axis to relative fluorescent units. The inner box shows the zoomed in trace where the first peak corresponds with 30 repeats on the x axis.

3.2.4 Re-designed RP-PCR

3.2.4.1 5'RP-PCR

Following the vast improvement that was obtained with the flanking PCR when applying the HPE PCR conditions, I went on to try these for the RP-PCR assays. Applying this PCR mix and cycling conditions for the 5' RP-PCR assay, and using the previously optimised primer concentrations (for F2, Repeat R and Tail R), revealed a greatly improved amplification pattern. I ran a gradient PCR to establish the optimal annealing temperature for the primers, which was 62°C (data not shown). As for the flanking PCR, I investigated whether the heat pulses were necessary by comparing samples run with heat pulses or with a constant temperature extension of 6 minutes. This showed that there was a higher fluorescence at 30 repeats (350 with pulses compared to 480 without), the maximum size of the products were similar and there was less evidence of split peaks with a constant temperature extension (Figure 3.14).

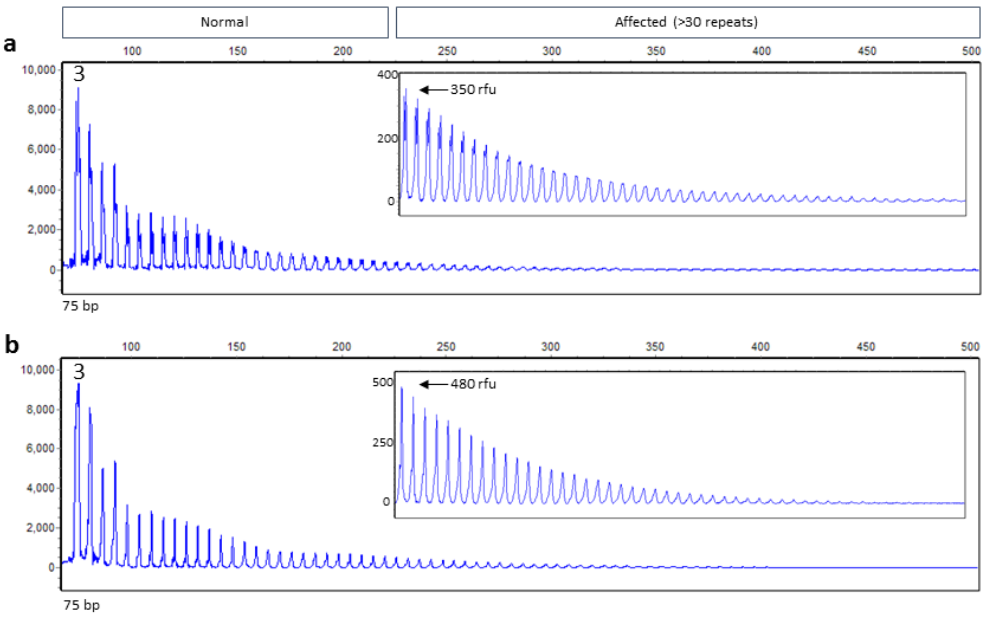

Figure 3.14 5'RP-PCR assay with heat pulse extension compared to constant temperature extension

Capillary electrophoresis traces of 5'RP-PCR with a *C9orf72* expansion carrier with (a) heat pulse extension PCR (b) constant temperature extension. The inner box shows an image of the baseline in the affected range. All traces are from GeneMarker (Soft Genetics) and x axis corresponds to size (bp) and y axis to relative fluorescent units. The inner box shows the zoomed in trace where the first peak corresponds with 30 repeats on the x axis.

Comparing samples tested by the original and newly optimised 5' RP-PCR assay showed that the new conditions promoted superior amplification. The resulting PCR products from the newly optimised conditions gave a brighter trace (3000 versus 100 rfu at 30 repeats) after capillary electrophoresis, and consistently larger products when an expansion was present, with reduced preferential amplification of the normal allele as shown (Figure 3.15a,b). Previously, it was necessary to closely scrutinise the baseline of each trace to determine whether there was an expansion present, whereas the new assay gave a more striking pattern in expansion positive samples. To validate this assay, 14 previously identified expansion carriers and 16 normal controls were tested and gave the expected result in all cases. An example capillary electrophoresis trace of a normal control following the original assay compared to the re-designed one is shown (Figure 3.15c,d).

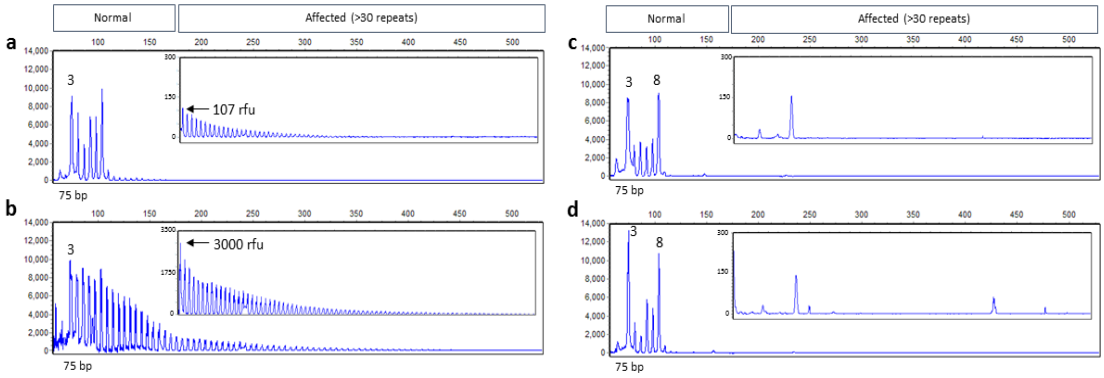

Figure 3.15 Improved PCR amplification of expanded alleles using the re-designed 5' RP-PCR assay compared to the original assay

(a) Capillary electrophoresis trace from the original 5' RP-PCR assay of an expansion carrier (b) a trace from the HPE 5' RP-PCR assay showing improved amplification. (c) Capillary electrophoresis trace from the original 5' RP-PCR assay of a normal control (2/8 repeats) compared to (d) a trace from the HPE 5' RP-PCR assay for the same normal control sample. All traces are from GeneMarker (Soft Genetics) and x axis corresponds to size (bp) and y axis to relative fluorescent units. The inner box shows the zoomed in trace where the first peak corresponds with 30 repeats on the x axis.

3.2.4.2 3'RP-PCR

For the 3'RP-PCR, as for the flanking PCR, it was important to consider the genomic variability of the region adjacent to the repeat expansion, and the impact that this may have on PCR amplification. Indeed, it proved challenging to optimise the 3' RP-PCR assay, although in this case the genomic variability did not seem to be the problem. Initially, as for the 5' RP-PCR assay, I tried the PCR mix and conditions described by Orpana *et al*., with the previously optimised RP-PCR primer concentrations (R2, Repeat F and Tail R), and then investigated the various aspects of the cycling conditions as for the flanking PCR (Figure 3.9a). As for the 5'RP-PCR assay, constant temperature extension gave a slightly higher fluorescence signal at 30 repeats than heat pulse extension so we used the latter (data not shown). It appeared that there was more amplification with slow (12%) ramping and a two-step denaturation improved amplification so these conditions were used (representative images, Figure 3.16).

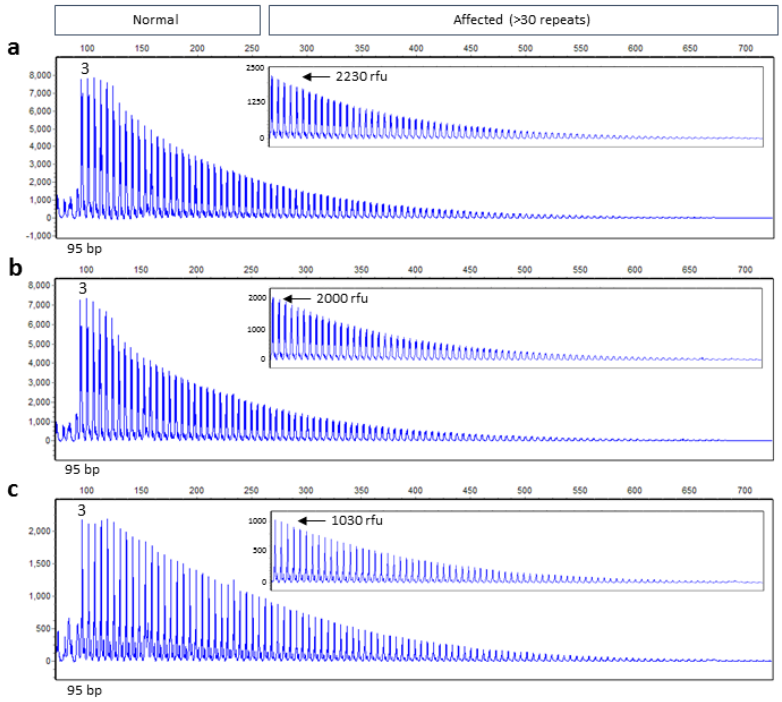

Figure 3.16 Comparison of 3'RP-PCR with varying ramp rate and denaturation temperature

Capillary electrophoresis traces of 3'RP-PCR products from a *C9orf72* expansion carrier with (a) Two-step denaturation and 12% ramp rate (b) single-step denaturation and 12% ramp rate and (c) two-step denaturation and 100% ramp rate. The inner box shows an image of the baseline in the affected range. All traces are from GeneMarker (Soft Genetics) and x axis corresponds to size (bp) and y axis to relative fluorescent units. The inner box shows the zoomed in trace where the first peak corresponds with 30 repeats on the x axis.

The resulting PCR was higher yielding as shown by the higher fluorescence on the capillary electrophoresis traces comparing the new assay to the original one for expansion carriers (Figure 3.17a-b), but it was notable that in the presence of an expansion, there was a lack of amplification from the normal allele, giving a notable pattern whereby the size of the first peak varied, which would be expected in the presence of insertions and deletions within the PCR amplicon (Figure 3.17c-d). However, this PCR also gave weak false positive results for two negative controls (Representative example; Figure 3.17e), both of which had two normal alleles on flanking PCR and no expansion detected by 5' RP-PCR (data not shown). To try and increase the reaction specificity, I tried altering the annealing temperature. I ran a gradient (62-67°C) and found that increasing the annealing temperature appeared to reduce the false positive effect (T_a=62°C, Figure 3.16e; T_a=65°C, Figure 3.17f), but that it also reduced the

yield of the expected product from the normal and expanded alleles and so this did not offer an ideal solution.

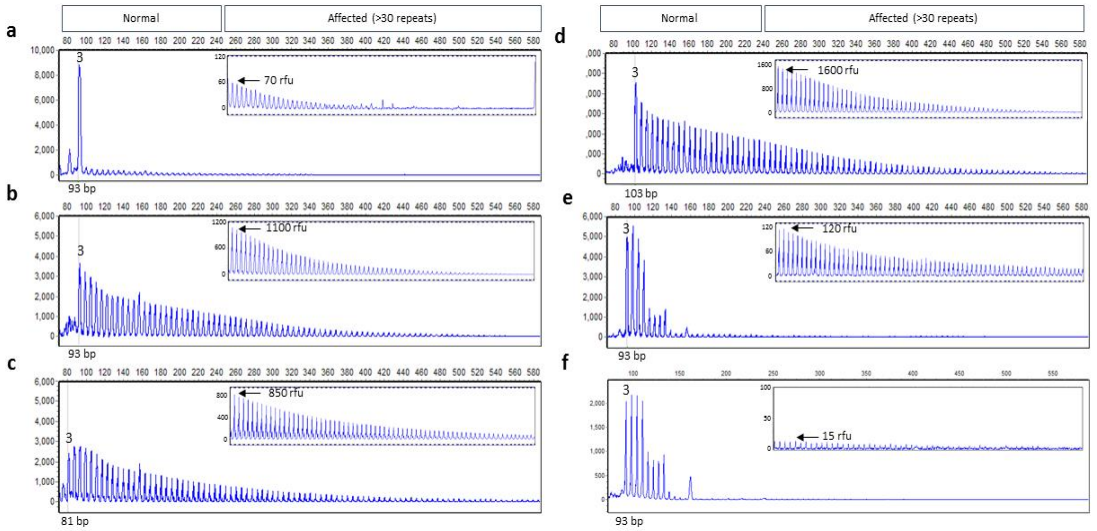

Figure 3.17 Optimisation of the re-designed 3' RP-PCR assay

(a) Capillary electrophoresis trace from the original 3' RP-PCR assay of an expansion carrier compared to (b) a trace from the re-designed 3' RP-PCR assay showing improved amplification. (c) A sample with an apparent deletion within the PCR amplicon indicated by the shifted start position (from 93 bp to 81 bp) of the saw-tooth pattern (d) Result from a sample with an apparent insertion within the PCR amplicon indicated by the shifted start position (from 93 bp to 103 bp) of the saw-tooth pattern. (e) A negative control sample with weak saw-tooth pattern indicating a false positive result (T_a=62°C) (f) A negative control sample with weaker saw-tooth pattern (T_a=65°C). The x axis corresponds to size in base pairs (bp) and y axis to relative fluorescent units. The inner box shows the zoomed in trace where the first peak corresponds with 30 repeats on the x axis.

To try and establish whether the primer choices were the cause of the false positive effect, I carried out PCR with several different flanking primers (R6, R7, R8, R9). None of these overcame the problem, as either they gave no product or they showed the same effect (data not shown), and therefore it seemed more likely that the repeat-binding primer needed to be re-designed. I removed one repeat unit from the primer and also altered the phase so that it had a different start point along the repeat tract. This primer, in combination with R6, eliminated the effect in most normal samples, with false positives being limited to samples with large normal alleles, with those over 15 repeats being affected (Figure 3.18). I tried reducing cycle number, reducing polymerase concentration and altering primer concentrations but these did not overcome the effect without having a significant impact on the yield of the expected product. I also designed a primer which was 'clamped' to the 5' end of the repeat by the addition of 2 bases complementary to this region, to try and encourage specific binding from

the end of the repeat and reduce replication slippage but this did not eliminate the effect either (data not shown).

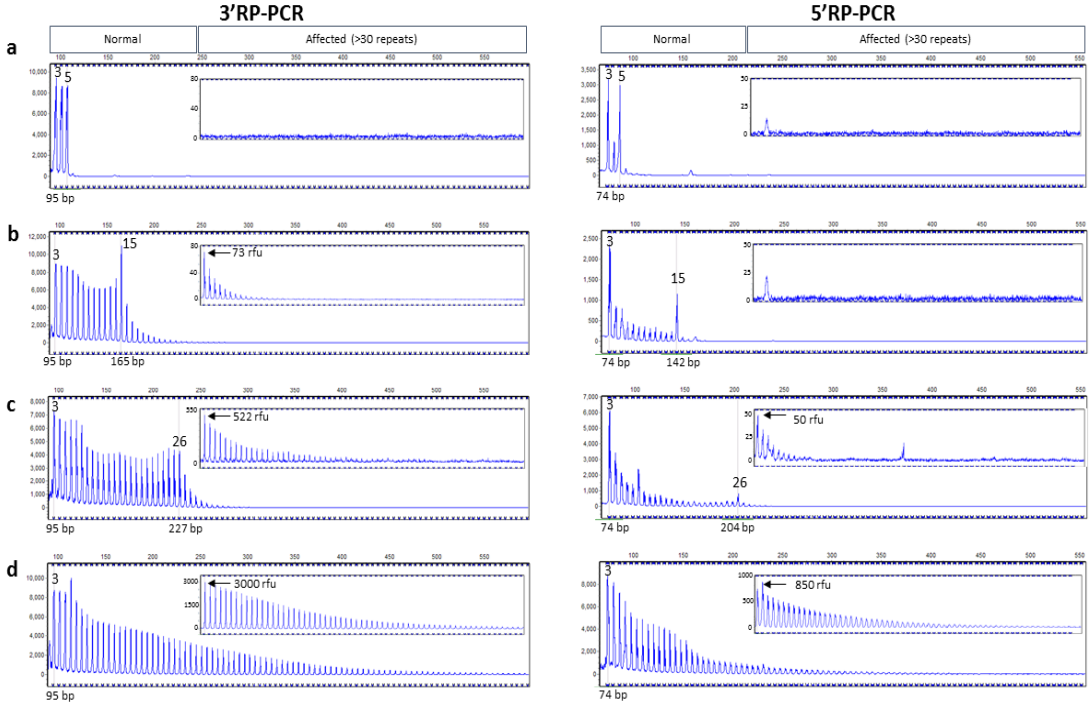

Figure 3.18 3'RP-PCR artefact which is only present in the presence of normal alleles greater than 15 repeats, which is not observed for 5'RP-PCR.

(a) Heterozygous normal sample (2;5 repeats) (b) Heterozygous normal sample (2;15 repeats) amplified with 3'RP-PCR showing weak stuttering into the affected range, with 5'RP-PCR showing no presence of product >30 repeats. (c) Heterozygous normal sample (8;26 repeats) amplified with 3'RP-PCR showing stuttering into the affected range, with 5'RP-PCR showing 10-fold weaker stuttering into the expanded range. (d) Heterozygous expansion carrier showing stronger signal in the affected (>30 repeat) size range in both assays compared to the samples with large normal alleles. All capillary electrophoresis traces are for 3'RP-PCR (left) and 5'RP-PCR (right), and are from GeneMarker (Soft Genetics). The x axis corresponds to size in base pairs (bp) and y axis to relative fluorescent units. The inner box shows the zoomed in trace where the first peak corresponds with 30 repeats on the x axis.

Using the new primer combinations (R8 and Repeat F3), the traces for expansion carriers showed higher yield than for the original assay and larger products with this assay, as was also the case for the 5'RP-PCR. This assay was validated with 15 previously identified expansion carriers and 17 normal controls, which all gave concordant results.

Although it appears from the pattern of altered start sites that this assay is detecting expansions even in the presence of insertions and deletions within the region, to confirm this I exploited the lack of amplification of normal alleles that was apparent during optimisation using primer

R6, to sequence the 3' region of expanded repeat alleles following RP-PCR. The full results of this analysis are shown in Table 3. This showed that the optimised 3'RP-PCR was still amplifying product even in the presence of genomic variability at the 3' end of the repeat expansion.

Variation detected; (NM_031977.1)	**Number of *C9orf72* positive alleles**
g.5353_5364dupGCGGGCCCGGGG	**2**
g.5342_5343dupG	**1**
g.5344_5353dupGTGGTCGGGG	**1**
g.5344_5353delGTGGTCGGGG	**6**
g.5345_5349delTGGTCinsG	**1**
g.5344_5353delGTGGTCGGGGinsGCGGGCCCG	**3**
g.5344_5348delGTGGT	**1**
g.5343_5347delCGTGG	**1**

Table 3.1 Variability detected at 3' end of the repeat expansion in *C9orf72* positive ALS patients

To determine the sensitivity of the assay for mosaicism, I carried out admixture experiments for both RP-PCR assays (Fig 3.19). These showed that even when expanded material was diluted 1% in normal control DNA, the presence of the expansion was still just detectable with 30 repeats corresponding to 85-150 rfu (Figure 3.19d).

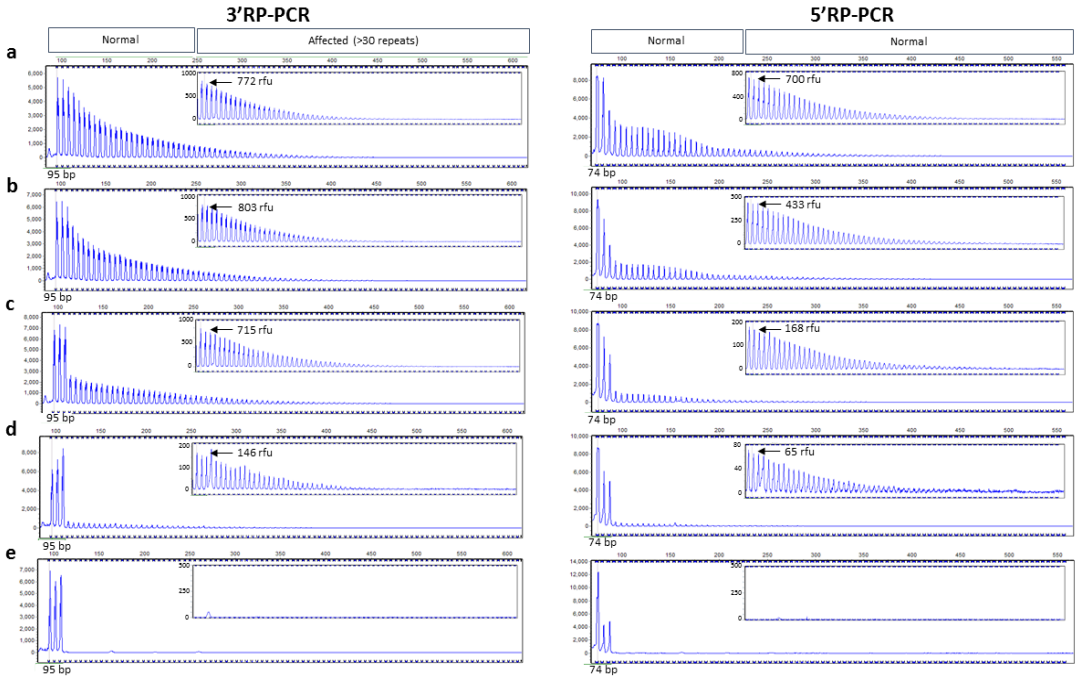

Figure 3.19 Sensitivity of RP-PCR for mosaicism

Figure 3.19 Sensitivity of RP-PCR for mosaicism

Capillary electrophoresis traces from 3'RP-PCR products (left) and 5'RP-PCR products (right) from GeneMarker (Soft Genetics). The x axis corresponds to size in base pairs (bp) and y axis to relative fluorescent units (box shows zoomed in trace where the first peak corresponds with 30 repeats on the x axis**)**. The traces show amplification of heterozygous expanded DNA (2 and expansion) at varying degrees of dilution (a) 100% (b) 50% (c) 10% (d) 1% and (e) 0% in heterozygous normal control DNA with 2 and 5 repeats.

3.2.5 Screening for *C9orf72* HRE in the Scottish ALS population

I screened for the presence of a *C9orf72* HRE in 529 DNA samples from the Scottish Regenerative Neurology Tissue Bank (1989-2015), which were linked to the Scottish MND Register (2010-2015). These samples were obtained from patients who fulfilled either the diagnostic criteria for MND as defined by the Modified World Federation of Neurology (1989-1994) or 'El Escorial' (1995 onwards) (Brooks, 1994; Chancellor, 1992). All samples were first tested by conventional flanking PCR, and the 187 which were apparently homozygous for a normal allele were reflex tested for the presence of an expansion using both 3'RP-PCR and 5'RP-PCR. Of the 528 samples for which results were obtained, 50 (9.5%) were found to have an HRE greater than 100 repeats. There was one equivocal result due to discordance between the two RP-PCR assays. One sample failed due to low DNA concentration and quality.

The equivocal result was in a sample which was apparently homozygous for 15 repeats, but which was negative for an expansion by 5'RP-PCR and positive by 3'RP-PCR. Due to insufficient DNA, it was not possible to test whether there was a primer binding site polymorphism inhibiting the 5'RP-PCR assay, or whether this was simply affected by the PCR artefact observed in the 3'RP-PCR assay, on samples with such large normal repeat alleles. There was also no information on the ethnic origin of the patient or whether there was a history of consanguinity, which may have made homozygosity more likely.

The frequency of the repeat sizes that were detected are shown in Figure 3.. The commonest allele size is 2 repeats (48.8% of alleles), with 5 (13.4% of alleles) and 8 repeats (11.7%) also being relatively common. Only 12% of alleles have between 10 and 29 repeats.

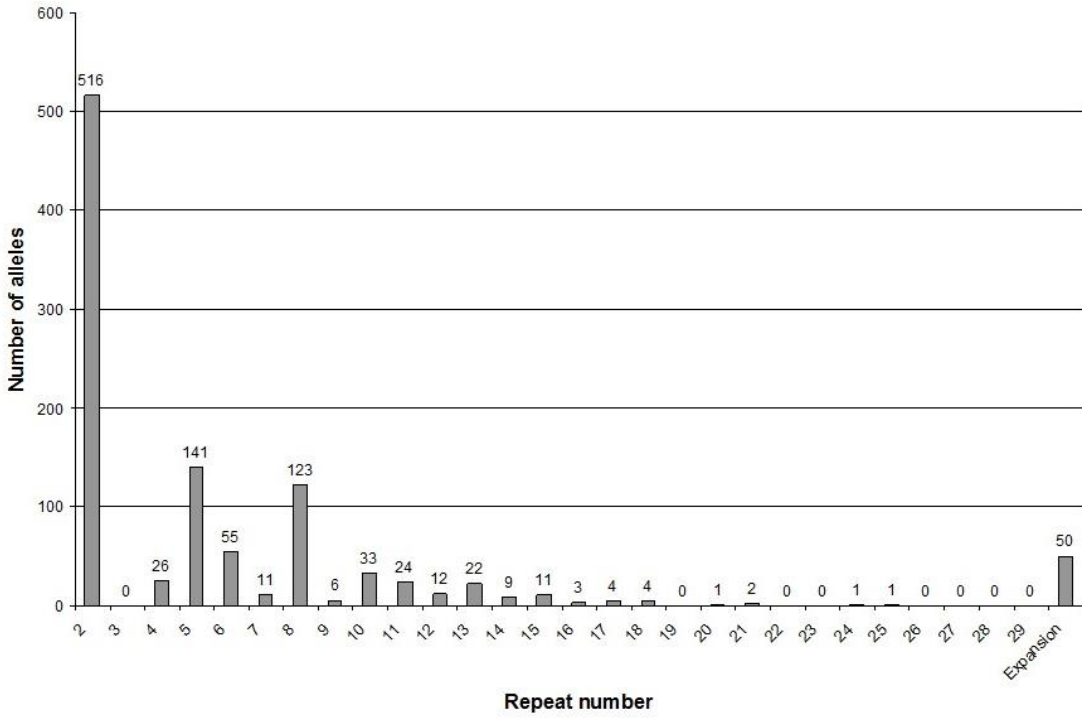

Figure 3.20 Distribution of repeat lengths of the *C9orf72* $(GGGGCC)_n$ tract in Scottish ALS patients.

Histogram of GGGGCC repeat numbers in Scottish patients from the MND Registry (1989-2015), with expansions represented as 100+ repeats.

Of these patients, there was clinical phenotypic data available for 47/50 *C9orf72* HRE carriers. There was a wide range of ages of onset, from 26-84 years. The average disease duration was 38 months (range 8-247 months). 18 patients (38%) were recorded as having a positive family history. 19 (40%) had bulbar onset disease and 24 (51%) were male (Leighton, personal communication).

3.2.6 Clinical diagnostic testing for *C9orf72* HRE in the Scottish MND and FTLD population

These PCR assays were validated within the South East Scotland Genetics Service for diagnostic use, and used to test 163 patients for a *C9orf72* HRE between 2013-2016. These patients had a variety of clinical phenotypes including dementia, motor neuron disease and Huntington disease-like symptoms. For all of these patients, all three PCR assays were performed. Out of the 163 patients tested, 23 were found to have a *C9orf72* HRE, giving a pick-up rate of 14.6%. A number of presymptomatic tests have also been performed, providing family members with information of their risk of developing *C9orf72*-related symptoms in the future. I will discuss two case studies that were of interest.

Case 1

A 41-year-old patient was referred with a diagnosis of dementia, having had severe memory problems for one year. He had word-finding difficulties, and attention and concentration problems. His mother had also suffered from dementia from a young age and died of the disorder in her forties.

C9orf72 testing revealed the presence of two alleles of 8 and 26 repeats. Because of the uncertainty surrounding the pathogenic range of *C9orf72* HRE, and because this was the largest normal sized allele which we had detected, and the family history was strong, I was prompted to investigate reports in the literature of similar size expansions. There was a report in the literature of a patient with FTD and ALS in whom a 26 repeat allele was present, however it did not segregate with disease in the family (Simón-Sánchez et al., 2012).

As it was decided that this allele was unlikely to be causative, this patient's sample was then tested for variants in a number of other genes which are associated with ALS, FTD or early onset AD (APP, CHMP2B, FUS, GRN, MAPT, PSEN1, PSEN2, SOD1, SQSTM1, TARDBP, UBQLN, VAPB and VCP) using next generation sequencing. This revealed a known pathogenic variant in PSEN1 (c.436C>A; p.Met146Leu in NM_000021.3), which has been implicated in early-onset AD (Bruni et al., 2010; Sherrington et al., 1995; Sorbi et al., 1995). Due to the differences in disease aetiology of FTD and AD, it is likely that the PSEN1 mutation is the cause of this patient's symptoms. However, we cannot rule out that the 26 repeats in *C9orf72* are contributing to his phenotype, particularly as others have suggested that repeats of this size may predispose to neurological disease (Gómez-Tortosa et al., 2013). If family studies had been possible, this would have been interesting and potentially informative as to the influence of the *C9orf72* short expansion. If post-mortem pathology was to be carried out on this individual, it would be interesting to establish whether there were TDP-43 inclusions present, or any other signs of *C9orf72* involvement, in addition to the amyloid-beta plaques as predicted from a PSEN1 mutation (Russo et al., 2000).

Case 2

A 59-year-old patient was referred for testing as he had a five-year history of progressive cognitive impairment, with short term memory loss and expressive speech disturbance. There was a strong family history of early onset dementia.

The *C9orf72* flanking PCR revealed an apparent 7 repeat homozygote, and this was confirmed by both RP-PCR assays. Because this was a relatively rare allele size, I sequenced the flanking PCR products, which revealed that there was apparently a normal 7 repeat allele, plus an allele

with 5 repeats and a 12 base pair insertion, which made it appear as a 7 repeat allele. This was a reassuring result confirming the presence of two normal alleles.

3.3 Discussion

3.3.1 PCR assays for detecting C9orf72 expansions

I have described the design and optimisation of PCR-based methods for testing for the presence of the *C9orf72* HRE, within a clinical diagnostic setting. The extreme GC richness of the expansion makes PCR a challenge, and I have had to optimise numerous aspects of the reaction conditions to bring about incremental improvements in both the flanking and RP-PCR assays.

One factor which has been key to the success of the assays has been the Taq polymerase which has been used. I have tried the Roche Fast Start polymerase, Qiagen HotStart polymerase (Figure 3.3a, Figure 3.12), and DyNAzyme EXT polymerase (Figure 3.9), and found that the latter gives a higher yield and permits larger fragments to be amplified in all of the assays. Since each polymerase has different manufacturer's recommendations for optimal cycling conditions, I have not performed a direct comparison of each Taq polymerase under the same conditions.

Another factor which I investigated with the original assays, which used Qiagen HotStart Taq polymerase, was the effect of co-solvents, such as DMSO, betaine and deaza-dGTP on the reaction success (Figure 3.4; Figure 3.12). It was clear that a combination of betaine and DMSO, and the addition of deaza-dGTP were beneficial for the amplification of larger fragments, and in particular allowed the RP-PCR to amplify longer fragments more effectively (Figure 3.12). Because the DyNAzyme EXT polymerase allowed amplification of even larger fragments with betaine alone, I decided not to investigate other co-solvents (Figure 3.15). The addition of deaza-dGTP interferes with detection of PCR products with intercalating dyes after agarose gel electrophoresis so was not desirable as the optimised assay amplified fragments which were larger than could be detected using the capillary electrophoresis instruments available.

PCR cycling conditions were optimised for the assays in various ways. For the original RP-PCR assays, it appeared to be beneficial for the generation of larger products if the early cycles had a high annealing temperature, which was then dropped in later cycles to promote amplification with Tail R (Figure 3.12g). For the re-designed assays, I investigated further how the cycling conditions affected the success of this PCR. It appeared that the heat pulse

extension step of the PCR, which was expected from the literature to be beneficial (Orpana et al., 2012), did not have a significant impact on the generation of RP-PCR products, and actually constant temperature extension gave a higher yield of product (Figure 3.14). The inclusion of slow ramping and two-step denaturation were also optimal for RP-PCR (Figure 3.16). For flanking PCR, there was a slight increase in the yield of larger product with HPE, compared to constant temperature extension, but as the capillary electrophoresis traces show signs of saturation, it would have been better to re-run these at a lower concentration to allow a fairer comparison. It is likely that the two-step denaturation, which includes a 10 second step at 98°C, is beneficial for such a highly GC-rich amplicon as complete denaturation is required for efficient PCR. This is consistent with the observation that the effect is more pronounced for RP-PCR of expansions, which generate larger products which are more susceptible to secondary structure formation, than flanking PCR of normal sized alleles. It was, however clear that slow ramping was beneficial to the yield of larger products for the flanking assay (Figure 3.9). Slow ramping from annealing to extension is thought to give primers slightly longer to bind, and allow some polymerase activity to begin to help clamp the products to the template (Orpana et al., 2012).

The re-designed and optimised flanking PCR allows detection of alleles which are larger than have previously been reported using similar methods. The largest alleles which were detected in blood were approximately 70-100 repeats in size, and revealed a high level of somatic mosaicism in two such samples (Figure 3.10d-f). There was a slight discrepancy between the sizing by PCR or Southern blot, however the higher resolution of capillary electrophoresis compared to agarose gel electrophoresis would enable PCR to provide more accurate sizing than Southern blotting. Whilst validating the optimised flanking PCR on blood derived DNA, I observed that some HRE positive samples revealed a background smear when the PCR products were separated by agarose gel electrophoresis. It was particularly striking that increasing the extension time enhanced the smear signal (Figure 3.9e). I suspected that this may reflect the amplification of the expanded allele, but the signal was weak due to somatic mosaicism. Although the pattern was not robust enough to be useful in a diagnostic setting, it suggested that the PCR was efficient and prompted me to investigate the upper size limit of detection.

Using cell line DNA allowed detection of larger expanded material than had been detected in blood. The largest band detected corresponded to approximately 900 repeats. Although cell line DNA is not a source routinely used in a diagnostic setting, the sharp bands observed for cell line DNA containing *C9orf72* expansions suggest that the PCR is reliable in this range,

and the mosaicism seen in blood-derived DNA from the short expansion carriers is likely to be a real effect and not a PCR artefact caused by replication slippage. The ability to detect such expansions in cell line DNA was useful for my later studies using hiPSC derived models.

Somatic mosaicism has been widely reported in *C9orf72* expansions (Beck et al., 2013; Dols-Icardo et al., 2014), with size varying between tissues within the same individual. For diagnostic purposes, DNA is normally isolated from whole blood or saliva samples, and therefore derives from lymphocytes. Lymphocytes have been shown to contain different sized expansions compared to neural tissue from the same patient, with the shortest expansions observed in cerebellum (van Blitterswijk et al., 2013b). Since neural tissue is usually only available to test post mortem, it is unclear whether there may be a change in size in *C9orf72* expansions over time, and that this may be involved in the triggering of the disease in middle-age. Such an age-dependent effect has been observed for myotonic dystrophy type I (Radvansky and Kadasi, 2010). When interpreting results from Southern blotting, the large size range of expanded material makes detection more challenging, and makes it particularly difficult to correlate repeat size to clinical variables such as age at onset, disease severity and progression because the size range within each patient is mosaic. Some have observed a positive correlation between the median repeat number, and the range of the repeat sizes, which suggests that the repeat becomes increasingly unstable with increasing size. This can be observed even for normal alleles, as there appears to be more stutter peaks present in larger alleles (26 and 20) compared to shorter alleles (7 and 13) (Figure 3.10a-c).

I have calibrated the flanking PCR assay using a variety of methods. As the original flanking PCR produced very short products in normal controls, direct Sanger sequencing of the products was not possible. To confirm the specificity of the products, I performed a nested PCR with the repeat containing primer used in in RP-PCR, which revealed a saw-tooth pattern with ~6 bp periodicity, as would be expected from the region (Figure 3.5). This suggested that the PCR was specific and also helped to confirm the relative sizing of alleles. A second flanking PCR had to be performed to allow sequencing and confirm the repeat number in a normal control sample. Upon redesigning the assay, direct sequencing of the PCR products allowed confirmation that the reaction was specific and allowed calibration between fragment size and repeat number. Furthermore, a number of previously tested DNA samples were re-tested and had their repeat numbers confirmed with the new assay. Unless sequenced though, the repeat number from flanking PCR is an estimate based on the presence of normal sequence surrounding the GGGGCC locus. Genomic variability adjacent to the repeat may affect the apparent repeat number based on size, as was observed in case study 2, who was apparently

homozygous for 7 repeats, but actually had one 7 repeat allele and one 5 repeat with a 12bp insertion.

The RP-PCR assays that I have developed appear to be higher yielding and produce a ladder of fragments corresponding with over 100 repeats, which is longer than has previously been published (DeJesus-Hernandez et al., 2011; Renton et al., 2011). Importantly, our 3' RP-PCR assay has been shown to be robust even in the presence of a number of genomic variations next to the HRE. During the optimisation of the 3'RP PCR, conditions were observed which resulted in a failure of the shorter normal allele to amplify. These difficulties were exploited to allow sequencing of the expanded allele to be carried out, without the complicating factor of heterozygosity in data analysis. We detected a relatively higher degree of variation than has been reported in studies based on Southern UK populations, and detected six HRE cases with a 10 base pair deletion which has also been proposed to be common in a Northern England cohort (Rollinson et al., 2015).

The admixture experiments which were carried out, where expansions can still be detected even when diluted to 1% in a normal background, suggest that these assays are not severely affected by preferential amplification, and the conditions seem to be optimal for PCR of longer fragments, and particularly of the expanded allele over the normal one.

However, I have observed that in the 3'RP-PCR, normal alleles of greater than 15 repeats can lead to a PCR artefact with low level expanded material being observed. This presumed primer-product interaction, leading to replication slippage can only be reduced by measures which also drastically reduce the production of expanded material in HRE positive cases. Thus, this may be a limitation for product length for *C9orf72* RP-PCR, as the 5'RP does not generate as large products and does not suffer from this artefact. The prevalence of false positive results in the recent blinded quality assurance style study (Akimoto et al., 2014) suggests that laboratories should be aware of such test limitations. Clearly elimination of false positive results would be desirable, however reduction of cycle number, reduction in polymerase quantity, alteration of primer concentrations and altering the repeat binding primer phase, all failed to solve this artefact. Another group have recently reported that they can overcome the problem by using a flanking primer slightly further from the repeat expansion than ours (Biasiotto et al., 2016).

3.3.2 C9orf72 repeat expansions in the Scottish ALS population

I used the PCR methods described to screen a cohort of 528 Scottish ALS patients (1989-2014) for the HRE. Overall, this revealed that 9.5% of patients had a *C9orf72* HRE, which is in line with what has been observed in other UK ALS cohorts (8.1%) (Beck et al., 2013). It appears that the number of *C9orf72* HRE carriers in the MND registry with a positive family history is relatively low, but this may reflect that these are historical samples, and it is unlikely that given the knowledge at the time, that patients were questioned with regards to a more extensive family history to include dementia, for example, as the links between ALS and FTLD were not known.

For clinical diagnostic testing, it is important to be aware of the common repeat sizes within the population as this can guide testing. Suspicion arises when a patient is apparently homozygous for a rare repeat size, particularly if these are in the 15-30 range which could hamper PCR amplification (Rollinson et al., 2015). In our experience, sequencing of the flanking PCR products in apparently homozygous cases can also reveal normal alleles with genomic variability, which has also been reported by others (Akimoto et al., 2014). For the sample from the MND Registry which was apparently a 15 repeat homozygote, it was unfortunate that there was insufficient DNA for further testing. Sequencing of the flanking PCR products, or trying alternative primers at the 5' end may have allowed a result to be obtained more confidently, before Southern blotting would have been required to elucidate a result.

3.3.3 Future directions

The advances in PCR based detection of *C9orf72* expansions allow accurate sizing of alleles although it is still unclear how large the expansions that can be detected in blood are. It was observed that some *C9orf72* expansion positive blood samples did appear to give a large smear after flanking PCR, when ran on an agarose gel but this was not consistent across samples, and relatively difficult to distinguish from background. One way to determine whether these smears are from amplification of mosaic expanded material would be to carry out a Southern blot of PCR products. However, current PCR methods may be unable to assess the exact size of the largest repeat expansions which are reported to be up to 4 400 repeats, and so these would not be detected (Beck et al., 2013). Traditional Southern blotting is therefore required for studies to determine whether there is a genotype-phenotype correlation involving repeat size (Hubers et al., 2014). It may also be of interest and value to perform large scale studies to

determine the stability of repeat size in individuals, over time, in different tissues (van Blitterswijk et al., 2013b).

Sanger sequencing is of limited use in determining repeat number, as it only works on alleles up to 20 repeats in size. Current next generation sequencing technologies also perform poorly on long repetitive DNA tract, precluding their use (Lyons et al., 2015). The latest sequencing technologies, such as single molecule real time sequencing may be capable of estimating *C9orf72* repeat size in future (Loomis et al., 2013), but these are not readily available technologies and may not be capable of sequencing 100% GC rich fragments from large expansions.

Several studies have also suggested that methylation status of the repeat can also influence the clinical phenotype, and this has not been assessed here. There has been some suggestion that higher levels of methylation are correlated with a shorter disease duration (Xi et al., 2014; Xi et al., 2015b; Xi et al., 2013), however it is not clear whether this association can be detected reliably in blood, and further work would be required before this could be used as a prognostic marker for disease progression, for example.

3.4 Conclusion

I strongly recommend carrying out all three PCR assays, which I have designed and optimised, in a clinical diagnostic setting. Results between the assays should be concordant before reporting, with the exception of rare cases which are affected by the 3'RP PCR artefact (where a large normal allele is detected on flanking PCR). There may be rare cases (1/528 in this study), where reflex testing with Southern blotting may be necessary, to distinguish between cases which are homozygous normal, and where an expansion is only apparent in one direction. In the particular case which gave an equivocal result in this study, it should be noted that further PCR based testing may have enabled a clear result to be obtained, but efforts were hampered by insufficient DNA.

Both RP-PCR assays should be used together to minimise the risk of any rare genomic variability, including single nucleotide polymorphisms under primer binding sites, from affecting the test accuracy. This is in line with recommendations for other repeat expansion disorders, such as Myotonic Dystrophy type 1, where rare cases have been reported which have interspersed repeats at one end (Kamsteeg et al., 2012). Although this hasn't been specifically documented in any *C9orf72* expansion positive cases to date, there was a suggestion that this may explain a sample which gave a discrete banding pattern, rather than a typical smear, following Southern blotting with a repeat containing probe (Beck et al., 2013).

In conclusion, the PCR assays which I have developed are robust and allow detection of larger repeat expansions than previous published methods. The ability to accurately detect and size short repeat expansions (60-120 repeats) from blood samples may help to define the lower pathogenic range of *C9orf72* HREs. Southern blotting for *C9orf72* HRE in a diagnostic setting provides information on the size of large expansions, although as discussed previously the expansions are usually heterogeneous and mosaic in nature making it challenging to correlate size with phenotype and prognosis (Beck et al., 2013; Hubers et al., 2014).

.

Chapter 4. Derivation of oligodendrocytes from patient derived induced pluripotent stem cells with *C9orf72* hexanucleotide expansions

4.1 Introduction

The capacity to produce differentiated cells from patient derived hiPSCs allows the study of cell autonomous factors in disease. For neurodegenerative disorders, such as ALS, hiPSC technology is particularly useful as the cells of interest cannot be easily studied *in vivo* during disease progression, and pathological studies tend to be focussed around end-stage disease. The technology also allows the contribution of non-neuronal cells to the degenerative process to be investigated. Loss of gray matter spinal oligodendrocytes has been observed in a SOD1 mouse model, and selective ablation of the mutation in oligodendrocytes was found to delay the onset of disease and enhance survival (Kang et al., 2013). Therefore, studying oligodendrocytes in the context of ALS is of interest. To generate oligodendrocytes from hiPSCs, knowledge of their *in vivo* development has been used to guide *in vitro* differentiation protocols based on the recapitulation of this process. Generating hiPSCs from patients with disease-causing mutations, and directing their differentiation to a cell type of interest is a widely recognised approach. The power of this has been demonstrated for *C9orf72* HREs in the context of motor neurons (Donnelly et al., 2013; Sareen et al., 2013). A major limitation of this technique is the differing genetic backgrounds of carriers and controls ((Bock et al., 2011; Rouhani et al., 2014). To overcome this problem, CRISPR/Cas-9 technology can be used to generate isogenic controls through the specific removal of the (GGGGCC)n expansion from hiPSCs.

4.1.1 Generation of human oligodendrocytes from hiPSCs

The first differentiation protocols to generate OPCs and oligodendrocytes from pluripotent cells were developed for rodents, and these were subsequently adapted for human systems (Li et al., 2009). The earliest published protocols for human cells take several months to produce oligodendrocytes from ES cells, compared to weeks for mouse cells (Hu et al., 2009a; Izrael et al., 2007; Kang et al., 2007; Nistor et al., 2005; Stacpoole et al., 2013). The application of such differentiation protocols to hiPSCs gave a low yield of cells (less than 0.01% O4 positive) and few cells went on to express mature markers such as MBP (Ogawa et al., 2011; Pouya et al., 2011). Most of the oligodendrocyte differentiation protocols which had been published

prior to the beginning of this study were only optimised for ES cells and their success when starting from hiPSC was not clear (Alsanie et al., 2013).

4.1.2 Signalling for oligodendrocyte conversion

Most differentiation protocols which have been developed for spinal oligodendrocytes rely on recapitulation of the events that occur during embryonic development. Within the blastocyst, the inner cell mass forms the three germ layers (ectoderm, mesoderm and endoderm) during gastrulation. The dorsal portion of ectoderm is specified to neuroectoderm by inhibition of activin and BMP signalling and activation of Wnt and FGF signalling. The neural tube then forms and the early specification of spinal cord derived oligodendrocytes occurs in the ventral ventricular zone of the neural tube, and is related to patterning of the rostral-caudal and dorsal-ventral axes by morphogenic gradients of Shh and BMP (Emery and Lu, 2015; Richardson et al., 2000). Patterning along the rostral-caudal axis of the neural tube occurs via an RA gradient which helps form a boundary between spinal cord and hindbrain (Davis-Dusenbery et al., 2014).

Following caudalization, anterior-posterior patterning occurs through a gradient of Shh, which is secreted from the floor plate and notochord leading to ventral patterning. Opposing BMP and Wnt signalling from the roof plate results in the formation of the dorsal neural tube, and is inhibitory to formation of the oligodendrocyte lineage (He and Lu, 2013). The Shh gradient leads to the formation of six distinct progenitor domains along the dorsal-ventral axis, which are defined by their expression of specific transcription factors (Briscoe et al., 2000). The oligodendrocyte lineage mainly arises from the ventral pMN domain, after motor neurons have been produced from neural precursors which express the transcription factor Olig2 (Jacob and Briscoe, 2003; Richardson et al., 2000). Olig2 initially promotes the formation of motor neurons through binding to neurogenin-1 and neurogenin-2 (Zhou et al., 2001). It is then dephosphorylated at Ser147 which results in a switch to promote oligodendrocyte fate via preferential binding to different partner transcription factors (Li et al., 2011). Cells which co-express Olig2 and Nkx2.2 develop into OPCs, and Olig2 is a consistent marker for the ventral oligodendrocyte lineage (Li et al., 2011; Ribes and Briscoe, 2009).

Once OPCs have formed they begin to migrate throughout the CNS, with Olig2 expression continuing, along with Sox10 and Nkx2.2 (Liu et al., 2007; Zhou et al., 2001). These transcription factors promote PDGFR-α expression (Finzsch et al., 2008), which enhances survival and proliferation of OPCs via the binding of its ligand PDGF (Barres et al., 1993; Calver et al., 1998). PDGFR-α expression is characteristic of OPCs (Pringle et al., 1992) and

these cells have either bipolar morphology, or a few short branches (Jakovcevski and Zecevic, 2005b)

The differentiation of OPCs to oligodendrocytes requires that OPCs exit the cell cycle in a highly regulated manner such that myelination occurs at the correct time and whilst ensuring there is a remaining pool of OPCs (Emery and Lu, 2015). The Notch, BMP and Wnt signalling pathways inhibit OPC production and differentiation during development, and there are prodifferentiation factors which act to antagonize these inhibitory effects allowing differentiation to occur (Emery and Lu, 2015). The differentiation of OPCs to oligodendrocytes is characterised by the sequential expression of different immunomarkers, including the O4 sulfatide which is a late OPC-early oligodendrocyte marker (Jakovcevski and Zecevic, 2005b; Schachner et al., 1981) and then MBP which is expressed by pre-myelinating oligodendrocytes (Jakovcevski et al., 2009). As they differentiate, oligodendrocytes undergo morphology changes and extend elaborate process to contact axons, most of which are subsequently retracted after axons are ensheathed (Emery and Lu, 2015). Myelination begins in the final trimester and continues over several decades (Back et al., 2001; Jakovcevski et al., 2007).

4.1.3 Protocol for oligodendrocyte generation

Our lab has developed a protocol for generating differentiated oligodendrocytes from hiPSCs (Livesey et al., 2016). This protocol first involves neuralizing hiPSCs by dual-SMAD inhibition (Chambers et al., 2009). This method (Phase I) causes differentiation by blocking two signaling pathways utilized by SMADs: BMP and transforming growth factor β (TGF-β). SB431542 is an inhibitor of the Lefty/Activin/TGFβ pathways, and reduces Nanog expression in pluripotent cells, leading to a loss of pluripotency (Chambers et al., 2009). The original protocol has been adapted, such that Noggin has been replaced with LDN193189, a dorsomorphin derivative which blocks BMP signalling. Overall, dual-SMAD inhibition results in rapid and high (>80%) conversion to neural cell fates by preventing the development of trophoectoderm, mesendoderm and endoderm (Chambers et al., 2009).

The resulting neuroectoderm cells can then be patterned to become many types of neural cells. To generate spinal oligodendrocytes, we first produce ventral spinal cord progenitors. This is carried out by adding RA as a caudalising signal (Phase II), followed by the addition of the Shh agonist purmorphamine, as a ventralizing signal (Phase III) (Hu et al., 2009a; Li et al., 2008). Fibroblast growth factor (FGF), which has an inhibitory effect on BMP signalling, is required for the self-renewal of human NPCs, and thus its removal during the next stage (Phase

III minus FGF) promotes the differentiation of NPCs (Gorris et al., 2015), which then undergo further specification to generate oligodendrocytes (Figure 4.1).

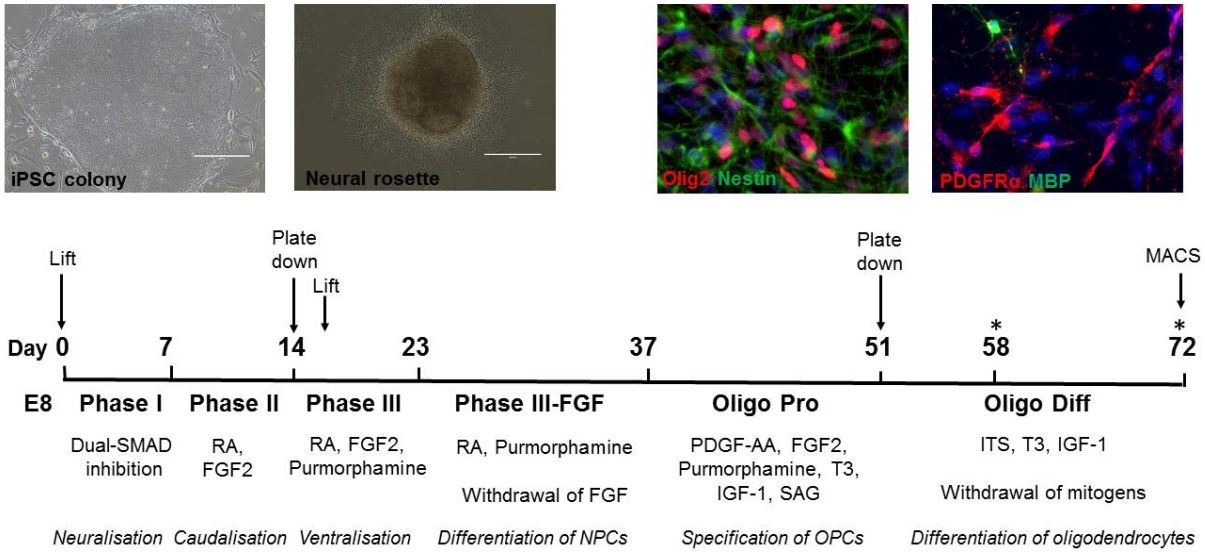

Figure 4.1. Schematic of protocol used to generate oligodendrocytes from hiPSCs

hiPSCs are lifted (day 0) to generate spheres which are neuralised by feeding for 7 days in Phase I medium. Neurospheres are then patterned in Phase II (7 days), where exposure to RA gives a caudal identity. At the end of Phase II, spheres are plated down for 2-3 days, before neural cells are selected. These are lifted to generate spheres which are then fed Phase III medium, containing RA and the Shh agonist Purmorphamine to promote a ventral cell identity. Further differentiation then occurs when the cells are exposed to Phase III-FGF medium for a further two weeks, generating spinal cord neural precursor cells (scNPCs). Spheres are then transferred into Oligo Pro medium, which promotes glial cell specification. After two weeks, spheres can be dissociated with Papain and plated down in Oligo Diff media. Withdrawal of PDGF-AA, FGF2 and SAG promote differentiation of oligodendrocytes, with the presence of insulin-transferrin and selenium (ITS), T3 and IGF-1 promoting survival and maturation. Spheres in Oligo Pro can be maintained for up to two months by chopping every few weeks. Experimental time points are indicated with the *, at week 1 and week 3 post plate down. MACS was carried out at week 3 to enrich for O4 positive cells for biochemical experiments.

To generate OPCs from NPCs *in vitro*, FGF and PDGF-AA are used in our protocol (Alsanie et al., 2013). PDGF-AA is thought to play a role in the timing of oligodendrocyte differentiation via the promotion of OPC differentiation (Hu et al., 2008). It is an essential mitogen for OPC proliferation (Calver et al., 1998). Fibroblast growth factor 2 (FGF2) may promote the proliferation of OPCs by the upregulation of Olig2 and PDGFRα (Naruse et al., 2006), and so these are added to Oligo Pro medium to accelerate OPC proliferation via the activation of multiple kinases (He and Lu, 2013). Insulin Growth Factor 1 (IGF-1) and

Triiodothyronine (T3) are also thought to support the development of OPCs (Hu et al., 2009a; Sundberg et al., 2011; Sundberg et al., 2010). IGF-1 has been shown to support the development and maturation of OPCs in rodents (Barres et al., 1993; Carson et al., 1993), and may act partially by inhibiting BMP signalling (Hsieh et al., 2004). The addition of Shh agonists has been reported by others to increase OPC numbers (Sundberg et al., 2011), and previous work in our lab had shown that a combination of purmorphamine and Smoothened agonist (SAG) increased the yield of oligodendrocytes.

When OPCs are dissociated using Papain and plated down, the substrate upon which they are cultured is important to cell proliferation, survival and differentiation (Alsanie et al., 2013). In this protocol we used a combination of poly-L-ornithine, laminin, matrigel and fibronectin. All of these components have been shown to promote these processes when tested on rat derived OPCs (Hu et al., 2009b). After plate down, mitogens are removed from the medium as FGF and PDGF-AA inhibit the maturation of these cells into oligodendrocytes (Bansal and Pfeiffer, 1997). The addition of IGF-1 and insulin promotes the survival of oligodendrocytes *in vitro* (Barres et al., 1993). T3 is thought to be important for the survival and proliferation of OPCs and may also promote differentiation to oligodendrocytes (Sundberg et al., 2010).

The *in vitro* differentiation process can be followed using immunocytochemistry for selected cell surface markers such as PDGFRα, O4 and MBP, which represent increasing stages of differentiation (Figure 1.7; for more details see Materials and Methods). Oligodendrocyte precursor cells express PDGFRα, immature oligodendrocytes are positive for O4, while MBP is expressed by mature oligodendrocytes (Barateiro and Fernandes, 2014). Where required the differentiating oligodendrocytes can be purified using magnetic activated cell sorting (MACS) with the O4 marker.

4.1.4 Objectives

The aim of this chapter was to produce oligodendrocytes from hiPSC lines derived from patients with *C9orf72*-related ALS and controls, including an isogenic control which has been generated using CRISPR/Cas9 mediated gene editing. The presence or absence of the repeat expansion was verified in patient derived cells and controls respectively. The generation of oligodendrocyte lineage cells from each of the cell lines was compared using quantitative immunocytochemistry for OPC and oligodendrocyte specific markers. The presence of astrocytes and neurons were also quantified in each of the cell lines.

4.2 Results

4.2.1 Maintenance of the *C9orf72* hexanucleotide expansion *in vitro*

To confirm the genotype of both carrier and control lines, flanking PCR and RP-PCR were used (Fig 4.2 a-e). These assays were used regularly to ensure that the cell lines were of the expected genotype. Interestingly, one of the samples from Carrier 2 hiPSCs showed the presence of an approximately 88 ± 2 repeat allele (Fig 4.2b). This was lower in intensity than was detected in blood samples with repeats of this size, suggesting that it represented mosaicism within the sample. However, there was no evidence of this shorter repeat allele at later passages of the same line (which was confirmed to be the same cell line by fingerprint analysis, data not shown), it is likely that cells with the shorter repeat were lost in culture. I tested DNA from cells at different stages of conversion from hiPSCs to oligodendrocytes and found no evidence of shorter repeat alleles at any of the stages tested (Fig 4.2e). In light of the reported presence of genomic instability in the 3' region of the repeat expansion, I sequenced this in both carrier lines, and showed that while Carrier 1 matched the reference sequence, Carrier 2 had the common 10 base pair deletion (Fig 4.2f). It is currently unclear whether this difference has any impact on pathology, as only one study has made suggested a link between the 10 bp deletion and reduced risk of psychosis (Snowden et al., 2016).

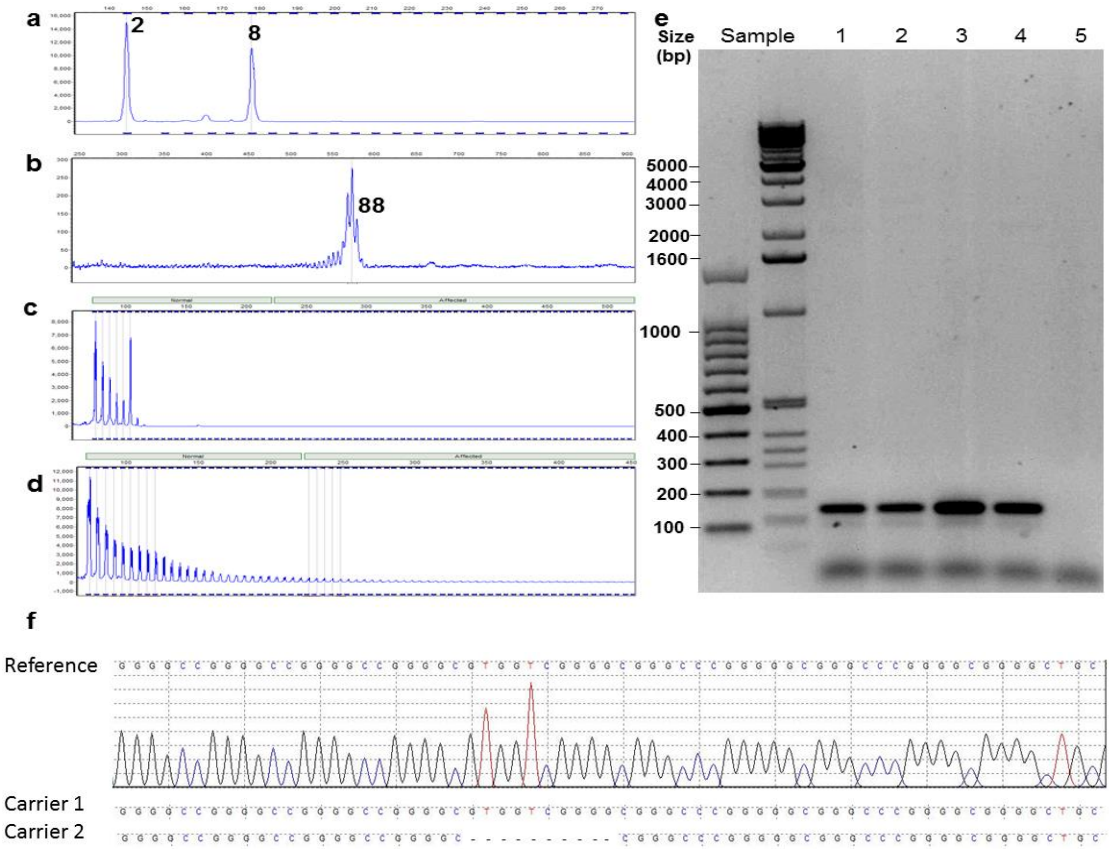

Figure 4.2 Genotyping results from hiPSC lines

Figure 4.2 Genotyping results from hiPSC lines

(a) *C9orf72* flanking PCR for control 2 hiPSC showing two normal alleles with 2 and 8 repeats. (b) C9orf72 flanking PCR for carrier 2 hiPSC showing an allele with 88 ± 2 repeats. (c) 5' RP-PCR result for Control 2 hiPSC showing no ladder and confirming the negative flanking PCR result. (d) 5' RP-PCR result for carrier 2 hiPSC showing a ladder extending into the affected size range (> 30 repeats) indicating the *C9orf72* hexanucleotide repeat expansion. (e) Agarose gel electrophoresis of flanking PCR products from cells at the following stages of conversion for carrier 2: Lane 1. iPSC. 2. Phases III-FGF 3. Oligodendrocyte precursor cells. 4. Differentiated oligodendrocytes. 5. No DNA control (Note that no positive controls are shown but these samples were tested alongside those in Figure 3.9f). (f) Sanger sequencing results of the region 3' to the repeat expansion in both carrier lines compared to reference sequence (NG_031977.1), showing the common 10 base pair deletion which is present in Carrier 2.

4.2.3 Creation of an isogenic control line

CRISPR/Cas-9 technology was used to specifically remove the (GGGGCC)n expansion from Carrier 2 iPS cells, and create an isogenic control line, which is referred to as Carrier 2 $\Delta(GGGGCC)_n$. This work was performed by Dr Bhuvaneish Selvaraj, and I contributed to the PCR screening for the cell lines. Two CRISPR guide (g) RNAs were designed (gRNA-1 and gRNA-2) which targeted each side of the GGGGCC repeat in intron 1 of the *C9orf72* gene. Without a repair template, the double strand breaks introduced by Cas9 will re-ligate via non-homologous end joining, so that the $(GGGGCC)_n$ repeats are removed. The gRNAs were initially tested in HEK-293 cells which contain three GGGGCC repeat units in the *C9orf72* locus, by transfection of gRNAs and Cas9 plasmid. PCR based screening was performed, which showed the presence of a truncated product following transfection, compared to wild-type cells (data not shown). This suggested that the system and gRNAs was functioning as expected. Therefore, hiPSC from Carrier 2, which contained one allele with two repeats, and an expanded allele with around 750 repeats, were then nucleofected with Cas9 and the gRNAs. Flanking PCR results show the presence of the normal allele only (Fig 4.3a) as the larger allele is too large to amplify. Screening 164 individual single-cell-derived clones using flanking PCR identified 22 clones in which there was a truncated PCR product compared to that from Carrier 2 hiPSCs. Testing these with 5'RP-PCR revealed that the expansion was still present in these clones (data not shown), and thus it appeared that the normal allele containing two GGGGCC repeats had been targeted for correction. Fortunately, there was one clone which had two truncated PCR products following flanking PCR, which suggested that both alleles had been targeted (Fig 4.3b). This was confirmed by 5'RP-PCR, which shows the presence of an expansion in the unedited iPSC (Fig 4.4 c) and the subsequent loss after editing (Fig 4.3d). This result was confirmed by Southern blotting and Sanger sequencing (Selvaraj, submitted).

The hiPSC cells were shown to be karyotypically normal and retained the pluripotency markers OCT3/4, TRA-1-60 and NANOG. (Selvaraj, submitted).

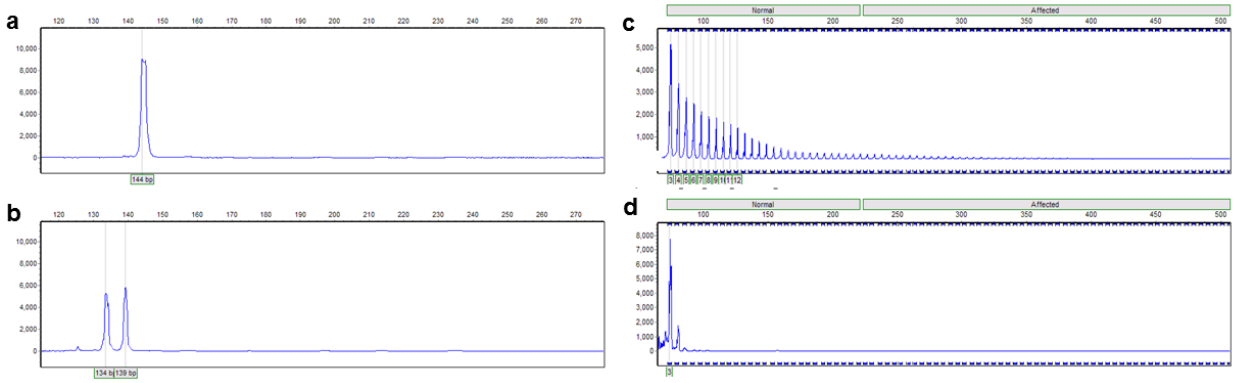

Figure 4.3 Genotyping results for creation of isogenic line

Capillary electrophoresis traces for flanking PCR products from (a) Carrier 2 (b) Carrier 2 after gene editing to remove $(GGGGCC)_n$ expansion. Capillary electrophoresis traces for 5'RP-PCR products from (a) Carrier 2 showing presence of expansion (b) Carrier 2 after gene editing to remove the $(GGGGCC)_n$ expansion in *C9orf72*.

4.2.4 Derivation of OPCs and oligodendrocytes from neural precursor cells

It has been reported that different hiPSC lines may have variable differentiation capabilities (Boulting et al., 2011), and therefore I wanted to characterise each of the control and *C9orf72* expansion carrying lines to determine if they produced equivalent numbers of differentiated cells.

Quantitative immunocytochemistry was carried out 7 days after plate down of OPC spheres and mitogen withdrawal (Oligo Diff). Representative images and graphical representations of quantification are shown in Figure 4.4. This analysis revealed that the cultures contained a majority of Olig2 positive cells (Control 1, 74.5 ± SE 4.3%; Control 2, 61.9 ± SE 3.8%; Carrier 1, 66.4 ± SE 8.9%; Carrier 2, 56.7 ± SE 3.6%; Carrier 2 $\Delta(GGGGCC)_n$, 52.1 ± SE 2.5%). There was no overall difference in Olig2 positive cells present in carrier and control cell lines ($p=0.83$, Mann-Whitney test). Oligodendrocyte precursor cells, identified by expression of PDGFR-α, were present at this time point (Control 1, 19.7 ± SE 2.5%; Control 2, 12.4 ± SE 1.2%; Carrier 1, 11.7 ± SE 1.3%; Carrier 2, 13.4 ± SE 1.1%; Carrier 2 $\Delta(GGGGCC)_n$, 15.5 ± SE 0.7%). Overall, there is no difference between the percentage of cells which are PDGFRα positive between carrier and control cell lines ($p=0.45$, Mann-Whitney test). The cultures also contained O4 positive oligodendrocytes (Control 1, 2.4 ± SE 0.5%; Control 2, 3.0 ± SE 0.5%;

Carrier 1, 4.4 ± SE 0.6%; Carrier 2, 3.9 ± SE 0.7%; Carrier 2 Δ$(GGGGCC)_n$, 2.0 ± SE 0.2%). Comparing carrier to control, there was no difference in the percentage of O4 positive cells generated by the cell lines (p=0.37, Mann-Whitney test).

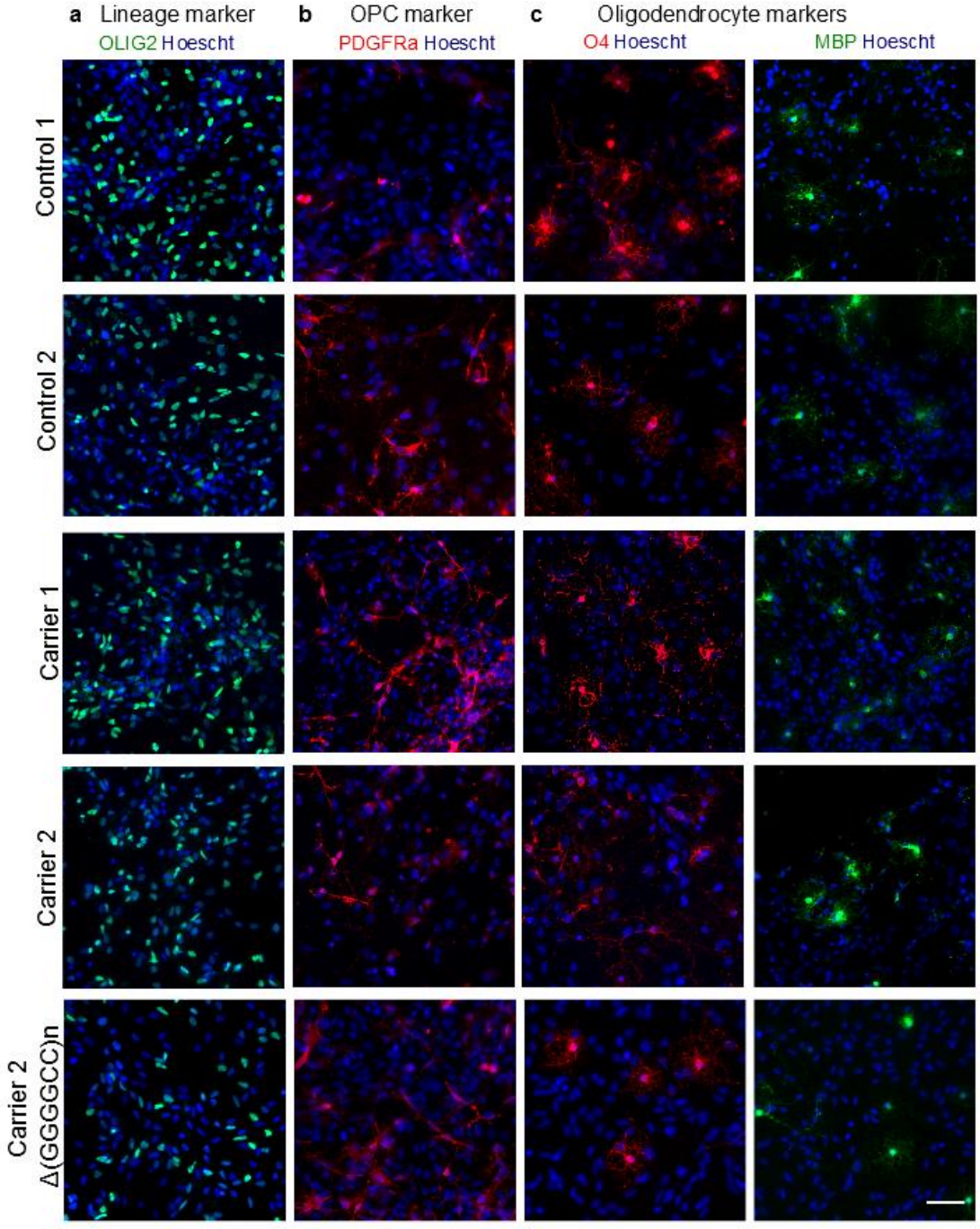

Figure 4.4 Immunocytochemical staining and quantification of oligodendrocyte lineage markers

d

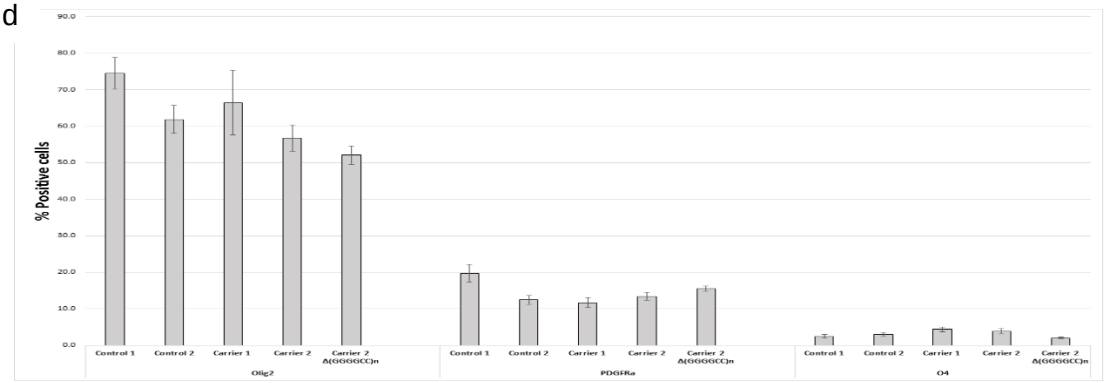

Figure 4.4 Immunocytochemical staining and quantification of oligodendrocyte lineage markers

(a) Immunocytochemical staining of the ventral transcription factor Olig2 (b) Immunocytochemical staining of the OPC marker PDGFR-α (c) Immunocytochemical staining of the oligodendrocyte markers O4 and MBP. Scale bar = 50μm. (d) Graph showing quantification of Olig2 (Control 1/Control 2/Carrier 1/Carrier 2/Carrier 2 Δ$(GGGGCC)_n$: n=5/7/6/6/7), PDGFR-α (Control 1/Control 2/Carrier 1/Carrier 2/Carrier 2 Δ$(GGGGCC)_n$: n=6/13/10/16/15) and O4 (Control 1/Control 2/Carrier 1/Carrier 2/Carrier 2 Δ$(GGGGCC)_n$: n=5/8/10/9/8) positive cells after 7 days in Oligo Diff medium by immunocytochemistry.

FACS analysis performed after three weeks of culture in Oligo Diff media showed a higher proportion of O4+ cells (Control 1, 76.4 ± SE 3.5%; Control 2, 54.6 ± SE 13.9%; Carrier 1, 56.2 ± SE 9.4%; Carrier 2, 53.3 ± SE 7.9%; Carrier 2 Δ$(GGGGCC)_n$, 34.9 ± SE 3.7%) as shown in Figure 4.5. Comparison of carrier with control cells revealed no difference overall between the cell lines (p=0.72, Mann-Whitney test). However, direct comparison between carrier 2 and the isogenic control line suggests there may be a trend towards a higher number of O4 positive cells in carrier 2 (p=0.066, Mann-Whitney test). For biochemical studies, this time point was selected and to further enrich for O4 positive cells, MAC sorting using O4 microbeads was performed.

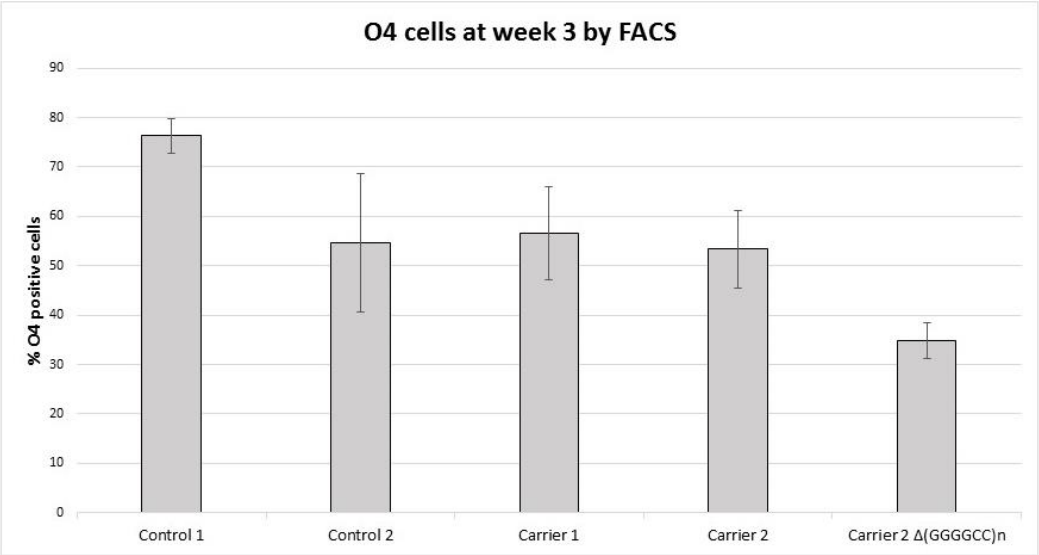

Figure 4.5 Quantification of O4 positive cells at week 3 by FACS

Graph displaying the percentage of O4 positive cells after three weeks in Oligo Diff medium by FACS analysis (Control 1/Control 2/Carrier 1/Carrier 2/Carrier 2 $\Delta(GGGGCC)_n$: n=3/4/6/3/5).

To investigate the maturation of the oligodendrocyte lineage cells, I quantified the overlap of the PDGFR-α and O4, and O4 and MBP positive cells. There was a high level of co-expression between the O4 marker and MBP (Control 1, 92.5 ± SE 2.1%; Control 2, 87.9 ± SE 3.0%; Carrier 1, 84.0 ± SE 5.6%; Carrier 2, 73.6 ± SE 6.7%; Carrier 2 $\Delta(GGGGCC)_n$: 83.5 ± SE 3.9%) as shown in Figure 4.6. Overall there was no difference between carrier and control lines in this respect (p=0.60, Mann-Whitney test). There was a lower overlap between O4 and PDGFR-α (Control 1, 7.4 ± SE 2.4%; Control 2, 8.0 ± SE 1.6%; Carrier 1, 9.1 ± SE 2.9%; Carrier 2, 9.2 ± SE 1.4%; Carrier 2 $\Delta(GGGGCC)_n$: 16.5 ± SE 3.9%) as shown in Figure 4.6. Comparison between carrier and control lines did not reveal any difference (p=0.87, Mann-Whitney test).

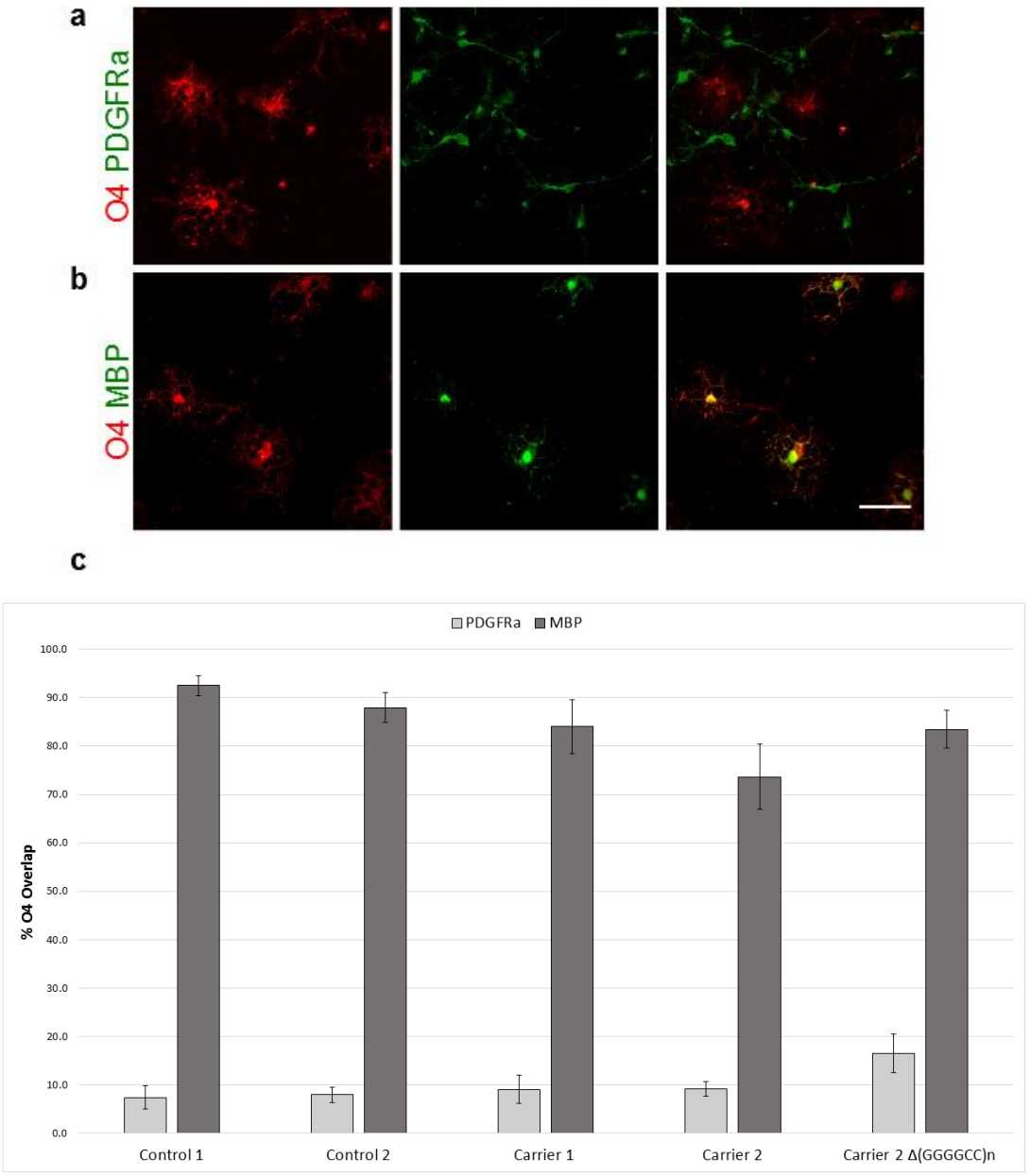

Figure 4.6 Overlap of O4 marker with PDGFRa and MBP

Representative images of immunocytochemistry showing (a) lack of overlap of PDGFR-α positive and O4 positive cells (b) substantial overlap between O4 and MBP markers. Scale bar = 50µm (c) Mean percentage of O4 positive cells which express PDGFR-α (Control 1/Control 2/Carrier 1/Carrier 2/ Carrier 2 $\Delta(GGGGCC)_n$: n=3/5/4/5/5) and MBP (Control 1/Control 2/Carrier 1/Carrier 2/ Carrier 2 $\Delta(GGGGCC)_n$: n=6/8/8/8/5). Cellular specification was equivalent across the five cell lines.

4.2.5 Presence of other cell types

At week 1 post-plate down, quantitative immunostaining was also performed for the astrocyte marker glial fibrillary acidic protein (GFAP) and neuronal marker β-III-tubulin as shown in

Figure 4.7. GFAP positive cells were found to be present in the cultures (Control 2, 24.7± SE 3.7%; Carrier 1, 25.2 ± SE 3%; Carrier 2, 20.0 ± SE 3.2%; Carrier 2 $\Delta(GGGGCC)_n$, 14.9 ± SE 1.4%), with no overall difference between carrier and control cell lines (p=0.14, Mann-Whitney test. There was also a low level of β-III-tubulin positive cells in the cultures (Control 2, 5.4± SE 1.1%; Carrier 1, 6.3 ± SE 0.9%; Carrier 2, 9.3 ± SE 2.0%; Carrier 2 $\Delta(GGGGCC)_n$, 8.8 ± SE 2.7%), which was equivalent between carrier and control lines (p=0.72, Mann-Whitney test).

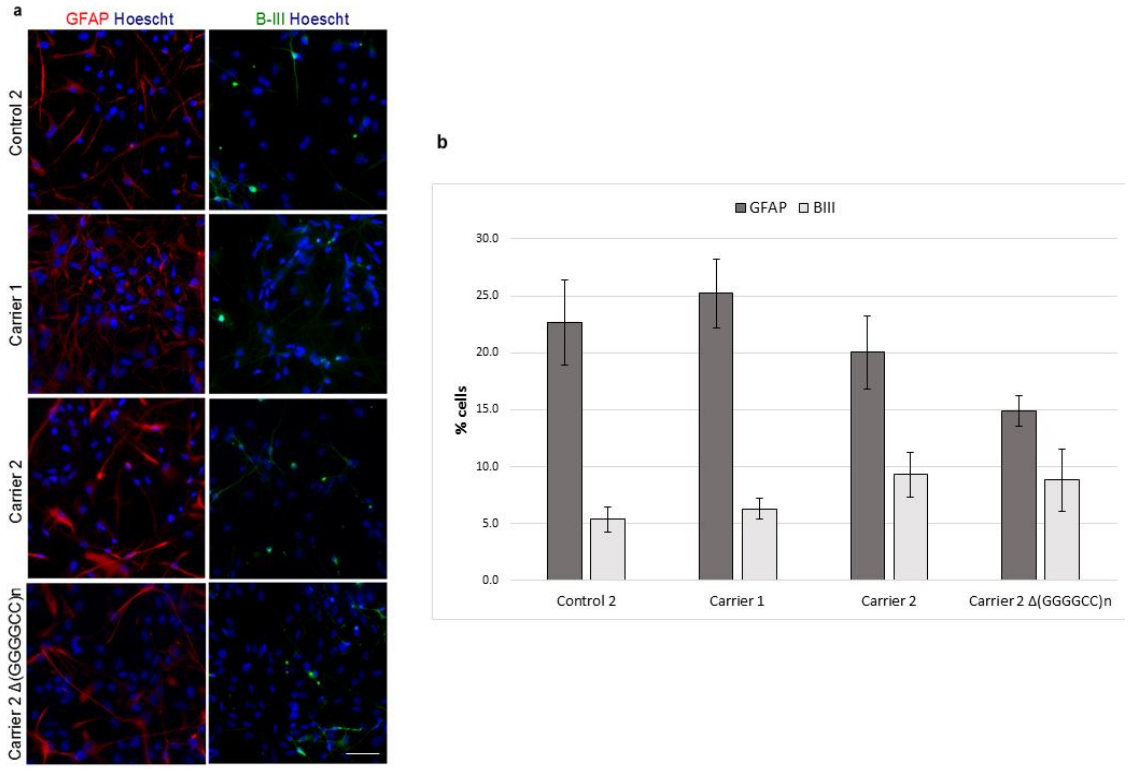

Figure 4.7 Immunocytochemical staining of GFAP and β-III tubulin positive cells and quantification

(a) Representative images of GFAP and β-III tubulin positive cells present. Scale bar = 50µm. (b) Graphs showing quantification of GFAP (Control 2/Carrier 1/Carrier 2/ Carrier 2 $\Delta(GGGGCC)_n$: n=7/8/8/8) and β-III tubulin (Control 2/Carrier 1/Carrier 2/ Carrier 2 $\Delta(GGGGCC)_n$: n=4/6/8/8) positive cells after 7 days in Oligo Diff medium.

4.2.6 Maturation of *C9orf72* HRE oligodendrocytes from hiPSCs

Electrophysiological recordings were made from PDGFR-α positive and O4 positive cells from both carrier and control cells to compare their maturation. This work was carried out by Dr Matt Livesey and Dr Owain James. In O4 positive cells at week 3, the percentage depression of rectification indices were measured (Control 1, 11.97 ± SE 3.8; Control 2, 12.4 ± SE 2.5; Carrier 1, 9 ± SE 3.6; Carrier 2, 16.3 ± SE 3.7) and found to be equivalent between control and carrier (p>0.27, unpaired t-test). At week 3 post plate-down, O4 positive cells

showed a strong functional downregulation of delayed-outwardly rectifying potassium channel and A-type potassium channel conductance, which was equivalent between control and carrier lines (Livesey et al., 2016). There was also no difference in whole cell capacitance and input resistance between control and carrier cells (Livesey et al., 2016). AMPA receptor unitary conductances reduce upon maturation from OPC to oligodendrocyte, and again there was no difference in the reduction between carrier and control cell lines (Livesey et al., 2016).

4.3 Discussion

In this chapter, I have shown that the *C9orf72* HRE was present in the carrier hiPSC lines, and was maintained in culture. There were no differences observed in the differentiation and maturation of oligodendrocytes containing *C9orf72* HREs, compared to controls from studies on cellular specification.

4.3.1 Validation of hiPSC lines

All four cell lines used in this study generated hiPSCs which expressed pluripotency markers NANOG, SOX2, TRA-1-60 and OCT3/4 (see Materials and methods). They were shown to be capable of generating all three germ layers, demonstrating that the cells were indeed pluripotent, regardless of whether they were reprogrammed using retrovirus or Sendai virus. Ideally, the cell lines would be matched in terms of sex and the age at which fibroblasts were obtained. In this respect, control 1 and carrier 1 are well matched, as are control 2 and carrier 2, although the latter differ in their reprogramming method.

Karyotyping was performed and showed the presence of normal karyotypes, with the exception of one of the control lines (Control 1), which developed an abnormality in culture (47, XYY). For this reason, some of the later characterisation was not completed on this line as it was subsequently excluded from the study. Similarly, Control 2 developed trisomy 12 in culture and some data was therefore excluded from later analysis, reducing the number of conversions which it was possible to analyse. The development of karyotypic abnormalities have been well described in iPSC cultures, with one study showing 12.5% of hiPSC cultures showing some abnormality (Taapken et al., 2011). Karyotypic abnormalities include changes in chromosomal number and structure and copy number variations such as insertions/duplications, deletions and loss of heterozygosity due to acquired uniparental disomy (Martins-Taylor and Xu, 2012).

Rates of aneuploidy increase with increasing passages, although they can occur at both early and late passages, so it is important that they are checked regularly (Taapken et al., 2011). The hiPSCs were also regularly tested for mycoplasma, and treated when required. This was

important as the presence of mycoplasma can have a substantial effect on gene expression and cellular behaviour, as well as influencing the differentiation capacity of pluripotent cells (Markoullis et al., 2009; Miller et al., 2003).

4.3.2 Presence of the *C9orf72* HRE

The presence of a *C9orf72* hexanucleotide repeat expansion in each of the two carrier cell lines was demonstrated using repeat-primed PCR. The control lines gave a negative result using this assay. Flanking PCR revealed that the size of the expansion changed during iPSC culture, with carrier 2 showing a repeat length of around 88 repeats, although there also appeared to be mosaicism for larger repeat expansions, which were exclusively present during other passages. This observation highlights the importance of checking the repeat size regularly and demonstrates the utility of the HPE assays, as this would not have been detected on the original PCR assays. Such instability is not unexpected and reveals the importance of having a reliable sizing assay and for strict quality control measures during culture. Studies on repeat stability in other repeat expansion disorders including myotonic dystrophy type 1 and Fragile X syndrome have shown high levels of instability in hES cells, with a tendency towards increasing size with passaging, however differentiation appears to be associated with a stabilization of repeat size (De Temmerman et al., 2008; Eiges et al., 2007; Seriola et al., 2011). It has been shown that skin-derived fibroblasts with *C9orf72* expansions have a lower number of repeats than in blood from the same patients, which may reflect a selective advantage for cells in culture with shorter expansions (van Blitterswijk et al., 2013b). Cell lines were checked at the iPSC stage or during differentiation for each derivation of cells used in this study, and consistently showed the presence of at least 100 repeats at the C9orf72 HRE locus. The technique used did not allow assessment of the actual size of expansion present.

4.3.3 Creation of isogenic control

The creation of the isogenic control for Carrier 2 was a significant advance in reducing the background variation between control and carrier lines. This allows for increased confidence that any differences between control and carrier lines are due to the presence of the C9orf72 HRE, and not simply due to background genetic differences between the lines. The generation of the isogenic line was an inefficient process, and this may have been related to design of the guide RNAs, which did not take into account the presence of a 10 bp deletion adjacent to the HRE, as this was only detected following the creation of the isogenic control. Ideally, of course, it would be desirable to have isogenic controls available for each of the carrier cell lines that are used, and this work is ongoing in the laboratory. The other cell lines have the

expected sequence adjacent to the HRE and therefore the efficiency of deletion of the HRE may be higher than for the line used in this study.

It is worth noting, that even with the use of an isogenic control, there may still be differences which emerge through epigenetic changes which are specific to one or other of the cell lines, which may be related to passage number. The stringent checks on karyotypes and mycoplasma presence are still required to minimise the risk of differences emerging due to some other factor than the *C9orf72* HRE.

4.3.4 Differentiation of hiPSC to oligodendrocytes

The protocol for generating OPCs and oligodendrocytes has been shown to be reproducible and consistent across the five hiPSC lines tested. There were no significant differences between the control and *C9orf72* hexanucleotide expansion cell lines in their generation of oligodendrocyte lineage cells, as shown by the quantification of Olig2, PDGFR-α, O4 and MBP positive cells. There appeared to be more variation in the percentage of Olig2 positive cells and this may reflect more variable staining and subjective counting of positive cells with this nuclear marker. However, there is no trend apparent between control and carrier lines.

When performing quantitative immunocytochemistry, I cultured the cells on glass coverslips, and this protocol appeared to produce a relatively low yield of O4 positive cells, however there appeared to be a greater percentage of O4 positive cells when the cells were cultured on plastic (Livesey et al., 2016). There were differences apparent in the cell adhesion to these different surfaces, with each requiring different fibronectin concentrations which may further contribute to the differences observed in the number of O4 positive cells. For much of the later analysis that I have performed (RNA-FISH, Sholl analysis and TDP-43/p62 staining), microscopy constraints required that the cells were cultured on glass, hence why I chose to quantify the cells under the same conditions.

There was no apparent difference between the proportions of O4 cells which also display PDGFR-α or MBP between the lines. This gives a crude measure of the cell maturation pattern. The expected expression pattern would be that PDGFR-α positive cells differentiate to O4 positive cells, before finally expressing MBP. The overlap between O4 and MBP is approximately 90%, and given the absence of cells solely expressing MBP, suggests that these cells are not yet terminally differentiated in the cultures as the levels of O4 sulfatide decrease during differentiation (Schachner et al., 1981). The similar levels of overlap seen for each of the cell lines suggests that there is not a gross differentiation abnormality present in the *C9orf72* expansion carrying oligodendrocytes, although further work with regards to cell

proliferation and survival would be needed to investigate this more fully. The proliferation rates of control and carrier OPCs were investigated by Dr. Navneet Vasistha, using ethynyl deoxy-uridine (EdU) and Ki67, and these assays showed no consistent differences (Livesey et al., 2016).

As well as showing consistent generation of oligodendrocyte lineage cells, the percentage of GFAP and βIII-tubulin positive cells were also similar between control and carrier cell lines. Other oligodendrocyte generating protocols have reported higher levels of GFAP positive cells from hiPSC lines, up to 40-50% of total cells, and suggest that these can arise from OPCs (Wang et al., 2013). Earlier studies on ES derived oligodendrocytes showed less than 5% neurons and astrocytes were present (Kang et al., 2007).

For assays which were based on population studies rather than looking at individual cells, this cellular composition was particularly important, which was why MACS was used to enrich for O4 positive cells prior to these assays. For biochemical studies, the cells were cultured on plastic as this appeared to generate a much greater yield of O4 positive cells as described previously. MACS was then performed, which generated cell pellets with up to 90% O4 positive cells for other cell lines (Magnani, personal communication).

4.3.5 Maturation of *C9orf72* HRE oligodendrocytes from hiPSCs

During differentiation and maturation of OPCs to oligodendrocytes, the excitable membrane properties of the cells have been shown to change significantly in rodent systems. The maturation of oligodendrocytes from OPCs using the protocol described, has suggested that the electrophysiological changes which occur during this transition are conserved between rodents and humans (Livesey et al., 2016). Using an array of electrophysiological, immunocytochemical and biochemical approaches, these properties have been investigated in our hiPSC derived OPCs and oligodendrocytes. We found that as human oligodendrocytes develop and express more mature markers, there is a progressive decline in voltage-gated sodium and potassium channel activity, and a loss of tetrodotoxin-sensitive spiking activity (Livesey et al., 2016). At the same time, there is an increase in inwardly rectifying potassium channel activity and a change in the AMPA receptor composition (Livesey et al., 2016). These changes are observed equivalently in both control and *C9orf72* HRE carrier oligodendrocytes (Livesey et al., 2016). In this study, we have only investigated the process of oligodendrocyte development and therefore cannot exclude changes that occur in the context of myelination, or at later stages of disease.

4.4 Conclusion

In this chapter, I have described the protocol which has been used to generate oligodendrocytes from hiPSCS. I have used this protocol to derive oligodendrocytes which carry the *C9orf72* HRE as well as controls. I have shown that the *C9orf72* HRE has been maintained during cell culture, and described how an isogenic control was generated. Studies on cellular specification has shown that the cell lines with and without the *C9orf72* HRE behaved in a similar manner with regards to the differentiation and maturation of oligodendrocytes.

Chapter 5. Investigating pathological features of oligodendrocytes from patient derived induced pluripotent stem cells with C9orf72 hexanucleotide expansions

5.1 Introduction

The involvement of oligodendrocytes in the pathogenesis of ALS has been investigated mainly through studies on SOD1 mutant rodents (Kang et al., 2013; Lee et al., 2012; Philips et al., 2013). In $SOD1^{G93A}$ mice, oligodendrocyte progenitor cells in the spinal cord proliferate rapidly but fail to differentiate and mature effectively, which leads to progressive demyelination, before the onset of disease symptoms (Kang et al., 2013; Lee et al., 2012). In ALS patients, reactive changes in oligodendrocytes in the motor cortex have been reported, along with demyelination in the spinal cord and motor cortex in both sporadic and familial cases (Kang et al., 2013; Lee et al., 2012). Elegant studies whereby the $SOD1^{G93A}$ mutation has been selectively ablated from the oligodendrocyte lineage in mice resulted in delayed onset of disease and increased survival (Kang et al., 2013). Such experiments have highlighted the importance of non-cell autonomous mechanisms in ALS pathogenesis, but in a complex *in vivo* model it is very difficult to tease apart the individual cellular roles contributing to motor neuron degeneration. *In vitro* cellular models give a unique opportunity to study cells without the complexity of the *in vivo* environment. The effect of the commonest ALS causing genetic mutation, *C9orf72* HRE, on oligodendrocytes is an area which has not been thoroughly investigated. The presence of RNA foci has been reported in oligodendrocytes from the frontal cortex of *C9orf72* related frontotemporal dementia cases at post-mortem (Mizielinska et al., 2013). One recent publication has used a similar methodology to that described in this thesis to investigate the influence of various ALS associated mutations in oligodendrocytes, on wild-type motor neurons (Ferraiuolo et al., 2016).

5.1.1 Pathological features of *C9orf72* HRE

There are three main proposed mechanisms by which the *C9orf72* HRE results in pathology (see section 1.3.4). These are loss of function by reduced gene expression, or gain of function by either RNA toxicity or formation of dipeptide repeat protein production by RAN translation (Ling et al., 2013). Although these mechanisms have been investigated by others in the context of motor neurons, it is of interest to determine whether there is evidence for any of the

associated pathological signs in other cell types which could contribute to disease pathogenesis.

5.1.2 Oligodendrocyte pathology in ALS

Oligodendrocytes from patients with ALS have been found to contain p62 and TDP-43 intracytoplasmic inclusions (Mackenzie et al., 2011; Neumann et al., 2006; Seilhean et al., 2009). Post-mortem spinal cord and motor cortex samples from ALS patients show reduced myelin compared to unaffected controls (Kang et al., 2013). The rat $SOD1^{G93A}$ ALS model displays altered myelin composition, which is reported to occur even in pre-symptomatic stages of the disease, although it is not clear whether this is a secondary effect to axonal dysfunction (Niebroj-Dobosz et al., 2007). In the $SOD1^{G93A}$ mouse ALS model, oligodendrocytes have an altered morphology, even before symptoms appear (Philips et al., 2013). In this model, oligodendrocytes have an increased turnover, with more cells dying and an apparent compensatory increase in oligodendrocyte precursor cell proliferation and differentiation (Kang et al., 2013; Philips et al., 2013). The resulting cells are dysfunctional in terms of myelination and trophic support, as indicated by reduced myelin basic protein (MBP) and monocarboxylate transporter (MCT1) expression respectively (Kang et al., 2013; Philips et al., 2013). The loss of MCT1 from oligodendrocytes is thought to contribute to neurodegeneration (Lee et al., 2012).

5.1.3 Objectives

The aims of this chapter were to investigate the pathological features in hiPSC derived oligodendrocytes related to the *C9orf72* expansion, including C9orf72 mRNA levels, presence of RNA foci and DPR. Furthermore, I wanted to investigate whether there were any morphology differences apparent in *C9orf72* HRE hiPSC derived oligodendrocytes. I also wanted to determine whether the *C9orf72* HRE influence the mRNA levels of MBP and MCT1, whether there was evidence of TDP-43 mislocalisation or p62 accumulation and whether there was a susceptibility of these cells to endoplasmic reticulum (ER) stress.

5.2 Results

5.2.1 *C9orf72* mRNA expression levels in O4+ cells

To check whether there was evidence for a loss of function of *C9orf72* in oligodendrocytes, I carried out qRT-PCR experiments to investigate mRNA levels in control versus carrier cells. I investigated the expression of the three mRNA isoforms of *C9orf72* (Fig 5.1a) on cells which had been cultured for 3 weeks in Oligo Differentiation medium, and then MACS sorted for O4. The most abundant transcript was found to be variant 2, followed by variant 3 and then

variant 1 (data not shown). The relative fold change (all data normalised to the geometric mean of glyceraldehyde-3-phosphate dehydrogenase (*GAPDH*) and *β-actin*, and calculated relative to one sample from control 2 using the ΔΔCt method) was calculated for variant 1 (Control 1, 3.9 ± SE 1.4; Control 2, 5.4 ± SE 1.5; Carrier 1, 4.6 ± SE 1.0; Carrier 2, 4.6 ± SE 1.2, Carrier 2 $\Delta(GGGGCC)_n$: 2.2 ± SE 0.3, N=5, Fig 5.1b), variant 2 (Control 1, 3.2 ± SE 0.8; Control 2, 2.1 ± SE 0.6; Carrier 1, 1.1 ± SE 0.1; Carrier 2, 1.8 ± SE 0.7, Carrier 2 $\Delta(GGGGCC)_n$: 1.6 ± SE 0.4, N=5, Fig 5.1b) and variant 3 (Control 1, 2.5 ± SE 0.9; Control 2, 4.2 ± SE 1.6; Carrier 1, 4.1 ± SE 0.8; Carrier 2, 8.3 ± SE 2.3, Carrier 2 $\Delta(GGGGCC)_n$: 3.7 ± SE 0.5, N=5, Fig 5.1b).

No consistent reduction was observed in *C9orf72* mutant oligodendrocytes compared to controls. The effects were variant specific with no difference for variant 1 (p=0.28, Mann-Whitney test), while for variant 2, there was a trend for lower expression in carriers than controls (p=0.06, Mann-Whitney test). For variant 3, the trend was reversed with higher expression in carriers than controls (p=0.07, Mann-Whitney test). The observed variability may be due to the low expression levels of all *C9orf72* transcripts in oligodendrocytes, which make it challenging to interpret as the assays are at the limit of sensitivity of qPCR. Comparison of expression levels to cortical neurons (n=1) suggested that levels in O4+ cells were lower (relative fold expression with respect to hiPSC derived control cortical neurons: V1, 41.7%; V2, 11%; V3, 3.9%) which is consistent with reports in the literature of low *C9orf72* expression levels in glial cells (Suzuki et al., 2013).

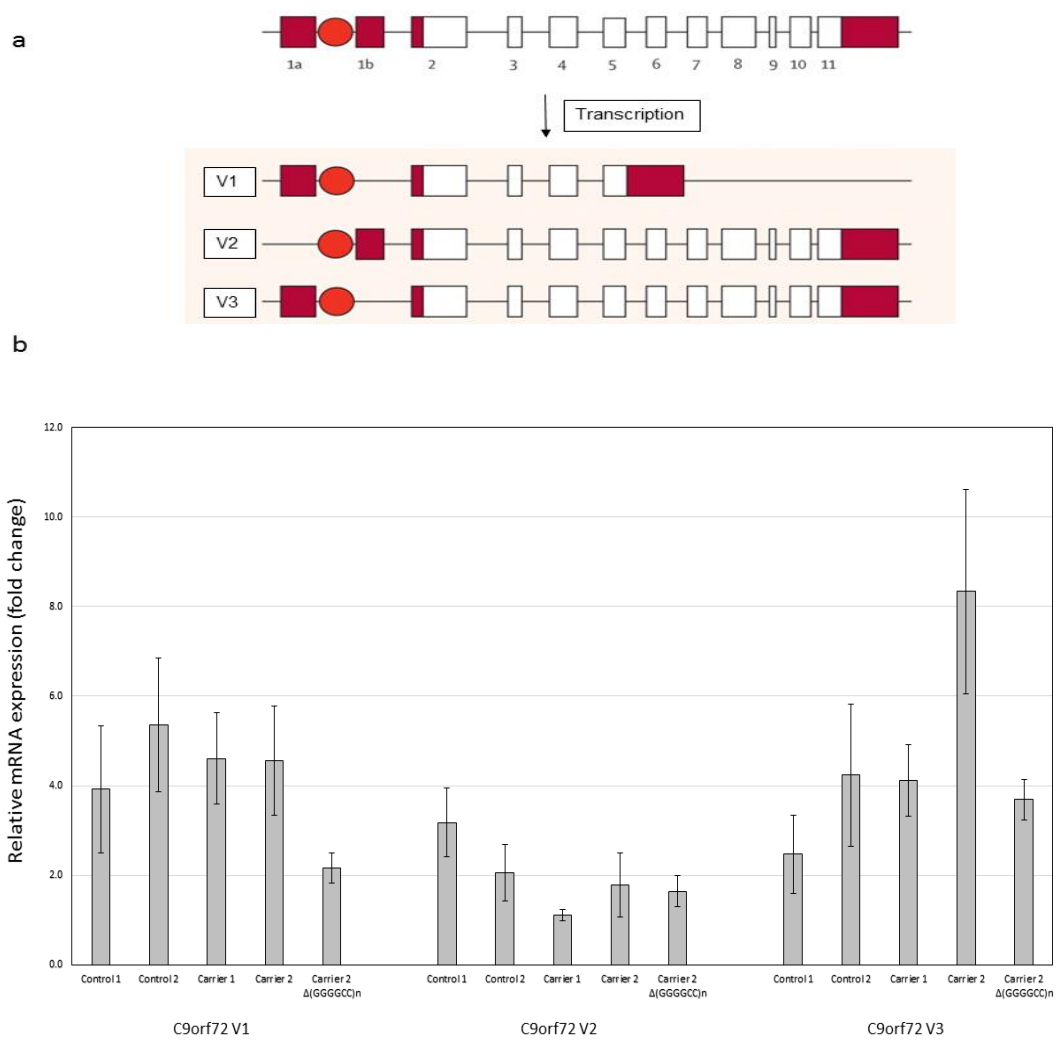

Figure 5.1 Transcript levels of *C9orf72* in oligodendrocytes

a. Schematic of the three transcript variants generated from the *C9orf72* gene (top): variant 1 (V1: NM_145005.5), variant 2 (V2: NM_01835.4) and variant 3 (V3: NM_001256054.1). The UTRs are represented by the pink boxes, coding exons by white boxes and the location of the hexanucleotide repeat expansion is represented by the red circle. Adapted (Rohrer et al., 2015). **b**. qRT-PCR analysis of the three *C9orf72* transcripts on mRNA extracted from cell pellets (N=5 for each cell line) obtained after three weeks of differentiation and MACS sorting for O4. Data were analysed by normalising to *GAPDH* and *β-actin* and comparing to a control using the ΔΔCt method.

5.2.2 Presence of RNA foci

To check whether RNA foci were present in *C9orf72* HRE hiPSC derived oligodendrocytes, I optimised a previously published RNA fluorescence in situ hybridization (FISH) protocol by increasing the hybridisation temperature and used this to show the presence of sense RNA foci in oligodendrocyte lineage cells derived from hiPSCs (Almeida et al., 2013). I initially

optimized the RNA-FISH protocol on two hiPSC lines carrying *C9orf72* repeat expansions and one control. As shown in Figure 5.2, the presence of nuclear, and occasional cytoplasmic, $(GGGGCC)_n$ foci were observed in the expansion containing lines, but not in controls. Treatment with RNase A prior to probe hybridisation prevented detection of any foci, suggesting that the foci contain RNA. Hybridisation with a control probe targeting an unrelated CCTG repeat (probe $(CAGG)_6$ showed no RNA foci containing such a repeat, supporting the specificity of the $(CCCCGG)_4$ probe.

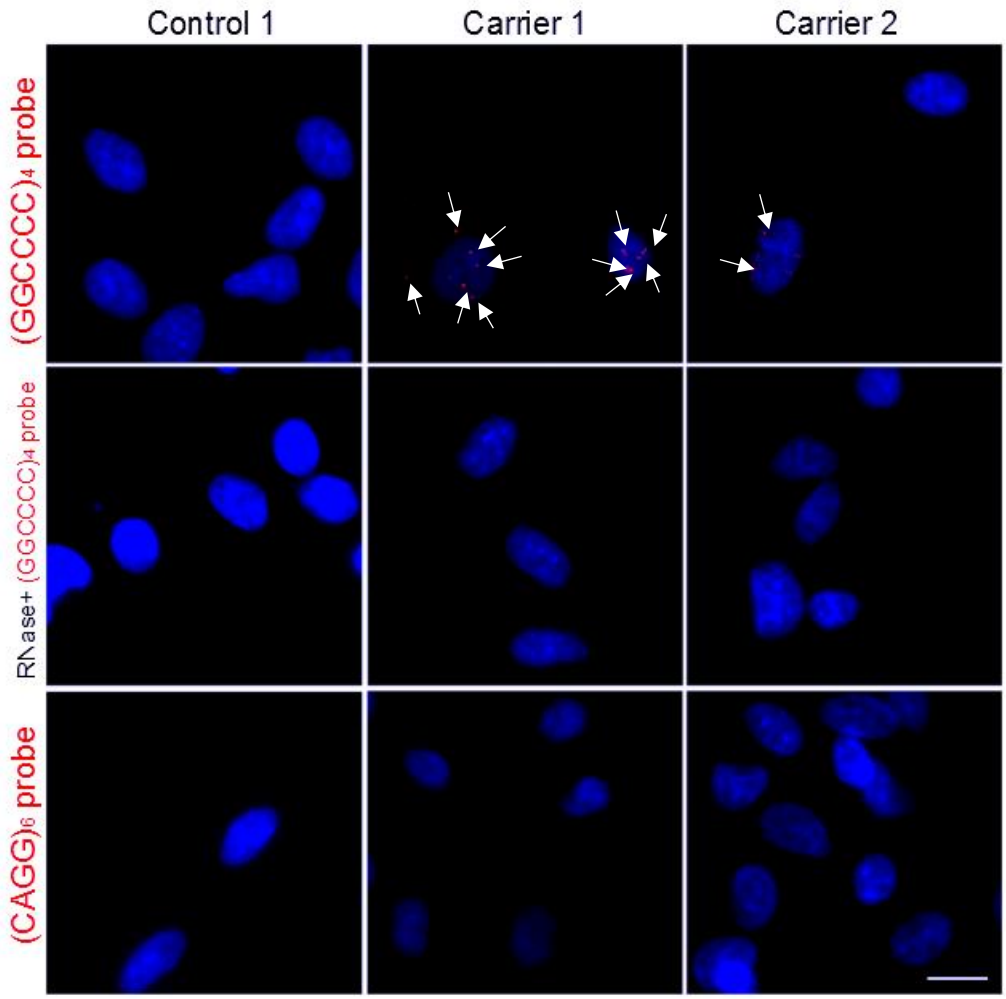

Figure 5.2 RNA-FISH validation with controls and carriers

RNA FISH with a $(CCCCGG)_4$ probe on control cells reveals that no GGGGCC foci (red) are observed, whereas these are present in both hiPSC derived cell lines from a patient carrying the *C9orf72* hexanucleotide repeat expansion. These foci are mainly nuclear, and occasionally cytoplasmic. Treatment with RNase A prior to performing RNA-FISH results in loss of GGGGCC foci (red) which suggests that the observed signal is from an RNA containing structure. RNA FISH with a $(CAGG)_6$ probe (red) does not result in detection of foci, as would be expected. All counterstained with Hoescht. Scale bar 10µm.

Following the optimisation of the RNA-FISH technique for sense RNA foci, I then combined it with immunocytochemistry to determine if foci were present in different cell types derived from *C9orf72* hexanucleotide repeat expansion hiPSCs. Sense RNA foci were detected in PDGFR-α (Figure 5.3a) positive cells, O4 positive cells (Figure 5.4a), and cells labelled with MBP and GFAP (Figure 5.5).

It was clear that not all cells contained sense RNA foci, and therefore I quantified the number of cells which contained foci. Using RNA-FISH, I observed that hiPSC-derived PDGFR-α positive cells contain nuclear sense RNA foci one week post plate-down (Control 2, 1.8 ± SE 1.5%; Carrier 1, 20.5 ± SE 9.4%; Carrier 2, 27.1 ± SE 5.8%, N=3, Fig 5.3b). There were significantly more foci in carriers compared to controls ($p=0.02$, Student's unpaired t-test). Although it was expected that there would not be any RNA foci present in controls, there was very occasional cells in which a single foci were detected, which is likely to represent very low level background signal in the control.

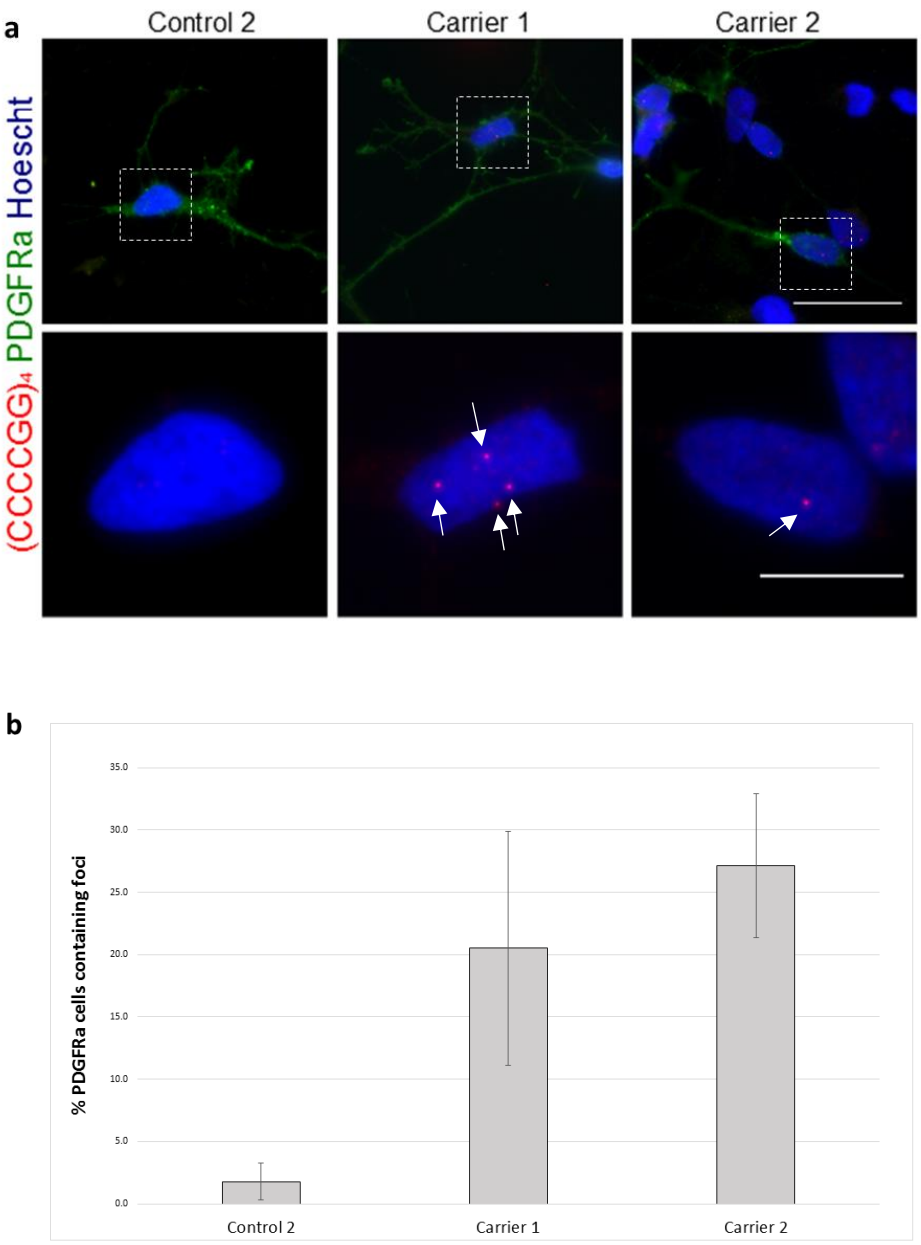

Figure 5.3 hiPSC derived PDGFR-α positive oligodendrocyte precursor cells with *C9orf72* HRE exhibit nuclear GGGGCCexp RNA foci while controls do not.

(a) RNA-FISH with $(CCCCGG)_4$ probe in control and carrier cell lines, with staining of O4 positive cells in upper panel. Dashed box indicates area which is shown in lower panel. Scale bar upper panel 30µm; lower panel 10 µm. All counterstained with Hoescht. (b) Graph of quantification of PDGFRα positive cells which have nuclear sense RNA foci at week 1 post plate-down (N=3, minimum of 100 cells analysed).

Quantification of RNA foci in hiPSC derived O4 positive cells was performed at weeks 1 and 3 post plate-down. (Control 2 week 1, 0.5 ± SE 0.5%, N=6; Control 2 week 3, 1.2 ± SE 0.7%, N=4; Carrier 1 week 1, 38.6 ± SE 3.8%, N=6; Carrier 1 week 3, 42.2 ± SE 5.2%, N=6; Carrier 2 week 1, 49 ± SE 7.1%, N=6; Carrier 2 week 3, 61.0 ± SE 3.8%, Carrier 2 $\Delta(GGGGCC)_n$ week 1: 0 ± SE 0%, Carrier 2 $\Delta(GGGGCC)_n$ week 3: 0 ± SE 0%, Fig 5.4b). There was a significantly higher number of cells with RNA foci in carriers than controls (week 1: p=0.0034; week 3: p=0.0008, Mann-Whitney test). To investigate whether there was a change in the number of foci containing cells over time, I compared matched batches of cells which were quantified at weeks 1 and 3 (Figure 5.4c). There was not a significant difference between RNA foci at weeks 1 and 3 (Carrier 1 (N=3), p=0.0669; Carrier 2 (N=3), p=0.2117, Student's paired t-test), although there is a trend for Carrier 1 to show an increase in foci over time. In the O4 positive cells which contained nuclear foci, the average number of foci per cell was 3.7 for Carrier 1 and 5.6 for Carrier 2, with the mode being 1 RNA foci for both cell lines. It was not possible to compare OPCs and oligodendrocytes directly because the combined immunostaining had to be done differently for each of the markers. In particular, PDGFRα staining was poor unless the ethanol incubation step was omitted, however, this permeabilization step increased the number of RNA foci detected by 57 ± SD 13% when no staining was performed (N=2) and therefore the number of PDGRFα positive cells which appear positive for RNA foci will be underestimated for this reason.

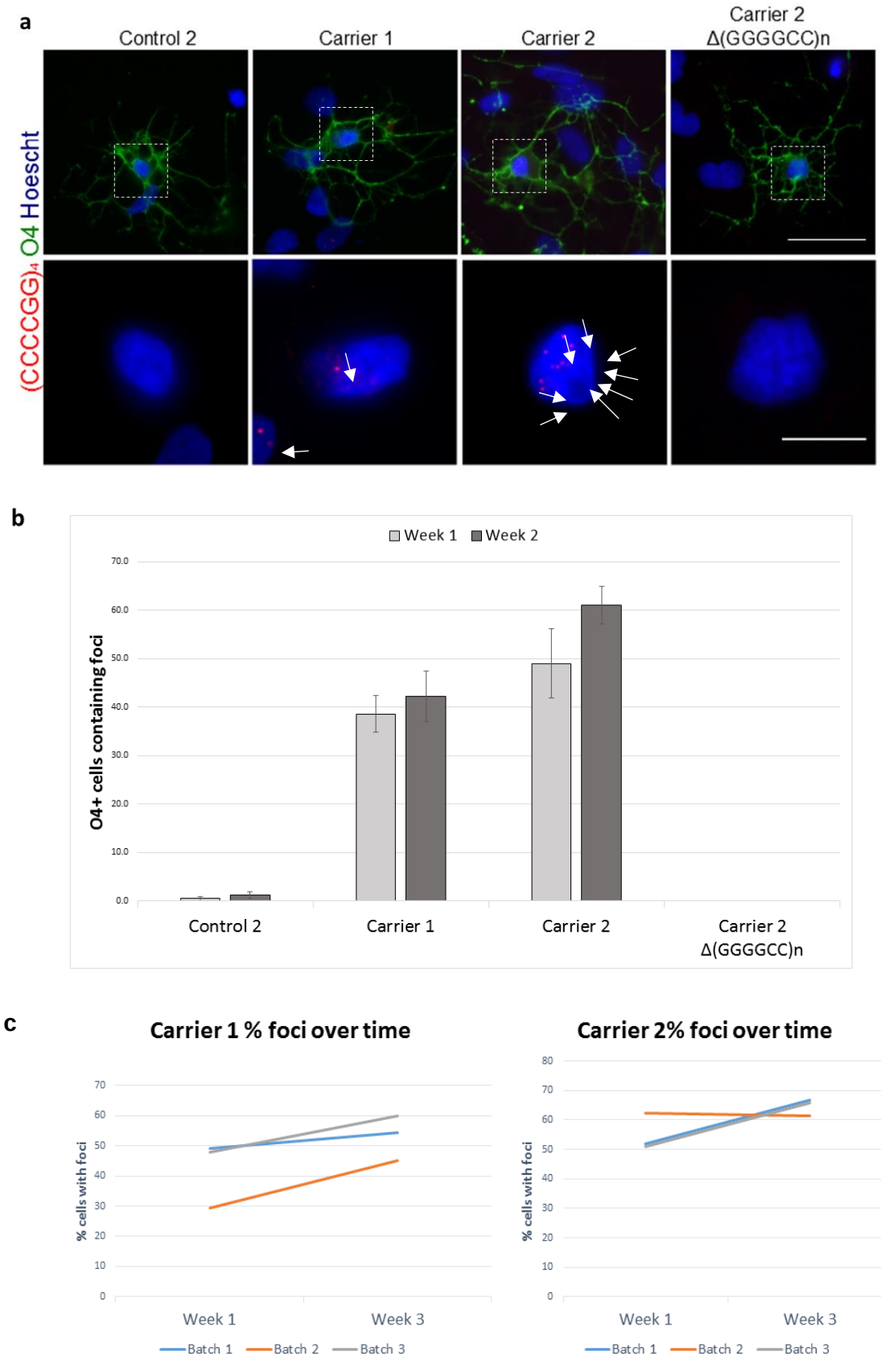

Figure 5.4 hiPSC derived O4-positive oligodendrocytes with *C9orf72* HRE exhibit nuclear GGGGCCexp RNA foci.

Figure 5.4 hiPSC derived O4-positive oligodendrocytes with *C9orf72* HRE exhibit nuclear GGGGCCexp RNA foci.

(a) RNA-FISH with $(CCCCGG)_4$ probe (red) in control and carrier cell lines, with staining of O4 positive cells (green) in upper panel. Dashed box indicates area which is shown magnified in lower panel. Scale bar upper panel 30µm; lower panel 10 µm. All counterstained with Hoescht. (b) Graph of quantification of PDGFRα positive cells which have nuclear sense RNA foci at week 1 post plate-down (N=3). (c) Graph of quantification of O4+ cells which have nuclear sense RNA foci at both week 1 and week 3 post plate-down for carrier 1 and carrier 2 (N=3, minimum of 200 cells analysed).

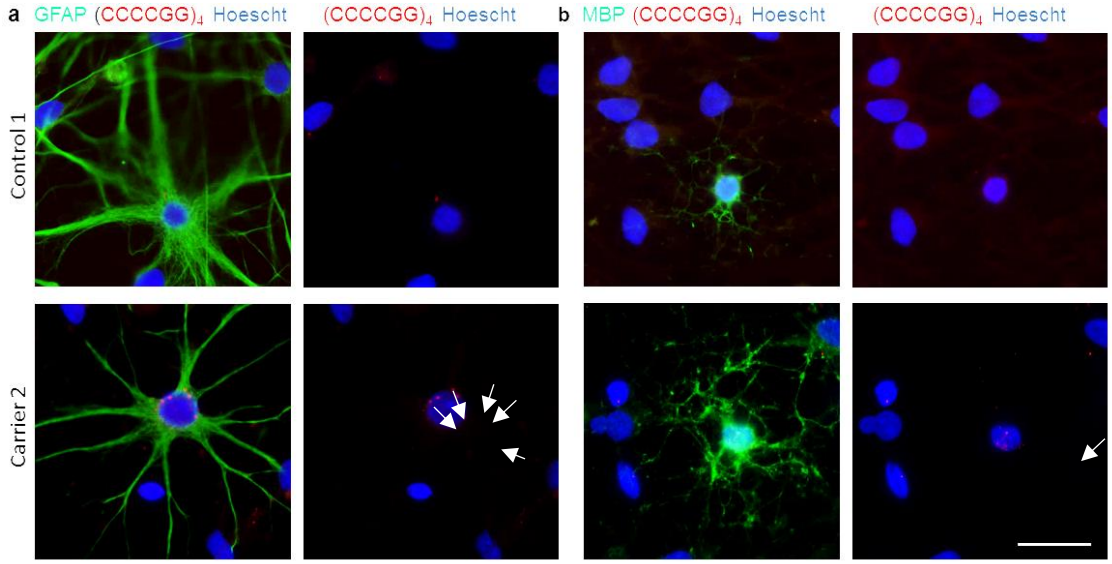

Figure 5.5 hiPSC derived GFAP-positive astrocytes and MBP-positive oligodendrocytes with *C9orf72* HRE exhibit nuclear GGGGCCexp RNA foci.
(a) RNA-FISH with $(CCCCGG)_4$ probe (red) in control and carrier cell lines, with staining of GFAP positive cells (green) in left hand panel. (b) RNA-FISH with $(CCCCGG)_4$ probe (red) in control and carrier cell lines, with staining of MBP positive cells (green) in left hand panel. Scale bar panel 20µm. All counterstained with Hoescht.

I went on to perform Sholl analysis on O4 positive cells, to investigate whether there was a morphology difference between cells which contain RNA foci or not. There does not appear to be any consistent differences between the number of branches observed in cells which contain foci compared to those which do not. This suggests that the RNA foci are not associated with a change in the morphology of the cells (Figure 5.6).

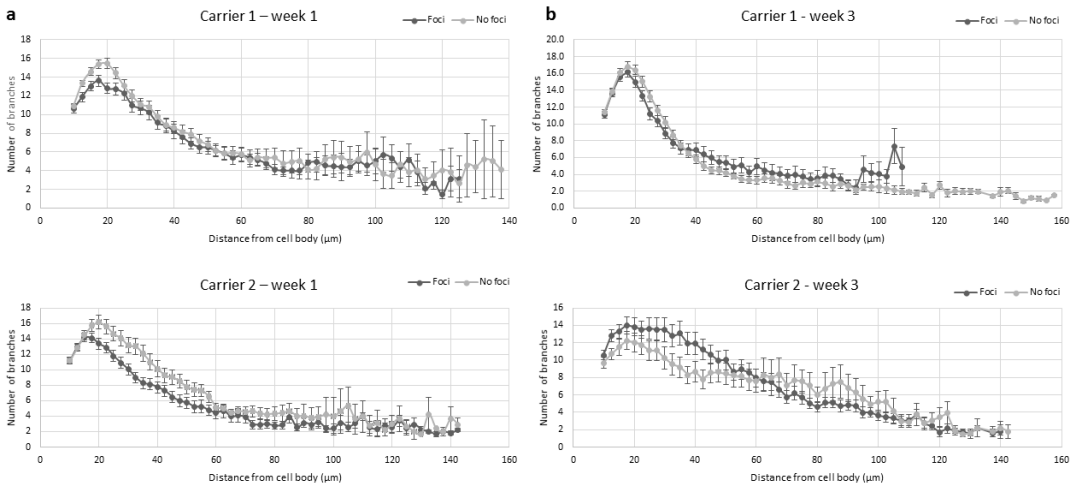

Figure 5.6 Sholl analysis on O4 positive cells with and without RNA foci

(a) Sholl analysis performed on O4 positive cells at 1 week post-plate down, stratified for presence of absence of sense RNA foci. Carrier 1 (Foci, n=95 cells; no foci, n=149 cells), Carrier 2 (Foci, n=106 cells; no foci, n=108 cells). (b) Sholl analysis performed on O4 positive cells at 3 weeks post-plate down, stratified for presence of absence of sense RNA foci. Carrier 1 (Foci, n=112 cells; no foci, n=143 cells), Carrier 2 (Foci, n=66 cells; no foci, n=54 cells).

5.2.3 Presence of DPR

To investigate the presence of DPR in hiPSC derived *C9orf72* expansion carrying oligodendrocytes reliable antibodies against these were required. To test whether the commercially available C9 RAN antibodies could detect DPR, I ectopically expressed each of the DPR in human embryonic kidney (HEK) cells by transfecting with a plasmid that encoded a specific DPR (GA, GP, GR, PA or PR), along with a V5 tag, and then tested the antibodies by immunocytochemistry. By comparing the expression pattern of the V5 tag, which acted as a positive control for the transfection, to that of the DPR antibody, the specificity of the C9RAN antibodies could be tested. Overlapping staining by antibodies against V5 and DPR were the desired result from a reliable antibody. Another PhD student within the laboratory tested the antibodies in parallel using Western blotting.

The first commercial C9RAN antibody (Novus) revealed non-specific binding, predominantly in nuclei. There is also background present in the non-transfected negative control. However, it did appear to detect poly-GP and poly-PA dipeptides in cells expressing these (Figure 5.7).

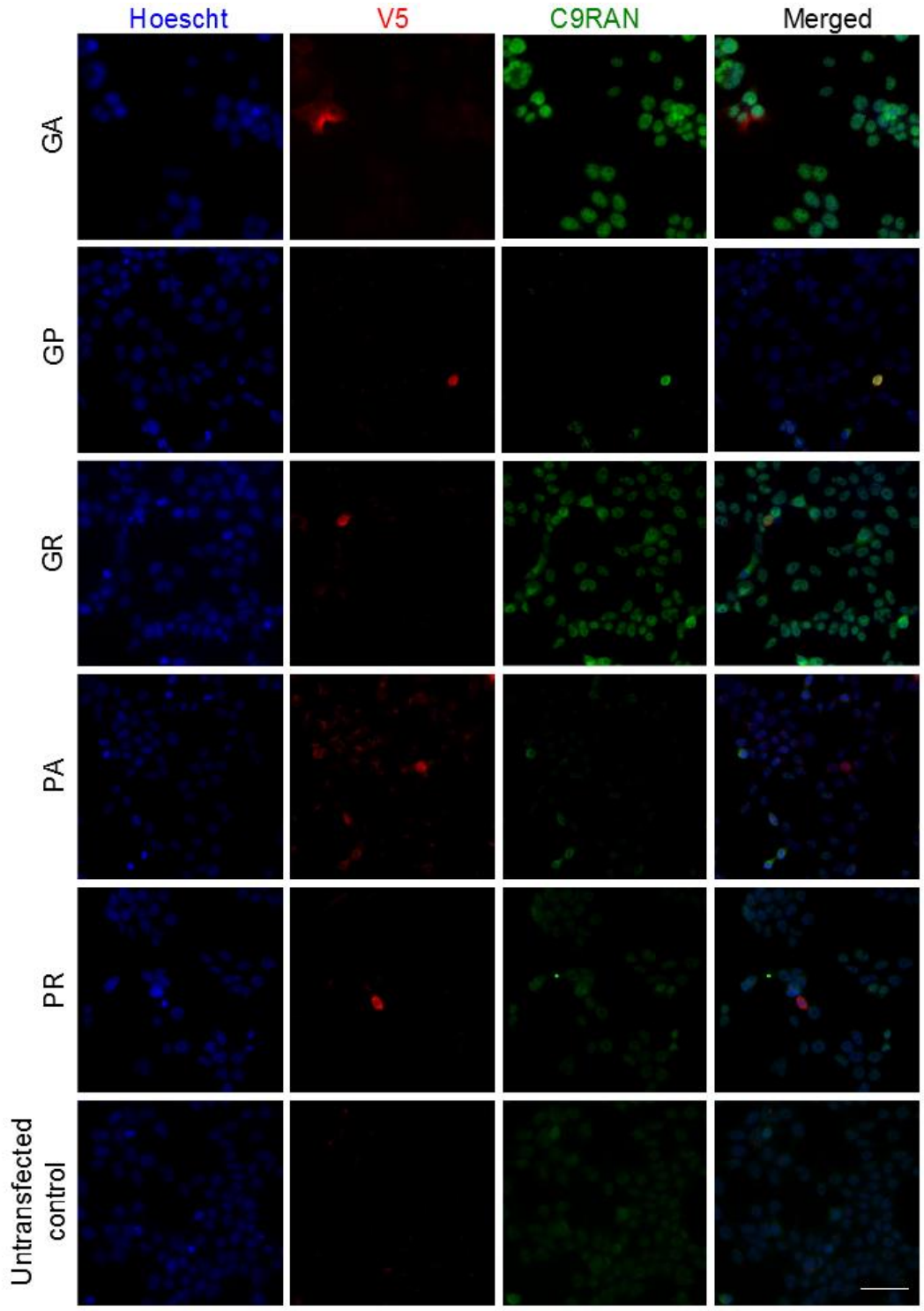

Figure 5.7 Novus C9RAN antibody testing on transfected HEK cells

HEK cells transfected with each of the DPR plasmids, followed by immunocytochemistry using the V5 tag and Novus C9RAN antibody. Counterstained with Hoescht. Scale bar 50µm.

The second antibody (Millipore) also gave non-specific background staining, but appeared to pick up poly-GA dipeptides in cells expressing these, and showed weak staining for poly-PR and poly-GP (Figure 5.8).

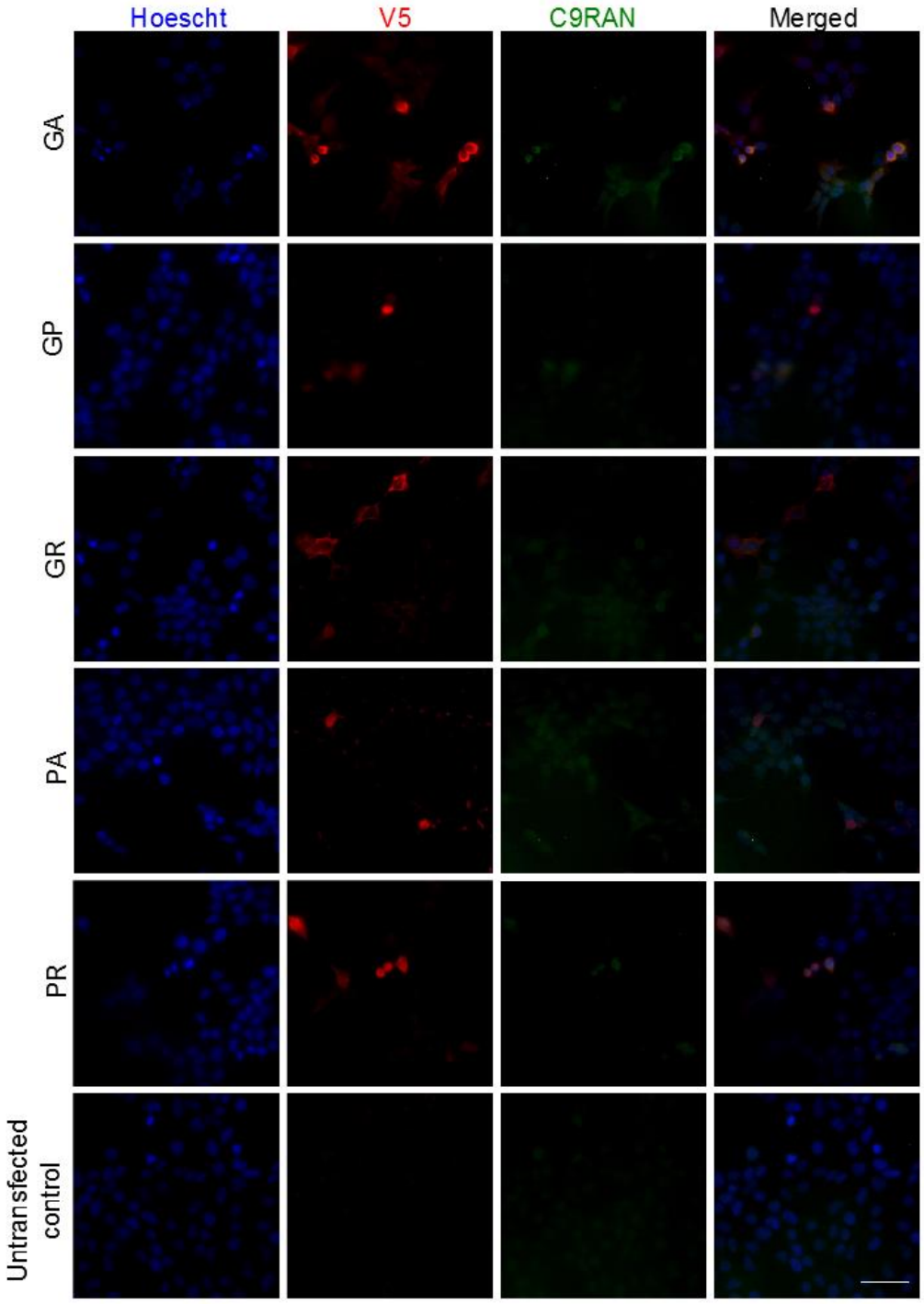

Figure 5.8 Millipore C9RAN antibody testing on transfected HEK cells

HEK cells transfected with each of the DPR plasmids, followed by immunocytochemistry using the V5 tag and Millipore C9RAN antibody. Counterstained with Hoescht. Scale bar 50µm.

Because both of these commercially available antibodies suggested that there were issues with background, non-specific staining, and to enable the detection of individual DPRs rather than several, Biogen Idec generated antibodies which were shared with us to try. Again, I used HEK cells transfected with each of the DPR plasmids to test these (Figure 5.9). Anti-GA antibody staining overlapped with GFP staining. Anti-GP appeared to stain appropriately but was not completely specific as there was some background staining. Anti-GR staining completely failed. Anti-PA antibody appeared to be both sensitive and specific, while anti-PR gave non-specific nuclear staining.

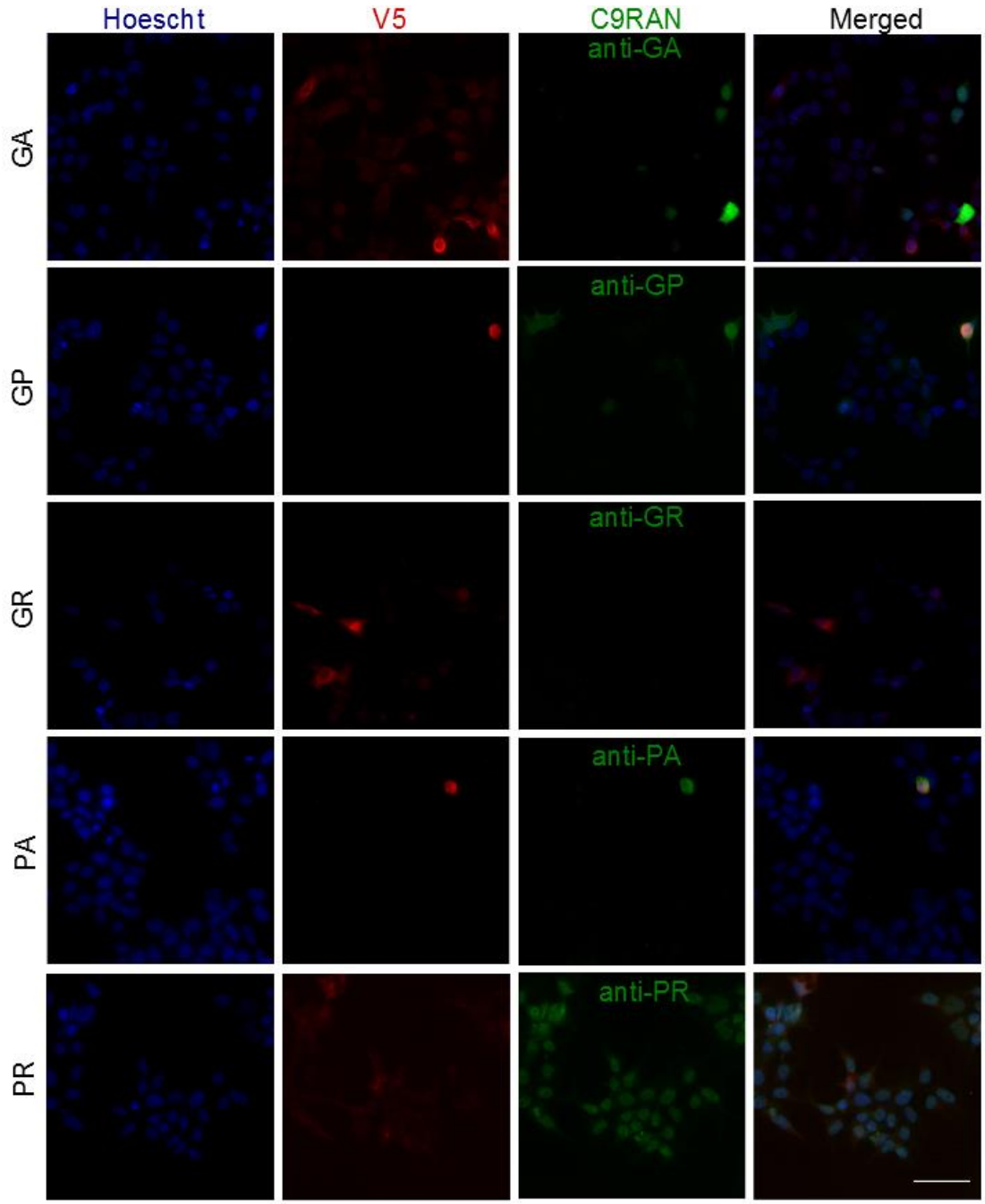

Figure 5.9 Biogen C9RAN antibody testing on transfected HEK cells

HEK cells transfected with each of the DPR plasmids, followed by immunocytochemistry using the V5 tag and specific Biogen antibody for that DPR. Counterstained with Hoescht. Scale bar 50µm.

As the anti-PA antibody appeared in the previous experiments to bind specifically, I went on to test this further in post-mortem brain material. Material was kindly supplied from three *C9orf72* HRE cases from Colin Smith's laboratory (University of Edinburgh), who prepared the tissue and provided slices for staining. Control material was obtained from the Netherlands brain bank. This was stained using anti-PA, which did not provide conclusive evidence that inclusions were *C9orf72* HRE specific, as there was some evidence of inclusion-like staining in controls as well as shown in Figure 5.10.

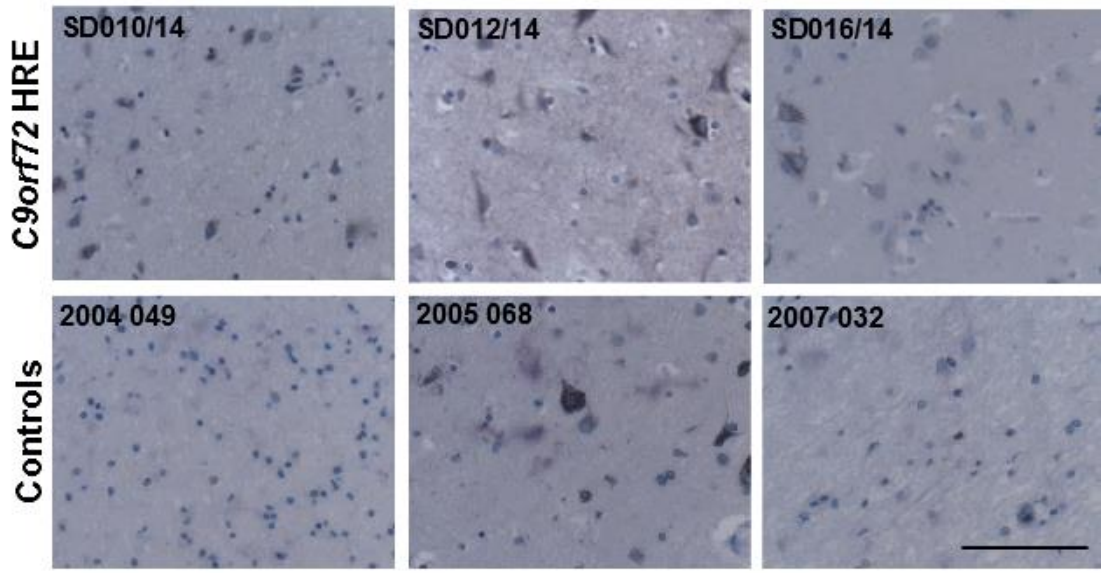

Figure 5.10 Immunohistochemistry using Biogen anti-PA antibody

Immunohistochemistry using Biogen anti-PA antibody on post-mortem material from three *C9orf72* HRE carriers (upper panels: SD010/14, SD012/14 and SD016/14) and three control patients (2004 049, 2005 068, 2007 032). Scale bar 100µm. Counterstained with haematoxylin.

Because of the difficulties in detecting DPR with the available antibodies, extracted protein from control and *C9orf72* hiPSC derived oligodendrocytes was sent to Chris Shaw's laboratory where Younbok Lee (King's College, London) performed Western blots with anti-GA, anti-GP and anti-PA antibodies (Figure 5.11). The anti-GA antibody showed a high degree of non-specific binding, and a protein of the correct size was detected in both control and *C9orf72* HRE carriers. This suggests that the antibody is not specific to the DPR. The Western blot with anti-GP and anti-PA antibodies showed no GP or PA DPRs in any of the hiPSC derived oligodendrocytes.

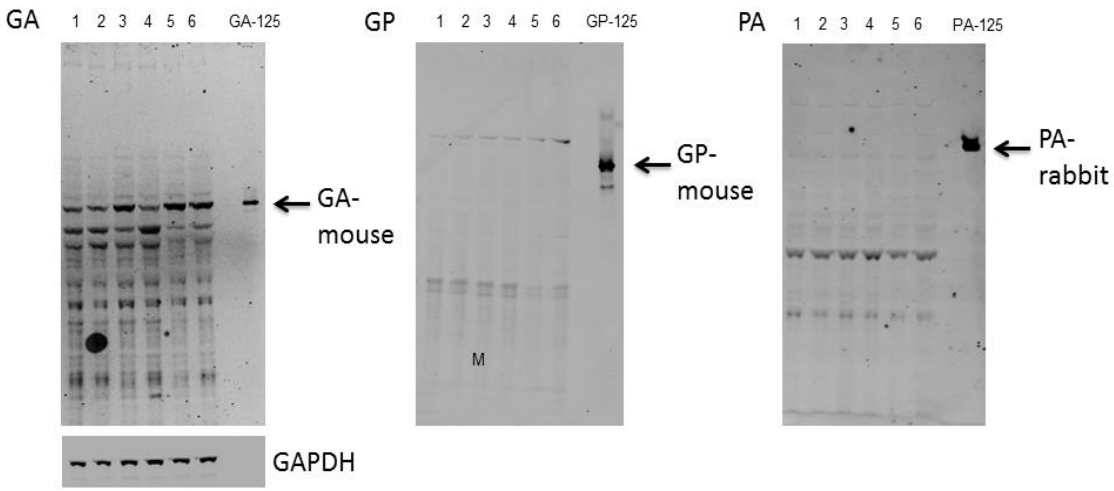

Figure 5.11 Western blots with anti-GA, anti-GP and anti-PA antibodies

Western blots with DPR specific antibodies carried out by Younbok Lee (Kings College London) with anti-GA, anti GP and anti-PA antibodies, with GAPDH as a loading control. Samples 1, 2: Control 2; Samples 3, 4: Carrier 2; Samples 5, 6: Carrier 1.

5.2.4 TDP-43 and p62 pathology

I investigated the mRNA expression levels of TDP-43 using in control and carrier O4 positive cells (Control 1, 0.64 ± SE 0.4; Control 2, 0.76 ± 0.3; Carrier 1, 0.53 ± SE 0.1; Carrier 2, 0.97 ± 0.3, Carrier 2 $\Delta(GGGGCC)_n$: 0.67 ± SE 0.2, N=5, Figure 5.12a). These results reveal that there is no difference between the TDP-43 mRNA levels between carrier and control O4 positive cells (p=0.749, Mann-Whitney test). Using immunocytochemistry at week 3 post plate-down, no TDP-43 mislocalisation was detected in any of the hiPSC derived O4 positive cells (N=3, >156 cells images per line, representative image Figure 5.12b).

Inclusions containing p62 were detected in a small number of cells at week 3 post plate-down (Control 2, 0.6 ± SE 0.6%; Carrier 1, 2.4 ± SE 2.4%; Carrier 2, 1.1 ± SE 0.7%, N=3, >189 cells per line, representative image Figure 5.12b). The presence of areas of punctate staining (such as in the lower right panel of Figure 5.12b) were taken as positive. As long as there were such areas on the slides, the staining was assumed to have been successful, as such staining was not observed in a secondary only control.

Preliminary investigations by Western blotting were performed but as these were only performed on two independent cultures in one experiment, conclusions cannot be drawn from this data. The suggested trend is for the control to have higher levels of TDP-43 and p62, however this needs to be repeated on more cell pellets to reveal whether this is a true representation.

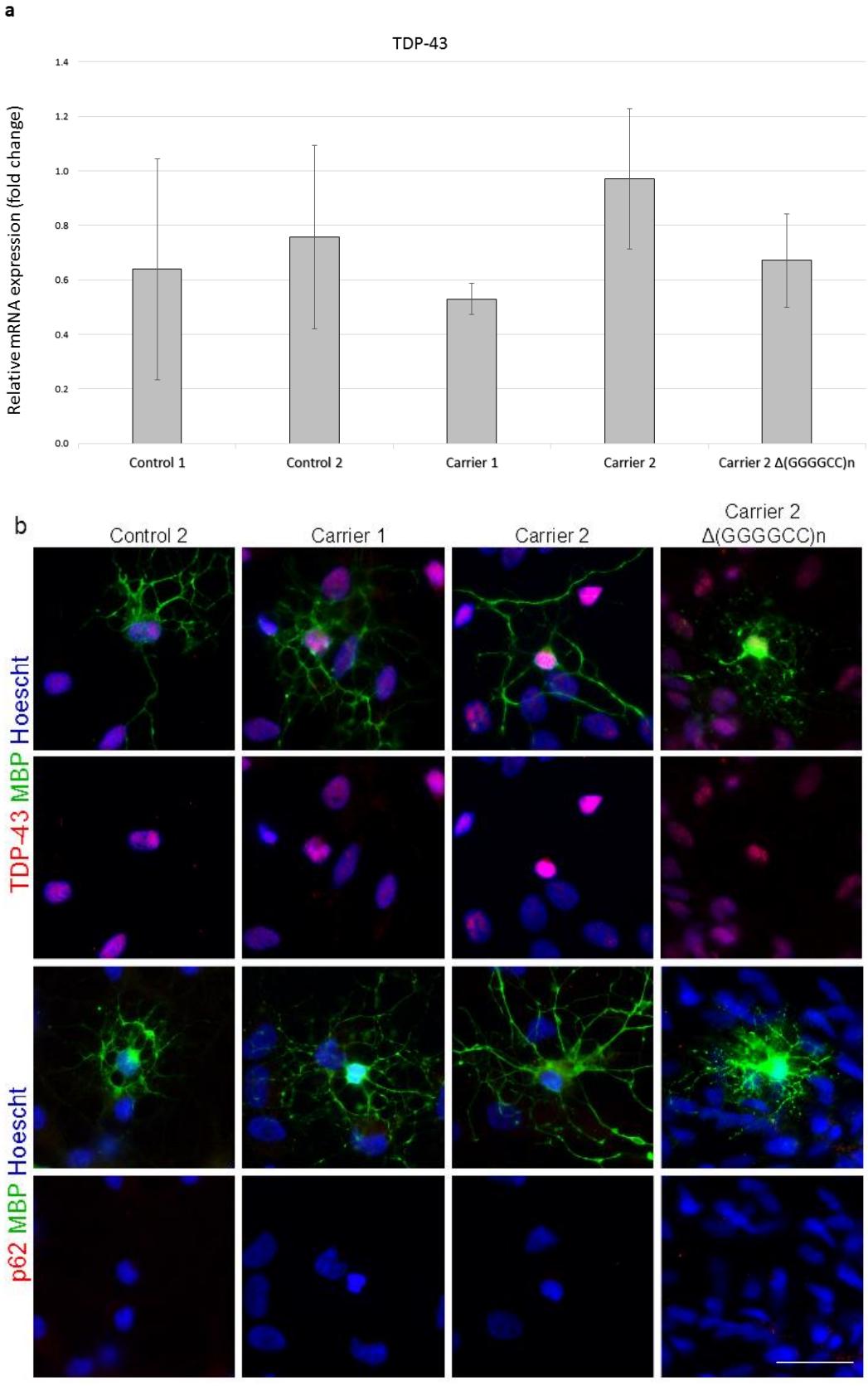

Figure 5.12 TDP-43 mRNA expression levels, TDP-43 and p62 immunocytochemistry and Western blots

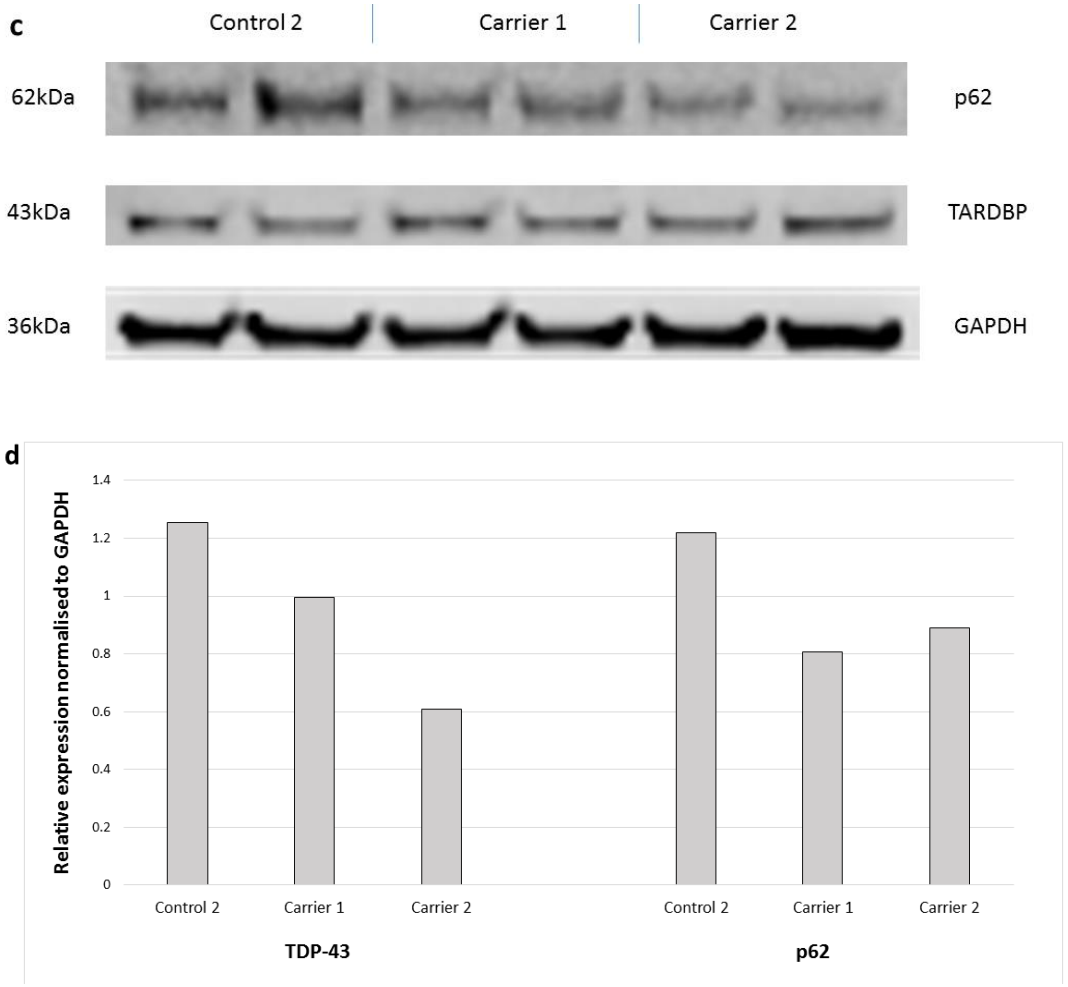

Figure 5.12 TDP-43 mRNA expression levels, TDP-43 and p62 immunocytochemistry and Western blots

(a) qRT-PCR results for TDP-43 mRNA expression from cell pellets (N=5 for each cell line) obtained after three weeks differentiation and MACS sorting for O4. Data were analysed by normalising to *GAPDH* and *β-actin* and comparing to a control using the ΔΔCt method. (b) Representative images following immunocytochemistry for control and carrier cell lines showing nuclear TDP-43 localisation in O4 positive cells and a lack of p62 inclusions in O4 positive cells. Scale bar 30 µm. All counterstained with Hoescht. (c) Western blot image of TDP-43, p62 and GAPDH. (d) Preliminary quantification data for TDP-43 and p62 Western blots, normalised to GAPDH (N=2 for each cell line).

5.2.5 MBP and MCT1 mRNA expression levels

Based on reports that MBP and MCT1 levels are reduced in ALS oligodendrocytes, I performed qRT-PCR on week 3 MACS sorted O4 positive cell pellets, to investigate mRNA expression levels. qRT-PCR was used to determine the relative expression levels of MBP in

C9orf72 HRE carrier O4 positive cells compared to controls (Control 1, 1.09 ± 0.24; Control 2, 1.11 ± 0.33; Carrier 1, 0.53 ± 0.13; Carrier 2, 1.06 ± 0.30, Carrier 2 $\Delta(GGGGCC)_n$: 0.56 ± SE 0.3, N=5, Figure 5.13). There was no difference in MBP mRNA levels between carrier and control O4 positive controls, and inter-cell line variability is apparent (p=0.95, Mann-Whitney test). The MCT1 mRNA levels were compared between control and carrier O4 positive cells (Control 1, 1.31 ± 0.18; Control 2, 1.44 ± 0.25; Carrier 1, 1.01 ± 0.13; Carrier 2, 1.30 ± 0.39, Carrier 2 $\Delta(GGGGCC)_n$: 1.36 ± SE 0.4, N=5, Figure 5.13). This analysis revealed that there was no difference in MCT1 mRNA levels between carrier and control O4 positive cells, which were quite consistent across the cell lines (p=0.85, Mann-Whitney test).

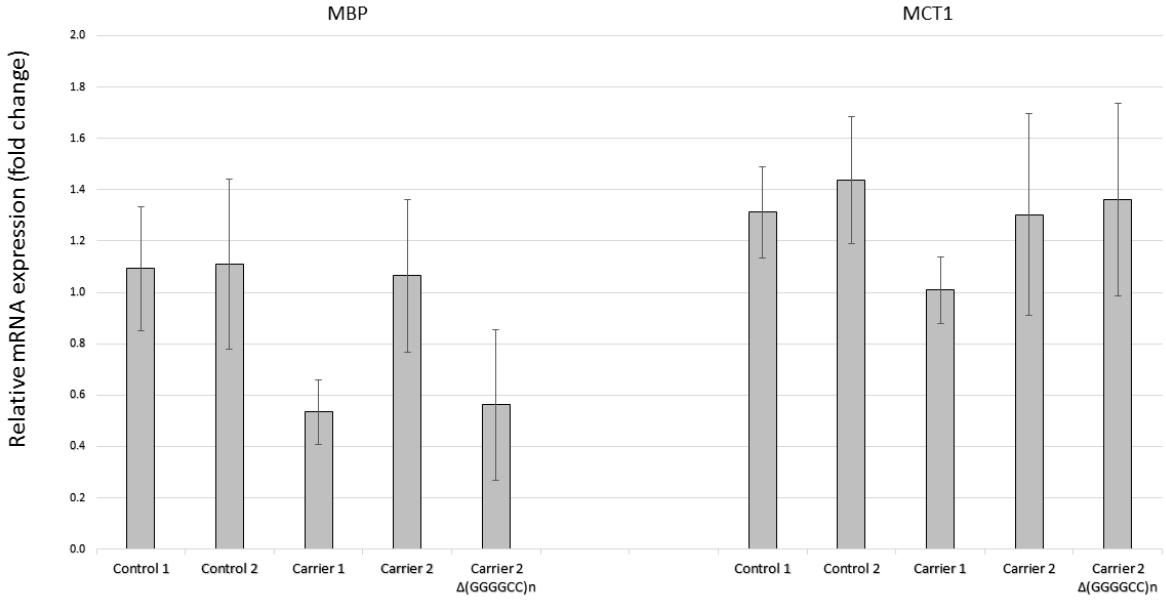

Figure 5.13 mRNA expression levels of MBP and MCT1

Graphical representation of results from qRT-PCR analysis of MBP and MCT1 on mRNA extracted from cell pellets (N=5 for each cell line) obtained after three weeks differentiation and MACS sorting for O4. Data were analysed by normalising to *GAPDH* and *β-actin* and comparing to a control using the ΔΔCt method.

5.2.6 Baseline cell death and susceptibility to tunicamycin

To investigate cell death in the cultures, FACS analysis was performed on cells which had been differentiated for three weeks. The baseline levels of O4 positive cells which stained for cleaved caspase-3, which is an apoptotic marker, were measured. The results showed that there were fairly consistent levels of caspase-3 activation in O4 positive cells from each of the cell lines (Control 1, 26.9 ± 4.4; Control 2, 27.1 ± 1.1; Carrier 1, 22.4 ± 3.9; Carrier 2, 30.9 ± 6.0, Carrier 2 $\Delta(GGGGCC)_n$: 29.8 ± SE 3.4, N=4/3/3/6/5, Figure 5.14a). Overall, there was no

difference observed between carrier and control cells in terms of their baseline levels of caspase-3 activation (p=0.66, Mann-Whitney test).

Because oligodendrocytes are cells which produce a vast amount of protein, and given that ER stress has been implicated in ALS (Walker and Atkin, 2011), I decided to investigate the effect of tunicamycin on hiPSC derived oligodendrocytes. The number of caspase-3 activated O4 positive cells which were present after exposure to tunicamycin for 24 hours were measured, and normalised to baseline, to give an indication of the percentage change in cell death. The results were quite variable between the cell lines, and also within, particularly in the case of carrier 2 (Control 1, 23.9 ± 13.9; Control 2, -0.5 ± 3.1; Carrier 1, 6.5 ± 2.3; Carrier 2, 40.5 ± 17.7, Carrier 2 $\Delta(GGGGCC)_n$: 23.0 ± 11.1, N=4/3/3/6/5, Figure 5.14b). Overall, there was no difference between carrier and control lines in terms of their activation of caspase-3 in response to tunicamycin induced ER stress (p=0.93, Mann-Whitney test).

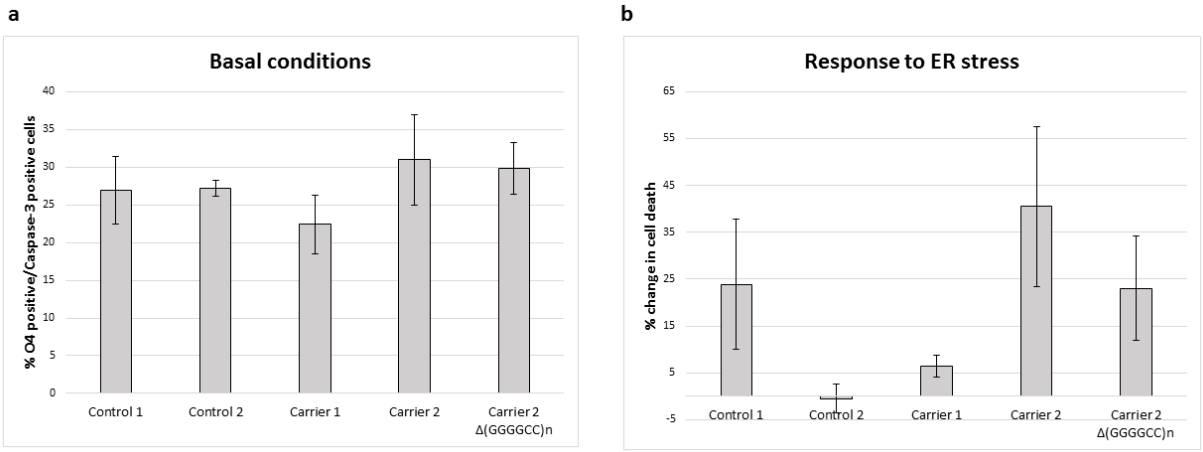

Figure 5.14 GGGGCCexp carrying oligodendrocytes show no baseline survival phenotype (population) by FACS and response to ER stress

(a) Graph of caspase-3 positive O4 positive cells in basal conditions, three weeks post-plate down, measured using FACS. (b) Graph of caspase-3 positive, O4 positive cells after 48 hours of tunicamycin treatment to induce ER stress, measured using FACS.

5.3 Discussion

5.3.1 Loss of function of C9orf72

The low mRNA expression levels that were detected are consistent with observations that C9orf72 is not highly expressed in glia, which have come from a mouse model generated with a LacZ insertion targeted to the *C9orf72* orthologue suggested that the gene was highly expressed in neuronal specific nuclear marker (NeuN) positive cells in the cortex and spinal cord, but not in activated microglia or GFAP positive cells (Suzuki et al., 2013). These low

levels make it difficult to quantify levels accurately as qRT-PCR is not sensitive enough when threshold cycle (Ct) values are greater than 30, as was the case for *C9orf72* variants 1 and 3. For variant 2, which is the most highly expressed isoform, there were no consistent differences between controls and carriers. Comparison of control 1 and carrier 1 for this variant suggests that there is downregulation, but this is not the case for carrier 2 and the carrier 2 isogenic control so may be an effect related to genetic background. For variant 3, there appears to be an increase in expression in carrier 2 compared to controls. This has been observed in another study which suggested that there was a shift in transcription from variant 2 to variants 1 and 3 (Sareen et al., 2013). The observed variability is likely to be partly due to low expression levels, but may also reflect intrinsic differences in the particular cell lines. Repeating these experiments using a more sensitive technique, such as droplet digital PCR or RNA-seq may help to elucidate whether there is indeed altered expression. Hypermethylation of the *C9orf72* promoter has been associated with reduced mRNA expression (Liu et al., 2014), and I have not investigated whether the *C9orf72* HRE carrier lines tested differ in their methylation status. Another possibility is that the 10 base pair deletion at the 3' end of the HRE detected in carrier 2, or some *cis*-acting locus, has a differential impact on transcription.

Although O4 positive cells were selected by MACS prior to these experiments, the enrichment may not reach 100%, and therefore other contaminating cell types may be present. However, previous data has shown that the proportions of different cell types are consistent between the cell lines tested using this protocol. In the context of *C9orf72*, because it is expressed at a higher level in neurons than glia (Suzuki et al., 2013), contamination of the cell pellet by neurons could be a source of potential variability, although the low levels of neurons prior to MACS reduces this possibility.

It would be of interest to determine whether there is reduced expression at the protein level, as even if there is no detectable difference in mRNA levels, the presence of the expansion in the transcript may affect its translation, particularly with regards to undergoing RAN translation. However, a lack of reliable commercial antibodies for C9orf72 at the time of this study, made this unfeasible (DeJesus-Hernandez et al., 2011).

5.3.2 RNA foci detected in OPCs and oligodendrocytes

The results obtained during optimisation of the RNA FISH protocol showed the presence of $(GGGGCC)_n$ sense RNA foci specifically in HRE carriers and not in controls. Treatment of cells with RNase A ablated the signal, suggesting that the foci detected are indeed RNA, rather than DNA. Using a control probe of equal length $(CAGG)_6$ resulted in no signal, which supports the specificity of the $(CCCCGG)_4$ probe for the *C9orf72* HRE.

Combining the RNA-FISH protocol with immunostaining allowed identification of the cell types which contained RNA foci. RNA foci were detected in OPCs, oligodendrocytes (labelled with either O4 or MBP) and also astrocytes (labelled with GFAP). It proved challenging to combine RNA-FISH with staining for the OPC marker PDGFRα, as the inclusion of ethanol to permeabilise membranes prior to RNA-FISH appeared to prevent immunostaining of the marker. The addition of this permeabilization step nearly doubled the number of cells in which RNA foci were detected, and therefore it is not possible to comment on the number of foci detected between different cell types. To try and elucidate whether there was a change in the number of cells containing foci over time, I compared this at one and three weeks post-plate down. This did not show a significant difference although it is not possible, using this technique, to identify whether the number of foci may increase over time in individual cells.

There has been one report following a post mortem study of the presence of sense RNA foci in approximately 10% of oligodendrocytes in the frontal cortex, whereas 37% of neurons displayed RNA foci using the same technique, which focused on *C9orf72*-related FTD (Mizielinska et al., 2013). In this study, I have detected RNA foci in approximately 40-50% of oligodendrocytes *in vitro* (indicated by O4 marker). This difference might be due to a higher sensitivity of the technique in our cell culture system compared to post-mortem tissue, where RNA may be degraded and the RNA-FISH technique is necessarily harsher, requiring extended heating times at 80°C. It may also reflect a difference in the oligodendrocyte marker used, with CAII used in the post-mortem study (Mizielinska et al., 2013). Another possible explanation could be the influence of disease stage on foci number. It may be that the hiPSC derived cells are representative of cells earlier in disease progression than end stage cells studied in post-mortem tissue. Foci containing cells may have undergone cell death during disease progression, as studies in cells transfected with 38 or 74 GGGGCC repeats, which showed RNA foci, had increased caspase-3 activation (Lee *et al.*, 2013). Other studies on hiPSC derived cells have thus far excluded oligodendrocytes. In studies of hiPSC derived neurons, approximately 20-50% of cells were found to contain sense RNA foci (Almeida et al., 2013; Donnelly et al., 2013; Sareen et al., 2013). Methodological differences could account for the variation in RNA foci detection as there are many factors which differ between studies. These include fixing and permeabilisation methods, the type of probe used (RNA, DNA, locked nucleic acid), type of probe label, hybridisation conditions including temperature and time, and imaging methods. The protocol I used was most similar to the that used in the study reporting the highest proportion of cells with RNA foci, with sense RNA detected in up to 68% of hiPSCs (Almeida et al., 2013).

Because of the observation of altered oligodendrocyte morphology in the SOD1 mouse model (Kang et al., 2013), and because of the hypothesis that the presence of RNA foci in oligodendrocytes may result in sequestration of key RNA binding proteins, I undertook Sholl analysis to compare the morphology of O4 positive cells which contained foci versus those with no foci. There were no consistent differences in the number of branches that were detected in cells with or without RNA foci, suggesting that the presence of RNA foci do not alter cellular pathways which influence cellular branching. Further investigation could be carried out using imaging platforms such as the Image Express which may allow detection of subtle morphology differences between the oligodendrocytes from different cell lines.

5.3.3 RAN translation

My investigations into whether hiPSC derived oligodendrocytes from *C9orf72* HRE carriers express DPRs proved challenging due to a lack of reliable antibodies against these species. Both commercial antibodies which I tried did not give reliable staining patterns when they were used on HEK cells which had been transfected with plasmids to overexpress specific DPRs. It is likely that due to the nature of DPR, they are difficult to raise antibodies to, and there may be interactions with other proteins which contain similar regions resulting in non-specificity. Unfortunately, the antibodies that were obtained from Biogen Idec did not give specific staining either. Although the results for anti-PA were promising on transfected HEK cells, the staining patterns were similar in *C9orf72* carrier and control post-mortem brain. Protein samples were sent to King's College London for analysis with antibodies which were thought to be more reliable, and these results suggested that there were no GP or PA DPR present in the oligodendrocytes.

Several studies on hiPSC derived neurons from *C9orf72* patients have shown the presence of RNA foci, but the presence of DPR inclusions has not been reported, with only low level expression detectable (Almeida et al., 2013; Donnelly et al., 2013; Sareen et al., 2013). It may be that the formation of DPR inclusions is a slow process and there is insufficient time in these *in vitro* cell cultures for these to accumulate to an appreciable level (Edbauer and Haass, 2015).

Therefore, using hiPSC derived oligodendrocytes may not be the best system for assessing whether DPR are present, and studies in post-mortem tissue are required specifically to investigate the presence of DPR inclusions in oligodendrocytes. This type of approach has proved challenging due to difficulties in immunostaining oligodendrocytes in formalin fixed tissue, meaning that early studies which suggested that these cells were affected by TDP-43 relied on cell morphology. More recently, the use of the p25α oligodendrocyte specific antibody has allowed double-labelling to be carried out with pTDP-43 (Fatima et al., 2015).

Similar studies using p25α alongside DPR antibodies are required to determine if these are present *in vivo*. IHC studies on post-mortem have the disadvantage, however, of only assessing end-stage disease in the vast majority of cases, and it is possible that the cells expressing DPR may have already died, particularly if these are produced in the mid-stage of disease as has been suggested (Edbauer and Haass, 2015).

It has been suggested that the occurrence of RNA foci and DPRs are mutually exclusive (Donnelly et al., 2013), however others have found an equal proportion of poly-GA in neurons which either contained RNA foci or did not, arguing against this model (Cooper-Knock et al., 2014). Further studies showed that cerebellar Purkinje neurons and motor neurons, which have with higher levels of antisense foci, also have higher levels of antisense DPR. A correlation between higher levels of sense foci in cerebellar granular cells, and sense DPR products have also been observed (Cooper-Knock et al., 2015).

5.3.4 TDP-43 mislocalisation and p62 accumulation

I have performed qRT-PCR for TDP-43 on hiPSC derived oligodendrocytes selected by MACS for O4 and found that the mRNA expression levels are approximately the same for controls and *C9orf72* HRE carriers. This result was expected given that TDP-43 is autoregulated and maintains a constant level of mRNA in cells (Ayala et al., 2011). Western blot analysis also suggested that there was no increase in TDP-43 or p62 protein levels. There was insufficient insoluble protein to allow assessment of TDP-43 levels in this fraction, which is unfortunate and should be investigated in future work. Immunocytochemistry provide no evidence that *C9orf72* carrying hiPSC derived oligodendrocytes display TDP-43 mislocalisation or a significant increase in p62 inclusions compared to controls. Where available, hiPSC derived oligodendrocytes which contain pathogenic variants in *TARDBP* were used as a positive control for this technique. Although these cells were not always available to stain alongside the C9orf72 cells, the nuclear staining of TDP-43 indicates that the antibody staining has been successful. For p62, areas of punctate staining were taken as an indication that the staining had been successful, as a secondary only control was clear of staining. Preliminary results from quantitative Western blots suggest that there is no difference in levels of TDP-43 or p62 in the soluble protein fractions from *C9orf72* HRE carriers and controls. However, this needs to be repeated to confirm in further plate downs, and importantly the insoluble fraction should also be investigated. The protein levels were too low in the insoluble fractions that I extracted and therefore more starting material needs to be used to generate this for future studies.

5.3.5 MBP and MCT1 mRNA expression levels

I investigated the mRNA expression levels of MBP and MCT1 using qRT-PCR, and found that there was no difference for either of these transcripts in hiPSC derived oligodendrocytes containing the *C9orf72* HRE compared to controls. No difference in MCT1 mRNA levels in *C9orf72* HRE containing hiPSC derived oligodendrocytes was observed in another study, although the gene was downregulated in hiPSC derived oligodendrocytes with *SOD1* mutations (Ferraiuolo et al., 2016).

Only one of the two studies reporting downregulation of MCT1 found this to be at the mRNA level (Lee et al., 2012). The other study suggested that the reduction in MCT1 occurred only at the protein level (Philips et al., 2013). Further work to investigate MCT1 levels at the protein level is therefore warranted, but none of the antibodies that were tried within our lab appeared to be reliable for Western blotting. Ideally, a functional assay for lactate transport to neurons would be beneficial to help elucidate whether the *C9orf72* HRE causes any defects in this process. The recent publication on *C9orf72* HRE carrier oligodendrocytes investigated lactate levels in conditioned media using a colorimetric assay, and found no lactate deficit in these cells (Ferraiuolo et al., 2016), although confirming these findings on hiPSC derived cells from more carrier lines would still be beneficial.

5.3.6 Cell death and susceptibility to ER stress

To investigate the baseline levels of apoptosis, I assessed the levels of caspase-3 activation in O4 positive cells by FACS, and found that they were similar between control and *C9orf72* HRE lines. This suggests that the *C9orf72* HRE does not result in a survival difference in hiPSC derived oligodendrocytes. Ideally, this should be confirmed by longitudinal live cell imaging which permits individual cells to be followed over time (Bilican et al., 2012). It proved challenging to set up such a system for oligodendrocytes as expression of the mCherry protein was not well tolerated but this remains an area worthy of future work.

When examining the response of hiPSC derived oligodendrocytes to ER stress, the effect of the *C9orf72* HRE was not entirely clear. Carrier 2 showed a variable response, which I had hoped to clarify by repeating these experiments several more times, but this was not possible as the hiPSC cells developed karyotypic abnormalities in culture and so were unsuitable. These experiments need to be repeated, ideally on additional cell lines to clarify whether there is a response. It would also be useful to perform a dose response to tunicamycin on the carrier cell lines and also investigate levels of ER stress markers such as *BIP*, *CHOP* and spliced *XBP1* to confirm the increased susceptibility (Numasawa-Kuroiwa et al., 2014).

5.4 Conclusions

The aim of this chapter was to investigate *C9orf72* related pathology in hiPSC derived oligodendrocytes. There was no difference found in mRNA levels in *C9orf72* carrier versus control hiPSC derived oligodendrocyte, although it was noted that the expression levels were lower than in neuronal cultures. Sense RNA foci were detected in *C9orf72* HRE carrier hiPSC derived oligodendrocytes, as well as astrocytes and OPCs. These were not associated with any altered morphology as detected by Sholl analysis. It proved challenging to establish whether there were DPR present in the cells, due to a lack of reliable antibodies and so this was inconclusive. There was no evidence of alteration in TDP-43 and p62 accumulation in the *C9orf72* HRE hiPSC derived oligodendrocytes, athough further Western blotting would be required to confirm this as there were technical issues which prevented a fuller investigation. There was no evidence of reduced gene expression of MBP or MCT associated with the *C9orf72* HRE. Finally, the baseline levels of cell death were similar between carrier and control hiPSC derived oligodendrocytes, and there was no clear difference observed in the response of the cells to ER stress.

Chapter 6: General Discussion

The main aim of this study was to determine the effect of the *C9orf72* HRE on hiPSC derived oligodendrocytes, and to my knowledge this was the first study to examine this. A recent publication overlaps with some of my work (Ferraiuolo et al., 2016). An important aspect of this work was developing PCR based assays to detect the presence of the pathogenic expansion, which was required as a key quality control measure of the cell culture based work and in screening during the creation of an isogenic control line. The assays which I developed and optimised were used not only in this context, but also in screening an archival cohort of Scottish MND patients, and have also been implemented within a diagnostic setting for patients with MND and FTD.

The effect of the *C9orf72* HRE in oligodendrocytes was investigated by applying a protocol for oligodendrocyte differentiation to hiPSCs. My aim was to determine whether there was any difference in the production of glial and neuronal cell types using this protocol, between control and *C9orf72* HRE containing cell lines. After establishing that these cell lines responded in an equivalent manner to the differentiation protocol, I went on to investigate whether the *C9orf72* HRE hiPSC derived oligodendrocytes showed any pathological features associated with this variant. The proposed mechanisms by which the *C9orf72* HRE results in disease include loss of function through haploinsufficiency, or gain of function by either RNA foci or dipeptide repeat proteins. Although I found that *C9orf72* was expressed at low levels in hiPSC derived oligodendrocytes, there was no significant change in mRNA expression levels in carrier versus controls. I detected the presence of sense RNA foci in a proportion of hiPSC derived oligodendrocytes with the *C9orf72* HRE, and showed that the presence of these was not associated with a change in branching pattern as assessed by Sholl analysis. I had difficulty detecting DPR, so cannot conclusively say whether these were present or not in the hiPSC derived oligodendrocytes. Furthermore, I went on to investigate whether any downstream changes which are associated with the *C9orf72* HRE, including mislocalisation of pTDP-43 or accumulation of p62, were present. These preliminary results suggested that there was no change in the levels or localisation of these proteins between carrier and control hiPSC derived oligodendrocytes. Finally, the study concluded with an examination of cell death in basal conditions and in the presence of tunicamycin induced ER stress, which suggested that there was no difference in the basal cell death rates or response to ER stress in *C9orf72* HRE carrier hiPSC derived oligodendrocytes compared to controls.

6.1 Genetic testing for C9orf72

Our understanding of the genetic basis for ALS and FTD has improved dramatically over the last few years, particularly with the discovery of the *C9orf72* HRE which is implicated in not only familial, but also apparently sporadic cases (DeJesus-Hernandez et al., 2011; Renton et al., 2011).

The *C9orf72* HRE, by its GC-rich and highly repetitive sequence, provides technical challenges for detection which have been highlighted in a large international study (Akimoto et al., 2014). Sequencing by Sanger methodology, or second generation sequencing technologies does not permit detection and therefore RP-PCR and/or Southern blotting is required. Although widely regarded as the 'gold standard method', Southern blotting for *C9orf72* HREs which are heterogeneous in size due to somatic mosaicism is challenging: it requires large amounts of DNA and is slow and labour intensive (Beck et al., 2013; Nordin et al., 2015). The exact size of the repeat may be estimated from Southern blotting, but the clinical utility of this is debatable and certainly unclear at this stage (Beck et al., 2013; van Blitterswijk et al., 2013b). As PCR based methods can use 100-1000 times less DNA than Southern blotting, and are rapid and high-throughput, it is desirable to develop these to robustly detect the presence or absence of the HRE.

There has been an increased demand from patients and clinicians for genetic testing for ALS and FTD. Although the results do not currently inform clinical treatment, owing to a lack of effective ALS treatments, they can help to speed up diagnosis, prevent other unnecessary investigations from being carried out and inform other family members of a potential increased risk of ALS and FTD. In addition, to accurately carry out investigations using hiPSC derived cells, it is important to genotype the cell lines periodically and ideally this should be carried out using as few cells, and therefore as little DNA, as possible to allow there to be sufficient material for other experiments. There were therefore a number of reasons why developing PCR-based methods to detect the *C9orf72* HRE was important in this study.

I developed three PCR based assays: a flanking PCR for sizing the repeat, and RP-PCR of both 3' and 5' directions from the repeat. The first set of conditions which were developed were later improved upon by the use of a different Taq polymerase and extensive optimisation of cycling conditions, using heat-pulse PCR are a starting point (Orpana et al., 2012).

The flanking PCR in particular can be applied to DNA derived from cell cultures to check repeat sizes. A particular strength of the assay developed here was the detection of expansions of up to 900 repeats in cell line DNA. This makes the assay able to identify accurately whether

there has been shrinkage of the expansion in culture. This assay may prove useful to help determine the lower range of disease causing repeat sizes, and I showed that samples of even 100 repeats in blood can be highly mosaic in nature, which has also been observed by others (Gijselinck et al., 2016; Nordin et al., 2015). The ability to visualise alleles in this range following fluorescent PCR and capillary electrophoresis should make this assay more sensitive for such HREs than Southern blotting. However, Southern blotting may still be required to establish whether there is a mosaicism for a larger repeat in such cases, as was detected in one sample in this study (Fratta et al., 2015).

The observation of somatic mosaicism for *C9orf72* HRE lengths highlights a possible challenge for genetic testing as a disparity could arise between the size of an expansion in lymphocytes, which are typically where DNA is obtained for testing, and the length in neuronal tissue (Nordin et al., 2015). A study on 38 paired blood and CNS tissues from sporadic ALS patients showed concordant results for the presence of an expansion between these tissues, and suggested that misdiagnosis is unlikely when results are based on lymphocyte derived DNA (Pamphlett et al., 2013). There does remain a possibility that differences in the exact size of the HRE could occur between these tissues, and this may be confounding efforts to link expansion size to phenotype. Another factor which remains to be intensively investigated for *C9orf72* is whether the size of the HRE changes over a patient's lifetime, as has been observed in myotonic dystrophy type 1 (Higham et al., 2012).

It would be interesting to investigate whether there are any differences in the expansion size between neuronal and glial cells. Since neuronal cells are terminally differentiated and glial cells undergo more cell division throughout life, it is possible that glial cells have more potential for repeat size changes throughout life. A similar hypothesis has been postulated with regards to the smaller repeat size detected in the cerebellum compared to frontal cortex tissue and blood, which may be due to the abundance of non-dividing terminally differentiated cells in this region (van Blitterswijk et al., 2013b). If neuronal and glial cells were to be separated following post-mortem, the relative size of the expansion could be compared, and it may be of interest to determine if there was a correlation with any clinical phenotypes. Somatic mosaicism for repeat sizes is also thought to arise during DNA repair processes, including mismatch repair (Gomes-Pereira et al., 2004), base excision repair (Kovtun et al., 2004) and nucleotide excision repair (Hubert et al., 2011). The particular pathways used depends on both the transcriptional activity of the locus and the expression level of particular repair proteins in the cell type (Usdin et al., 2015), and therefore these factors may differ between glia and neurons too.

The original RP-PCR assays which were published only allowed determination of whether alleles were up to around 30 repeats in length (DeJesus-Hernandez et al., 2011; Renton et al., 2011). The first RP-PCR assays which I developed were similarly limited. The further work that I carried out to optimise the RP-PCR assays permitted amplification of up to 100 repeats in blood samples, which was an improvement on previously published methods. Given that the lower size range for pathogenic alleles has still not been well established, it is important to be able to extend the size range of detection. From a clinical diagnostic viewpoint, establishing that an expanded allele is greater than 100 repeats in size is important in view of a report of an unaffected individual who had 70 repeats on an allele which then expanded in his offspring who were affected (Xi et al., 2015a). Although conclusions cannot be drawn from one case, this highlights the importance of identifying such cases to aid understanding of how alleles of different sizes behave upon meiotic transmission. Short repeat expansions (45-78 repeats) have been found to co-segregate with disease in another two families studied (Gijselinck et al., 2016). It is well established in other repeat expansion disorders such as Fragile X syndrome and Huntington's disease that premutations, which are alleles not implicated in disease but are at risk of expansion into the affected size range, exist (Fu et al., 1991; Goldberg et al., 1993). There also tends to be a predominant sex through which expansions occur in these disorders (Rousseau et al., 1991). The emerging evidence with *C9orf72* suggests that indeed such phenomena occur, and this is an area which requires further research and is highly important to genetic counselling. In time, and with increased genetic testing for the disorder, more family studies should emerge which will contribute to our knowledge of how *C9orf72* HREs behave through meiosis. In the recent study which detailed the familial association of disease to alleles of as few as 50 repeats, there was some evidence of anticipation in a few of the families studied (Gijselinck et al., 2016).

One key issue which had to be overcome with the RP-PCR assays was ensuring they were robust in the presence of genomic variability at the 3' end of the repeat (Rollinson et al., 2015). By carefully selecting primers outwith the known variable region, I overcame these issues and developed a method which allowed Sanger sequencing to be performed across the repeat. This allowed identification of a range of indels which were present next to the repeat. It has been suggested that the presence of indels can affect the clinical phenotype, and further studies are required to investigate this (Snowden et al., 2016). There is some evidence that the presence of either 5 or 23 bp deletions are associated with decreased transcription levels (Gijselinck et al., 2016). Whether variation next to the repeat expansion affects its stability upon meiotic transmission is unknown but of interest. It is also possible that indels at the 3' end of the HRE could affect the production of DPRs, for example leading to a predominance of a specific type,

which could lead to differing cellular toxicity profiles and consequent phenotype. Investigating a correlation between these sequence variants and clinical phenotypes could offer insight into why *C9orf72* HRE lead to such a vastly variable phenotype.

For genetic testing purposes, it is important that the RP-PCR methods are highly sensitive at picking up the expanded allele. Using a series of dilutions of *C9orf72* positive carrier DNA in a normal DNA background, I showed that we could detect an expansion even at when only present at 1%. This shows that the mutation could be detected in a mosaic state, but is also something to be aware of in terms of the risk of contamination giving false positive results. This would be particularly important in the context of prenatal testing, which although unlikely to be requested in a late-onset condition in which the penetrance is not well established, should be taken into consideration. Appropriate, sensitive controls should be included in the event of such testing and it would be pertinent to back up results with analysis of linked markers given the sensitivity of the RP-PCR assay to contamination.

The observation that false positive results can occur using 3' RP-PCR in samples with normal alleles in the >15 repeat allele range is significant, and shows the importance of using several PCR based assays to ensure that results are accurate. This was something which, despite extensive efforts, was minimised but unfortunately not eliminated. It may be due to the products of incomplete amplification forming megaprimers, and annealing out of register to generate PCR products of different sizes (Hommelsheim et al., 2014). This PCR artefact has been noted by others, who suggest that the flanking primer needs to be moved by several nucleotides to eliminate this effect (Biasiotto et al., 2016).

When investigating the frequency of the *C9orf72* HRE in an archival collection of DNA samples from Scottish MND cases, which were a mixture of sporadic and familial cases, I found that it was detected in ~10% of cases. This corroborates with other studies from Northern European populations (Byrne et al., 2012; Majounie et al., 2012).

In the future, genetic testing is likely to be used within the context of clinical trials for ALS and FTD to determine whether mutations in particular genes cause a differential response to new drug therapies (Picher-Martel et al., 2016). In a research context, imaging studies of unaffected individuals, who have undergone presymptomatic testing and carry a *C9orf72* HRE could provide insight into early disease processes. My future work on genetic testing in ALS will focus on further investigating the genetic epidemiology of ALS in Scotland, by introducing test for a larger set of genes by next generation sequencing. This will allow genotype-phenotype correlations to be made between different genetic forms of ALS and may help inform future patients of their prognosis, based on their genetic findings.

6.2 Disease modelling in ALS with hiPSC derived cells

Human iPSC derived cells have most commonly been used to investigate motor neurons in the context of ALS, with some additional studies on astrocytes (Almeida et al., 2013; Donnelly et al., 2013; Sareen et al., 2013; Serio et al., 2013). This was the first study to my knowledge using this technology to investigate ALS pathology in oligodendrocytes. hiPSC derived oligodendrocytes have been used by others to investigate demyelinating disorders and multiple sclerosis, showing the validity of this technique (Douvaras et al., 2014; Numasawa-Kuroiwa et al., 2014). A recent publication investigating hiPSC and iNPC derived oligodendrocytes from sporadic and genetic ALS (*SOD1* D90A, *FIG4* C27T, *TARDBP* G298S, and *C9orf72* HRE) has replicated many of the findings, particularly with regards to lactate metabolism, from the $SOD1^{G93A}$ mouse model and demonstrates the power of this methodology (Ferraiuolo et al., 2016). Interestingly their observations suggest that the disease mechanism in *C9orf72* HRE cases is distinct from SOD1 mutant and sporadic cases (Ferraiuolo et al., 2016).

For disease modelling in ALS, a clear advantage of this approach is the physiological expression levels of *C9orf72*, as one of the significant disadvantages of animal models would be that the expression levels of a transgene may be significantly different from the true disease context (McGoldrick et al., 2013). Due to the GC-rich, complex secondary structures and large size of *C9orf72* HRE, these are also difficult to handle experimentally and therefore hiPSC derived models allow the pathogenesis relating to the mutation to occur in its native state, without requiring cloning or other challenging manipulations. Although it is possible to obtain neural precursor cells at post-mortem for use in disease studies and drug screening, this is also technically demanding and the tissue is in short supply (Haidet-Phillips et al., 2011). These cells also represent end-stage disease and therefore are unlikely to be informative of early disease processes, which the hiPSC approach can potentially overcome (Meyer et al., 2014).

6.2.1 Reprogramming methods

The first step in disease modelling using hiPSCs is reprogramming of somatic cells to a pluripotent state, and this can be performed from a variety of starting cell types and methodologies. Both control cell lines and carrier 1 were reprogrammed from fibroblasts using a retroviral method, which involves the integration of the factors into the genome (Brock et al., 2012). This may result in random mutagenesis, which is a major reason why there has been significant developments in the field to develop integration free methods (Yu et al., 2009). Another issue that can arise with integrated methods is residual expression of reprogramming factors (Kang et al., 2015). Reprogramming with Sendai virus is a preferable method, as it is non-integrating, and was the method used for carrier 2 (Fusaki et al., 2009; Zhou and Freed,

2009). Ideally, all cell lines used would have been reprogrammed using the same method to make the lines as consistent as possible and, now that episomal-based methods have emerged, this would be the method of choice (Yu et al., 2009). Although carrier 2 was reprogrammed using a different method compared to the controls, an isogenic control was created for this line.

6.2.2 Gender of cell line donors

Another factor to consider when comparing cell lines is the gender of the donor. It has been shown that there is greater variation in transcriptional and DNA methylation between female cell lines than male ones which is thought to be due to sporadic reactivation of the inactive X chromosome (Mekhoubad et al., 2012; Tomoda et al., 2012). Because there are a large number of X-linked genes which function in the nervous system, a perturbation in dosage compensation could impact studies such as this one (Tomoda et al., 2012). For example, one known X-linked oligodendrocyte gene is proteolipid protein 1 (PLP1), mutations in which are associated with the leukodystrophy Pelizaeus-Merzbacher disease (Sistermans et al., 1998). In this study, control 1 and carrier 1 are male, whereas control 2 and carrier 2 are female, and hence pairwise comparisons are best between each of these.

6.2.3 Isogenic controls

Because of the previously mentioned factors, as well as variation intrinsic to cell lines, the use of isogenic controls which can be generated by gene editing technologies offer an advantage over generic controls. The generation of isogenic controls for more *C9orf72* carrier hiPSC lines was ongoing while this project was being carried out, however given the time taken to carry this out, these were not available to me in a feasible time scale for my project. This should offer a more robust platform with which to perform future studies since the background genomic variability between control and carrier lines has been essentially removed. There will still be epigenetic differences between the lines but they still offer the best controls that we can currently create, and deriving cells from these concurrently offers the most robust platform with which to detect phenotypic differences relating to a particular genetic change.

During the creation of isogenic lines, there is a risk of off-target effects from the gene editing process. Typically, these have been identified by exome sequencing and array comparative genome hybridisation (Soldner et al., 2011). In our study, we assessed highly homologous targets which were predicted to be the likeliest regions to be targeted, by Sanger sequencing (Selvaraj et al, submitted). As the creation of isogenic lines involves clonal selection, it is possible that due to random mutagenesis, coincidental genetic variants could appear, which may affect the phenotypic outcome (Ding et al., 2013). Because of this, it is recommended that

multiple clones should be produced so that there are several isogenic controls available (Sandoe and Eggan, 2013). For the *C9orf72* gene targeting, the efficiency of HRE excision was very low for carrier 2 and therefore this was not possible for this line: only 1 clone out of 164 was successfully targeted. It is probable that the 10 base pair deletion, which was not detected until after the gene editing process, was the reason behind the low efficiency. There are two more *C9orf72* hiPSC lines for which isogenic controls have now been created in the lab, which will allow future studies to be performed in a more robust manner. These lines had no indels at the 3' end and the efficiency of excision of the *C9orf72* HRE was subsequently higher, and several isogenic control lines were created for each (Selvaraj et al, submitted). Another consideration in relation to the generation of isogenic controls is the effect of the transformation process on the hiPSC, as such it may be preferable to transfect cells without using gRNA as a control for this, so that the process itself can be ruled out as the cause of any observed differences.

6.2.4 Genomic stability of hiPSCs

Conventional karyotyping using G-banding has been the most commonly used method for checking the genomic integrity of hiPSCs (Lund et al., 2012a) and is the method that has been used in this study. This allows accurate detection of abnormalities in heterogeneous populations, although the analysis is usually only performed on a small number of cells rather than the entire population, and the technique is expensive, labour intensive and slow which limits the regularity with which it can be carried out (Lund et al., 2012a). Using array comparative genome hybridisation allows a higher resolution analysis to be carried out, and can be cheaper and quicker than conventional karyotyping. Expertise, as well as specialised analysis software is still required, particularly for interpretation when small scale copy number changes are detected, which are of unknown significance (Lund et al., 2012a). For interpretation of such changes, it is important that DNA from the patient is available to confirm whether these have arisen *in vitro*. There are also differences in the types of abnormalities which can be detected, as karyotyping is required to detect balanced translocations, while single nucleotide polymorphism (SNP) arrays may allow detection of loss of heterozygosity, which would not be detectable by other methods but may have phenotypic consequences. It may be that as array technology becomes cheaper, that this is a more suitable approach than karyotyping, given that the results may be obtained more quickly. This is important when differentiated cells may have already been used experimentally before karyotyping results are obtained, and therefore subsequent abnormal karyotype results mean that data needs to be excluded, which has clear cost implications. The drawbacks of detecting smaller copy number variations can be reduced by comparing fibroblast DNA and excluding common variants

between this and hiPSC DNA, and also filtering for only common variants which are known to affect differentiation and malignant potentials of the cells.

During this study, chromosomal abnormalities were detected on two occasions. Control 1 hiPSCs were found to have developed an XYY karyotype, and this line was therefore subsequently removed from the study. It is difficult to assess the impact of this chromosomal at the cellular level, but this karyotype occurs in 1 in 1000 live male births, and is associated with tall stature and impaired language and motor skills (Geerts et al., 2003; Linden et al., 2002; Ratcliffe et al., 1992). In a small study on eight XYY males, there was a trend for increased grey and white matter volumes (Bryant et al., 2012), which suggests that this karyotypic abnormality may impact cell growth and division. However, there is likely to be an ascertainment bias in such studies as healthy XYY individuals may never be diagnosed and so the phenotype may be milder than these studies suggest (Bryant et al., 2012). Carrier 2 hiPSCs developed trisomy 12, which is one of the most common cytogenetic abnormalities which arises *in vitro* (Taapken et al., 2011). This abnormality is also observed in both solid tumours and haematological malignancies, and it may be that such an abnormality occurs during *in vitro* culture as it is a permissive aneuploidy which is not selected against (Taapken et al., 2011). Because karyotypic abnormalities in cell lines are likely to result in changes in gene expression, and aneuploidy leads to deficiencies in cellular processes (Mayshar et al., 2010; Upender et al., 2004), experimental results from cells with these changes are unreliable and as such cannot be used in disease modelling.

6.2.5 Verification of pluripotency of cell lines

Pluripotency measurement has been carried out by qualitative immunostaining, which showed that each of the cell lines were able to generate all three germ layers are required (Devlin et al., 2015). Recently, quantitative approaches have been developed and these would be better suited to highlight any differences between the hiPSCs studied (Bock et al., 2011; Müller et al., 2011).

6.3 Derivation of hiPSC derived oligodendrocytes

There are several recent published protocols for generating oligodendrocytes from hiPSCs, The first report of the generation of O4 positive cells from hiPSCs showed very low efficiency (<0.01%), despite attempts using two protocols previously optimised on hESCs (Ogawa et al., 2011). Several groups have focused their efforts towards cell transplantation, and therefore assessed the production of OPCs with less focus on *in vitro* differentiation and maturation of oligodendrocytes (Wang et al., 2013). In this case, the protocol contained six stages as ours did, but took longer (190 days) to generate terminally differentiated cells (Wang et al., 2013).

This protocol generated a yield of 4-12% O4 positive cells but in their case was at a later time point than when a similar yield was present using our protocol (Wang et al., 2013).

More recently, protocols with higher yield and shorter differentiation times have been published (Douvaras and Fossati, 2015). The major differences between our protocol and this one is that they combine RA with the dual SMAD inhibitors (SBN431542 and LDN193189) and use adherent cultures for a larger proportion of time, which would be predicted to expose cells to a more consistent concentration of morphogens (Douvaras and Fossati, 2015). Our protocol is largely based on neurospheres, and therefore the cells are exposed to a different morphogen concentration depending on their location within the sphere, and this likely contributes to the generation of undesired cell types, and is also why maintenance of spheres by regular chopping is important.

Another protocol that has been developed demonstrates the utility of deriving cells in hypoxic conditions, showing a two fold increase in Olig2 expression at 3% oxygen compared to 20% (Stacpoole et al., 2013). Low oxygen levels are more physiologically relevant to *in vivo* conditions, and have been suggested to enhance oligodendrocyte survival, as this lineage has been shown to be particularly sensitive to oxidative stress (Casaccia-Bonnefil, 2000; Stacpoole et al., 2013).

Using a similar approach to ours, another group have used patient derived hiPSCs with *PLP1* mutations to investigate their effect on oligodendrocytes (Numasawa-Kuroiwa et al., 2014). Their derivation protocol was similar to ours in their use of RA and Shh agonists in the initial stages, while their OPC proliferation stage utilised epidermal growth factor (EGF) and neurotrophin-3 (NT-3) and lacked SAG compared to ours, and they used leukaemia inhibitory factor (LIF) and ciliary neurotrophic factor (CNTF) rather than IGF-1 in the differentiation phase (Numasawa-Kuroiwa et al., 2014). It is difficult to compare the efficiency of this protocol to others as they used a unique scoring method for number of O4 positive cells.

All of the protocols are similar in that they take several months to form mature oligodendrocytes, and it would therefore be useful to have a stable and expandable intermediate precursor cell population which can be used so that the entire differentiation process does not need to be performed each time. This has been achieved in one protocol, where radial glia-like cells are used in this manner (Gorris et al., 2015). In our protocol, OPCs can be maintained as spheres for up to two months, but the efficiency of oligodendrocyte differentiation may vary over this time period.

Interestingly, development of more direct methods of cell generation from fibroblasts have emerged which bypass the hiPSC stage, allowing neurons and oligodendrocyte precursor cells to be generated from human fibroblasts by direct reprogramming using a combination of transcription factors (Ferraiuolo et al., 2016; Meyer et al., 2014). Such approaches are potentially time saving, and a reduced time in culture means there is less time for potential genetic defects to occur and reduced infection risk, as well as being more economical.

In the protocol which I have used in this study, the cell purity is a limitation. As the yield of oligodendrocytes was less than 100% after three weeks of oligodendrocyte differentiation, to carry out biochemical studies, it was necessary to enrich for cells of interest with MAC sorting. However, it is technically challenging to perform a quality check each time, as material is limiting and therefore I cannot exclude contamination with different cell types including astrocytes and neurons. I also therefore cannot exclude that the results obtained have been influenced by the non-cell autonomous effects of other cell types. Switching to a protocol which is higher yielding and has few contaminating cell types would be a significant advance and allow for more cell population based assays to be performed. One simple alteration which could improve yield would be to try a higher IGF-1 concentration in the differentiation medium (50ng/ml), as this was found to give a higher yield of MBP positive cells in a recent study (Ferraiuolo et al., 2016).

Other ways in which the protocol could be altered include optimisation of RA and Shh concentrations early on to mimic the embryonic spinal cord. (Douvaras et al., 2014). In this protocol, adherent cultures were used for a longer duration of time, which results in cells being exposed to a more consistent concentration of morphogens than if they are within a neurosphere. In the latter, cells will have different exposure levels depending on their position within the sphere. Douvaras et al. also used a significantly lower RA concentration than others (Nistor et al., 2005) and no FGF. Although FGF has been shown to promote Olig2 expression in chicken, and has been used in several hES and hiPSC (Nistor et al., 2005), protocols have now emerged which show that this factor is not required for oligodendrocyte production (Douvaras et al., 2014).

Additional survival factors could be added to try and maintain oligodendrocytes in culture for longer. Neurotrophins including NT-3, CNTF, LIF and interleukin 6 are thought to work together to promote survival additively in rat cells *in vitro* (Barres et al., 1993). NT-3 is thought to be a potent mitogen for OPCs, as well as being a survival factor and further work to investigate whether this factor could increase yield in this protocol could be useful. This could

improve the yield of these cells, allowing more population based assays to be used without cell sorting.

Others have recently investigated oligodendrocyte differentiation from hiPSC and iNPCs in the context of ALS-associated mutations, and also found that there was no difference in marker expression between ALS samples and controls (Ferraiuolo et al., 2016). Because this group used samples from multiple sources and their protocol was different to ours, this backs up our findings and suggests that differentiation defects are not present in *C9orf72* HRE oligodendrocytes, which is also consistent with the disease being late-onset and not arising early in development. However, it is not possible to exclude that defects in differentiation and maturation of newly formed oligodendrocytes could contribute to the development of ALS at a later stage. Indeed, cell aging is an important consideration in disease modelling using hiPSCs, particularly given that increased age is the main risk factor for neurodegenerative diseases such as ALS. It is important to consider how reprogramming and directed differentiation affects cellular aging, and it may be that direct conversion of fibroblasts to oligodendrocytes might allow this to be retained as has been suggested for neurons (Mertens et al., 2015).

There is a gap in knowledge of the regional identities of oligodendrocytes, and this has not been addressed in current hiPSC derivation protocols. With regards to the *C9orf72* HRE, it is of interest to investigate cortical oligodendrocytes, given that this mutation also causes FTD. There is even less known about oligodendrocytes in FTD than in ALS, and therefore many of the investigations on spinal oligodendrocytes should be repeated on cortical oligodendrocytes. This work is ongoing by another member of the laboratory (Barton, personal communication).

6.4 Pathology of C9orf72 HRE hiPSC derived oligodendrocytes

Any of the proposed pathological mechanisms relating to *C9orf72* HREs that have been suggested could be affecting cell types other than neurons. Therefore, I investigated whether any of these features were apparent in hiPSC derived oligodendrocytes.

6.4.1 Loss of function

At the beginning of this study, very little was known with regards to the role of *C9orf72* HRE in oligodendrocytes, and it was not clear whether these cells were affected by the presence of the mutation, or to what extent they might contribute to the development of disease. Using hiPSC derived oligodendrocytes was a novel approach to addressing some of these questions, mostly with regards to cell autonomous effects of the *C9orf72* HRE on oligodendrocytes.

It has subsequently emerged, from a mouse model with LacZ expressed from the *C9orf72* promoter, and human gene expression studies that C9orf72 is mostly expressed in neurons and macrophages, with low expression levels in glia (Rizzu et al., 2016; Suzuki et al., 2013). This was backed up by the results which I obtained from mRNA expression analysis using qPCR which showed low expression levels in hiPSC derived oligodendrocytes compared to hiPSC derived cortical neurons, and similar to the levels detected in the laboratory for astrocytes (Zhao, personal communication). There was not a significant difference in the expression levels between carrier and control hiPSC derived oligodendrocytes, although there was some variability between the lines. This is probably due to the low expression levels and subsequent limitations in the sensitivity of the technique. Within the literature, similar experiments on hiPSC derived neurons have shown variable results, with some showing a reduction in C9orf72 mRNA expression of specific transcripts (Almeida et al., 2013) and others showing that other transcripts are upregulated (Sareen et al., 2013). Some reasons for inconsistencies between studies examining mRNA levels include variability in sample sizes, nomenclature differences, methodology, tissue types investigated and RNA quality (van Blitterswijk et al., 2015). As yet it is still unclear to what extent a loss of function of C9orf72 contributes to pathogenesis.

Due to a lack of reliable antibodies to C9orf72, I have not investigated the expression of the protein in hiPSC derived oligodendrocytes. It would have been interesting to check for co-expression with oligodendrocyte markers using immunohistochemistry, as well as look at expression levels of purified cell lysates by Western blot. Further work to investigate the epigenetic status of the *C9orf72* HRE and surrounding genomic region could potentially be interesting, particularly if there were any differences detected between the cell lines as this is a potential source of variation.

6.4.2 Gain of function (RNA)

Using RNA FISH, I detected sense RNA foci in hiPSC derived oligodendrocytes, which corroborates findings from post-mortem studies showing RNA foci in oligodendrocytes in the frontal cortex of FTD patients (Mizielinska et al., 2013). I detected RNA foci in a higher percentage of oligodendrocytes (40-50%) than this study (10%), however this likely reflects the differences between an *in vitro* system and analysis on post-mortem tissue. RNA-FISH for the latter requires harsh sample treatment including heating to 80°C, which is likely to result in RNA degradation. The stage of disease studied using post-mortem tissue is also unlikely to be replicated in hiPSC derived cells, so this is likely to influence the number of foci containing cells. Studies have shown that in cells which have been transfected with 38 or 74 GGGGCC repeats, those which display RNA foci are associated with increased caspase-3 activation (Lee

et al., 2013). In other studies of hiPSC derived neurons, sense RNA foci were detected in 20-50% of cells (Almeida et al., 2013; Donnelly et al., 2013; Sareen et al., 2013). Variation in the detection of RNA foci may reflect procedural differences in the RNA-FISH technique, including fixation and permeabilisation methods, type of probe used (RNA, DNA, locked nucleic acid), type of probe label, hybridisation conditions including temperature and time, and imaging methods. The protocol I used was based on that used in the study reporting the highest proportion of cells with RNA foci, with sense RNA detected in up to 68% of hiPSCs (Almeida et al., 2013).

The presence of RNA foci has been reported in most cell types that have been investigated, including fibroblasts, peripheral blood leukocytes, immortalized lymphoblasts, astrocytes, microglia and various neuronal types including motor neurons, cortical neurons, lumbar interneurons, cerebellar Purkinje cells and hippocampal neurons (Donnelly et al., 2013; Lagier-Tourenne et al., 2013; Mizielinska et al., 2013; Zu et al., 2013). Since there is no overt clinical phenotype affecting cell types such as fibroblasts and leukocytes, this suggests that the presence of RNA foci alone is not cytotoxic. If RNA foci are sequestering proteins, it may be that the various cell types have different RNA binding proteins which are perturbed, and how crucial these are to cellular function determines whether there is a cellular phenotype or not. Various RNA binding proteins, including ADARB2, hnRNPA1, hnRNPA3, Pur-α and nucleolin have been proposed to be involved but no real consensus on which are important (Donnelly et al., 2013; Haeusler et al., 2014; Mori et al., 2013b; Sareen et al., 2013; Xu et al., 2013). Among the most elegant experiments carried out to establish binding partners of C9orf72 sense RNA foci in the central nervous system involved pull down assays with subsequent mass spectrometry to identify candidate binding proteins (Cooper-Knock et al., 2014). This study identified multiple targets and co-expression studies revealed colocalization of RNA foci with hnRNP A1, hnRNP H1/F, ALYREF and SRSF2 in motor neurons (Cooper-Knock et al., 2014). It would be interesting to investigate whether there are differences in which proteins are sequestered by RNA foci in oligodendrocytes compared to neurons or astrocytes. This could be done on hiPSC derived cells, or following cell purification on post-mortem samples. So far, most studies have focused on neurons and have failed to reach a consensus on the factors involved, and therefore there does not appear to be a 'master' factor, unlike in myotonic dystrophy where sequestration of muscleblind proteins by RNA foci are significantly implicated in disease pathogenesis (Miller et al., 2000).

The morphology of oligodendrocytes in the $SOD1^{G93A}$ mouse model, and in ALS post mortem tissue is thought to be abnormal (Kang et al., 2013). Because of this, I investigated whether

the branching pattern of oligodendrocytes was affected by the presence of RNA foci using Sholl analysis. There was not a clear and consistent effect on the number of branches as determined by Sholl analysis, which suggests that the presence of RNA foci is not disrupting any of the cellular pathways involved in creating the branching network in oligodendrocytes. Clearly, however this analysis does not exclude an influence of RNA foci on many other cellular processes.

Further work is required to determine whether hiPSC derived oligodendrocytes contain antisense RNA foci. Despite numerous attempts, I did not manage to get a protocol for this to work, possibly due to the formation of secondary structures in the $(GGGGCC)_4$ probe. Repeats of GGGGCC are thought to form highly stable G-quadruplexes *in vitro* and it may be that despite attempts to denature the probe with extended heating times, that this may be contributing to the lack of signal obtained (Fratta et al., 2012; Reddy et al., 2013). Published methods for RNA-FISH to detect antisense foci have tended to be optimised for post-mortem tissue or peripheral blood cells and have included longer hybridisation at temperatures greater than 60°C, which may be too harsh for the cells used in this study (Cooper-Knock et al., 2015; Mizielinska et al., 2013; Zu et al., 2013). Locked nucleic acid probes have also been used by several groups as these are thought to reduce secondary structure formation and improve probe specificity and sensitivity for RNA-FISH (Lagier-Tourenne et al., 2013).

6.4.3 Gain of function (protein)

The difficulties that I had with specificity and sensitivity of the available antibodies to DPR highlight the challenges of working with these proteins as reliable antibodies are still scarce. I cannot confirm or exclude from my work whether DPR were present in the hiPSC derived carrier oligodendrocytes or not. The Western blots that were carried out suggest that PA and GP dipeptides were not present, however the experiments were only carried out once using two cell pellets from each of control 2, carrier 1 and carrier 2, and so ideally they would be repeated to confirm the results.

I had intended to investigate the presence of DPR in oligodendrocytes from post-mortem tissue from *C9orf72* HRE positive patients, however again this work was hampered by the lack of reliable antibodies. Had this worked, it would have been very interesting to see if the results were similar in hiPSC derived oligodendrocytes compared to those present at end stage disease.

There have not been any other studies to investigate the presence of DPR in oligodendrocytes carrying *C9orf72* HRE in the literature that I am aware of. There has been one report of

transmission of DPR from conditioned media obtained from GFP-DPR expressing cortical neurons to mature oligodendrocytes *in vitro* (Westergard et al., 2016). This study suggests that DPR can be transmitted between CNS cell types and that this may provide an explanation for the progressive spread of the disease (Westergard et al., 2016).

6.4.4 TDP-43 and p62 accumulation

I found no evidence of TDP-43 mislocalisation related to the *C9orf72* HRE in hiPSC derived O4 positive cells using immunocytochemistry, and there was no increase in TDP-43 in the soluble fraction following protein extraction and Western blotting. Unfortunately, insufficient protein was obtained from the insoluble fraction to allow assessment of TDP-43 levels, which needs to be repeated on fresh material. This contrasts with evidence from post-mortem material which suggests that TDP-43 becomes mislocalised in oligodendrocytes in ALS cases (Brettschneider et al., 2014; Rohan et al., 2014). However, the literature focuses on sporadic cases and this has not specifically been assessed in oligodendrocytes which have a *C9orf72* HRE. It may be that TDP-43 mislocalisation has not been detected in this study due to the kinetics of the accumulation with regards to the development of the disease. Although the accumulation of TDP-43 in oligodendrocytes it is thought to reflect an early disease process, it may be that the cultured cells have not been exposed to the appropriate cellular conditions which trigger this *in vivo* (Brettschneider et al., 2014; Rohan et al., 2014).

It is possible that *in vivo*, the TDP-43 mislocalisation observed in oligodendrocytes could be due to the presence of damaged motor neurons. This could still occur prior to symptom onset, for example, excitotoxicity in motor neurons in the early disease stages could have a detrimental effect on surrounding oligodendrocytes, which ultimately leads them to mislocalise TDP-43. Alternatively, TDP-43 could also spread between cell types as has been suggested for DPR (Fatima et al., 2015; Feiler et al., 2015).

There was no evidence of increased p62 using either immunocytochemistry or Western blotting in *C9orf72* HRE containing hiPSC derived oligodendrocytes. However, further work is required to verify these results as there was limited protein available for analysis.

6.4.5 Cell death and ER stress susceptibility

In this study, I have used FACS to determine the levels of caspase-3 activation, which is a cell death marker, within O4 positive cells. I did not find any difference in levels of caspase-3 activation between carrier and control O4 positive cells under basal conditions. This finding has been supported by another group who transduced human oligodendrocytes with red fluorescent protein under the MBP promoter and showed that when cultured with motor

neurons, there was no difference between control and ALS derived oligodendrocyte number (Ferraiuolo et al., 2016). A caveat here is that the ALS patients are a pooled group and it is not stated how many of these were *C9orf72* HRE carriers, and the study could have benefited from time lapse survival analysis rather than a cell count at the end of co-culture.

The application of tunicamycin to cells to induce ER stress, followed by FACS analysis to determine levels of caspase-3 activation revealed no significant susceptibility of *C9orf72* HRE carriers to ER stress. There was variability between the cell lines however, and ideally this experiment would be repeated using more isogenic controls as this would help reveal whether the difference is specifically due to the presence or absence of the *C9orf72* HRE. If a difference was revealed after further analysis, it would be pertinent to perform a dose response curve to determine that the effect is specifically due to the application of tunicamycin. Furthermore, checking whether any response was reversed by agents which inhibit the ER stress response, such as salubrinal or tauroursodeoxycholic acid, would back up such results. This type of experimental approach could also be used to investigate whether there is a susceptibility to many other types of cellular stress, such as oxidative stress which have been implicated in ALS.

6.4.6 Other potential pathogenic mechanisms in oligodendrocytes

I investigated expression levels of MBP and MCT1 as they have previously been reported to be reduced in *SOD1* mutant oligodendrocytes (Kang et al., 2013; Philips et al., 2013). I did not observe a significant difference in mRNA levels for either of these markers in *C9orf72* HRE oligodendrocytes. Given that one report of reduced MCT1 appeared to be a post-transcriptional effect (Philips et al., 2013), an obvious next step would be to measure expression at the protein level.

Another area worthy of investigation is lactate metabolism, to investigate whether there is any difference in how well the oligodendrocytes may be able to support motor neurons. Recently, lactate release has been measured in conditioned media from control and ALS oligodendrocytes by another group, who found that there was no difference at the beginning of differentiation, but after three weeks in culture there is a decrease in lactate production by human ALS oligodendrocytes compared to controls (Ferraiuolo et al., 2016). However, looking specifically at *C9orf72* HRE oligodendrocytes, there did not appear to be a reduction in lactate release, intracellular lactate concentration or MCT1 mRNA expression levels, suggesting that this effect is specific to *SOD1* and *TARDBP* mutant oligodendrocytes (Ferraiuolo et al., 2016).

6.5 Further research

The key question regarding the role of oligodendrocytes in the pathogenesis of *C9orf72* HRE related ALS is whether there is an impact on neuronal health and function. To extend this study, the functionality of hiPSC derived oligodendrocytes needs to be investigated. Ideally, this requires a reliable *in vitro* protocol for co-culturing human oligodendrocytes and neurons, so that cell non-autonomous effects can be examined.

A recent publication describes an *in vitro* human co-culture system between wild type Hb9-GFP+ motor neurons and either hiPSC or induced neural progenitor cell derived oligodendrocytes with various ALS-associated genetic variants. In the presence of oligodendrocytes carrying either a *C9orf72* HRE, or pathogenic variants in *SOD1*, *TARDBP* or *FIG4*, motor neurons displayed reduced survival (Ferraiuolo et al., 2016). The application of conditioned media from human ALS oligodendrocytes to motor neurons resulted in a 15-40% increase in motor neuron death compared to control oligodendrocytes, suggesting that part of this effect is mediated via soluble factors (Ferraiuolo et al., 2016). It would be of great interest to determine what biochemical differences there are between conditioned media from control and *C9orf72* HRE oligodendrocytes. In order to investigate this, a higher yielding protocol would be required, otherwise it is possible that there would be a significant influence from contaminating astrocytes. From preliminary experiments that I carried out on co-cultures with hiPSC derived neurons, the most effective contact between oligodendrocytes and neurons appeared to occur when OPC spheres were used, rather than MACS sorted O4 positive cells. This meant using cells from earlier in the protocol, and as such the oligodendrocyte yield was low and the cell population included astrocytes. Therefore, it would be impossible to tease apart whether any detected changes in neuronal function were due to oligodendrocytes or astrocytes.

A further challenge following on from this study is to show that the hiPSC derived oligodendrocytes can function and form myelin sheaths. The widely regarded ‘gold-standard’ method for showing function is *in vivo* transplantation into the congenitally hypomyelinated *shiverer* mouse model (Douvaras et al., 2014; Wang et al., 2013). This work is currently ongoing by others in the laboratory and external collaborators. In addition, another student in the laboratory has had success using oligodendrocytes derived using the same method as this project, with slice cultures from the MBP-lacking *shiverer* mouse. These have given promising results suggesting that the oligodendrocytes are indeed functional in respect to myelination (James, personal communication).

References

Akimoto, C., A. E. Volk, M. van Blitterswijk, M. Van den Broeck, C. S. Leblond, S. Lumbroso, W. Camu, B. Neitzel, O. Onodera, W. van Rheenen, S. Pinto, M. Weber, B. Smith, M. Proven, K. Talbot, P. Keagle, A. Chesi, A. Ratti, J. van der Zee, H. Alstermark, A. Birve, D. Calini, A. Nordin, D. C. Tradowsky, W. Just, H. Daoud, S. Angerbauer, M. DeJesus-Hernandez, T. Konno, A. Lloyd-Jani, M. de Carvalho, K. Mouzat, J. E. Landers, J. H. Veldink, V. Silani, A. D. Gitler, C. E. Shaw, G. A. Rouleau, L. H. van den Berg, C. Van Broeckhoven, R. Rademakers, P. M. Andersen, and C. Kubisch, 2014, A blinded international study on the reliability of genetic testing for GGGGCC-repeat expansions in C9orf72 reveals marked differences in results among 14 laboratories: J Med Genet, v. 51, p. 419-24.

Al-Chalabi, A., F. Fang, M. F. Hanby, P. N. Leigh, C. E. Shaw, W. Ye, and F. Rijsdijk, 2010, An estimate of amyotrophic lateral sclerosis heritability using twin data: J Neurol Neurosurg Psychiatry, v. 81, p. 1324-6.

Al-Chalabi, A., and O. Hardiman, 2013, The epidemiology of ALS: a conspiracy of genes, environment and time: Nat Rev Neurol, v. 9, p. 617-28.

Al-Chalabi, A., A. Jones, C. Troakes, A. King, S. Al-Sarraj, and L. H. van den Berg, 2012, The genetics and neuropathology of amyotrophic lateral sclerosis: Acta Neuropathol, v. 124, p. 339-52.

Almad, A. A., A. Doreswamy, S. K. Gross, J. P. Richard, Y. Huo, N. Haughey, and N. J. Maragakis, 2016, Connexin 43 in astrocytes contributes to motor neuron toxicity in amyotrophic lateral sclerosis: Glia, v. 64, p. 1154-69.

Almeida, S., E. Gascon, H. Tran, H. J. Chou, T. F. Gendron, S. Degroot, A. R. Tapper, C. Sellier, N. Charlet-Berguerand, A. Karydas, W. W. Seeley, A. L. Boxer, L. Petrucelli, B. L. Miller, and F. B. Gao, 2013, Modeling key pathological features of frontotemporal dementia with C9ORF72 repeat expansion in iPSC-derived human neurons: Acta Neuropathol, v. 126, p. 385-99.

Alonso, A., G. Logroscino, S. S. Jick, and M. A. Hernán, 2009, Incidence and lifetime risk of motor neuron disease in the United Kingdom: a population-based study: Eur J Neurol, v. 16, p. 745-51.

Alsanie, W. F., J. C. Niclis, and S. Petratos, 2013, Human Embryonic Stem Cell-Derived Oligodendrocytes: Protocols and Perspectives, Stem Cells Dev, v. 22, p. 2459-76.

An, M. C., R. N. O'Brien, N. Zhang, B. N. Patra, M. De La Cruz, A. Ray, and L. M. Ellerby, 2014, Polyglutamine Disease Modeling: Epitope Based Screen for Homologous Recombination using CRISPR/Cas9 System: PLoS Curr, v. 6.

Appel, S. H., W. Zhao, D. R. Beers, and J. S. Henkel, 2011, The microglial-motoneuron dialogue in ALS: Acta Myol, v. 30, p. 4-8.

Arai, T., T. Nonaka, M. Hasegawa, H. Akiyama, M. Yoshida, Y. Hashizume, K. Tsuchiya, T. Oda, and K. Ikeda, 2003, Neuronal and glial inclusions in frontotemporal dementia with or without motor neuron disease are immunopositive for p62: Neurosci Lett, v. 342, p. 41-4.

Ash, P. E., K. F. Bieniek, T. F. Gendron, T. Caulfield, W. L. Lin, M. Dejesus-Hernandez, M. M. van Blitterswijk, K. Jansen-West, J. W. Paul, 3rd, R. Rademakers, K. B. Boylan, D. W. Dickson, and L. Petrucelli, 2013, Unconventional translation of C9ORF72 GGGGCC expansion generates insoluble polypeptides specific to c9FTD/ALS: Neuron, v. 77, p. 639-46.

Atanasio, A., V. Decman, D. White, M. Ramos, B. Ikiz, H. C. Lee, C. J. Siao, S. Brydges, E. LaRosa, Y. Bai, W. Fury, P. Burfeind, R. Zamfirova, G. Warshaw, J. Orengo, A. Oyejide, M. Fralish, W. Auerbach, W. Poueymirou, J.

Freudenberg, G. Gong, B. Zambrowicz, D. Valenzuela, G. Yancopoulos, A. Murphy, G. Thurston, and K. M. Lai, 2016, C9orf72 ablation causes immune dysregulation characterized by leukocyte expansion, autoantibody production, and glomerulonephropathy in mice: Sci Rep, v. 6, p. 23204.

Ayala, Y. M., L. De Conti, S. E. Avendaño-Vázquez, A. Dhir, M. Romano, A. D'Ambrogio, J. Tollervey, J. Ule, M. Baralle, E. Buratti, and F. E. Baralle, 2011, TDP-43 regulates its mRNA levels through a negative feedback loop: EMBO J, v. 30, p. 277-88.

Baborie, A., T. D. Griffiths, E. Jaros, R. Perry, I. G. McKeith, D. J. Burn, M. Masuda-Suzukake, M. Hasegawa, S. Rollinson, S. Pickering-Brown, A. C. Robinson, Y. S. Davidson, and D. M. Mann, 2015, Accumulation of dipeptide repeat proteins predates that of TDP-43 in frontotemporal lobar degeneration associated with hexanucleotide repeat expansions in C9ORF72 gene: Neuropathol Appl Neurobiol, v. 41, p. 601-12.

Back, S. A., N. L. Luo, N. S. Borenstein, J. M. Levine, J. J. Volpe, and H. C. Kinney, 2001, Late oligodendrocyte progenitors coincide with the developmental window of vulnerability for human perinatal white matter injury: J Neurosci, v. 21, p. 1302-12.

Baker, D. E., N. J. Harrison, E. Maltby, K. Smith, H. D. Moore, P. J. Shaw, P. R. Heath, H. Holden, and P. W. Andrews, 2007, Adaptation to culture of human embryonic stem cells and oncogenesis in vivo: Nat Biotechnol, v. 25, p. 207-15.

Baker, M., I. R. Mackenzie, S. M. Pickering-Brown, J. Gass, R. Rademakers, C. Lindholm, J. Snowden, J. Adamson, A. D. Sadovnick, S. Rollinson, A. Cannon, E. Dwosh, D. Neary, S. Melquist, A. Richardson, D. Dickson, Z. Berger, J. Eriksen, T. Robinson, C. Zehr, C. A. Dickey, R. Crook, E. McGowan, D. Mann, B. Boeve, H. Feldman, and M. Hutton, 2006, Mutations in progranulin cause tau-negative frontotemporal dementia linked to chromosome 17: Nature, v. 442, p. 916-9.

Bang, J., S. Spina, and B. L. Miller, 2015, Frontotemporal dementia: Lancet, v. 386, p. 1672-82.

Bansal, R., and S. E. Pfeiffer, 1997, FGF-2 converts mature oligodendrocytes to a novel phenotype: J Neurosci Res, v. 50, p. 215-28.

Barateiro, A., and A. Fernandes, 2014, Temporal oligodendrocyte lineage progression: in vitro models of proliferation, differentiation and myelination: Biochim Biophys Acta, v. 1843, p. 1917-29.

Barres, B. A., R. Schmid, M. Sendnter, and M. C. Raff, 1993, Multiple extracellular signals are required for long-term oligodendrocyte survival: Development, v. 118, p. 283-95.

Bechler, M. E., L. Byrne, and C. Ffrench-Constant, 2015, CNS Myelin Sheath Lengths Are an Intrinsic Property of Oligodendrocytes: Curr Biol, v. 25, p. 2411-6.

Beck, J., M. Poulter, D. Hensman, J. D. Rohrer, C. J. Mahoney, G. Adamson, T. Campbell, J. Uphill, A. Borg, P. Fratta, R. W. Orrell, A. Malaspina, J. Rowe, J. Brown, J. Hodges, K. Sidle, J. M. Polke, H. Houlden, J. M. Schott, N. C. Fox, M. N. Rossor, S. J. Tabrizi, A. M. Isaacs, J. Hardy, J. D. Warren, J. Collinge, and S. Mead, 2013, Large C9orf72 hexanucleotide repeat expansions are seen in multiple neurodegenerative syndromes and are more frequent than expected in the UK population: Am J Hum Genet, v. 92, p. 345-53.

Belzil, V. V., P. O. Bauer, M. Prudencio, T. F. Gendron, C. T. Stetler, I. K. Yan, L. Pregent, L. Daughrity, M. C. Baker, R. Rademakers, K. Boylan, T. C. Patel, D. W. Dickson, and L. Petrucelli, 2013, Reduced C9orf72 gene expression in c9FTD/ALS is caused by histone trimethylation, an epigenetic event detectable in blood: Acta Neuropathol, v. 126, p. 895-905.

Benatar, M., 2007, Lost in translation: treatment trials in the SOD1 mouse and in human ALS: Neurobiol Dis, v. 26, p. 1-13.
Biasiotto, G., S. Archetti, D. Di Lorenzo, F. Merola, G. Paiardi, B. Borroni, A. Alberici, A. Padovani, M. Filosto, C. Bonvicini, L. Caimi, and I. Zanella, 2016, A PCR-based protocol to accurately size C9orf72 intermediate-length alleles: Mol Cell Probes.
Bieniek, K. F., M. van Blitterswijk, M. C. Baker, L. Petrucelli, R. Rademakers, and D. W. Dickson, 2014, Expanded C9ORF72 hexanucleotide repeat in depressive pseudodementia: JAMA Neurol, v. 71, p. 775-81.
Bilican, B., A. Serio, S. J. Barmada, A. L. Nishimura, G. J. Sullivan, M. Carrasco, H. P. Phatnani, C. A. Puddifoot, D. Story, J. Fletcher, I. H. Park, B. A. Friedman, G. Q. Daley, D. J. Wyllie, G. E. Hardingham, I. Wilmut, S. Finkbeiner, T. Maniatis, C. E. Shaw, and S. Chandran, 2012, Mutant induced pluripotent stem cell lines recapitulate aspects of TDP-43 proteinopathies and reveal cell-specific vulnerability: Proc Natl Acad Sci U S A, v. 109, p. 5803-8.
Bock, C., E. Kiskinis, G. Verstappen, H. Gu, G. Boulting, Z. D. Smith, M. Ziller, G. F. Croft, M. W. Amoroso, D. H. Oakley, A. Gnirke, K. Eggan, and A. Meissner, 2011, Reference Maps of human ES and iPS cell variation enable high-throughput characterization of pluripotent cell lines: Cell, v. 144, p. 439-52.
Boeynaems, S., E. Bogaert, E. Michiels, I. Gijselinck, A. Sieben, A. Jovičić, G. De Baets, W. Scheveneels, J. Steyaert, I. Cuijt, K. J. Verstrepen, P. Callaerts, F. Rousseau, J. Schymkowitz, M. Cruts, C. Van Broeckhoven, P. Van Damme, A. D. Gitler, W. Robberecht, and L. Van Den Bosch, 2016, Drosophila screen connects nuclear transport genes to DPR pathology in c9ALS/FTD: Sci Rep, v. 6, p. 20877.
Boillée, S., and D. W. Cleveland, 2008, Revisiting oxidative damage in ALS: microglia, Nox, and mutant SOD1: J Clin Invest, v. 118, p. 474-8.
Boillée, S., K. Yamanaka, C. S. Lobsiger, N. G. Copeland, N. A. Jenkins, G. Kassiotis, G. Kollias, and D. W. Cleveland, 2006, Onset and progression in inherited ALS determined by motor neurons and microglia: Science, v. 312, p. 1389-92.
Boulting, G. L., E. Kiskinis, G. F. Croft, M. W. Amoroso, D. H. Oakley, B. J. Wainger, D. J. Williams, D. J. Kahler, M. Yamaki, L. Davidow, C. T. Rodolfa, J. T. Dimos, S. Mikkilineni, A. B. MacDermott, C. J. Woolf, C. E. Henderson, H. Wichterle, and K. Eggan, 2011, A functionally characterized test set of human induced pluripotent stem cells: Nat Biotechnol, v. 29, p. 279-86.
Boylan, K., 2015, Familial Amyotrophic Lateral Sclerosis: Neurol Clin, v. 33, p. 807-30.
Bradl, M., and H. Lassmann, 2010, Oligodendrocytes: biology and pathology: Acta Neuropathol, v. 119, p. 37-53.
Brettschneider, J., K. Arai, K. Del Tredici, J. B. Toledo, J. L. Robinson, E. B. Lee, S. Kuwabara, K. Shibuya, D. J. Irwin, L. Fang, V. M. Van Deerlin, L. Elman, L. McCluskey, A. C. Ludolph, V. M. Lee, H. Braak, and J. Q. Trojanowski, 2014, TDP-43 pathology and neuronal loss in amyotrophic lateral sclerosis spinal cord: Acta Neuropathol, v. 128, p. 423-37.
Briscoe, J., A. Pierani, T. M. Jessell, and J. Ericson, 2000, A homeodomain protein code specifies progenitor cell identity and neuronal fate in the ventral neural tube: Cell, v. 101, p. 435-45.
Brock, A., H. T. Goh, B. Yang, Y. Lu, H. Li, and Y. H. Loh, 2012, Cellular reprogramming: a new technology frontier in pharmaceutical research: Pharm Res, v. 29, p. 35-52.
Brooks, B. R., 1994, El Escorial World Federation of Neurology criteria for the diagnosis of amyotrophic lateral sclerosis. Subcommittee on Motor Neuron Diseases/Amyotrophic Lateral Sclerosis of the World Federation of Neurology

Research Group on Neuromuscular Diseases and the El Escorial "Clinical limits of amyotrophic lateral sclerosis" workshop contributors: J Neurol Sci, v. 124 Suppl, p. 96-107.

Bruni, A. C., L. Bernardi, R. Colao, E. Rubino, N. Smirne, F. Frangipane, B. Terni, S. A. Curcio, M. Mirabelli, A. Clodomiro, R. Di Lorenzo, R. Maletta, M. Anfossi, M. Gallo, S. Geracitano, C. Tomaino, M. G. Muraca, A. Leotta, S. G. Lio, L. Pinessi, I. Rainero, S. Sorbi, L. Nee, G. Milan, S. Pappatà, A. Postiglione, N. Abbamondi, G. Forloni, P. St George Hyslop, E. Rogaeva, O. Bugiani, G. Giaccone, J. F. Foncin, M. G. Spillantini, and G. Puccio, 2010, Worldwide distribution of PSEN1 Met146Leu mutation: a large variability for a founder mutation: Neurology, v. 74, p. 798-806.

Bryant, D. M., F. Hoeft, S. Lai, J. Lackey, D. Roeltgen, J. Ross, and A. L. Reiss, 2012, Sex chromosomes and the brain: a study of neuroanatomy in XYY syndrome: Dev Med Child Neurol, v. 54, p. 1149-56.

Buchman, V. L., J. Cooper-Knock, N. Connor-Robson, A. Higginbottom, J. Kirby, O. D. Razinskaya, N. Ninkina, and P. J. Shaw, 2013, Simultaneous and independent detection of C9ORF72 alleles with low and high number of GGGGCC repeats using an optimised protocol of Southern blot hybridisation: Mol Neurodegener, v. 8, p. 12.

Bunge, M. B., R. P. BUNGE, and G. D. PAPPAS, 1962, Electron microscopic demonstration of connections between glia and myelin sheaths in the developing mammalian central nervous system: J Cell Biol, v. 12, p. 448-53.

Bunge, R. P., 1968, Glial cells and the central myelin sheath: Physiol Rev, v. 48, p. 197-251.

Burns, L. T., and S. R. Wente, 2012, Trafficking to uncharted territory of the nuclear envelope: Curr Opin Cell Biol, v. 24, p. 341-9.

Burrell, J. R., G. M. Halliday, J. J. Kril, L. M. Ittner, J. Götz, M. C. Kiernan, and J. R. Hodges, 2016, The frontotemporal dementia-motor neuron disease continuum: Lancet.

Burrell, J. R., M. C. Kiernan, S. Vucic, and J. R. Hodges, 2011, Motor neuron dysfunction in frontotemporal dementia: Brain, v. 134, p. 2582-94.

Byrne, S., P. Bede, M. Elamin, K. Kenna, C. Lynch, R. McLaughlin, and O. Hardiman, 2011a, Proposed criteria for familial amyotrophic lateral sclerosis: Amyotroph Lateral Scler, v. 12, p. 157-9.

Byrne, S., M. Elamin, P. Bede, A. Shatunov, C. Walsh, B. Corr, M. Heverin, N. Jordan, K. Kenna, C. Lynch, R. L. McLaughlin, P. M. Iyer, C. O'Brien, J. Phukan, B. Wynne, A. L. Bokde, D. G. Bradley, N. Pender, A. Al-Chalabi, and O. Hardiman, 2012, Cognitive and clinical characteristics of patients with amyotrophic lateral sclerosis carrying a C9orf72 repeat expansion: a population-based cohort study: Lancet Neurol, v. 11, p. 232-40.

Byrne, S., C. Walsh, C. Lynch, P. Bede, M. Elamin, K. Kenna, R. McLaughlin, and O. Hardiman, 2011b, Rate of familial amyotrophic lateral sclerosis: a systematic review and meta-analysis: J Neurol Neurosurg Psychiatry, v. 82, p. 623-7.

Cai, J., Y. Qi, X. Hu, M. Tan, Z. Liu, J. Zhang, Q. Li, M. Sander, and M. Qiu, 2005, Generation of oligodendrocyte precursor cells from mouse dorsal spinal cord independent of Nkx6 regulation and Shh signaling: Neuron, v. 45, p. 41-53.

Calver, A. R., A. C. Hall, W. P. Yu, F. S. Walsh, J. K. Heath, C. Betsholtz, and W. D. Richardson, 1998, Oligodendrocyte population dynamics and the role of PDGF in vivo: Neuron, v. 20, p. 869-82.

Carson, M. J., R. R. Behringer, R. L. Brinster, and F. A. McMorris, 1993, Insulin-like growth factor I increases brain growth and central nervous system myelination in transgenic mice: Neuron, v. 10, p. 729-40.

Casaccia-Bonnefil, P., 2000, Cell death in the oligodendrocyte lineage: a molecular perspective of life/death decisions in development and disease: Glia, v. 29, p. 124-35.

Chamberlain, C. E., J. Jeong, C. Guo, B. L. Allen, and A. P. McMahon, 2008, Notochord-derived Shh concentrates in close association with the apically positioned basal body in neural target cells and forms a dynamic gradient during neural patterning: Development, v. 135, p. 1097-106.

Chambers, S. M., C. A. Fasano, E. P. Papapetrou, M. Tomishima, M. Sadelain, and L. Studer, 2009, Highly efficient neural conversion of human ES and iPS cells by dual inhibition of SMAD signaling: Nat Biotechnol, v. 27, p. 275-80.

Chan, E. M., S. Ratanasirintrawoot, I. H. Park, P. D. Manos, Y. H. Loh, H. Huo, J. D. Miller, O. Hartung, J. Rho, T. A. Ince, G. Q. Daley, and T. M. Schlaeger, 2009, Live cell imaging distinguishes bona fide human iPS cells from partially reprogrammed cells: Nat Biotechnol, v. 27, p. 1033-7.

Chancellor, A., 1992, The Scottish Motor Neuron Disease Register: a prospective study of adult onset motor neuron disease in Scotland. Methodology, demography and clinical features of incident cases in 1989: J Neurol Neurosurg Psychiatry, v. 55, p. 536-41.

Chang, Y. J., U. S. Jeng, Y. L. Chiang, I. S. Hwang, and Y. R. Chen, 2016, The Glycine-Alanine Dipeptide Repeat from C9orf72 Hexanucleotide Expansions Forms Toxic Amyloids Possessing Cell-to-Cell Transmission Properties: J Biol Chem, v. 291, p. 4903-11.

Chew, J., T. F. Gendron, M. Prudencio, H. Sasaguri, Y. J. Zhang, M. Castanedes-Casey, C. W. Lee, K. Jansen-West, A. Kurti, M. E. Murray, K. F. Bieniek, P. O. Bauer, E. C. Whitelaw, L. Rousseau, J. N. Stankowski, C. Stetler, L. M. Daughrity, E. A. Perkerson, P. Desaro, A. Johnston, K. Overstreet, D. Edbauer, R. Rademakers, K. B. Boylan, D. W. Dickson, J. D. Fryer, and L. Petrucelli, 2015, Neurodegeneration. C9ORF72 repeat expansions in mice cause TDP-43 pathology, neuronal loss, and behavioral deficits: Science, v. 348, p. 1151-4.

Chiò, A., G. Mora, M. Sabatelli, C. Caponnetto, C. Lunetta, B. J. Traynor, J. O. Johnson, M. A. Nalls, A. Calvo, C. Moglia, G. Borghero, F. Trojsi, V. La Bella, P. Volanti, I. Simone, F. Salvi, F. O. Logullo, N. Riva, P. Carrera, F. Giannini, J. Mandrioli, R. Tanel, M. Capasso, L. Tremolizzo, S. Battistini, M. R. Murru, P. Origone, M. Zollino, S. Penco, L. Mazzini, S. D'Alfonso, G. Restagno, M. Brunetti, M. Barberis, F. L. Conforti, I. consortium, and S. consortium, 2016, ATNX2 is not a regulatory gene in Italian amyotrophic lateral sclerosis patients with C9ORF72 GGGGCC expansion: Neurobiol Aging, v. 39, p. 218.e5-8.

Ciura, S., S. Lattante, I. Le Ber, M. Latouche, H. Tostivint, A. Brice, and E. Kabashi, 2013, Loss of function of C9orf72 causes motor deficits in a zebrafish model of amyotrophic lateral sclerosis: Ann Neurol, v. 74, p. 180-7.

Ciura, S., C. Sellier, M. L. Campanari, N. Charlet-Berguerand, and E. Kabashi, 2016, The most prevalent genetic cause of ALS-FTD, C9orf72 synergizes the toxicity of ATXN2 intermediate polyglutamine repeats through the autophagy pathway: Autophagy, v. 12, p. 1406-8.

Clayton, B. L., and B. Popko, 2016, Endoplasmic reticulum stress and the unfolded protein response in disorders of myelinating glia: Brain Res.

Cohen-Hadad, Y., G. Altarescu, T. Eldar-Geva, E. Levi-Lahad, M. Zhang, E. Rogaeva, M. Gotkine, O. Bartok, R. Ashwal-Fluss, S. Kadener, S. Epsztejn-Litman, and R. Eiges, 2016, Marked Differences in C9orf72 Methylation Status and Isoform Expression between C9/ALS Human Embryonic and Induced Pluripotent Stem Cells: Stem Cell Reports, v. 7, p. 927-940.

Consortium, H. i., 2012, Induced pluripotent stem cells from patients with Huntington's disease show CAG-repeat-expansion-associated phenotypes: Cell Stem Cell, v. 11, p. 264-78.

Cooper-Knock, J., C. Hewitt, J. R. Highley, A. Brockington, A. Milano, S. Man, J. Martindale, J. Hartley, T. Walsh, C. Gelsthorpe, L. Baxter, G. Forster, M. Fox, J. Bury, K. Mok, C. J. McDermott, B. J. Traynor, J. Kirby, S. B. Wharton, P. G. Ince, J. Hardy, and P. J. Shaw, 2012, Clinico-pathological features in amyotrophic lateral sclerosis with expansions in C9ORF72: Brain, v. 135, p. 751-64.

Cooper-Knock, J., A. Higginbottom, M. J. Stopford, J. R. Highley, P. G. Ince, S. B. Wharton, S. Pickering-Brown, J. Kirby, G. M. Hautbergue, and P. J. Shaw, 2015, Antisense RNA foci in the motor neurons of C9ORF72-ALS patients are associated with TDP-43 proteinopathy: Acta Neuropathol, v. 130, p. 63-75.

Cooper-Knock, J., M. J. Walsh, A. Higginbottom, J. Robin Highley, M. J. Dickman, D. Edbauer, P. G. Ince, S. B. Wharton, S. A. Wilson, J. Kirby, G. M. Hautbergue, and P. J. Shaw, 2014, Sequestration of multiple RNA recognition motif-containing proteins by C9orf72 repeat expansions: Brain, v. 137, p. 2040-51.

Cowan, C. A., I. Klimanskaya, J. McMahon, J. Atienza, J. Witmyer, J. P. Zucker, S. Wang, C. C. Morton, A. P. McMahon, D. Powers, and D. A. Melton, 2004, Derivation of embryonic stem-cell lines from human blastocysts: N Engl J Med, v. 350, p. 1353-6.

D'Antonio, M., M. L. Feltri, and L. Wrabetz, 2009, Myelin under stress: J Neurosci Res, v. 87, p. 3241-9.

D'Aquila, R. T., L. J. Bechtel, J. A. Videler, J. J. Eron, P. Gorczyca, and J. C. Kaplan, 1991, Maximizing sensitivity and specificity of PCR by pre-amplification heating: Nucleic Acids Res, v. 19, p. 3749.

Davidson, Y., A. C. Robinson, X. Liu, D. Wu, C. Troakes, S. Rollinson, M. Masuda-Suzukake, G. Suzuki, T. Nonaka, J. Shi, J. Tian, H. Hamdalla, J. Ealing, A. Richardson, M. Jones, S. Pickering-Brown, J. S. Snowden, M. Hasegawa, and D. M. Mann, 2016, Neurodegeneration in frontotemporal lobar degeneration and motor neurone disease associated with expansions in C9orf72 is linked to TDP-43 pathology and not associated with aggregated forms of dipeptide repeat proteins: Neuropathol Appl Neurobiol, v. 42, p. 242-54.

Davis-Dusenbery, B. N., L. A. Williams, J. R. Klim, and K. Eggan, 2014, How to make spinal motor neurons: Development, v. 141, p. 491-501.

De Temmerman, N., S. Seneca, A. Van Steirteghem, P. Haentjens, J. Van der Elst, I. Liebaers, and K. D. Sermon, 2008, CTG repeat instability in a human embryonic stem cell line carrying the myotonic dystrophy type 1 mutation: Mol Hum Reprod, v. 14, p. 405-12.

DeJesus-Hernandez, M., I. R. Mackenzie, B. F. Boeve, A. L. Boxer, M. Baker, N. J. Rutherford, A. M. Nicholson, N. A. Finch, H. Flynn, J. Adamson, N. Kouri, A. Wojtas, P. Sengdy, G. Y. Hsiung, A. Karydas, W. W. Seeley, K. A. Josephs, G. Coppola, D. H. Geschwind, Z. K. Wszolek, H. Feldman, D. S. Knopman, R. C. Petersen, B. L. Miller, D. W. Dickson, K. B. Boylan, N. R. Graff-Radford, and R. Rademakers, 2011, Expanded GGGGCC hexanucleotide repeat in noncoding region of C9ORF72 causes chromosome 9p-linked FTD and ALS: Neuron, v. 72, p. 245-56.

Deltcheva, E., K. Chylinski, C. M. Sharma, K. Gonzales, Y. Chao, Z. A. Pirzada, M. R. Eckert, J. Vogel, and E. Charpentier, 2011, CRISPR RNA maturation by trans-encoded small RNA and host factor RNase III: Nature, v. 471, p. 602-7.

Deng, H. X., W. Chen, S. T. Hong, K. M. Boycott, G. H. Gorrie, N. Siddique, Y. Yang, F. Fecto, Y. Shi, H. Zhai, H. Jiang, M. Hirano, E. Rampersaud, G. H. Jansen, S. Donkervoort, E. H. Bigio, B. R. Brooks, K. Ajroud, R. L. Sufit, J. L. Haines,

E. Mugnaini, M. A. Pericak-Vance, and T. Siddique, 2011, Mutations in UBQLN2 cause dominant X-linked juvenile and adult-onset ALS and ALS/dementia: Nature, v. 477, p. 211-5.

Deng, H. X., H. Zhai, E. H. Bigio, J. Yan, F. Fecto, K. Ajroud, M. Mishra, S. Ajroud-Driss, S. Heller, R. Sufit, N. Siddique, E. Mugnaini, and T. Siddique, 2010, FUS-immunoreactive inclusions are a common feature in sporadic and non-SOD1 familial amyotrophic lateral sclerosis: Ann Neurol, v. 67, p. 739-48.

Devenney, E., D. Foxe, C. Dobson-Stone, J. B. Kwok, M. C. Kiernan, and J. R. Hodges, 2015, Clinical heterogeneity of the C9orf72 genetic mutation in frontotemporal dementia: Neurocase, v. 21, p. 535-41.

Devlin, A. C., K. Burr, S. Borooah, J. D. Foster, E. M. Cleary, I. Geti, L. Vallier, C. E. Shaw, S. Chandran, and G. B. Miles, 2015, Human iPSC-derived motoneurons harbouring TARDBP or C9ORF72 ALS mutations are dysfunctional despite maintaining viability: Nat Commun, v. 6, p. 5999.

Di Giorgio, F. P., M. A. Carrasco, M. C. Siao, T. Maniatis, and K. Eggan, 2007, Non-cell autonomous effect of glia on motor neurons in an embryonic stem cell-based ALS model: Nat Neurosci, v. 10, p. 608-14.

Dierick, H., M. Stul, W. De Kelver, P. Marynen, and J. J. Cassiman, 1993, Incorporation of dITP or 7-deaza dGTP during PCR improves sequencing of the product: Nucleic Acids Res, v. 21, p. 4427-8.

Ding, Q., Y. K. Lee, E. A. Schaefer, D. T. Peters, A. Veres, K. Kim, N. Kuperwasser, D. L. Motola, T. B. Meissner, W. T. Hendriks, M. Trevisan, R. M. Gupta, A. Moisan, E. Banks, M. Friesen, R. T. Schinzel, F. Xia, A. Tang, Y. Xia, E. Figueroa, A. Wann, T. Ahfeldt, L. Daheron, F. Zhang, L. L. Rubin, L. F. Peng, R. T. Chung, K. Musunuru, and C. A. Cowan, 2013, A TALEN genome-editing system for generating human stem cell-based disease models: Cell Stem Cell, v. 12, p. 238-51.

Dobson-Stone, C., M. Hallupp, C. T. Loy, E. M. Thompson, E. Haan, C. M. Sue, P. K. Panegyres, C. Razquin, M. Seijo-Martinez, R. Rene, J. Gascon, J. Campdelacreu, B. Schmoll, A. E. Volk, W. S. Brooks, P. R. Schofield, P. Pastor, and J. B. Kwok, 2013, C9ORF72 repeat expansion in Australian and Spanish frontotemporal dementia patients: PLoS One, v. 8, p. e56899.

Dols-Icardo, O., A. García-Redondo, R. Rojas-García, R. Sánchez-Valle, A. Noguera, E. Gómez-Tortosa, P. Pastor, I. Hernández, J. Esteban-Pérez, M. Suárez-Calvet, S. Antón-Aguirre, G. Amer, S. Ortega-Cubero, R. Blesa, J. Fortea, D. Alcolea, A. Capdevila, A. Antonell, A. Lladó, J. L. Muñoz-Blanco, J. S. Mora, L. Galán-Dávila, F. J. Rodríguez De Rivera, A. Lleó, and J. Clarimón, 2014, Characterization of the repeat expansion size in C9orf72 in amyotrophic lateral sclerosis and frontotemporal dementia: Hum Mol Genet, v. 23, p. 749-54.

Don, R. H., P. T. Cox, B. J. Wainwright, K. Baker, and J. S. Mattick, 1991, 'Touchdown' PCR to circumvent spurious priming during gene amplification: Nucleic Acids Res, v. 19, p. 4008.

Donnelly, C. J., P. W. Zhang, J. T. Pham, A. R. Haeusler, N. A. Mistry, S. Vidensky, E. L. Daley, E. M. Poth, B. Hoover, D. M. Fines, N. Maragakis, P. J. Tienari, L. Petrucelli, B. J. Traynor, J. Wang, F. Rigo, C. F. Bennett, S. Blackshaw, R. Sattler, and J. D. Rothstein, 2013, RNA toxicity from the ALS/FTD C9ORF72 expansion is mitigated by antisense intervention: Neuron, v. 80, p. 415-28.

Douvaras, P., and V. Fossati, 2015, Generation and isolation of oligodendrocyte progenitor cells from human pluripotent stem cells: Nat Protoc, v. 10, p. 1143-54.

Douvaras, P., J. Wang, M. Zimmer, S. Hanchuk, M. A. O'Bara, S. Sadiq, F. J. Sim, J. Goldman, and V. Fossati, 2014, Efficient generation of myelinating

oligodendrocytes from primary progressive multiple sclerosis patients by induced pluripotent stem cells: Stem Cell Reports, v. 3, p. 250-9.
Draper, J. S., K. Smith, P. Gokhale, H. D. Moore, E. Maltby, J. Johnson, L. Meisner, T. P. Zwaka, J. A. Thomson, and P. W. Andrews, 2004, Recurrent gain of chromosomes 17q and 12 in cultured human embryonic stem cells: Nat Biotechnol, v. 22, p. 53-4.
Ebert, A. D., J. Yu, F. F. Rose, V. B. Mattis, C. L. Lorson, J. A. Thomson, and C. N. Svendsen, 2009, Induced pluripotent stem cells from a spinal muscular atrophy patient: Nature, v. 457, p. 277-80.
Edbauer, D., and C. Haass, 2015, An amyloid-like cascade hypothesis for C9orf72 ALS/FTD: Curr Opin Neurobiol, v. 36, p. 99-106.
Egawa, N., S. Kitaoka, K. Tsukita, M. Naitoh, K. Takahashi, T. Yamamoto, F. Adachi, T. Kondo, K. Okita, I. Asaka, T. Aoi, A. Watanabe, Y. Yamada, A. Morizane, J. Takahashi, T. Ayaki, H. Ito, K. Yoshikawa, S. Yamawaki, S. Suzuki, D. Watanabe, H. Hioki, T. Kaneko, K. Makioka, K. Okamoto, H. Takuma, A. Tamaoka, K. Hasegawa, T. Nonaka, M. Hasegawa, A. Kawata, M. Yoshida, T. Nakahata, R. Takahashi, M. C. Marchetto, F. H. Gage, S. Yamanaka, and H. Inoue, 2012, Drug screening for ALS using patient-specific induced pluripotent stem cells: Sci Transl Med, v. 4, p. 145ra104.
Eiges, R., A. Urbach, M. Malcov, T. Frumkin, T. Schwartz, A. Amit, Y. Yaron, A. Eden, O. Yanuka, N. Benvenisty, and D. Ben-Yosef, 2007, Developmental study of fragile X syndrome using human embryonic stem cells derived from preimplantation genetically diagnosed embryos: Cell Stem Cell, v. 1, p. 568-77.
Elamin, M., J. Phukan, P. Bede, N. Jordan, S. Byrne, N. Pender, and O. Hardiman, 2011, Executive dysfunction is a negative prognostic indicator in patients with ALS without dementia: Neurology, v. 76, p. 1263-9.
Ellis, J., B. G. Bruneau, G. Keller, I. R. Lemischka, A. Nagy, J. Rossant, D. Srivastava, P. W. Zandstra, and W. L. Stanford, 2009, Alternative induced pluripotent stem cell characterization criteria for in vitro applications: Cell Stem Cell, v. 4, p. 198-9; author reply 202.
Emery, B., and Q. R. Lu, 2015, Transcriptional and Epigenetic Regulation of Oligodendrocyte Development and Myelination in the Central Nervous System: Cold Spring Harb Perspect Biol, v. 7.
Esanov, R., K. C. Belle, M. van Blitterswijk, V. V. Belzil, R. Rademakers, D. W. Dickson, L. Petrucelli, K. B. Boylan, D. M. Dykxhoorn, J. Wuu, M. Benatar, C. Wahlestedt, and Z. Zeier, 2016, C9orf72 promoter hypermethylation is reduced while hydroxymethylation is acquired during reprogramming of ALS patient cells: Exp Neurol, v. 277, p. 171-7.
Farg, M. A., V. Sundaramoorthy, J. M. Sultana, S. Yang, R. A. Atkinson, V. Levina, M. A. Halloran, P. A. Gleeson, I. P. Blair, K. Y. Soo, A. E. King, and J. D. Atkin, 2014, C9ORF72, implicated in amytrophic lateral sclerosis and frontotemporal dementia, regulates endosomal trafficking: Hum Mol Genet, v. 23, p. 3579-95.
Fatima, M., R. Tan, G. M. Halliday, and J. J. Kril, 2015, Spread of pathology in amyotrophic lateral sclerosis: assessment of phosphorylated TDP-43 along axonal pathways: Acta Neuropathol Commun, v. 3, p. 47.
Feiler, M. S., B. Strobel, A. Freischmidt, A. M. Helferich, J. Kappel, B. M. Brewer, D. Li, D. R. Thal, P. Walther, A. C. Ludolph, K. M. Danzer, and J. H. Weishaupt, 2015, TDP-43 is intercellularly transmitted across axon terminals: J Cell Biol, v. 211, p. 897-911.
Ferraiuolo, L., J. Kirby, A. J. Grierson, M. Sendtner, and P. J. Shaw, 2011, Molecular pathways of motor neuron injury in amyotrophic lateral sclerosis: Nat Rev Neurol, v. 7, p. 616-30.

Ferraiuolo, L., K. Meyer, T. W. Sherwood, J. Vick, S. Likhite, A. Frakes, C. J. Miranda, L. Braun, P. R. Heath, R. Pineda, C. E. Beattie, P. J. Shaw, C. C. Askwith, D. McTigue, and B. K. Kaspar, 2016, Oligodendrocytes contribute to motor neuron death in ALS via SOD1-dependent mechanism: Proc Natl Acad Sci U S A.

Ferrari, R., D. Kapogiannis, E. D. Huey, and P. Momeni, 2011, FTD and ALS: a tale of two diseases: Curr Alzheimer Res, v. 8, p. 273-94.

Ferreira, T. A., A. V. Blackman, J. Oyrer, S. Jayabal, A. J. Chung, A. J. Watt, P. J. Sjöström, and D. J. van Meyel, 2014, Neuronal morphometry directly from bitmap images: Nat Methods, v. 11, p. 982-4.

Filippi, M., F. Agosta, S. Abrahams, F. Fazekas, J. Grosskreutz, S. Kalra, J. Kassubek, V. Silani, M. R. Turner, J. C. Masdeu, and E. F. o. N. Societies, 2010, EFNS guidelines on the use of neuroimaging in the management of motor neuron diseases: Eur J Neurol, v. 17, p. 526-e20.

Finzsch, M., C. C. Stolt, P. Lommes, and M. Wegner, 2008, Sox9 and Sox10 influence survival and migration of oligodendrocyte precursors in the spinal cord by regulating PDGF receptor alpha expression: Development, v. 135, p. 637-46.

Fogarty, M., W. D. Richardson, and N. Kessaris, 2005, A subset of oligodendrocytes generated from radial glia in the dorsal spinal cord: Development, v. 132, p. 1951-9.

Fong, J. C., A. M. Karydas, and J. S. Goldman, 2012, Genetic counseling for FTD/ALS caused by the C9ORF72 hexanucleotide expansion: Alzheimers Res Ther, v. 4, p. 27.

Fratta, P., S. Mizielinska, A. J. Nicoll, M. Zloh, E. M. Fisher, G. Parkinson, and A. M. Isaacs, 2012, C9orf72 hexanucleotide repeat associated with amyotrophic lateral sclerosis and frontotemporal dementia forms RNA G-quadruplexes: Sci Rep, v. 2, p. 1016.

Fratta, P., J. M. Polke, J. Newcombe, S. Mizielinska, T. Lashley, M. Poulter, J. Beck, E. Preza, A. Devoy, K. Sidle, R. Howard, A. Malaspina, R. W. Orrell, J. Clarke, C. H. Lu, K. Mok, T. Collins, M. Shoaii, T. Nanji, S. Wray, G. Adamson, A. Pittman, A. E. Renton, B. J. Traynor, M. G. Sweeney, T. Revesz, H. Houlden, S. Mead, A. M. Isaacs, and E. M. Fisher, 2015, Screening a UK amyotrophic lateral sclerosis cohort provides evidence of multiple origins of the C9orf72 expansion: Neurobiol Aging, v. 36, p. 546.e1-7.

Fratta, P., M. Poulter, T. Lashley, J. D. Rohrer, J. M. Polke, J. Beck, N. Ryan, D. Hensman, S. Mizielinska, A. J. Waite, M. C. Lai, T. F. Gendron, L. Petrucelli, E. M. Fisher, T. Revesz, J. D. Warren, J. Collinge, A. M. Isaacs, and S. Mead, 2013, Homozygosity for the C9orf72 GGGGCC repeat expansion in frontotemporal dementia: Acta Neuropathol, v. 126, p. 401-9.

Freibaum, B. D., Y. Lu, R. Lopez-Gonzalez, N. C. Kim, S. Almeida, K. H. Lee, N. Badders, M. Valentine, B. L. Miller, P. C. Wong, L. Petrucelli, H. J. Kim, F. B. Gao, and J. P. Taylor, 2015, GGGGCC repeat expansion in C9orf72 compromises nucleocytoplasmic transport: Nature, v. 525, p. 129-33.

Freischmidt, A., T. Wieland, B. Richter, W. Ruf, V. Schaeffer, K. Müller, N. Marroquin, F. Nordin, A. Hübers, P. Weydt, S. Pinto, R. Press, S. Millecamps, N. Molko, E. Bernard, C. Desnuelle, M. H. Soriani, J. Dorst, E. Graf, U. Nordström, M. S. Feiler, S. Putz, T. M. Boeckers, T. Meyer, A. S. Winkler, J. Winkelman, M. de Carvalho, D. R. Thal, M. Otto, T. Brännström, A. E. Volk, P. Kursula, K. M. Danzer, P. Lichtner, I. Dikic, T. Meitinger, A. C. Ludolph, T. M. Strom, P. M. Andersen, and J. H. Weishaupt, 2015, Haploinsufficiency of TBK1 causes familial ALS and fronto-temporal dementia: Nat Neurosci, v. 18, p. 631-6.

Frey, U. H., H. S. Bachmann, J. Peters, and W. Siffert, 2008, PCR-amplification of GC-rich regions: 'slowdown PCR': Nat Protoc, v. 3, p. 1312-7.

Fu, Y. H., D. P. Kuhl, A. Pizzuti, M. Pieretti, J. S. Sutcliffe, S. Richards, A. J. Verkerk, J. J. Holden, R. G. Fenwick, and S. T. Warren, 1991, Variation of the CGG repeat at the fragile X site results in genetic instability: resolution of the Sherman paradox: Cell, v. 67, p. 1047-58.

Funfschilling, U., L. M. Supplie, D. Mahad, S. Boretius, A. S. Saab, J. Edgar, B. G. Brinkmann, C. M. Kassmann, I. D. Tzvetanova, W. Mobius, F. Diaz, D. Meijer, U. Suter, B. Hamprecht, M. W. Sereda, C. T. Moraes, J. Frahm, S. Goebbels, and K. A. Nave, 2012, Glycolytic oligodendrocytes maintain myelin and long-term axonal integrity: Nature, v. 485, p. 517-21.

Fusaki, N., H. Ban, A. Nishiyama, K. Saeki, and M. Hasegawa, 2009, Efficient induction of transgene-free human pluripotent stem cells using a vector based on Sendai virus, an RNA virus that does not integrate into the host genome: Proc Jpn Acad Ser B Phys Biol Sci, v. 85, p. 348-62.

Gallagher, M. D., E. Suh, M. Grossman, L. Elman, L. McCluskey, J. C. Van Swieten, S. Al-Sarraj, M. Neumann, E. Gelpi, B. Ghetti, J. D. Rohrer, G. Halliday, C. Van Broeckhoven, D. Seilhean, P. J. Shaw, M. P. Frosch, I. Alafuzoff, A. Antonell, N. Bogdanovic, W. Brooks, N. J. Cairns, J. Cooper-Knock, C. Cotman, P. Cras, M. Cruts, P. P. De Deyn, C. DeCarli, C. Dobson-Stone, S. Engelborghs, N. Fox, D. Galasko, M. Gearing, I. Gijselinck, J. Grafman, P. Hartikainen, K. J. Hatanpaa, J. R. Highley, J. Hodges, C. Hulette, P. G. Ince, L. W. Jin, J. Kirby, J. Kofler, J. Kril, J. B. Kwok, A. Levey, A. Lieberman, A. Llado, J. J. Martin, E. Masliah, C. J. McDermott, A. McKee, C. McLean, S. Mead, C. A. Miller, J. Miller, D. G. Munoz, J. Murrell, H. Paulson, O. Piguet, M. Rossor, R. Sanchez-Valle, M. Sano, J. Schneider, L. C. Silbert, S. Spina, J. van der Zee, T. Van Langenhove, J. Warren, S. B. Wharton, C. L. White, R. L. Woltjer, J. Q. Trojanowski, V. M. Lee, V. Van Deerlin, and A. S. Chen-Plotkin, 2014, TMEM106B is a genetic modifier of frontotemporal lobar degeneration with C9orf72 hexanucleotide repeat expansions: Acta Neuropathol, v. 127, p. 407-18.

Gasiunas, G., R. Barrangou, P. Horvath, and V. Siksnys, 2012, Cas9-crRNA ribonucleoprotein complex mediates specific DNA cleavage for adaptive immunity in bacteria: Proc Natl Acad Sci U S A, v. 109, p. E2579-86.

Geerts, M., J. Steyaert, and J. P. Fryns, 2003, The XYY syndrome: a follow-up study on 38 boys: Genet Couns, v. 14, p. 267-79.

Gendron, T. F., V. V. Belzil, Y. J. Zhang, and L. Petrucelli, 2014, Mechanisms of toxicity in C9FTLD/ALS: Acta Neuropathol, v. 127, p. 359-76.

Gendron, T. F., K. F. Bieniek, Y. J. Zhang, K. Jansen-West, P. E. Ash, T. Caulfield, L. Daughrity, J. H. Dunmore, M. Castanedes-Casey, J. Chew, D. M. Cosio, M. van Blitterswijk, W. C. Lee, R. Rademakers, K. B. Boylan, D. W. Dickson, and L. Petrucelli, 2013, Antisense transcripts of the expanded C9ORF72 hexanucleotide repeat form nuclear RNA foci and undergo repeat-associated non-ATG translation in c9FTD/ALS: Acta Neuropathol, v. 126, p. 829-44.

Gijselinck, I., T. Van Langenhove, J. van der Zee, K. Sleegers, S. Philtjens, G. Kleinberger, J. Janssens, K. Bettens, C. Van Cauwenberghe, S. Pereson, S. Engelborghs, A. Sieben, P. De Jonghe, R. Vandenberghe, P. Santens, J. De Bleecker, G. Maes, V. Baumer, L. Dillen, G. Joris, I. Cuijt, E. Corsmit, E. Elinck, J. Van Dongen, S. Vermeulen, M. Van den Broeck, C. Vaerenberg, M. Mattheijssens, K. Peeters, W. Robberecht, P. Cras, J. J. Martin, P. P. De Deyn, M. Cruts, and C. Van Broeckhoven, 2012, A C9orf72 promoter repeat expansion in a Flanders-Belgian cohort with disorders of the frontotemporal lobar degeneration-amyotrophic lateral sclerosis spectrum: a gene identification study: Lancet Neurol, v. 11, p. 54-65.

Gijselinck, I., S. Van Mossevelde, J. van der Zee, A. Sieben, S. Engelborghs, J. De Bleecker, A. Ivanoiu, O. Deryck, D. Edbauer, M. Zhang, B. Heeman, V. Bäumer, M. Van den Broeck, M. Mattheijssens, K. Peeters, E. Rogaeva, P. De Jonghe, P. Cras, J. J. Martin, P. P. de Deyn, M. Cruts, and C. Van Broeckhoven, 2016, The C9orf72 repeat size correlates with onset age of disease, DNA methylation and transcriptional downregulation of the promoter: Mol Psychiatry, v. 21, p. 1112-24.

Gitler, A. D., and H. Tsuiji, 2016, There has been an awakening: Emerging mechanisms of C9orf72 mutations in FTD/ALS: Brain Res.

Goldberg, Y. P., B. Kremer, S. E. Andrew, J. Theilmann, R. K. Graham, F. Squitieri, H. Telenius, S. Adam, A. Sajoo, and E. Starr, 1993, Molecular analysis of new mutations for Huntington's disease: intermediate alleles and sex of origin effects: Nat Genet, v. 5, p. 174-9.

Goldman, J. S., J. M. Farmer, E. M. Wood, J. K. Johnson, A. Boxer, J. Neuhaus, C. Lomen-Hoerth, K. C. Wilhelmsen, V. M. Lee, M. Grossman, and B. L. Miller, 2005, Comparison of family histories in FTLD subtypes and related tauopathies: Neurology, v. 65, p. 1817-9.

Gomes-Pereira, M., M. T. Fortune, L. Ingram, J. P. McAbney, and D. G. Monckton, 2004, Pms2 is a genetic enhancer of trinucleotide CAG.CTG repeat somatic mosaicism: implications for the mechanism of triplet repeat expansion: Hum Mol Genet, v. 13, p. 1815-25.

Gomez-Deza, J., Y. B. Lee, C. Troakes, M. Nolan, S. Al-Sarraj, J. M. Gallo, and C. E. Shaw, 2015, Dipeptide repeat protein inclusions are rare in the spinal cord and almost absent from motor neurons in C9ORF72 mutant amyotrophic lateral sclerosis and are unlikely to cause their degeneration: Acta Neuropathol Commun, v. 3, p. 38.

Goodin, D. S., H. A. Rowley, and R. K. Olney, 1988, Magnetic resonance imaging in amyotrophic lateral sclerosis: Ann Neurol, v. 23, p. 418-20.

Gorris, R., J. Fischer, K. L. Erwes, J. Kesavan, D. A. Peterson, M. Alexander, M. M. Nöthen, M. Peitz, T. Quandel, M. Karus, and O. Brüstle, 2015, Pluripotent stem cell-derived radial glia-like cells as stable intermediate for efficient generation of human oligodendrocytes: Glia, v. 63, p. 2152-67.

Grolez, G., C. Moreau, V. Danel-Brunaud, C. Delmaire, R. Lopes, P. F. Pradat, M. M. El Mendili, L. Defebvre, and D. Devos, 2016, The value of magnetic resonance imaging as a biomarker for amyotrophic lateral sclerosis: a systematic review: BMC Neurol, v. 16, p. 155.

Gómez-Tortosa, E., J. Gallego, R. Guerrero-López, A. Marcos, E. Gil-Neciga, M. J. Sainz, A. Díaz, E. Franco-Macías, M. J. Trujillo-Tiebas, C. Ayuso, and J. Pérez-Pérez, 2013, C9ORF72 hexanucleotide expansions of 20-22 repeats are associated with frontotemporal deterioration: Neurology, v. 80, p. 366-70.

Haeusler, A. R., C. J. Donnelly, G. Periz, E. A. Simko, P. G. Shaw, M. S. Kim, N. J. Maragakis, J. C. Troncoso, A. Pandey, R. Sattler, J. D. Rothstein, and J. Wang, 2014, C9orf72 nucleotide repeat structures initiate molecular cascades of disease: Nature, v. 507, p. 195-200.

Haidet-Phillips, A. M., M. E. Hester, C. J. Miranda, K. Meyer, L. Braun, A. Frakes, S. Song, S. Likhite, M. J. Murtha, K. D. Foust, M. Rao, A. Eagle, A. Kammesheidt, A. Christensen, J. R. Mendell, A. H. Burghes, and B. K. Kaspar, 2011, Astrocytes from familial and sporadic ALS patients are toxic to motor neurons: Nat Biotechnol, v. 29, p. 824-8.

Hardy, J., and E. Rogaeva, 2014, Motor neuron disease and frontotemporal dementia: sometimes related, sometimes not: Exp Neurol, v. 262 Pt B, p. 75-83.

Harms, M. B., J. Cady, C. Zaidman, P. Cooper, T. Bali, P. Allred, C. Cruchaga, M. Baughn, A. Pestronk, A. Goate, J. Ravits, and R. H. Baloh, 2013, Lack of

C9ORF72 coding mutations supports a gain of function for repeat expansions in ALS: Neurobiol Aging, v. 34, p. 2234 e13-9.
He, L., and Q. R. Lu, 2013, Coordinated control of oligodendrocyte development by extrinsic and intrinsic signaling cues: Neurosci Bull, v. 29, p. 129-43.
Henke, W., K. Herdel, K. Jung, D. Schnorr, and S. A. Loening, 1997, Betaine improves the PCR amplification of GC-rich DNA sequences: Nucleic Acids Res, v. 25, p. 3957-8.
Hećimović, S., I. Barisić, A. Müller, I. Petković, I. Barić, I. Ligutić, and K. Pavelić, 1997, Expand Long PCR for fragile X mutation detection: Clin Genet, v. 52, p. 147-54.
Higham, C. F., F. Morales, C. A. Cobbold, D. T. Haydon, and D. G. Monckton, 2012, High levels of somatic DNA diversity at the myotonic dystrophy type 1 locus are driven by ultra-frequent expansion and contraction mutations: Hum Mol Genet, v. 21, p. 2450-63.
Hommelsheim, C. M., L. Frantzeskakis, M. Huang, and B. Ülker, 2014, PCR amplification of repetitive DNA: a limitation to genome editing technologies and many other applications: Sci Rep, v. 4, p. 5052.
Hou, P., Y. Li, X. Zhang, C. Liu, J. Guan, H. Li, T. Zhao, J. Ye, W. Yang, K. Liu, J. Ge, J. Xu, Q. Zhang, Y. Zhao, and H. Deng, 2013, Pluripotent stem cells induced from mouse somatic cells by small-molecule compounds: Science, v. 341, p. 651-4.
Hsieh, J., J. B. Aimone, B. K. Kaspar, T. Kuwabara, K. Nakashima, and F. H. Gage, 2004, IGF-I instructs multipotent adult neural progenitor cells to become oligodendrocytes: J Cell Biol, v. 164, p. 111-22.
Hsu, P. D., D. A. Scott, J. A. Weinstein, F. A. Ran, S. Konermann, V. Agarwala, Y. Li, E. J. Fine, X. Wu, O. Shalem, T. J. Cradick, L. A. Marraffini, G. Bao, and F. Zhang, 2013, DNA targeting specificity of RNA-guided Cas9 nucleases: Nat Biotechnol, v. 31, p. 827-32.
Hu, B. Y., Z. W. Du, X. J. Li, M. Ayala, and S. C. Zhang, 2009a, Human oligodendrocytes from embryonic stem cells: conserved SHH signaling networks and divergent FGF effects: Development, v. 136, p. 1443-52.
Hu, B. Y., J. P. Weick, J. Yu, L. X. Ma, X. Q. Zhang, J. A. Thomson, and S. C. Zhang, 2010, Neural differentiation of human induced pluripotent stem cells follows developmental principles but with variable potency: Proc Natl Acad Sci U S A, v. 107, p. 4335-40.
Hu, J., L. Deng, X. Wang, and X. M. Xu, 2009b, Effects of extracellular matrix molecules on the growth properties of oligodendrocyte progenitor cells in vitro: J Neurosci Res, v. 87, p. 2854-62.
Hu, J. G., S. L. Fu, Y. X. Wang, Y. Li, X. Y. Jiang, X. F. Wang, M. S. Qiu, P. H. Lu, and X. M. Xu, 2008, Platelet-derived growth factor-AA mediates oligodendrocyte lineage differentiation through activation of extracellular signal-regulated kinase signaling pathway: Neuroscience, v. 151, p. 138-47.
Hubers, A., N. Marroquin, B. Schmoll, S. Vielhaber, M. Just, B. Mayer, J. Hogel, J. Dorst, T. Mertens, W. Just, A. Aulitzky, V. Wais, A. C. Ludolph, C. Kubisch, J. H. Weishaupt, and A. E. Volk, 2014, Polymerase chain reaction and Southern blot-based analysis of the C9orf72 hexanucleotide repeat in different motor neuron diseases: Neurobiol Aging, v. 35, p. 1214.e1-6.
Hubert, L., Y. Lin, V. Dion, and J. H. Wilson, 2011, Xpa deficiency reduces CAG trinucleotide repeat instability in neuronal tissues in a mouse model of SCA1: Hum Mol Genet, v. 20, p. 4822-30.
Hussein, S. M., N. N. Batada, S. Vuoristo, R. W. Ching, R. Autio, E. Närvä, S. Ng, M. Sourour, R. Hämäläinen, C. Olsson, K. Lundin, M. Mikkola, R. Trokovic, M. Peitz, O. Brüstle, D. P. Bazett-Jones, K. Alitalo, R. Lahesmaa, A. Nagy, and

T. Otonkoski, 2011, Copy number variation and selection during reprogramming to pluripotency: Nature, v. 471, p. 58-62.
Hutton, M., C. L. Lendon, P. Rizzu, M. Baker, S. Froelich, H. Houlden, S. Pickering-Brown, S. Chakraverty, A. Isaacs, A. Grover, J. Hackett, J. Adamson, S. Lincoln, D. Dickson, P. Davies, R. C. Petersen, M. Stevens, E. de Graaff, E. Wauters, J. van Baren, M. Hillebrand, M. Joosse, J. M. Kwon, P. Nowotny, L. K. Che, J. Norton, J. C. Morris, L. A. Reed, J. Trojanowski, H. Basun, L. Lannfelt, M. Neystat, S. Fahn, F. Dark, T. Tannenberg, P. R. Dodd, N. Hayward, J. B. Kwok, P. R. Schofield, A. Andreadis, J. Snowden, D. Craufurd, D. Neary, F. Owen, B. A. Oostra, J. Hardy, A. Goate, J. van Swieten, D. Mann, T. Lynch, and P. Heutink, 1998, Association of missense and 5'-splice-site mutations in tau with the inherited dementia FTDP-17: Nature, v. 393, p. 702-5.
Izrael, M., P. Zhang, R. Kaufman, V. Shinder, R. Ella, M. Amit, J. Itskovitz-Eldor, J. Chebath, and M. Revel, 2007, Human oligodendrocytes derived from embryonic stem cells: Effect of noggin on phenotypic differentiation in vitro and on myelination in vivo: Mol Cell Neurosci, v. 34, p. 310-23.
Jacob, J., and J. Briscoe, 2003, Gli proteins and the control of spinal-cord patterning: EMBO Rep, v. 4, p. 761-5.
Jain, N., and S. Ganesh, 2016, Emerging nexus between RAB GTPases, autophagy and neurodegeneration: Autophagy, v. 12, p. 900-4.
Jakovcevski, I., R. Filipovic, Z. Mo, S. Rakic, and N. Zecevic, 2009, Oligodendrocyte Development and the Onset of Myelination in the Human Fetal Brain: Front Neuroanat, v. 3.
Jakovcevski, I., Z. Mo, and N. Zecevic, 2007, Down-regulation of the axonal PSA-NCAM expression coincides with the onset of myelination in the human fetal forebrain: Neuroscience, v. 149, p. 328-37.
Jakovcevski, I., and N. Zecevic, 2005a, Olig transcription factors are expressed in oligodendrocyte and neuronal cells in human fetal CNS: J Neurosci, v. 25, p. 10064-73.
Jakovcevski, I., and N. Zecevic, 2005b, Sequence of oligodendrocyte development in the human fetal telencephalon: Glia, v. 49, p. 480-91.
Jarjour, A. A., H. Zhang, N. Bauer, C. Ffrench-Constant, and A. Williams, 2012, In vitro modeling of central nervous system myelination and remyelination: Glia, v. 60, p. 1-12.
Jaworska, E., E. Kozlowska, P. M. Switonski, and W. J. Krzyzosiak, 2016, Modeling simple repeat expansion diseases with iPSC technology: Cell Mol Life Sci, v. 73, p. 4085-100.
Jiang, W., D. Bikard, D. Cox, F. Zhang, and L. A. Marraffini, 2013, RNA-guided editing of bacterial genomes using CRISPR-Cas systems: Nat Biotechnol, v. 31, p. 233-9.
Johnston, C. A., B. R. Stanton, M. R. Turner, R. Gray, A. H. Blunt, D. Butt, M. A. Ampong, C. E. Shaw, P. N. Leigh, and A. Al-Chalabi, 2006, Amyotrophic lateral sclerosis in an urban setting: a population based study of inner city London: J Neurol, v. 253, p. 1642-3.
Jovicic, A., J. Mertens, S. Boeynaems, E. Bogaert, N. Chai, S. B. Yamada, J. W. Paul, 3rd, S. Sun, J. R. Herdy, G. Bieri, N. J. Kramer, F. H. Gage, L. Van Den Bosch, W. Robberecht, and A. D. Gitler, 2015, Modifiers of C9orf72 dipeptide repeat toxicity connect nucleocytoplasmic transport defects to FTD/ALS: Nat Neurosci, v. 18, p. 1226-9.
Kabashi, E., P. N. Valdmanis, P. Dion, D. Spiegelman, B. J. McConkey, C. Vande Velde, J. P. Bouchard, L. Lacomblez, K. Pochigaeva, F. Salachas, P. F. Pradat, W. Camu, V. Meininger, N. Dupre, and G. A. Rouleau, 2008, TARDBP

mutations in individuals with sporadic and familial amyotrophic lateral sclerosis: Nat Genet, v. 40, p. 572-4.
Kamsteeg, E. J., W. Kress, C. Catalli, J. M. Hertz, M. Witsch-Baumgartner, M. F. Buckley, B. G. van Engelen, M. Schwartz, and H. Scheffer, 2012, Best practice guidelines and recommendations on the molecular diagnosis of myotonic dystrophy types 1 and 2: Eur J Hum Genet, v. 20, p. 1203-8.
Kang, S. H., Y. Li, M. Fukaya, I. Lorenzini, D. W. Cleveland, L. W. Ostrow, J. D. Rothstein, and D. E. Bergles, 2013, Degeneration and impaired regeneration of gray matter oligodendrocytes in amyotrophic lateral sclerosis: Nat Neurosci, v. 16, p. 571-9.
Kang, S. M., M. S. Cho, H. Seo, C. J. Yoon, S. K. Oh, Y. M. Choi, and D. W. Kim, 2007, Efficient induction of oligodendrocytes from human embryonic stem cells: Stem Cells, v. 25, p. 419-24.
Kang, X., Q. Yu, Y. Huang, B. Song, Y. Chen, X. Gao, W. He, X. Sun, and Y. Fan, 2015, Effects of Integrating and Non-Integrating Reprogramming Methods on Copy Number Variation and Genomic Stability of Human Induced Pluripotent Stem Cells: PLoS One, v. 10, p. e0131128.
Kerman, B. E., H. J. Kim, K. Padmanabhan, A. Mei, S. Georges, M. S. Joens, J. A. Fitzpatrick, R. Jappelli, K. J. Chandross, P. August, and F. H. Gage, 2015, In vitro myelin formation using embryonic stem cells: Development, v. 142, p. 2213-25.
Kim, H., and J. S. Kim, 2014, A guide to genome engineering with programmable nucleases: Nat Rev Genet, v. 15, p. 321-34.
Kim, K., A. Doi, B. Wen, K. Ng, R. Zhao, P. Cahan, J. Kim, M. J. Aryee, H. Ji, L. I. Ehrlich, A. Yabuuchi, A. Takeuchi, K. C. Cunniff, H. Hongguang, S. McKinney-Freeman, O. Naveiras, T. J. Yoon, R. A. Irizarry, N. Jung, J. Seita, J. Hanna, P. Murakami, R. Jaenisch, R. Weissleder, S. H. Orkin, I. L. Weissman, A. P. Feinberg, and G. Q. Daley, 2010, Epigenetic memory in induced pluripotent stem cells: Nature, v. 467, p. 285-90.
Kiskinis, E., J. Sandoe, L. A. Williams, G. L. Boulting, R. Moccia, B. J. Wainger, S. Han, T. Peng, S. Thams, S. Mikkilineni, C. Mellin, F. T. Merkle, B. N. Davis-Dusenbery, M. Ziller, D. Oakley, J. Ichida, S. Di Costanzo, N. Atwater, M. L. Maeder, M. J. Goodwin, J. Nemesh, R. E. Handsaker, D. Paull, S. Noggle, S. A. McCarroll, J. K. Joung, C. J. Woolf, R. H. Brown, and K. Eggan, 2014, Pathways disrupted in human ALS motor neurons identified through genetic correction of mutant SOD1: Cell Stem Cell, v. 14, p. 781-95.
Koch, P., P. Breuer, M. Peitz, J. Jungverdorben, J. Kesavan, D. Poppe, J. Doerr, J. Ladewig, J. Mertens, T. Tüting, P. Hoffmann, T. Klockgether, B. O. Evert, U. Wüllner, and O. Brüstle, 2011, Excitation-induced ataxin-3 aggregation in neurons from patients with Machado-Joseph disease: Nature, v. 480, p. 543-6.
Kolind, S., R. Sharma, S. Knight, H. Johansen-Berg, K. Talbot, and M. R. Turner, 2013, Myelin imaging in amyotrophic and primary lateral sclerosis: Amyotroph Lateral Scler Frontotemporal Degener, v. 14, p. 562-73.
Koppers, M., A. M. Blokhuis, H. J. Westeneng, M. L. Terpstra, C. A. Zundel, R. Vieira de Sa, R. D. Schellevis, A. J. Waite, D. J. Blake, J. H. Veldink, L. H. van den Berg, and R. J. Pasterkamp, 2015, C9orf72 ablation in mice does not cause motor neuron degeneration or motor deficits: Ann Neurol, v. 78, p. 426-38.
Kovtun, I. V., A. R. Thornhill, and C. T. McMurray, 2004, Somatic deletion events occur during early embryonic development and modify the extent of CAG expansion in subsequent generations: Hum Mol Genet, v. 13, p. 3057-68.
Kreutzberg, G. W., 1996, Microglia: a sensor for pathological events in the CNS: Trends Neurosci, v. 19, p. 312-8.

Kwiatkowski, T. J., D. A. Bosco, A. L. Leclerc, E. Tamrazian, C. R. Vanderburg, C. Russ, A. Davis, J. Gilchrist, E. J. Kasarskis, T. Munsat, P. Valdmanis, G. A. Rouleau, B. A. Hosler, P. Cortelli, P. J. de Jong, Y. Yoshinaga, J. L. Haines, M. A. Pericak-Vance, J. Yan, N. Ticozzi, T. Siddique, D. McKenna-Yasek, P. C. Sapp, H. R. Horvitz, J. E. Landers, and R. H. Brown, 2009, Mutations in the FUS/TLS gene on chromosome 16 cause familial amyotrophic lateral sclerosis: Science, v. 323, p. 1205-8.

Kwon, I., S. Xiang, M. Kato, L. Wu, P. Theodoropoulos, T. Wang, J. Kim, J. Yun, Y. Xie, and S. L. McKnight, 2014, Poly-dipeptides encoded by the C9orf72 repeats bind nucleoli, impede RNA biogenesis, and kill cells: Science, v. 345, p. 1139-45.

Laaksovirta, H., T. Peuralinna, J. C. Schymick, S. W. Scholz, S. L. Lai, L. Myllykangas, R. Sulkava, L. Jansson, D. G. Hernandez, J. R. Gibbs, M. A. Nalls, D. Heckerman, P. J. Tienari, and B. J. Traynor, 2010, Chromosome 9p21 in amyotrophic lateral sclerosis in Finland: a genome-wide association study: Lancet Neurol, v. 9, p. 978-85.

Lagier-Tourenne, C., M. Baughn, F. Rigo, S. Sun, P. Liu, H. R. Li, J. Jiang, A. T. Watt, S. Chun, M. Katz, J. Qiu, Y. Sun, S. C. Ling, Q. Zhu, M. Polymenidou, K. Drenner, J. W. Artates, M. McAlonis-Downes, S. Markmiller, K. R. Hutt, D. P. Pizzo, J. Cady, M. B. Harms, R. H. Baloh, S. R. Vandenberg, G. W. Yeo, X. D. Fu, C. F. Bennett, D. W. Cleveland, and J. Ravits, 2013, Targeted degradation of sense and antisense C9orf72 RNA foci as therapy for ALS and frontotemporal degeneration: Proc Natl Acad Sci U S A, v. 110, p. E4530-9.

Landre, P. A., D. H. Gelfand, and R. M. Watson, 1995, 1 - The Use of Cosolvents to Enhance Amplification by the Polymerase Chain Reaction, *in* M. A. I. H. Gelfand, and J. J. Sninsky, eds., PCR Strategies: San Diego, Academic Press, p. 3-16.

Lashley, T., J. D. Rohrer, C. Mahoney, E. Gordon, J. Beck, S. Mead, J. Warren, M. Rossor, and T. Revesz, 2014, A pathogenic progranulin mutation and C9orf72 repeat expansion in a family with frontotemporal dementia: Neuropathol Appl Neurobiol, v. 40, p. 502-13.

Le Ber, I., 2013, Genetics of frontotemporal lobar degeneration: an up-date and diagnosis algorithm: Rev Neurol (Paris), v. 169, p. 811-9.

Lee, S., and E. J. Huang, 2015, Modeling ALS and FTD with iPSC-derived neurons: Brain Res.

Lee, Y., B. M. Morrison, Y. Li, S. Lengacher, M. H. Farah, P. N. Hoffman, Y. Liu, A. Tsingalia, L. Jin, P. W. Zhang, L. Pellerin, P. J. Magistretti, and J. D. Rothstein, 2012, Oligodendroglia metabolically support axons and contribute to neurodegeneration: Nature, v. 487, p. 443-8.

Lee, Y. B., H. J. Chen, J. N. Peres, J. Gomez-Deza, J. Attig, M. Stalekar, C. Troakes, A. L. Nishimura, E. L. Scotter, C. Vance, Y. Adachi, V. Sardone, J. W. Miller, B. N. Smith, J. M. Gallo, J. Ule, F. Hirth, B. Rogelj, C. Houart, and C. E. Shaw, 2013, Hexanucleotide repeats in ALS/FTD form length-dependent RNA foci, sequester RNA binding proteins, and are neurotoxic: Cell Rep, v. 5, p. 1178-86.

Leitch, H. G., K. R. McEwen, A. Turp, V. Encheva, T. Carroll, N. Grabole, W. Mansfield, B. Nashun, J. G. Knezovich, A. Smith, M. A. Surani, and P. Hajkova, 2013, Naive pluripotency is associated with global DNA hypomethylation: Nat Struct Mol Biol, v. 20, p. 311-6.

Levine, T. P., R. D. Daniels, A. T. Gatta, L. H. Wong, and M. J. Hayes, 2013, The product of C9orf72, a gene strongly implicated in neurodegeneration, is structurally related to DENN Rab-GEFs: Bioinformatics, v. 29, p. 499-503.

Li, H., J. P. de Faria, P. Andrew, J. Nitarska, and W. D. Richardson, 2011, Phosphorylation regulates OLIG2 cofactor choice and the motor neuron-oligodendrocyte fate switch: Neuron, v. 69, p. 918-29.
Li, X. J., B. Y. Hu, S. A. Jones, Y. S. Zhang, T. Lavaute, Z. W. Du, and S. C. Zhang, 2008, Directed Differentiation of Ventral Spinal Progenitors and Motor Neurons from Human Embryonic Stem Cells by Small Molecules: Stem Cells, v. 26, p. 886-93.
Li, X. J., X. Zhang, M. A. Johnson, Z. B. Wang, T. Lavaute, and S. C. Zhang, 2009, Coordination of sonic hedgehog and Wnt signaling determines ventral and dorsal telencephalic neuron types from human embryonic stem cells: Development, v. 136, p. 4055-63.
Lin, W., and B. Popko, 2009, Endoplasmic reticulum stress in disorders of myelinating cells: Nat Neurosci, v. 12, p. 379-85.
Linden, M. G., B. G. Bender, and A. Robinson, 2002, Genetic counseling for sex chromosome abnormalities: Am J Med Genet, v. 110, p. 3-10.
Lindquist, S. G., M. Duno, M. Batbayli, A. Puschmann, H. Braendgaard, S. Mardosiene, K. Svenstrup, L. H. Pinborg, K. Vestergaard, L. E. Hjermind, J. Stokholm, B. B. Andersen, P. Johannsen, and J. E. Nielsen, 2013, Corticobasal and ataxia syndromes widen the spectrum of C9ORF72 hexanucleotide expansion disease: Clin Genet, v. 83, p. 279-83.
Ling, S. C., M. Polymenidou, and D. W. Cleveland, 2013, Converging mechanisms in ALS and FTD: disrupted RNA and protein homeostasis: Neuron, v. 79, p. 416-38.
Liu, E. Y., J. Russ, K. Wu, D. Neal, E. Suh, A. G. McNally, D. J. Irwin, V. M. Van Deerlin, and E. B. Lee, 2014, C9orf72 hypermethylation protects against repeat expansion-associated pathology in ALS/FTD: Acta Neuropathol, v. 128, p. 525-41.
Liu, F., Q. Liu, C. X. Lu, B. Cui, X. N. Guo, R. R. Wang, M. S. Liu, X. G. Li, L. Y. Cui, and X. Zhang, 2016, Identification of a novel loss-of-function C9orf72 splice site mutation in a patient with amyotrophic lateral sclerosis: Neurobiol Aging, v. 47, p. 219.e1-219.e5.
Liu, Z., X. Hu, J. Cai, B. Liu, X. Peng, M. Wegner, and M. Qiu, 2007, Induction of oligodendrocyte differentiation by Olig2 and Sox10: evidence for reciprocal interactions and dosage-dependent mechanisms: Dev Biol, v. 302, p. 683-93.
Livesey, M. R., D. Magnani, E. M. Cleary, N. A. Vasistha, O. T. James, B. T. Selvaraj, K. Burr, D. Story, C. E. Shaw, P. C. Kind, G. E. Hardingham, D. J. Wyllie, and S. Chandran, 2016, Maturation and electrophysiological properties of human pluripotent stem cell-derived oligodendrocytes: Stem Cells.
Lobsiger, C. S., and D. W. Cleveland, 2007, Glial cells as intrinsic components of non-cell-autonomous neurodegenerative disease: Nat Neurosci, v. 10, p. 1355-60.
Loh, Y. H., Q. Wu, J. L. Chew, V. B. Vega, W. Zhang, X. Chen, G. Bourque, J. George, B. Leong, J. Liu, K. Y. Wong, K. W. Sung, C. W. Lee, X. D. Zhao, K. P. Chiu, L. Lipovich, V. A. Kuznetsov, P. Robson, L. W. Stanton, C. L. Wei, Y. Ruan, B. Lim, and H. H. Ng, 2006, The Oct4 and Nanog transcription network regulates pluripotency in mouse embryonic stem cells: Nat Genet, v. 38, p. 431-40.
Lomen-Hoerth, C., T. Anderson, and B. Miller, 2002, The overlap of amyotrophic lateral sclerosis and frontotemporal dementia: Neurology, v. 59, p. 1077-9.
Lomen-Hoerth, C., J. Murphy, S. Langmore, J. H. Kramer, R. K. Olney, and B. Miller, 2003, Are amyotrophic lateral sclerosis patients cognitively normal?: Neurology, v. 60, p. 1094-7.
Loomis, E. W., J. S. Eid, P. Peluso, J. Yin, L. Hickey, D. Rank, S. McCalmon, R. J. Hagerman, F. Tassone, and P. J. Hagerman, 2013, Sequencing the

unsequenceable: expanded CGG-repeat alleles of the fragile X gene: Genome Res, v. 23, p. 121-8.
Lund, R. J., T. Nikula, N. Rahkonen, E. Närvä, D. Baker, N. Harrison, P. Andrews, T. Otonkoski, and R. Lahesmaa, 2012a, High-throughput karyotyping of human pluripotent stem cells: Stem Cell Res, v. 9, p. 192-5.
Lund, R. J., E. Närvä, and R. Lahesmaa, 2012b, Genetic and epigenetic stability of human pluripotent stem cells: Nat Rev Genet, v. 13, p. 732-44.
Luty, A. A., J. B. Kwok, E. M. Thompson, P. Blumbergs, W. S. Brooks, C. T. Loy, C. Dobson-Stone, P. K. Panegyres, J. Hecker, G. A. Nicholson, G. M. Halliday, and P. R. Schofield, 2008, Pedigree with frontotemporal lobar degeneration--motor neuron disease and Tar DNA binding protein-43 positive neuropathology: genetic linkage to chromosome 9: BMC Neurol, v. 8, p. 32.
Lyons, J. I., G. R. Kerr, and P. W. Mueller, 2015, Fragile X Syndrome: Scientific Background and Screening Technologies: J Mol Diagn, v. 17, p. 463-71.
Mackenzie, I. R., 2016, The role of dipeptide-repeat protein pathology in C9orf72 mutation cases: Neuropathol Appl Neurobiol, v. 42, p. 217-9.
Mackenzie, I. R., O. Ansorge, M. Strong, J. Bilbao, L. Zinman, L. C. Ang, M. Baker, H. Stewart, A. Eisen, R. Rademakers, and M. Neumann, 2011, Pathological heterogeneity in amyotrophic lateral sclerosis with FUS mutations: two distinct patterns correlating with disease severity and mutation: Acta Neuropathol, v. 122, p. 87-98.
Mackenzie, I. R., T. Arzberger, E. Kremmer, D. Troost, S. Lorenzl, K. Mori, S. M. Weng, C. Haass, H. A. Kretzschmar, D. Edbauer, and M. Neumann, 2013, Dipeptide repeat protein pathology in C9ORF72 mutation cases: clinico-pathological correlations: Acta Neuropathol, v. 126, p. 859-79.
Mackenzie, I. R., E. H. Bigio, P. G. Ince, F. Geser, M. Neumann, N. J. Cairns, L. K. Kwong, M. S. Forman, J. Ravits, H. Stewart, A. Eisen, L. McClusky, H. A. Kretzschmar, C. M. Monoranu, J. R. Highley, J. Kirby, T. Siddique, P. J. Shaw, V. M. Lee, and J. Q. Trojanowski, 2007, Pathological TDP-43 distinguishes sporadic amyotrophic lateral sclerosis from amyotrophic lateral sclerosis with SOD1 mutations: Ann Neurol, v. 61, p. 427-34.
Mackenzie, I. R., P. Frick, F. A. Grässer, T. F. Gendron, L. Petrucelli, N. R. Cashman, D. Edbauer, E. Kremmer, J. Prudlo, D. Troost, and M. Neumann, 2015, Quantitative analysis and clinico-pathological correlations of different dipeptide repeat protein pathologies in C9ORF72 mutation carriers: Acta Neuropathol, v. 130, p. 845-61.
Mackenzie, I. R., P. Frick, and M. Neumann, 2014, The neuropathology associated with repeat expansions in the C9ORF72 gene: Acta Neuropathol, v. 127, p. 347-57.
Mackenzie, I. R., M. Neumann, E. H. Bigio, N. J. Cairns, I. Alafuzoff, J. Kril, G. G. Kovacs, B. Ghetti, G. Halliday, I. E. Holm, P. G. Ince, W. Kamphorst, T. Revesz, A. J. Rozemuller, S. Kumar-Singh, H. Akiyama, A. Baborie, S. Spina, D. W. Dickson, J. Q. Trojanowski, and D. M. Mann, 2009, Nomenclature for neuropathologic subtypes of frontotemporal lobar degeneration: consensus recommendations: Acta Neuropathol, v. 117, p. 15-8.
Mackenzie, I. R., J. Shi, C. L. Shaw, D. Duplessis, D. Neary, J. S. Snowden, and D. M. Mann, 2006, Dementia lacking distinctive histology (DLDH) revisited: Acta Neuropathol, v. 112, p. 551-9.
Majounie, E., A. E. Renton, K. Mok, E. G. Dopper, A. Waite, S. Rollinson, A. Chio, G. Restagno, N. Nicolaou, J. Simon-Sanchez, J. C. van Swieten, Y. Abramzon, J. O. Johnson, M. Sendtner, R. Pamphlett, R. W. Orrell, S. Mead, K. C. Sidle, H. Houlden, J. D. Rohrer, K. E. Morrison, H. Pall, K. Talbot, O. Ansorge, D. G. Hernandez, S. Arepalli, M. Sabatelli, G. Mora, M. Corbo, F. Giannini, A. Calvo,

E. Englund, G. Borghero, G. L. Floris, A. M. Remes, H. Laaksovirta, L. McCluskey, J. Q. Trojanowski, V. M. Van Deerlin, G. D. Schellenberg, M. A. Nalls, V. E. Drory, C. S. Lu, T. H. Yeh, H. Ishiura, Y. Takahashi, S. Tsuji, I. Le Ber, A. Brice, C. Drepper, N. Williams, J. Kirby, P. Shaw, J. Hardy, P. J. Tienari, P. Heutink, H. R. Morris, S. Pickering-Brown, and B. J. Traynor, 2012, Frequency of the C9orf72 hexanucleotide repeat expansion in patients with amyotrophic lateral sclerosis and frontotemporal dementia: a cross-sectional study: Lancet Neurol, v. 11, p. 323-30.

Markoullis, K., D. Bulian, G. Hölzlwimmer, L. Quintanilla-Martinez, K. J. Heiliger, H. Zitzelsberger, H. Scherb, J. Mysliwietz, C. C. Uphoff, H. G. Drexler, T. Adler, D. H. Busch, J. Schmidt, and E. Mahabir, 2009, Mycoplasma contamination of murine embryonic stem cells affects cell parameters, germline transmission and chimeric progeny: Transgenic Res, v. 18, p. 71-87.

Martins-Taylor, K., and R. H. Xu, 2012, Concise review: Genomic stability of human induced pluripotent stem cells: Stem Cells, v. 30, p. 22-7.

Matus, S., V. Valenzuela, D. B. Medinas, and C. Hetz, 2013, ER Dysfunction and Protein Folding Stress in ALS: Int J Cell Biol, v. 2013, p. 674751.

May, S., D. Hornburg, M. H. Schludi, T. Arzberger, K. Rentzsch, B. M. Schwenk, F. A. Grässer, K. Mori, E. Kremmer, J. Banzhaf-Strathmann, M. Mann, F. Meissner, and D. Edbauer, 2014, C9orf72 FTLD/ALS-associated Gly-Ala dipeptide repeat proteins cause neuronal toxicity and Unc119 sequestration: Acta Neuropathol, v. 128, p. 485-503.

Mayshar, Y., U. Ben-David, N. Lavon, J. C. Biancotti, B. Yakir, A. T. Clark, K. Plath, W. E. Lowry, and N. Benvenisty, 2010, Identification and classification of chromosomal aberrations in human induced pluripotent stem cells: Cell Stem Cell, v. 7, p. 521-31.

McConlogue, L., M. A. Brow, and M. A. Innis, 1988, Structure-independent DNA amplification by PCR using 7-deaza-2'-deoxyguanosine: Nucleic Acids Res, v. 16, p. 9869.

McDermott, C. J., and P. J. Shaw, 2008, Diagnosis and management of motor neurone disease: BMJ, v. 336, p. 658-62.

McDowell, D. G., N. A. Burns, and H. C. Parkes, 1998, Localised sequence regions possessing high melting temperatures prevent the amplification of a DNA mimic in competitive PCR: Nucleic Acids Res, v. 26, p. 3340-7.

McGoldrick, P., P. I. Joyce, E. M. Fisher, and L. Greensmith, 2013, Rodent models of amyotrophic lateral sclerosis: Biochim Biophys Acta, v. 1832, p. 1421-36.

Meadowcroft, M. D., N. J. Mutic, D. C. Bigler, J. L. Wang, Z. Simmons, J. R. Connor, and Q. X. Yang, 2015, Histological-MRI correlation in the primary motor cortex of patients with amyotrophic lateral sclerosis: J Magn Reson Imaging, v. 41, p. 665-75.

Mekhoubad, S., C. Bock, A. S. de Boer, E. Kiskinis, A. Meissner, and K. Eggan, 2012, Erosion of dosage compensation impacts human iPSC disease modeling: Cell Stem Cell, v. 10, p. 595-609.

Mercy, L., J. R. Hodges, K. Dawson, R. A. Barker, and C. Brayne, 2008, Incidence of early-onset dementias in Cambridgeshire, United Kingdom: Neurology, v. 71, p. 1496-9.

Mertens, J., A. C. Paquola, M. Ku, E. Hatch, L. Böhnke, S. Ladjevardi, S. McGrath, B. Campbell, H. Lee, J. R. Herdy, J. T. Gonçalves, T. Toda, Y. Kim, J. Winkler, J. Yao, M. W. Hetzer, and F. H. Gage, 2015, Directly Reprogrammed Human Neurons Retain Aging-Associated Transcriptomic Signatures and Reveal Age-Related Nucleocytoplasmic Defects: Cell Stem Cell, v. 17, p. 705-18.

Meyer, K., L. Ferraiuolo, C. J. Miranda, S. Likhite, S. McElroy, S. Renusch, D. Ditsworth, C. Lagier-Tourenne, R. A. Smith, J. Ravits, A. H. Burghes, P. J.

Shaw, D. W. Cleveland, S. J. Kolb, and B. K. Kaspar, 2014, Direct conversion of patient fibroblasts demonstrates non-cell autonomous toxicity of astrocytes to motor neurons in familial and sporadic ALS: Proc Natl Acad Sci U S A, v. 111, p. 829-32.

Meyer, K., and B. K. Kaspar, 2016, Glia-neuron interactions in neurological diseases: Testing non-cell autonomy in a dish: Brain Res.

Mikkelsen, T. S., J. Hanna, X. Zhang, M. Ku, M. Wernig, P. Schorderet, B. E. Bernstein, R. Jaenisch, E. S. Lander, and A. Meissner, 2008, Dissecting direct reprogramming through integrative genomic analysis: Nature, v. 454, p. 49-55.

Miller, C. J., H. S. Kassem, S. D. Pepper, Y. Hey, T. H. Ward, and G. P. Margison, 2003, Mycoplasma infection significantly alters microarray gene expression profiles: Biotechniques, v. 35, p. 812-4.

Miller, J. D., Y. M. Ganat, S. Kishinevsky, R. L. Bowman, B. Liu, E. Y. Tu, P. K. Mandal, E. Vera, J. W. Shim, S. Kriks, T. Taldone, N. Fusaki, M. J. Tomishima, D. Krainc, T. A. Milner, D. J. Rossi, and L. Studer, 2013a, Human iPSC-based modeling of late-onset disease via progerin-induced aging: Cell Stem Cell, v. 13, p. 691-705.

Miller, J. W., C. R. Urbinati, P. Teng-Umnuay, M. G. Stenberg, B. J. Byrne, C. A. Thornton, and M. S. Swanson, 2000, Recruitment of human muscleblind proteins to (CUG)(n) expansions associated with myotonic dystrophy: EMBO J, v. 19, p. 4439-48.

Miller, R. G., J. D. Mitchell, and D. H. Moore, 2012, Riluzole for amyotrophic lateral sclerosis (ALS)/motor neuron disease (MND): Cochrane Database Syst Rev, v. 3, p. CD001447.

Miller, T. M., A. Pestronk, W. David, J. Rothstein, E. Simpson, S. H. Appel, P. L. Andres, K. Mahoney, P. Allred, K. Alexander, L. W. Ostrow, D. Schoenfeld, E. A. Macklin, D. A. Norris, G. Manousakis, M. Crisp, R. Smith, C. F. Bennett, K. M. Bishop, and M. E. Cudkowicz, 2013b, An antisense oligonucleotide against SOD1 delivered intrathecally for patients with SOD1 familial amyotrophic lateral sclerosis: a phase 1, randomised, first-in-man study: Lancet Neurol, v. 12, p. 435-42.

Mirkin, S. M., 2007, Expandable DNA repeats and human disease: Nature, v. 447, p. 932-40.

Mitsis, E. M., S. Riggio, L. Kostakoglu, D. L. Dickstein, J. Machac, B. Delman, M. Goldstein, D. Jennings, E. D'Antonio, J. Martin, T. P. Naidich, A. Aloysi, C. Fernandez, J. Seibyl, S. T. DeKosky, G. A. Elder, K. Marek, W. Gordon, P. R. Hof, M. Sano, and S. Gandy, 2014, Tauopathy PET and amyloid PET in the diagnosis of chronic traumatic encephalopathies: studies of a retired NFL player and of a man with FTD and a severe head injury: Transl Psychiatry, v. 4, p. e441.

Mizielinska, S., S. Grönke, T. Niccoli, C. E. Ridler, E. L. Clayton, A. Devoy, T. Moens, F. E. Norona, I. O. Woollacott, J. Pietrzyk, K. Cleverley, A. J. Nicoll, S. Pickering-Brown, J. Dols, M. Cabecinha, O. Hendrich, P. Fratta, E. M. Fisher, L. Partridge, and A. M. Isaacs, 2014, C9orf72 repeat expansions cause neurodegeneration in Drosophila through arginine-rich proteins: Science, v. 345, p. 1192-4.

Mizielinska, S., T. Lashley, F. E. Norona, E. L. Clayton, C. E. Ridler, P. Fratta, and A. M. Isaacs, 2013, C9orf72 frontotemporal lobar degeneration is characterised by frequent neuronal sense and antisense RNA foci: Acta Neuropathol, v. 126, p. 845-57.

Mori, K., T. Arzberger, F. A. Grasser, I. Gijselinck, S. May, K. Rentzsch, S. M. Weng, M. H. Schludi, J. van der Zee, M. Cruts, C. Van Broeckhoven, E. Kremmer, H.

A. Kretzschmar, C. Haass, and D. Edbauer, 2013a, Bidirectional transcripts of the expanded C9orf72 hexanucleotide repeat are translated into aggregating dipeptide repeat proteins: Acta Neuropathol, v. 126, p. 881-93.

Mori, K., S. Lammich, I. R. Mackenzie, I. Forné, S. Zilow, H. Kretzschmar, D. Edbauer, J. Janssens, G. Kleinberger, M. Cruts, J. Herms, M. Neumann, C. Van Broeckhoven, T. Arzberger, and C. Haass, 2013b, hnRNP A3 binds to GGGGCC repeats and is a constituent of p62-positive/TDP43-negative inclusions in the hippocampus of patients with C9orf72 mutations: Acta Neuropathol, v. 125, p. 413-23.

Mori, K., S. M. Weng, T. Arzberger, S. May, K. Rentzsch, E. Kremmer, B. Schmid, H. A. Kretzschmar, M. Cruts, C. Van Broeckhoven, C. Haass, and D. Edbauer, 2013c, The C9orf72 GGGGCC repeat is translated into aggregating dipeptide-repeat proteins in FTLD/ALS: Science, v. 339, p. 1335-8.

Morita, M., A. Al-Chalabi, P. M. Andersen, B. Hosler, P. Sapp, E. Englund, J. E. Mitchell, J. J. Habgood, J. de Belleroche, J. Xi, W. Jongjaroenprasert, H. R. Horvitz, L. G. Gunnarsson, and R. H. Brown, 2006, A locus on chromosome 9p confers susceptibility to ALS and frontotemporal dementia: Neurology, v. 66, p. 839-44.

Morris, H. R., A. J. Waite, N. M. Williams, J. W. Neal, and D. J. Blake, 2012, Recent advances in the genetics of the ALS-FTLD complex: Curr Neurol Neurosci Rep, v. 12, p. 243-50.

Mukai, H., and T. Nakagawa, 1996, [Long and accurate PCR (LA PCR)]: Nihon Rinsho, v. 54, p. 917-22.

Munoz, D. G., M. Neumann, H. Kusaka, O. Yokota, K. Ishihara, S. Terada, S. Kuroda, and I. R. Mackenzie, 2009, FUS pathology in basophilic inclusion body disease: Acta Neuropathol, v. 118, p. 617-27.

Musso, M., R. Bocciardi, S. Parodi, R. Ravazzolo, and I. Ceccherini, 2006, Betaine, dimethyl sulfoxide, and 7-deaza-dGTP, a powerful mixture for amplification of GC-rich DNA sequences: J Mol Diagn, v. 8, p. 544-50.

Müller, F. J., B. M. Schuldt, R. Williams, D. Mason, G. Altun, E. P. Papapetrou, S. Danner, J. E. Goldmann, A. Herbst, N. O. Schmidt, J. B. Aldenhoff, L. C. Laurent, and J. F. Loring, 2011, A bioinformatic assay for pluripotency in human cells: Nat Methods, v. 8, p. 315-7.

Naruse, M., E. Nakahira, T. Miyata, S. Hitoshi, K. Ikenaka, and R. Bansal, 2006, Induction of oligodendrocyte progenitors in dorsal forebrain by intraventricular microinjection of FGF-2: Dev Biol, v. 297, p. 262-73.

Nave, K. A., 2010, Myelination and the trophic support of long axons: Nat Rev Neurosci, v. 11, p. 275-83.

Neary, D., J. S. Snowden, L. Gustafson, U. Passant, D. Stuss, S. Black, M. Freedman, A. Kertesz, P. H. Robert, M. Albert, K. Boone, B. L. Miller, J. Cummings, and D. F. Benson, 1998, Frontotemporal lobar degeneration: a consensus on clinical diagnostic criteria: Neurology, v. 51, p. 1546-54.

Neumann, M., R. Rademakers, S. Roeber, M. Baker, H. A. Kretzschmar, and I. R. Mackenzie, 2009, A new subtype of frontotemporal lobar degeneration with FUS pathology: Brain, v. 132, p. 2922-31.

Neumann, M., D. M. Sampathu, L. K. Kwong, A. C. Truax, M. C. Micsenyi, T. T. Chou, J. Bruce, T. Schuck, M. Grossman, C. M. Clark, L. F. McCluskey, B. L. Miller, E. Masliah, I. R. Mackenzie, H. Feldman, W. Feiden, H. A. Kretzschmar, J. Q. Trojanowski, and V. M. Lee, 2006, Ubiquitinated TDP-43 in frontotemporal lobar degeneration and amyotrophic lateral sclerosis: Science, v. 314, p. 130-3.

Nguyen, H. N., B. Byers, B. Cord, A. Shcheglovitov, J. Byrne, P. Gujar, K. Kee, B. Schüle, R. E. Dolmetsch, W. Langston, T. D. Palmer, and R. R. Pera, 2011,

LRRK2 mutant iPSC-derived DA neurons demonstrate increased susceptibility to oxidative stress: Cell Stem Cell, v. 8, p. 267-80.
Niebroj-Dobosz, I., J. Rafalowska, A. Fidzianska, R. Gadamski, and P. Grieb, 2007, Myelin composition of spinal cord in a model of amyotrophic lateral sclerosis (ALS) in SOD1G93A transgenic rats: Folia Neuropathol, v. 45, p. 236-41.
Nistor, G. I., M. O. Totoiu, N. Haque, M. K. Carpenter, and H. S. Keirstead, 2005, Human embryonic stem cells differentiate into oligodendrocytes in high purity and myelinate after spinal cord transplantation: Glia, v. 49, p. 385-96.
Nordin, A., C. Akimoto, A. Wuolikainen, H. Alstermark, P. Jonsson, A. Birve, S. L. Marklund, K. S. Graffmo, K. Forsberg, T. Brännström, and P. M. Andersen, 2015, Extensive size variability of the GGGGCC expansion in C9orf72 in both neuronal and non-neuronal tissues in 18 patients with ALS or FTD: Hum Mol Genet, v. 24, p. 3133-42.
Numasawa-Kuroiwa, Y., Y. Okada, S. Shibata, N. Kishi, W. Akamatsu, M. Shoji, A. Nakanishi, M. Oyama, H. Osaka, K. Inoue, K. Takahashi, S. Yamanaka, K. Kosaki, T. Takahashi, and H. Okano, 2014, Involvement of ER stress in dysmyelination of Pelizaeus-Merzbacher Disease with PLP1 missense mutations shown by iPSC-derived oligodendrocytes: Stem Cell Reports, v. 2, p. 648-61.
O'Rourke, J. G., L. Bogdanik, A. Yáñez, D. Lall, A. J. Wolf, A. K. Muhammad, R. Ho, S. Carmona, J. P. Vit, J. Zarrow, K. J. Kim, S. Bell, M. B. Harms, T. M. Miller, C. A. Dangler, D. M. Underhill, H. S. Goodridge, C. M. Lutz, and R. H. Baloh, 2016, C9orf72 is required for proper macrophage and microglial function in mice: Science, v. 351, p. 1324-9.
O'Rourke, J. R., and M. S. Swanson, 2009, Mechanisms of RNA-mediated Disease.
Ogawa, S., Y. Tokumoto, J. Miyake, and T. Nagamune, 2011, Induction of oligodendrocyte differentiation from adult human fibroblast-derived induced pluripotent stem cells: In Vitro Cell Dev Biol Anim, v. 47, p. 464-9.
Ornelas, I. M., L. E. McLane, A. Saliu, A. V. Evangelou, L. Khandker, and T. L. Wood, 2016, Heterogeneity in oligodendroglia: Is it relevant to mouse models and human disease?: J Neurosci Res, v. 94, p. 1421-1433.
Orpana, A. K., T. H. Ho, K. Alagrund, M. Ridanpää, K. Aittomäki, and J. Stenman, 2013, Novel heat pulse extension-PCR-based method for detection of large CTG-repeat expansions in myotonic dystrophy type 1: J Mol Diagn, v. 15, p. 110-5.
Orpana, A. K., T. H. Ho, and J. Stenman, 2012, Multiple heat pulses during PCR extension enabling amplification of GC-rich sequences and reducing amplification bias: Anal Chem, v. 84, p. 2081-7.
Osafune, K., L. Caron, M. Borowiak, R. J. Martinez, C. S. Fitz-Gerald, Y. Sato, C. A. Cowan, K. R. Chien, and D. A. Melton, 2008, Marked differences in differentiation propensity among human embryonic stem cell lines: Nat Biotechnol, v. 26, p. 313-5.
Pamphlett, R., P. L. Cheong, R. J. Trent, and B. Yu, 2013, Can ALS-associated C9orf72 repeat expansions be diagnosed on a blood DNA test alone?: PLoS One, v. 8, p. e70007.
Park, C. Y., T. Halevy, D. R. Lee, J. J. Sung, J. S. Lee, O. Yanuka, N. Benvenisty, and D. W. Kim, 2015, Reversion of FMR1 Methylation and Silencing by Editing the Triplet Repeats in Fragile X iPSC-Derived Neurons: Cell Rep, v. 13, p. 234-41.
Pasinelli, P., and R. H. Brown, 2006, Molecular biology of amyotrophic lateral sclerosis: insights from genetics: Nat Rev Neurosci, v. 7, p. 710-23.
Perry, D. C., and B. L. Miller, 2013, Frontotemporal dementia: Semin Neurol, v. 33, p. 336-41.

Peters, O. M., G. T. Cabrera, H. Tran, T. F. Gendron, J. E. McKeon, J. Metterville, A. Weiss, N. Wightman, J. Salameh, J. Kim, H. Sun, K. B. Boylan, D. Dickson, Z. Kennedy, Z. Lin, Y. J. Zhang, L. Daughrity, C. Jung, F. B. Gao, P. C. Sapp, H. R. Horvitz, D. A. Bosco, S. P. Brown, P. de Jong, L. Petrucelli, C. Mueller, and R. H. Brown, 2015, Human C9ORF72 Hexanucleotide Expansion Reproduces RNA Foci and Dipeptide Repeat Proteins but Not Neurodegeneration in BAC Transgenic Mice: Neuron, v. 88, p. 902-9.

Pfeiffer, S. E., A. E. Warrington, and R. Bansal, 1993, The oligodendrocyte and its many cellular processes: Trends in Cell Biology, v. 3, p. 191-197.

Philips, T., A. Bento-Abreu, A. Nonneman, W. Haeck, K. Staats, V. Geelen, N. Hersmus, B. Kusters, L. Van Den Bosch, P. Van Damme, W. D. Richardson, and W. Robberecht, 2013, Oligodendrocyte dysfunction in the pathogenesis of amyotrophic lateral sclerosis: Brain, v. 136, p. 471-82.

Picher-Martel, V., P. N. Valdmanis, P. V. Gould, J. P. Julien, and N. Dupré, 2016, From animal models to human disease: a genetic approach for personalized medicine in ALS: Acta Neuropathol Commun, v. 4, p. 70.

Pottier, C., K. F. Bieniek, N. Finch, M. van de Vorst, M. Baker, R. Perkersen, P. Brown, T. Ravenscroft, M. van Blitterswijk, A. M. Nicholson, M. DeTure, D. S. Knopman, K. A. Josephs, J. E. Parisi, R. C. Petersen, K. B. Boylan, B. F. Boeve, N. R. Graff-Radford, J. A. Veltman, C. Gilissen, M. E. Murray, D. W. Dickson, and R. Rademakers, 2015, Whole-genome sequencing reveals important role for TBK1 and OPTN mutations in frontotemporal lobar degeneration without motor neuron disease: Acta Neuropathol, v. 130, p. 77-92.

Pouya, A., L. Satarian, S. Kiani, M. Javan, and H. Baharvand, 2011, Human induced pluripotent stem cells differentiation into oligodendrocyte progenitors and transplantation in a rat model of optic chiasm demyelination: PLoS One, v. 6, p. e27925.

Pringle, N. P., H. S. Mudhar, E. J. Collarini, and W. D. Richardson, 1992, PDGF receptors in the rat CNS: during late neurogenesis, PDGF alpha-receptor expression appears to be restricted to glial cells of the oligodendrocyte lineage: Development, v. 115, p. 535-51.

Proudfoot, M., N. J. Gutowski, D. Edbauer, D. A. Hilton, M. Stephens, J. Rankin, and I. R. Mackenzie, 2014, Early dipeptide repeat pathology in a frontotemporal dementia kindred with C9ORF72 mutation and intellectual disability: Acta Neuropathol, v. 127, p. 451-8.

Qiang, L., R. Fujita, and A. Abeliovich, 2013, Remodeling neurodegeneration: somatic cell reprogramming-based models of adult neurological disorders: Neuron, v. 78, p. 957-69.

Radvansky, J., and L. Kadasi, 2010, The expanding world of myotonic dystrophies: how can they be detected?: Genet Test Mol Biomarkers, v. 14, p. 733-41.

Rakic, S., and N. Zecevic, 2003, Early oligodendrocyte progenitor cells in the human fetal telencephalon: Glia, v. 41, p. 117-27.

Ran, F. A., P. D. Hsu, J. Wright, V. Agarwala, D. A. Scott, and F. Zhang, 2013, Genome engineering using the CRISPR-Cas9 system: Nat Protoc, v. 8, p. 2281-308.

Ratcliffe, S. G., H. Pan, and M. McKie, 1992, Growth during puberty in the XYY boy: Ann Hum Biol, v. 19, p. 579-87.

Ravits, J., 2014, Focality, stochasticity and neuroanatomic propagation in ALS pathogenesis: Exp Neurol, v. 262 Pt B, p. 121-6.

Reddy, K., B. Zamiri, S. Y. Stanley, R. B. Macgregor, Jr., and C. E. Pearson, 2013, The disease-associated r(GGGGCC)n repeat from the C9orf72 gene forms

tract length-dependent uni- and multimolecular RNA G-quadruplex structures: J Biol Chem, v. 288, p. 9860-6.
Renton, A. E., A. Chio, and B. J. Traynor, 2014, State of play in amyotrophic lateral sclerosis genetics: Nat Neurosci, v. 17, p. 17-23.
Renton, A. E., E. Majounie, A. Waite, J. Simon-Sanchez, S. Rollinson, J. R. Gibbs, J. C. Schymick, H. Laaksovirta, J. C. van Swieten, L. Myllykangas, H. Kalimo, A. Paetau, Y. Abramzon, A. M. Remes, A. Kaganovich, S. W. Scholz, J. Duckworth, J. Ding, D. W. Harmer, D. G. Hernandez, J. O. Johnson, K. Mok, M. Ryten, D. Trabzuni, R. J. Guerreiro, R. W. Orrell, J. Neal, A. Murray, J. Pearson, I. E. Jansen, D. Sondervan, H. Seelaar, D. Blake, K. Young, N. Halliwell, J. B. Callister, G. Toulson, A. Richardson, A. Gerhard, J. Snowden, D. Mann, D. Neary, M. A. Nalls, T. Peuralinna, L. Jansson, V. M. Isoviita, A. L. Kaivorinne, M. Holtta-Vuori, E. Ikonen, R. Sulkava, M. Benatar, J. Wuu, A. Chio, G. Restagno, G. Borghero, M. Sabatelli, D. Heckerman, E. Rogaeva, L. Zinman, J. D. Rothstein, M. Sendtner, C. Drepper, E. E. Eichler, C. Alkan, Z. Abdullaev, S. D. Pack, A. Dutra, E. Pak, J. Hardy, A. Singleton, N. M. Williams, P. Heutink, S. Pickering-Brown, H. R. Morris, P. J. Tienari, and B. J. Traynor, 2011, A hexanucleotide repeat expansion in C9ORF72 is the cause of chromosome 9p21-linked ALS-FTD: Neuron, v. 72, p. 257-68.
Ribes, V., and J. Briscoe, 2009, Establishing and interpreting graded Sonic Hedgehog signaling during vertebrate neural tube patterning: the role of negative feedback: Cold Spring Harb Perspect Biol, v. 1, p. a002014.
Richard, J. P., and N. J. Maragakis, 2015, Induced pluripotent stem cells from ALS patients for disease modeling: Brain Res, v. 1607, p. 15-25.
Richardson, W. D., H. K. Smith, T. Sun, N. P. Pringle, A. Hall, and R. Woodruff, 2000, Oligodendrocyte lineage and the motor neuron connection: Glia, v. 29, p. 136-42.
Rizzu, P., C. Blauwendraat, S. Heetveld, E. M. Lynes, M. Castillo-Lizardo, A. Dhingra, E. Pyz, M. Hobert, M. Synofzik, J. Simón-Sánchez, M. Francescatto, and P. Heutink, 2016, C9orf72 is differentially expressed in the central nervous system and myeloid cells and consistently reduced in C9orf72, MAPT and GRN mutation carriers: Acta Neuropathol Commun, v. 4, p. 37.
Rohan, Z., R. Matej, R. Rusina, and G. G. Kovacs, 2014, Oligodendroglial response in the spinal cord in TDP-43 proteinopathy with motor neuron involvement: Neurodegener Dis, v. 14, p. 117-24.
Rohrer, J. D., R. Guerreiro, J. Vandrovcova, J. Uphill, D. Reiman, J. Beck, A. M. Isaacs, A. Authier, R. Ferrari, N. C. Fox, I. R. Mackenzie, J. D. Warren, R. de Silva, J. Holton, T. Revesz, J. Hardy, S. Mead, and M. N. Rossor, 2009, The heritability and genetics of frontotemporal lobar degeneration: Neurology, v. 73, p. 1451-6.
Rohrer, J. D., A. M. Isaacs, S. Mizielinska, S. Mead, T. Lashley, S. Wray, K. Sidle, P. Fratta, R. W. Orrell, J. Hardy, J. Holton, T. Revesz, M. N. Rossor, and J. D. Warren, 2015, C9orf72 expansions in frontotemporal dementia and amyotrophic lateral sclerosis: Lancet Neurol, v. 14, p. 291-301.
Rollinson, S., J. Bennion Callister, K. Young, S. J. Ryan, R. Druyeh, J. D. Rohrer, J. Snowden, A. Richardson, M. Jones, J. Harris, Y. Davidson, A. Robinson, J. Ealing, J. O. Johnson, B. Traynor, S. Mead, D. Mann, and S. M. Pickering-Brown, 2015, A small deletion in C9orf72 hides a proportion of expansion carriers in FTLD: Neurobiol Aging, v. 36, p. 1601.e1-5.
Rosen, D. R., T. Siddique, D. Patterson, D. A. Figlewicz, P. Sapp, A. Hentati, D. Donaldson, J. Goto, J. P. O'Regan, H. X. Deng, and et al., 1993, Mutations in Cu/Zn superoxide dismutase gene are associated with familial amyotrophic lateral sclerosis: Nature, v. 362, p. 59-62.

Rosso, S. M., L. Donker Kaat, T. Baks, M. Joosse, I. de Koning, Y. Pijnenburg, D. de Jong, D. Dooijes, W. Kamphorst, R. Ravid, M. F. Niermeijer, F. Verheij, H. P. Kremer, P. Scheltens, C. M. van Duijn, P. Heutink, and J. C. van Swieten, 2003, Frontotemporal dementia in The Netherlands: patient characteristics and prevalence estimates from a population-based study: Brain, v. 126, p. 2016-22.

Rouhani, F., N. Kumasaka, M. C. de Brito, A. Bradley, L. Vallier, and D. Gaffney, 2014, Genetic background drives transcriptional variation in human induced pluripotent stem cells: PLoS Genet, v. 10, p. e1004432.

Rousseau, F., D. Heitz, V. Biancalana, S. Blumenfeld, C. Kretz, J. Boué, N. Tommerup, C. Van Der Hagen, C. DeLozier-Blanchet, and M. F. Croquette, 1991, Direct diagnosis by DNA analysis of the fragile X syndrome of mental retardation: N Engl J Med, v. 325, p. 1673-81.

Rowitch, D. H., 2004, Glial specification in the vertebrate neural tube: Nat Rev Neurosci, v. 5, p. 409-19.

Rubin, L. L., 2008, Stem cells and drug discovery: the beginning of a new era?: Cell, v. 132, p. 549-52.

Russ, J., E. Y. Liu, K. Wu, D. Neal, E. Suh, D. J. Irwin, C. T. McMillan, M. B. Harms, N. J. Cairns, E. M. Wood, S. X. Xie, L. Elman, L. McCluskey, M. Grossman, V. M. Van Deerlin, and E. B. Lee, 2015, Hypermethylation of repeat expanded C9orf72 is a clinical and molecular disease modifier: Acta Neuropathol, v. 129, p. 39-52.

Russo, C., G. Schettini, T. C. Saido, C. Hulette, C. Lippa, L. Lannfelt, B. Ghetti, P. Gambetti, M. Tabaton, and J. K. Teller, 2000, Presenilin-1 mutations in Alzheimer's disease: Nature, v. 405, p. 531-2.

Saha, K., and R. Jaenisch, 2009, Technical challenges in using human induced pluripotent stem cells to model disease: Cell Stem Cell, v. 5, p. 584-95.

Sandoe, J., and K. Eggan, 2013, Opportunities and challenges of pluripotent stem cell neurodegenerative disease models: Nat Neurosci, v. 16, p. 780-9.

Sareen, D., J. G. O'Rourke, P. Meera, A. K. Muhammad, S. Grant, M. Simpkinson, S. Bell, S. Carmona, L. Ornelas, A. Sahabian, T. Gendron, L. Petrucelli, M. Baughn, J. Ravits, M. B. Harms, F. Rigo, C. F. Bennett, T. S. Otis, C. N. Svendsen, and R. H. Baloh, 2013, Targeting RNA foci in iPSC-derived motor neurons from ALS patients with a C9ORF72 repeat expansion: Sci Transl Med, v. 5, p. 208ra149.

Schachner, M., S. K. Kim, and R. Zehnle, 1981, Developmental expression in central and peripheral nervous system of oligodendrocyte cell surface antigens (O antigens) recognized by monoclonal antibodies: Dev Biol, v. 83, p. 328-38.

Schuchard, M., G. Sarkar, T. Ruesink, and T. C. Spelsberg, 1993, Two-step "hot" PCR amplification of GC-rich avian c-myc sequences: Biotechniques, v. 14, p. 390-4.

Schweizer Burguete, A., S. Almeida, F. B. Gao, R. Kalb, M. R. Akins, and N. M. Bonini, 2015, GGGGCC microsatellite RNA is neuritically localized, induces branching defects, and perturbs transport granule function: Elife, v. 4, p. e08881.

Seilhean, D., C. Cazeneuve, V. Thuriès, O. Russaouen, S. Millecamps, F. Salachas, V. Meininger, E. Leguern, and C. Duyckaerts, 2009, Accumulation of TDP-43 and alpha-actin in an amyotrophic lateral sclerosis patient with the K17I ANG mutation: Acta Neuropathol, v. 118, p. 561-73.

Sellier, C., M. L. Campanari, C. Julie Corbier, A. Gaucherot, I. Kolb-Cheynel, M. Oulad-Abdelghani, F. Ruffenach, A. Page, S. Ciura, E. Kabashi, and N. Charlet-Berguerand, 2016, Loss of C9ORF72 impairs autophagy and

synergizes with polyQ Ataxin-2 to induce motor neuron dysfunction and cell death: EMBO J, v. 35, p. 1276-97.

Serio, A., B. Bilican, S. J. Barmada, D. M. Ando, C. Zhao, R. Siller, K. Burr, G. Haghi, D. Story, A. L. Nishimura, M. A. Carrasco, H. P. Phatnani, C. Shum, I. Wilmut, T. Maniatis, C. E. Shaw, S. Finkbeiner, and S. Chandran, 2013, Astrocyte pathology and the absence of non-cell autonomy in an induced pluripotent stem cell model of TDP-43 proteinopathy: Proc Natl Acad Sci U S A, v. 110, p. 4697-702.

Seriola, A., C. Spits, J. P. Simard, P. Hilven, P. Haentjens, C. E. Pearson, and K. Sermon, 2011, Huntington's and myotonic dystrophy hESCs: down-regulated trinucleotide repeat instability and mismatch repair machinery expression upon differentiation: Hum Mol Genet, v. 20, p. 176-85.

Seto, D., J. Seto, P. Deshpande, and L. Hood, 1995, DMSO resolves certain compressions and signal dropouts in fluorescent dye labeled primer-based DNA sequencing reactions: DNA Seq, v. 5, p. 131-40.

Shatunov, A., K. Mok, S. Newhouse, M. E. Weale, B. Smith, C. Vance, L. Johnson, J. H. Veldink, M. A. van Es, L. H. van den Berg, W. Robberecht, P. Van Damme, O. Hardiman, A. E. Farmer, C. M. Lewis, A. W. Butler, O. Abel, P. M. Andersen, I. Fogh, V. Silani, A. Chiò, B. J. Traynor, J. Melki, V. Meininger, J. E. Landers, P. McGuffin, J. D. Glass, H. Pall, P. N. Leigh, J. Hardy, R. H. Brown, J. F. Powell, R. W. Orrell, K. E. Morrison, P. J. Shaw, C. E. Shaw, and A. Al-Chalabi, 2010, Chromosome 9p21 in sporadic amyotrophic lateral sclerosis in the UK and seven other countries: a genome-wide association study: Lancet Neurol, v. 9, p. 986-94.

Shefner, J. M., M. E. Cudkowicz, D. Schoenfeld, T. Conrad, J. Taft, M. Chilton, L. Urbinelli, M. Qureshi, H. Zhang, A. Pestronk, J. Caress, P. Donofrio, E. Sorenson, W. Bradley, C. Lomen-Hoerth, E. Pioro, K. Rezania, M. Ross, R. Pascuzzi, T. Heiman-Patterson, R. Tandan, H. Mitsumoto, J. Rothstein, T. Smith-Palmer, D. MacDonald, D. Burke, and N. Consortium, 2004, A clinical trial of creatine in ALS: Neurology, v. 63, p. 1656-61.

Sherrington, R., E. I. Rogaev, Y. Liang, E. A. Rogaeva, G. Levesque, M. Ikeda, H. Chi, C. Lin, G. Li, K. Holman, T. Tsuda, L. Mar, J. F. Foncin, A. C. Bruni, M. P. Montesi, S. Sorbi, I. Rainero, L. Pinessi, L. Nee, I. Chumakov, D. Pollen, A. Brookes, P. Sanseau, R. J. Polinsky, W. Wasco, H. A. Da Silva, J. L. Haines, M. A. Perkicak-Vance, R. E. Tanzi, A. D. Roses, P. E. Fraser, J. M. Rommens, and P. H. St George-Hyslop, 1995, Cloning of a gene bearing missense mutations in early-onset familial Alzheimer's disease: Nature, v. 375, p. 754-60.

Shibata, N., A. Hirano, M. Kobayashi, T. Siddique, H. X. Deng, W. Y. Hung, T. Kato, and K. Asayama, 1996, Intense superoxide dismutase-1 immunoreactivity in intracytoplasmic hyaline inclusions of familial amyotrophic lateral sclerosis with posterior column involvement: J Neuropathol Exp Neurol, v. 55, p. 481-90.

Simons, M., and K. A. Nave, 2016, Oligodendrocytes: Myelination and Axonal Support: Cold Spring Harb Perspect Biol, v. 8, p. a020479.

Simón-Sánchez, J., E. G. Dopper, P. E. Cohn-Hokke, R. K. Hukema, N. Nicolaou, H. Seelaar, J. R. de Graaf, I. de Koning, N. M. van Schoor, D. J. Deeg, M. Smits, J. Raaphorst, L. H. van den Berg, H. J. Schelhaas, C. E. De Die-Smulders, D. Majoor-Krakauer, A. J. Rozemuller, R. Willemsen, Y. A. Pijnenburg, P. Heutink, and J. C. van Swieten, 2012, The clinical and pathological phenotype of C9ORF72 hexanucleotide repeat expansions: Brain, v. 135, p. 723-35.

Singh, A. M., V. V. Adjan Steffey, T. Yeshi, and D. W. Allison, 2015, Gene Editing in Human Pluripotent Stem Cells: Choosing the Correct Path: J Stem Cell Regen Biol, v. 1.

Singh, B., and R. S. Gupta, 1985, Species-specific differences in the toxicity and mutagenicity of the anticancer drugs mithramycin, chromomycin A3, and olivomycin: Cancer Res, v. 45, p. 2813-20.

Sistermans, E. A., R. F. de Coo, I. J. De Wijs, and B. A. Van Oost, 1998, Duplication of the proteolipid protein gene is the major cause of Pelizaeus-Merzbacher disease: Neurology, v. 50, p. 1749-54.

Sivadasan, R., D. Hornburg, C. Drepper, N. Frank, S. Jablonka, A. Hansel, X. Lojewski, J. Sterneckert, A. Hermann, P. J. Shaw, P. G. Ince, M. Mann, F. Meissner, and M. Sendtner, 2016, C9ORF72 interaction with cofilin modulates actin dynamics in motor neurons: Nat Neurosci.

Sket, P., J. Pohleven, A. Kovanda, M. Stalekar, V. Zupunski, M. Zalar, J. Plavec, and B. Rogelj, 2015, Characterization of DNA G-quadruplex species forming from C9ORF72 G4C2-expanded repeats associated with amyotrophic lateral sclerosis and frontotemporal lobar degeneration: Neurobiol Aging, v. 36, p. 1091-6.

Snowden, J. S., J. Harris, J. Adams, J. C. Thompson, A. M. Richardson, M. S. Jones, D. Neary, Y. S. Davidson, A. C. Robinson, S. Rollinson, S. Pickering-Brown, and D. M. Mann, 2016, Psychosis associated with expansions in the C9orf72 gene: the influence of a 10 base pair gene deletion: J Neurol Neurosurg Psychiatry, v. 87, p. 562-3.

Sofroniew, M. V., and H. V. Vinters, 2010, Astrocytes: biology and pathology: Acta Neuropathol, v. 119, p. 7-35.

Soldner, F., J. Laganière, A. W. Cheng, D. Hockemeyer, Q. Gao, R. Alagappan, V. Khurana, L. I. Golbe, R. H. Myers, S. Lindquist, L. Zhang, D. Guschin, L. K. Fong, B. J. Vu, X. Meng, F. D. Urnov, E. J. Rebar, P. D. Gregory, H. S. Zhang, and R. Jaenisch, 2011, Generation of isogenic pluripotent stem cells differing exclusively at two early onset Parkinson point mutations: Cell, v. 146, p. 318-31.

Song, Y. J., D. M. Lundvig, Y. Huang, W. P. Gai, P. C. Blumbergs, P. Højrup, D. Otzen, G. M. Halliday, and P. H. Jensen, 2007, p25alpha relocalizes in oligodendroglia from myelin to cytoplasmic inclusions in multiple system atrophy: Am J Pathol, v. 171, p. 1291-303.

Sorbi, S., B. Nacmias, P. Forleo, S. Piacentini, R. Sherrington, E. Rogaev, P. St George Hyslop, and L. Amaducci, 1995, Missense mutation of S182 gene in Italian families with early-onset Alzheimer's disease: Lancet, v. 346, p. 439-40.

Spits, C., I. Mateizel, M. Geens, A. Mertzanidou, C. Staessen, Y. Vandeskelde, J. Van der Elst, I. Liebaers, and K. Sermon, 2008, Recurrent chromosomal abnormalities in human embryonic stem cells: Nat Biotechnol, v. 26, p. 1361-3.

Sreedharan, J., I. P. Blair, V. B. Tripathi, X. Hu, C. Vance, B. Rogelj, S. Ackerley, J. C. Durnall, K. L. Williams, E. Buratti, F. Baralle, J. de Belleroche, J. D. Mitchell, P. N. Leigh, A. Al-Chalabi, C. C. Miller, G. Nicholson, and C. E. Shaw, 2008, TDP-43 mutations in familial and sporadic amyotrophic lateral sclerosis: Science, v. 319, p. 1668-72.

Stacpoole, S. R., S. Spitzer, B. Bilican, A. Compston, R. Karadottir, S. Chandran, and R. J. Franklin, 2013, High yields of oligodendrocyte lineage cells from human embryonic stem cells at physiological oxygen tensions for evaluation of translational biology: Stem Cell Reports, v. 1, p. 437-50.

Sun, S., Y. Sun, S. C. Ling, L. Ferraiuolo, M. McAlonis-Downes, Y. Zou, K. Drenner, Y. Wang, D. Ditsworth, S. Tokunaga, A. Kopelevich, B. K. Kaspar, C. Lagier-Tourenne, and D. W. Cleveland, 2015, Translational profiling identifies a cascade of damage initiated in motor neurons and spreading to glia in mutant SOD1-mediated ALS: Proc Natl Acad Sci U S A, v. 112, p. E6993-7002.

Sun, Y., G. Hegamyer, and N. H. Colburn, 1993, PCR-direct sequencing of a GC-rich region by inclusion of 10% DMSO: application to mouse c-jun: Biotechniques, v. 15, p. 372-4.

Sundberg, M., A. Hyysalo, H. Skottman, S. Shin, M. Vemuri, R. Suuronen, and S. Narkilahti, 2011, A xeno-free culturing protocol for pluripotent stem cell-derived oligodendrocyte precursor cell production: Regen Med, v. 6, p. 449-60.

Sundberg, M., H. Skottman, R. Suuronen, and S. Narkilahti, 2010, Production and isolation of NG2+ oligodendrocyte precursors from human embryonic stem cells in defined serum-free medium: Stem Cell Res, v. 5, p. 91-103.

Suzuki, N., A. M. Maroof, F. T. Merkle, K. Koszka, A. Intoh, I. Armstrong, R. Moccia, B. N. Davis-Dusenbery, and K. Eggan, 2013, The mouse C9ORF72 ortholog is enriched in neurons known to degenerate in ALS and FTD: Nat Neurosci, v. 16, p. 1725-7.

Taapken, S. M., B. S. Nisler, M. A. Newton, T. L. Sampsell-Barron, K. A. Leonhard, E. M. McIntire, and K. D. Montgomery, 2011, Karotypic abnormalities in human induced pluripotent stem cells and embryonic stem cells: Nat Biotechnol, v. 29, p. 313-4.

Tabrizi, S. J., D. R. Langbehn, B. R. Leavitt, R. A. Roos, A. Durr, D. Craufurd, C. Kennard, S. L. Hicks, N. C. Fox, R. I. Scahill, B. Borowsky, A. J. Tobin, H. D. Rosas, H. Johnson, R. Reilmann, B. Landwehrmeyer, J. C. Stout, and T.-H. investigators, 2009, Biological and clinical manifestations of Huntington's disease in the longitudinal TRACK-HD study: cross-sectional analysis of baseline data: Lancet Neurol, v. 8, p. 791-801.

Takahashi, K., K. Tanabe, M. Ohnuki, M. Narita, T. Ichisaka, K. Tomoda, and S. Yamanaka, 2007, Induction of pluripotent stem cells from adult human fibroblasts by defined factors: Cell, v. 131, p. 861-72.

Takahashi, K., and S. Yamanaka, 2006, Induction of pluripotent stem cells from mouse embryonic and adult fibroblast cultures by defined factors: Cell, v. 126, p. 663-76.

Takebayashi, H., Y. Nabeshima, S. Yoshida, O. Chisaka, and K. Ikenaka, 2002, The basic helix-loop-helix factor olig2 is essential for the development of motoneuron and oligodendrocyte lineages: Curr Biol, v. 12, p. 1157-63.

Tang, B. L., 2016, C9orf72's Interaction with Rab GTPases-Modulation of Membrane Traffic and Autophagy: Front Cell Neurosci, v. 10, p. 228.

Taylor, J. P., R. H. Brown, and D. W. Cleveland, 2016, Decoding ALS: from genes to mechanism: Nature, v. 539, p. 197-206.

Therrien, M., G. A. Rouleau, P. A. Dion, and J. A. Parker, 2013, Deletion of C9ORF72 results in motor neuron degeneration and stress sensitivity in C. elegans: PLoS One, v. 8, p. e83450.

Thiruvalluvan, A., M. Czepiel, Y. A. Kap, I. Mantingh-Otter, I. Vainchtein, J. Kuipers, M. Bijlard, W. Baron, B. Giepmans, W. Brück, B. A. 't Hart, E. Boddeke, and S. Copray, 2016, Survival and Functionality of Human Induced Pluripotent Stem Cell-Derived Oligodendrocytes in a Nonhuman Primate Model for Multiple Sclerosis: Stem Cells Transl Med.

Thomson, J. A., J. Itskovitz-Eldor, S. S. Shapiro, M. A. Waknitz, J. J. Swiergiel, V. S. Marshall, and J. M. Jones, 1998, Embryonic stem cell lines derived from human blastocysts: Science, v. 282, p. 1145-7.

Todd, P. K., and H. L. Paulson, 2010, RNA-mediated neurodegeneration in repeat expansion disorders: Ann Neurol, v. 67, p. 291-300.
Tomoda, K., K. Takahashi, K. Leung, A. Okada, M. Narita, N. A. Yamada, K. E. Eilertson, P. Tsang, S. Baba, M. P. White, S. Sami, D. Srivastava, B. R. Conklin, B. Panning, and S. Yamanaka, 2012, Derivation conditions impact X-inactivation status in female human induced pluripotent stem cells: Cell Stem Cell, v. 11, p. 91-9.
Tran, H., S. Almeida, J. Moore, T. F. Gendron, U. Chalasani, Y. Lu, X. Du, J. A. Nickerson, L. Petrucelli, Z. Weng, and F. B. Gao, 2015, Differential Toxicity of Nuclear RNA Foci versus Dipeptide Repeat Proteins in a Drosophila Model of C9ORF72 FTD/ALS: Neuron, v. 87, p. 1207-14.
Turner, M. R., and E. Verstraete, 2015, What does imaging reveal about the pathology of amyotrophic lateral sclerosis?: Curr Neurol Neurosci Rep, v. 15, p. 45.
Upender, M. B., J. K. Habermann, L. M. McShane, E. L. Korn, J. C. Barrett, M. J. Difilippantonio, and T. Ried, 2004, Chromosome transfer induced aneuploidy results in complex dysregulation of the cellular transcriptome in immortalized and cancer cells: Cancer Res, v. 64, p. 6941-9.
Usdin, K., N. C. House, and C. H. Freudenreich, 2015, Repeat instability during DNA repair: Insights from model systems: Crit Rev Biochem Mol Biol, v. 50, p. 142-67.
Valdmanis, P. N., N. Dupre, J. P. Bouchard, W. Camu, F. Salachas, V. Meininger, M. Strong, and G. A. Rouleau, 2007, Three families with amyotrophic lateral sclerosis and frontotemporal dementia with evidence of linkage to chromosome 9p: Arch Neurol, v. 64, p. 240-5.
Vallstedt, A., J. M. Klos, and J. Ericson, 2005, Multiple dorsoventral origins of oligodendrocyte generation in the spinal cord and hindbrain: Neuron, v. 45, p. 55-67.
Valori, C. F., L. Brambilla, F. Martorana, and D. Rossi, 2014, The multifaceted role of glial cells in amyotrophic lateral sclerosis: Cell Mol Life Sci, v. 71, p. 287-97.
van Blitterswijk, M., M. C. Baker, M. DeJesus-Hernandez, R. Ghidoni, L. Benussi, E. Finger, G. Y. Hsiung, B. J. Kelley, M. E. Murray, N. J. Rutherford, P. E. Brown, T. Ravenscroft, B. Mullen, P. E. Ash, K. F. Bieniek, K. J. Hatanpaa, A. Karydas, E. M. Wood, G. Coppola, E. H. Bigio, C. Lippa, M. J. Strong, T. G. Beach, D. S. Knopman, E. D. Huey, M. Mesulam, T. Bird, C. L. White, A. Kertesz, D. H. Geschwind, V. M. Van Deerlin, R. C. Petersen, G. Binetti, B. L. Miller, L. Petrucelli, Z. K. Wszolek, K. B. Boylan, N. R. Graff-Radford, I. R. Mackenzie, B. F. Boeve, D. W. Dickson, and R. Rademakers, 2013a, C9ORF72 repeat expansions in cases with previously identified pathogenic mutations: Neurology, v. 81, p. 1332-41.
van Blitterswijk, M., M. DeJesus-Hernandez, E. Niemantsverdriet, M. E. Murray, M. G. Heckman, N. N. Diehl, P. H. Brown, M. C. Baker, N. A. Finch, P. O. Bauer, G. Serrano, T. G. Beach, K. A. Josephs, D. S. Knopman, R. C. Petersen, B. F. Boeve, N. R. Graff-Radford, K. B. Boylan, L. Petrucelli, D. W. Dickson, and R. Rademakers, 2013b, Association between repeat sizes and clinical and pathological characteristics in carriers of C9ORF72 repeat expansions (Xpansize-72): a cross-sectional cohort study: Lancet Neurol, v. 12, p. 978-88.
van Blitterswijk, M., T. F. Gendron, M. C. Baker, M. DeJesus-Hernandez, N. A. Finch, P. H. Brown, L. M. Daughrity, M. E. Murray, M. G. Heckman, J. Jiang, C. Lagier-Tourenne, D. Edbauer, D. W. Cleveland, K. A. Josephs, J. E. Parisi, D. S. Knopman, R. C. Petersen, L. Petrucelli, B. F. Boeve, N. R. Graff-Radford, K. B. Boylan, D. W. Dickson, and R. Rademakers, 2015, Novel clinical

associations with specific C9ORF72 transcripts in patients with repeat expansions in C9ORF72: Acta Neuropathol.

van Blitterswijk, M., B. Mullen, M. G. Heckman, M. C. Baker, M. DeJesus-Hernandez, P. H. Brown, M. E. Murray, G. Y. Hsiung, H. Stewart, A. M. Karydas, E. Finger, A. Kertesz, E. H. Bigio, S. Weintraub, M. Mesulam, K. J. Hatanpaa, C. L. White, M. Neumann, M. J. Strong, T. G. Beach, Z. K. Wszolek, C. Lippa, R. Caselli, L. Petrucelli, K. A. Josephs, J. E. Parisi, D. S. Knopman, R. C. Petersen, I. R. Mackenzie, W. W. Seeley, L. T. Grinberg, B. L. Miller, K. B. Boylan, N. R. Graff-Radford, B. F. Boeve, D. W. Dickson, and R. Rademakers, 2014a, Ataxin-2 as potential disease modifier in C9ORF72 expansion carriers: Neurobiol Aging, v. 35, p. 2421.e13-7.

van Blitterswijk, M., B. Mullen, A. M. Nicholson, K. F. Bieniek, M. G. Heckman, M. C. Baker, M. DeJesus-Hernandez, N. A. Finch, P. H. Brown, M. E. Murray, G. Y. Hsiung, H. Stewart, A. M. Karydas, E. Finger, A. Kertesz, E. H. Bigio, S. Weintraub, M. Mesulam, K. J. Hatanpaa, C. L. White, M. J. Strong, T. G. Beach, Z. K. Wszolek, C. Lippa, R. Caselli, L. Petrucelli, K. A. Josephs, J. E. Parisi, D. S. Knopman, R. C. Petersen, I. R. Mackenzie, W. W. Seeley, L. T. Grinberg, B. L. Miller, K. B. Boylan, N. R. Graff-Radford, B. F. Boeve, D. W. Dickson, and R. Rademakers, 2014b, TMEM106B protects C9ORF72 expansion carriers against frontotemporal dementia: Acta Neuropathol, v. 127, p. 397-406.

van Blitterswijk, M., M. A. van Es, E. A. Hennekam, D. Dooijes, W. van Rheenen, J. Medic, P. R. Bourque, H. J. Schelhaas, A. J. van der Kooi, M. de Visser, P. I. de Bakker, J. H. Veldink, and L. H. van den Berg, 2012, Evidence for an oligogenic basis of amyotrophic lateral sclerosis: Hum Mol Genet, v. 21, p. 3776-84.

Van Deerlin, V. M., P. M. Sleiman, M. Martinez-Lage, A. Chen-Plotkin, L. S. Wang, N. R. Graff-Radford, D. W. Dickson, R. Rademakers, B. F. Boeve, M. Grossman, S. E. Arnold, D. M. Mann, S. M. Pickering-Brown, H. Seelaar, P. Heutink, J. C. van Swieten, J. R. Murrell, B. Ghetti, S. Spina, J. Grafman, J. Hodges, M. G. Spillantini, S. Gilman, A. P. Lieberman, J. A. Kaye, R. L. Woltjer, E. H. Bigio, M. Mesulam, S. Al-Sarraj, C. Troakes, R. N. Rosenberg, C. L. White, I. Ferrer, A. Lladó, M. Neumann, H. A. Kretzschmar, C. M. Hulette, K. A. Welsh-Bohmer, B. L. Miller, A. Alzualde, A. Lopez de Munain, A. C. McKee, M. Gearing, A. I. Levey, J. J. Lah, J. Hardy, J. D. Rohrer, T. Lashley, I. R. Mackenzie, H. H. Feldman, R. L. Hamilton, S. T. Dekosky, J. van der Zee, S. Kumar-Singh, C. Van Broeckhoven, R. Mayeux, J. P. Vonsattel, J. C. Troncoso, J. J. Kril, J. B. Kwok, G. M. Halliday, T. D. Bird, P. G. Ince, P. J. Shaw, N. J. Cairns, J. C. Morris, C. A. McLean, C. DeCarli, W. G. Ellis, S. H. Freeman, M. P. Frosch, J. H. Growdon, D. P. Perl, M. Sano, D. A. Bennett, J. A. Schneider, T. G. Beach, E. M. Reiman, B. K. Woodruff, J. Cummings, H. V. Vinters, C. A. Miller, H. C. Chui, I. Alafuzoff, P. Hartikainen, D. Seilhean, D. Galasko, E. Masliah, C. W. Cotman, M. T. Tuñón, M. C. Martínez, D. G. Munoz, S. L. Carroll, D. Marson, P. F. Riederer, N. Bogdanovic, G. D. Schellenberg, H. Hakonarson, J. Q. Trojanowski, and V. M. Lee, 2010, Common variants at 7p21 are associated with frontotemporal lobar degeneration with TDP-43 inclusions: Nat Genet, v. 42, p. 234-9.

van der Zee, J., I. Gijselinck, L. Dillen, T. Van Langenhove, J. Theuns, S. Engelborghs, S. Philtjens, M. Vandenbulcke, K. Sleegers, A. Sieben, V. Baumer, G. Maes, E. Corsmit, B. Borroni, A. Padovani, S. Archetti, R. Perneczky, J. Diehl-Schmid, A. de Mendonca, G. Miltenberger-Miltenyi, S. Pereira, J. Pimentel, B. Nacmias, S. Bagnoli, S. Sorbi, C. Graff, H. H. Chiang, M. Westerlund, R. Sanchez-Valle, A. Llado, E. Gelpi, I. Santana, M. R.

Almeida, B. Santiago, G. Frisoni, O. Zanetti, C. Bonvicini, M. Synofzik, W. Maetzler, J. M. Vom Hagen, L. Schols, M. T. Heneka, F. Jessen, R. Matej, E. Parobkova, G. G. Kovacs, T. Strobel, S. Sarafov, I. Tournev, A. Jordanova, A. Danek, T. Arzberger, G. M. Fabrizi, S. Testi, E. Salmon, P. Santens, J. J. Martin, P. Cras, R. Vandenberghe, P. P. De Deyn, M. Cruts, C. Van Broeckhoven, J. Muller Vom Hagen, A. Ramirez, D. Kurzwelly, C. Sachtleben, W. Mairer, C. Firmo, A. Antonell, J. Molinuevo, A. Kinhult Stahlbom, H. Thonberg, I. Nennesmo, A. Borjesson-Hanson, V. Bessi, I. Piaceri, M. Helena Ribeiro, M. Rosario Almeida, C. Oliveira, J. Massano, C. Garret, P. Pires, A. Danel, G. Maria Fabrizi, S. Ferrari, and T. Cavallaro, 2013, A pan-European study of the C9orf72 repeat associated with FTLD: geographic prevalence, genomic instability, and intermediate repeats: Hum Mutat, v. 34, p. 363-73.

van Es, M. A., J. H. Veldink, C. G. Saris, H. M. Blauw, P. W. van Vught, A. Birve, R. Lemmens, H. J. Schelhaas, E. J. Groen, M. H. Huisman, A. J. van der Kooi, M. de Visser, C. Dahlberg, K. Estrada, F. Rivadeneira, A. Hofman, M. J. Zwarts, P. T. van Doormaal, D. Rujescu, E. Strengman, I. Giegling, P. Muglia, B. Tomik, A. Slowik, A. G. Uitterlinden, C. Hendrich, S. Waibel, T. Meyer, A. C. Ludolph, J. D. Glass, S. Purcell, S. Cichon, M. M. Nöthen, H. E. Wichmann, S. Schreiber, S. H. Vermeulen, L. A. Kiemeney, J. H. Wokke, S. Cronin, R. L. McLaughlin, O. Hardiman, K. Fumoto, R. J. Pasterkamp, V. Meininger, J. Melki, P. N. Leigh, C. E. Shaw, J. E. Landers, A. Al-Chalabi, R. H. Brown, W. Robberecht, P. M. Andersen, R. A. Ophoff, and L. H. van den Berg, 2009, Genome-wide association study identifies 19p13.3 (UNC13A) and 9p21.2 as susceptibility loci for sporadic amyotrophic lateral sclerosis: Nat Genet, v. 41, p. 1083-7.

Vance, C., A. Al-Chalabi, D. Ruddy, B. N. Smith, X. Hu, J. Sreedharan, T. Siddique, H. J. Schelhaas, B. Kusters, D. Troost, F. Baas, V. de Jong, and C. E. Shaw, 2006, Familial amyotrophic lateral sclerosis with frontotemporal dementia is linked to a locus on chromosome 9p13.2-21.3: Brain, v. 129, p. 868-76.

Vance, C., B. Rogelj, T. Hortobágyi, K. J. De Vos, A. L. Nishimura, J. Sreedharan, X. Hu, B. Smith, D. Ruddy, P. Wright, J. Ganesalingam, K. L. Williams, V. Tripathi, S. Al-Saraj, A. Al-Chalabi, P. N. Leigh, I. P. Blair, G. Nicholson, J. de Belleroche, J. M. Gallo, C. C. Miller, and C. E. Shaw, 2009, Mutations in FUS, an RNA processing protein, cause familial amyotrophic lateral sclerosis type 6: Science, v. 323, p. 1208-11.

Waite, A. J., D. Baumer, S. East, J. Neal, H. R. Morris, O. Ansorge, and D. J. Blake, 2014, Reduced C9orf72 protein levels in frontal cortex of amyotrophic lateral sclerosis and frontotemporal degeneration brain with the C9ORF72 hexanucleotide repeat expansion: Neurobiol Aging, v. 35, p. 1779.e5-1779.e13.

Walker, A. K., and J. D. Atkin, 2011, Stress signaling from the endoplasmic reticulum: A central player in the pathogenesis of amyotrophic lateral sclerosis: IUBMB Life, v. 63, p. 754-63.

Walter, P., and D. Ron, 2011, The unfolded protein response: from stress pathway to homeostatic regulation: Science, v. 334, p. 1081-6.

Wang, L., D. H. Gutmann, and R. P. Roos, 2011, Astrocyte loss of mutant SOD1 delays ALS disease onset and progression in G85R transgenic mice: Hum Mol Genet, v. 20, p. 286-93.

Wang, S., J. Bates, X. Li, S. Schanz, D. Chandler-Militello, C. Levine, N. Maherali, L. Studer, K. Hochedlinger, M. Windrem, and S. A. Goldman, 2013, Human iPSC-derived oligodendrocyte progenitor cells can myelinate and rescue a mouse model of congenital hypomyelination: Cell Stem Cell, v. 12, p. 252-64.

Warner, J. P., L. H. Barron, D. Goudie, K. Kelly, D. Dow, D. R. Fitzpatrick, and D. J. Brock, 1996, A general method for the detection of large CAG repeat expansions by fluorescent PCR: J Med Genet, v. 33, p. 1022-6.

Webster, C. P., E. F. Smith, A. J. Grierson, and K. J. De Vos, 2016, C9orf72 plays a central role in Rab GTPase-dependent regulation of autophagy: Small GTPases, p. 1-10.

Weng, Q., Y. Chen, H. Wang, X. Xu, B. Yang, Q. He, W. Shou, Y. Higashi, V. van den Berghe, E. Seuntjens, S. G. Kernie, P. Bukshpun, E. H. Sherr, D. Huylebroeck, and Q. R. Lu, 2012, Dual-mode modulation of Smad signaling by Smad-interacting protein Sip1 is required for myelination in the central nervous system: Neuron, v. 73, p. 713-28.

Westergard, T., B. K. Jensen, X. Wen, J. Cai, E. Kropf, L. Iacovitti, P. Pasinelli, and D. Trotti, 2016, Cell-to-Cell Transmission of Dipeptide Repeat Proteins Linked to C9orf72-ALS/FTD: Cell Rep, v. 17, p. 645-652.

Wingo, T. S., D. J. Cutler, N. Yarab, C. M. Kelly, and J. D. Glass, 2011, The heritability of amyotrophic lateral sclerosis in a clinically ascertained United States research registry: PLoS One, v. 6, p. e27985.

Xi, Z., I. Rainero, E. Rubino, L. Pinessi, A. C. Bruni, R. G. Maletta, B. Nacmias, S. Sorbi, D. Galimberti, E. I. Surace, Y. Zheng, D. Moreno, C. Sato, Y. Liang, Y. Zhou, J. Robertson, L. Zinman, M. C. Tartaglia, P. St George-Hyslop, and E. Rogaeva, 2014, Hypermethylation of the CpG-island near the C9orf72 G(4)C(2)-repeat expansion in FTLD patients: Hum Mol Genet, v. 23, p. 5630-7.

Xi, Z., M. van Blitterswijk, M. Zhang, P. McGoldrick, J. R. McLean, Y. Yunusova, E. Knock, D. Moreno, C. Sato, P. M. McKeever, R. Schneider, J. Keith, N. Petrescu, P. Fraser, M. C. Tartaglia, M. C. Baker, N. R. Graff-Radford, K. B. Boylan, D. W. Dickson, I. R. Mackenzie, R. Rademakers, J. Robertson, L. Zinman, and E. Rogaeva, 2015a, Jump from pre-mutation to pathologic expansion in C9orf72: Am J Hum Genet, v. 96, p. 962-70.

Xi, Z., M. Zhang, A. C. Bruni, R. G. Maletta, R. Colao, P. Fratta, J. M. Polke, M. G. Sweeney, E. Mudanohwo, B. Nacmias, S. Sorbi, M. C. Tartaglia, I. Rainero, E. Rubino, L. Pinessi, D. Galimberti, E. I. Surace, P. McGoldrick, P. McKeever, D. Moreno, C. Sato, Y. Liang, J. Keith, L. Zinman, J. Robertson, and E. Rogaeva, 2015b, The C9orf72 repeat expansion itself is methylated in ALS and FTLD patients: Acta Neuropathol, v. 129, p. 715-27.

Xi, Z., L. Zinman, D. Moreno, J. Schymick, Y. Liang, C. Sato, Y. Zheng, M. Ghani, S. Dib, J. Keith, J. Robertson, and E. Rogaeva, 2013, Hypermethylation of the CpG island near the G4C2 repeat in ALS with a C9orf72 expansion: Am J Hum Genet, v. 92, p. 981-9.

Xiao, S., L. MacNair, P. McGoldrick, P. M. McKeever, J. R. McLean, M. Zhang, J. Keith, L. Zinman, E. Rogaeva, and J. Robertson, 2015, Isoform-specific antibodies reveal distinct subcellular localizations of C9orf72 in amyotrophic lateral sclerosis: Ann Neurol, v. 78, p. 568-83.

Xu, Z., M. Poidevin, X. Li, Y. Li, L. Shu, D. L. Nelson, H. Li, C. M. Hales, M. Gearing, T. S. Wingo, and P. Jin, 2013, Expanded GGGGCC repeat RNA associated with amyotrophic lateral sclerosis and frontotemporal dementia causes neurodegeneration: Proc Natl Acad Sci U S A, v. 110, p. 7778-83.

Yamakawa, M., D. Ito, T. Honda, K. Kubo, M. Noda, K. Nakajima, and N. Suzuki, 2015, Characterization of the dipeptide repeat protein in the molecular pathogenesis of c9FTD/ALS: Hum Mol Genet, v. 24, p. 1630-45.

Yamanaka, K., S. Boillee, E. A. Roberts, M. L. Garcia, M. McAlonis-Downes, O. R. Mikse, D. W. Cleveland, and L. S. Goldstein, 2008a, Mutant SOD1 in cell types

other than motor neurons and oligodendrocytes accelerates onset of disease in ALS mice: Proc Natl Acad Sci U S A, v. 105, p. 7594-9.
Yamanaka, K., S. J. Chun, S. Boillee, N. Fujimori-Tonou, H. Yamashita, D. H. Gutmann, R. Takahashi, H. Misawa, and D. W. Cleveland, 2008b, Astrocytes as determinants of disease progression in inherited amyotrophic lateral sclerosis: Nat Neurosci, v. 11, p. 251-3.
Yokoyama, J. S., D. W. Sirkis, and B. L. Miller, 2014, C9ORF72 hexanucleotide repeats in behavioral and motor neuron disease: clinical heterogeneity and pathological diversity: Am J Neurodegener Dis, v. 3, p. 1-18.
Yu, J., K. Hu, K. Smuga-Otto, S. Tian, R. Stewart, I. I. Slukvin, and J. A. Thomson, 2009, Human induced pluripotent stem cells free of vector and transgene sequences: Science, v. 324, p. 797-801.
Yu, Y., Y. Chen, B. Kim, H. Wang, C. Zhao, X. He, L. Liu, W. Liu, L. M. Wu, M. Mao, J. R. Chan, J. Wu, and Q. R. Lu, 2013, Olig2 targets chromatin remodelers to enhancers to initiate oligodendrocyte differentiation: Cell, v. 152, p. 248-61.
Zhang, D., M. Pekkanen-Mattila, M. Shahsavani, A. Falk, A. I. Teixeira, and A. Herland, 2014a, A 3D Alzheimer's disease culture model and the induction of P21-activated kinase mediated sensing in iPSC derived neurons: Biomaterials, v. 35, p. 1420-8.
Zhang, K., C. J. Donnelly, A. R. Haeusler, J. C. Grima, J. B. Machamer, P. Steinwald, E. L. Daley, S. J. Miller, K. M. Cunningham, S. Vidensky, S. Gupta, M. A. Thomas, I. Hong, S. L. Chiu, R. L. Huganir, L. W. Ostrow, M. J. Matunis, J. Wang, R. Sattler, T. E. Lloyd, and J. D. Rothstein, 2015, The C9orf72 repeat expansion disrupts nucleocytoplasmic transport: Nature, v. 525, p. 56-61.
Zhang, Y. J., T. F. Gendron, J. C. Grima, H. Sasaguri, K. Jansen-West, Y. F. Xu, R. B. Katzman, J. Gass, M. E. Murray, M. Shinohara, W. L. Lin, A. Garrett, J. N. Stankowski, L. Daughrity, J. Tong, E. A. Perkerson, M. Yue, J. Chew, M. Castanedes-Casey, A. Kurti, Z. S. Wang, A. M. Liesinger, J. D. Baker, J. Jiang, C. Lagier-Tourenne, D. Edbauer, D. W. Cleveland, R. Rademakers, K. B. Boylan, G. Bu, C. D. Link, C. A. Dickey, J. D. Rothstein, D. W. Dickson, J. D. Fryer, and L. Petrucelli, 2016, C9ORF72 poly(GA) aggregates sequester and impair HR23 and nucleocytoplasmic transport proteins: Nat Neurosci.
Zhang, Y. J., K. Jansen-West, Y. F. Xu, T. F. Gendron, K. F. Bieniek, W. L. Lin, H. Sasaguri, T. Caulfield, J. Hubbard, L. Daughrity, J. Chew, V. V. Belzil, M. Prudencio, J. N. Stankowski, M. Castanedes-Casey, E. Whitelaw, P. E. Ash, M. DeTure, R. Rademakers, K. B. Boylan, D. W. Dickson, and L. Petrucelli, 2014b, Aggregation-prone c9FTD/ALS poly(GA) RAN-translated proteins cause neurotoxicity by inducing ER stress: Acta Neuropathol, v. 128, p. 505-24.
Zhou, Q., and D. J. Anderson, 2002, The bHLH transcription factors OLIG2 and OLIG1 couple neuronal and glial subtype specification: Cell, v. 109, p. 61-73.
Zhou, Q., G. Choi, and D. J. Anderson, 2001, The bHLH transcription factor Olig2 promotes oligodendrocyte differentiation in collaboration with Nkx2.2: Neuron, v. 31, p. 791-807.
Zhou, W., and C. R. Freed, 2009, Adenoviral gene delivery can reprogram human fibroblasts to induced pluripotent stem cells: Stem Cells, v. 27, p. 2667-74.
Zoccolella, S., E. Beghi, G. Palagano, A. Fraddosio, V. Guerra, V. Samarelli, V. Lepore, I. L. Simone, P. Lamberti, L. Serlenga, and G. Logroscino, 2008, Analysis of survival and prognostic factors in amyotrophic lateral sclerosis: a population based study: J Neurol Neurosurg Psychiatry, v. 79, p. 33-7.
Zu, T., B. Gibbens, N. S. Doty, M. Gomes-Pereira, A. Huguet, M. D. Stone, J. Margolis, M. Peterson, T. W. Markowski, M. A. Ingram, Z. Nan, C. Forster, W. C. Low, B. Schoser, N. V. Somia, H. B. Clark, S. Schmechel, P. B. Bitterman,

G. Gourdon, M. S. Swanson, M. Moseley, and L. P. Ranum, 2011, Non-ATG-initiated translation directed by microsatellite expansions: Proc Natl Acad Sci U S A, v. 108, p. 260-5.

Zu, T., Y. Liu, M. Bañez-Coronel, T. Reid, O. Pletnikova, J. Lewis, T. M. Miller, M. B. Harms, A. E. Falchook, S. H. Subramony, L. W. Ostrow, J. D. Rothstein, J. C. Troncoso, and L. P. W. Ranum, 2013, RAN proteins and RNA foci from antisense transcripts in C9ORF72 ALS and frontotemporal dementia: Proc Natl Acad Sci U S A, v. 110, p. E4968-77.